

Application and elucidation of enzymes involved in the utilization of  
marine carbohydrates

I n a u g u r a l d i s s e r t a t i o n

zur

Erlangung des akademischen Grades

Dr. rer. nat. (Doctor rerum naturalium)

der

Mathematisch-Naturwissenschaftlichen Fakultät

der

Universität Greifswald

vorgelegt von

Stefan Brott

Greifswald, September 2023

Dekan: Prof. Dr. Gerald Kerth

1. Gutachter: Prof. Dr. Uwe T. Bornscheuer

2. Gutachterin: Prof. Dr. Magali Remaud-Simeon

Tag der Promotion: 30.11.2023

---

## Table of Content

<b>Abbreviations</b> .....	V
<b>Scope and Outline</b> .....	VII
<b>1. Background</b> .....	1
1.1 Marine algae produce complex polysaccharides .....	1
1.2 Utilization of marine polysaccharides by heterotrophic bacteria .....	1
1.2.1 Carbohydrate-active enzymes and sulfatases .....	2
1.3 Green algae of the genus <i>Ulva</i> – An economic menace with biotechnology potential ..	4
1.3.1 The marine polysaccharide ulvan .....	4
1.3.1.1 Saccharification of ulvan by a bacterial enzyme cascade .....	5
1.4 Porphyran a marine red algal polysaccharide .....	8
1.4.1 Enzymatic porphyran degradation .....	8
1.4.1.1 Oxidative demethylation of G6Me by cytochrome P450 monooxygenases.....	11
1.5 Alcohol dehydrogenases .....	13
1.6 Formaldehyde: a cytotoxic metabolite .....	13
1.6.1 Detoxification of formaldehyde through different metabolic pathways .....	15
1.6.1.1 Formaldehyde dissimilation via thiol-dependent pathways .....	15
1.6.1.2 Pterin-dependent formaldehyde dissimilation .....	17
1.6.1.3 Formaldehyde dissimilation through cofactor-independent pathways.....	19
1.6.1.4 Formaldehyde assimilation via the ribulose monophosphate pathway .....	19
1.6.1.4.1 Formaldehyde induces gene expression of HPS and PHI.....	21
1.6.1.4.2 HPS and PHI are the unique key enzymes of the RuMP pathway .....	21
1.6.1.5 Alternative pathways for formaldehyde assimilation .....	22
<b>2. Aim of the thesis</b> .....	23
<b>3. Results &amp; Discussion</b> .....	24
3.1 Connecting porphyran degradation to formaldehyde detoxification .....	24
3.2 Alcohol dehydrogenases involved in G6Me utilization by marine bacteria .....	29
3.3 Application of ulvan as feedstock for a biotechnologically relevant strain .....	34
<b>4. Summary</b> .....	39
<b>5. References</b> .....	40
<b>Author Contributions</b> .....	48
<b>Articles</b> .....	51
<b>Article I</b> .....	53
<b>Article II</b> .....	71
<b>Article III</b> .....	123
<b>List of Publications</b> .....	161
<b>Acknowledgments</b> .....	163



## Abbreviations

Å	Ångström
AA	Auxiliary activity
ADH	Alcohol dehydrogenase
ADP	Adenosine diphosphate
AgaB	$\beta$ -Agarase from <i>Z. galactanivorans</i> Dsij <sup>T</sup>
AH6P	D-Arabino-3-hexulose-6-phosphate
ATP	Adenosine triphosphate
<i>B. licheniformis</i>	<i>Bacillus licheniformis</i>
<i>B. plebeius</i>	<i>Bacteroides plebeius</i>
<i>B. subtilis</i>	<i>Bacillus subtilis</i>
BSH	Bacillithiol
CAZymes	Carbohydrate-active enzymes
CBM	Carbohydrate-binding module
CE	Carbohydrate esterase
CYP	Cytochrome P450 monooxygenases
DNA	Deoxyribonucleic acid
DPC	DNA-protein crosslink
<i>E. coli</i>	<i>Escherichia coli</i>
<i>et al.</i>	<i>et alia</i>
<i>F. agariphila</i>	<i>Formosa agariphila</i> KMM 3901 <sup>T</sup>
F6P	D-Fructose-6-phosphate
FoADH	Alcohol dehydrogenase from <i>Formosa agariphila</i> KMM 3901 <sup>T</sup>
G6Me	6-O-Methyl-D-galactose
Gal	$\beta$ -D-Galactose
GH	Glycoside hydrolase
GlcA	$\beta$ -D-Glucuronic acid
GSH	Glutathione
GT	Glycosyltransferase
H <sub>4</sub> MPT	Tetrahydromethanopterin
HPS	3-Hexulose-6-phosphate synthase
IdoA	$\alpha$ -L-Iduronic acid
L6S	$\alpha$ -L-Galactose-6-sulfate

## Abbreviations

---

LA	3,6-Anhydro- $\alpha$ -L-galactose
MSH	Mycothioliol
NAD(P) <sup>+</sup>	Oxidized nicotinamide adenine dinucleotide (phosphate)
NADH(P)	Reduced nicotinamide adenine dinucleotide (phosphate)
OMPDC	Orotidine 5'-monophosphate decarboxylase
pH	<i>Pondus hydrogenii</i>
PHI	6-Phospho-3-hexuloisomerase
PL	Polysaccharide lyase
PLP	Pyridoxal-5'-phosphate
PorA	$\beta$ -Porphyrinase A from <i>Zobellia galactanivorans</i> Dsij <sup>T</sup>
PorB	$\beta$ -Porphyrinase B from <i>Zobellia galactanivorans</i> Dsij <sup>T</sup>
PorWf	$\beta$ -Porphyrinase from <i>Wenyingzhuangia fucanilytica</i>
PUL	Polysaccharide utilization loci
R5P	D-Ribulose-5-phosphate
Rha3S	$\alpha$ -L-Rhamnose-3-sulfate
RNA	Ribonucleic acid
RuMP	Ribulose monophosphate
Spp.	Species pluralis
Sus	Starch-utilization-system
THF	Tetrahydrofolate
U	Unit
<i>W. fucanilytica</i>	<i>Wenyingzhuangia fucanilytica</i>
w/o	Without
WT	Wild-type
Xyl	$\beta$ -D-Xylose
<i>Z. galactanivorans</i>	<i>Zobellia galactanivorans</i> Dsij <sup>T</sup>
ZoADH	Alcohol dehydrogenase from <i>Zobellia galactanivorans</i> Dsij <sup>T</sup>

In addition to the listed abbreviations, units based on the International System of Units (SI) as well as derived SI units are used. Furthermore, the one-letter code for proteinogenic amino acids were used.

## Scope and Outline

This dissertation focuses on the characterization of novel enzymes and metabolic pathways that fulfil crucial functions during marine carbohydrate degradation by *Bacteroidetes* and thus contributes to an advanced understanding of the global carbon cycle. Depolymerization and utilization of marine polysaccharides by *Bacteroidetes* requires a tremendous repertoire of enzymes with a wide range of functions. For instance, during the breakdown of the marine red algal polysaccharide porphyran, an oxidative demethylation of the methoxy sugar 6-O-methyl-D-galactose (G6Me) by cytochrome P450 monooxygenases occurs. This reaction produces huge amounts of cytotoxic formaldehyde, marine bacteria capable of degrading porphyran must therefore possess suitable formaldehyde detoxification pathways. Consequently, **Article I** focus on the identification of possible formaldehyde detoxification pathways in marine *Flavobacteriia*, which led to the discovery of the ribulose monophosphate pathway as specific pathway for the detoxification of formaldehyde in certain *Bacteroidetes* like *Zobellia galactanivorans*. Furthermore, it was demonstrated in **Article II** that alcohol dehydrogenases play an essential role in the microbial utilization of G6Me and therefore possess a function in porphyran degradation. Discovering novel enzymes, entire enzymatic cascades or biotechnologically important microorganisms that can metabolize these marine carbohydrates also contributes to the utilization of marine polysaccharides as feedstock for potential biotechnological applications. A prospective biorefinery process was proposed in **Article III** by the identification of *Bacillus licheniformis* as promising utilizer of marine carbohydrate-derived monosaccharides and the creation of a microbial cell factory capable of growing on ulvan, a marine carbohydrate obtainable from algal bloom-dominating green algae, enabling an industrial use of the renewable and abundant algal biomass in future.

### **Article I      Connecting algal polysaccharide degradation to formaldehyde detoxification**

S. Brott, F. Thomas, M. Behrens, K. Methling, D. Bartosik, T. Dutschei, M. Lalk, G. Michel, T. Schweder and U. T. Bornscheuer, *ChemBioChem* **2022**, 23, e202200269.

By combining gene knockouts, growth studies, gene expression analyses and biochemical characterizations, it was possible to demonstrate in this article that the ribulose monophosphate pathway exists as formaldehyde detoxification pathway in *Zobellia galactanivorans* and that it performs an essential role in the porphyran degradation by removing cytotoxic formaldehyde, which is produced by the oxidative demethylation of the methoxy sugar G6Me. In addition, computational analysis revealed that the ribulose monophosphate pathway is scarcely distributed in marine bacteria, but simultaneously represents a specific characteristic of microbes that grow predominantly on multicellular algae.

**Article II      Unique alcohol dehydrogenases involved in algal sugar utilization by marine bacteria**

S. Brott, K. H. Nam, F. Thomas, T. Dutschei, L. Reisky, M. Behrens, H. C. Grimm, G. Michel, T. Schweder and U. T. Bornscheuer, *Appl. Microbiol. Biotechnol.* **2023**, 107, 2363–2384.

This article describes the previously uncharacterized alcohol dehydrogenases from marine *Bacteroidetes*, whose genes appear in a cluster with the genes that encode for the enzymes of the oxidative demethylation as well as an esterase, and are presumably conserved in porphyrin-degrading *Flavobacteriia*. The combination of a gene knockout in *Zobellia galactanivorans* and subsequent growth studies demonstrated the involvement of this alcohol dehydrogenase in the microbial utilization of G6Me. The complete biochemical characterization as well as the elucidation of the crystal structures of the two alcohol dehydrogenases from *Formosa agariphila* and *Zobellia galactanivorans* were performed. A potential function of these enzymes in the metabolism of galactose or in the detoxification of formaldehyde was investigated. Despite the fact that neither of these functions was observed *in vitro*, these ADHs represent novel enzymes that either fulfill a pivotal role within porphyrin utilization as carbohydrate-active enzyme (CAZyme) with auxiliary activity or in uncharacterized formaldehyde detoxification pathways. This article thus introduces alcohol dehydrogenases as important enzymes in the utilization of porphyrin-derived methoxy sugars, contributes to an enhanced knowledge of the carbon cycle and provides the basis for further research.

**Article III      Metabolic engineering enables *Bacillus licheniformis* to grow on the marine polysaccharide ulvan**

T. Dutschei, M. K. Zühlke, N. Welsch, T. Eisenack, M. Hilkmann, J. Krull, C. Stühle, S. Brott, A. Dürwald, L. Reisky, J.-H. Hehemann, D. Becher, T. Schweder and U. T. Bornscheuer, *Microb. Cell Fact.* **2022**, 21, 207.

This article focuses on the implementation of the marine green algae polysaccharide ulvan as feedstock for an industrially important production strain to provide the foundation for a prospective biotechnological process. Various biotechnologically relevant microorganisms were screened for their physiological ability to grow on ulvan-derived monosaccharides as a sole carbon source. The best performing strain in the growth studies, *Bacillus licheniformis*, was subsequently developed into a self-sufficient strain capable of growing on ulvan as a sole carbon source by introducing two genes into the strain, which encode for essential enzymes of initial ulvan degradation. The creation of this microbial cell factory provides a groundwork for the potential utilization of abundant algal biomass in a future biorefinery process.



# 1. Background

## 1.1 Marine algae produce complex polysaccharides

Oceans cover about 70% of the earth's surface and serve as a habitat for countless organisms, including marine algae species.<sup>[1]</sup> Marine algae can be categorized into two large sub-groups namely macroalgae, which can be subdivided in green algae (Chlorophyta), red algae (Rhodophyta) and brown algae (Phaeophyta), and microalgae, also referred to as phytoplankton, in which dinoflagellates, diatoms, green algae and cyanobacteria represent the most prominent groups.<sup>[2,3]</sup> Marine algae fulfill a major role in the global carbon cycle by sequestering approximately 52 billion tons of carbon dioxide annually in form of organic matter such as carbohydrate structures,<sup>[4]</sup> which they utilize as intracellular energy storage, structural cell wall polysaccharides or extracellular polymeric substances.<sup>[5–8]</sup> Consequently, up to 70% of algae dry mass consists of carbohydrates.<sup>[8]</sup> Depending on the algae species, the function of the marine carbohydrate as well as its composition can vary considerably.<sup>[9,10]</sup> Compared to their terrestrial counterparts, marine polysaccharides possess a complicated backbone structure, which may contain various branching motifs and side group modifications such as methylations or acetylations.<sup>[5,10]</sup> In addition, a specific characteristic of marine carbohydrates represents the high degree of sulfatation, which is assumed to be an adaptation of marine seaweeds towards the marine habitat.<sup>[11–13]</sup> The composition as well as the structures of the sulfated carbohydrates ulvan derived from green algae and porphyran from red algae are presented in detail in chapters 1.3.1 and 1.4 as typical examples of marine polysaccharides.

## 1.2 Utilization of marine polysaccharides by heterotrophic bacteria

Heterotrophic bacteria contribute significantly to the marine carbon cycle by degrading algal-derived carbohydrates and utilizing the resulting monosaccharides as an energy and carbon source.<sup>[14–16]</sup> Members of the diverse bacterial phylum *Bacteroidetes*, which occurs abundantly in nature across various ecological niches,<sup>[17,18]</sup> are considered as specialists in the degradation of marine carbohydrates.<sup>[18,19]</sup> Observations that *Bacteroidetes* emerge as first responders after phytoplankton and macroalgal blooms,<sup>[20–22]</sup> which are annual occurring events characterized by excessive proliferation of algae,<sup>[23–25]</sup> can be attributed by their abilities of rapid growth on colonizable surfaces such as macroalgae<sup>[18,26,27]</sup> as well as the production and secretion of carbohydrate-active enzymes (CAZymes) that efficiently degrade complex polysaccharides.<sup>[18,19,21]</sup> A distinctive feature of *Bacteroidetes* is the occurrence of strictly regulated gene clusters in their genomes, which are termed polysaccharide utilization loci (PUL) and encode for CAZymes as well as the complete protein machinery involved in binding and transport of sugars.<sup>[17–19,28]</sup> It is assumed that one PUL is specifically responsible for the utilization of one particular carbohydrate.<sup>[19]</sup> One characteristic feature of a canonical PUL is the presence of a SusC- and SusD-like pair, which share structural and functional homology

with the original SusC and SusD proteins from the starch-utilization-system (Sus) of the human gut symbiont *Bacteroidetes thetaiotaomicron*.<sup>[17,29,30]</sup> The extracellular SusD-like protein displays carbohydrate-binding properties, while the SusC-like protein represents a member of the TonB-dependent transporters and is responsible for the transfer of oligosaccharides from the bacterial surface into the periplasmic space.<sup>[17,29,30]</sup> Both proteins form a complex in which SusD acts as a hinge-like lid of SusC, which facilitate the transport of bound oligosaccharides into the periplasm via a pedal-bin like mechanism.<sup>[30,31]</sup>

Currently, three prevailing models for marine carbohydrate utilization by heterotrophic bacteria are reported in literature.<sup>[32]</sup> The probably most widespread model is termed selfish uptake,<sup>[33]</sup> where polysaccharides are initially bound to the outer cell membrane and then partially degraded to larger oligosaccharides by surface-anchored CAZymes,<sup>[32–34]</sup> The oligosaccharides are then transported, for instance via the SusCD complex,<sup>[31]</sup> into the periplasm where saccharification proceeds by further CAZymes.<sup>[32–34]</sup> The generated monosaccharides are then transported into the cytoplasm and are utilized as a carbon and energy source.<sup>[32–34]</sup> The advantage of the selfish mechanism is the securing of substantial quantities of substrate in the periplasm, where it is protected from diffusion loss as well as other bacteria.<sup>[32–34]</sup> The second model consists of sharing bacteria, which employ surface-anchored but additionally also secreted CAZymes for the degradation of polysaccharides into suitable sizes for uptake.<sup>[32,33]</sup> As a result of CAZymes secretion, extracellular hydrolysis products also known as “public goods” are accessible for all microbes.<sup>[32,33]</sup> The third model is represented by scavenging bacteria, which are incapable of producing CAZymes and thus are unable to hydrolyze polysaccharides. Instead, scavengers take up and consume the public goods.<sup>[32,33]</sup>

### 1.2.1 Carbohydrate-active enzymes and sulfatases

Due to their complexity, the degradation of marine carbohydrates requires an enormous range of diverse CAZymes, which fulfil distinct functions and must interact synergistically to break down the polysaccharide to the level of monosaccharides.<sup>[10]</sup> CAZymes are listed in the CAZy database and are grouped into the classes of glycoside hydrolases (GH), polysaccharide lyases (PL), carbohydrate esterases (CE), glycosyltransferases (GT) and carbohydrate-binding modules (CBM).<sup>[35]</sup> An additional class was later introduced into the CAZy database, enzymes of this class possess an auxiliary activity (AA) and assist GHs and PLs in the degradation process.<sup>[36]</sup> Each class is subdivided into families based on experimentally characterized enzymes, protein folds, enzymatic mechanism and sequence similarities.<sup>[35,36]</sup> Depending on whether the CAZyme targets the sugar at a terminal end or within the backbone, they can be further classified as exo- or endo-acting enzymes.<sup>[37]</sup> Noteworthy, CAZymes include by definition not only enzymes that degrade carbohydrates, but also those such as

GTs that are involved in the formation of polysaccharides.<sup>[35,38]</sup> The largest CAZyme class in relation to the number of families represent the GHs,<sup>[35]</sup> which hydrolyze the glycosidic bonds of a carbohydrate.<sup>[39,40]</sup> GHs can be divided into two distinct classes based on their reaction mechanism, which can lead to either a retention or inversion of the anomeric configuration at the newly formed reducing end as result of hydrolysis.<sup>[40–42]</sup> However, diverging reaction mechanisms involving elimination and/or hydration steps may take place in certain GH families.<sup>[43]</sup> Glycosidic bond scission of uronic acid-containing polysaccharides can also proceed via PL-catalyzed  $\beta$ -elimination.<sup>[44,45]</sup> GHs and PLs can appear as multimodular enzymes containing non-catalytic modules like CBMs that potentiate prolonged association and interaction of the enzyme with the polysaccharide and thus accelerates depolymerization of the carbohydrate.<sup>[46–48]</sup> In addition, CBMs may cause non-catalytic disruption of a polysaccharide structure, resulting in increased accessibility for GHs or PLs to attack the glycosidic bonds of the carbohydrate.<sup>[49]</sup> Enzymes with auxiliary activity assist hydrolytic enzymes in the degradation of recalcitrant carbohydrates by creating new hydrolyzable target sites, for instance through an oxidative cleavage in a crystalline polymer chain.<sup>[36,50]</sup> The most prominent representatives of the AA family are lytic polysaccharide monooxygenases, which catalyze the  $O_2$ - or  $H_2O_2$ -dependent oxidative cleavage of crystalline cellulose or chitin.<sup>[36,51–53]</sup> In addition, marine cytochrome P450 monooxygenases which are involved in the degradation of the red algae polysaccharide porphyran belong to the AA class.<sup>[54]</sup> Variations in the polysaccharide composition due to the additional appearance of ester-based modifications such as acetylations at the sugar units, might negatively affect the activity and specificity of CAZymes for certain carbohydrates.<sup>[55]</sup> De-esterification of these interfering ester groups is therefore catalyzed by CEs, which provide new unsubstituted sugar moieties that are accepted in the substrate binding pockets of GHs or PLs and thus facilitate polysaccharide depolymerization.<sup>[56–60]</sup>

Many marine algal polysaccharides are frequently decorated with sulfate esters, which can also interfere in the enzymatic carbohydrate breakdown.<sup>[61]</sup> Consequently, the hydrolytic removal of sulfate groups by sulfatases represents an essential step in various phases of polysaccharide degradation.<sup>[61–63]</sup> Genes encoding for sulfatases often appear with GH or PL genes in PULs, indicating a synergy action between CAZymes and sulfatases.<sup>[12,63,64]</sup> In fact, some sulfatases may also occur as a catalytic module of multimodular CAZymes.<sup>[12]</sup> Sulfatases are classified by sequence homology, crystal structures and mechanisms into four classes and several subfamilies in the SulfAtlas database.<sup>[65]</sup> Sulfatases participating in marine carbohydrate degradation belong to class 1, which require an essential formylglycine residue for their catalytic activity.<sup>[12,66]</sup> The formylglycine is formed from a serine or cysteine residue belonging to the signature amino acid sequence C/S-X-P-X-R via co-translational conversion and is catalyzed in aerobic microbes by a formylglycine-generating enzyme.<sup>[12,66–68]</sup>

### **1.3 Green algae of the genus *Ulva* – An economic menace with biotechnology potential**

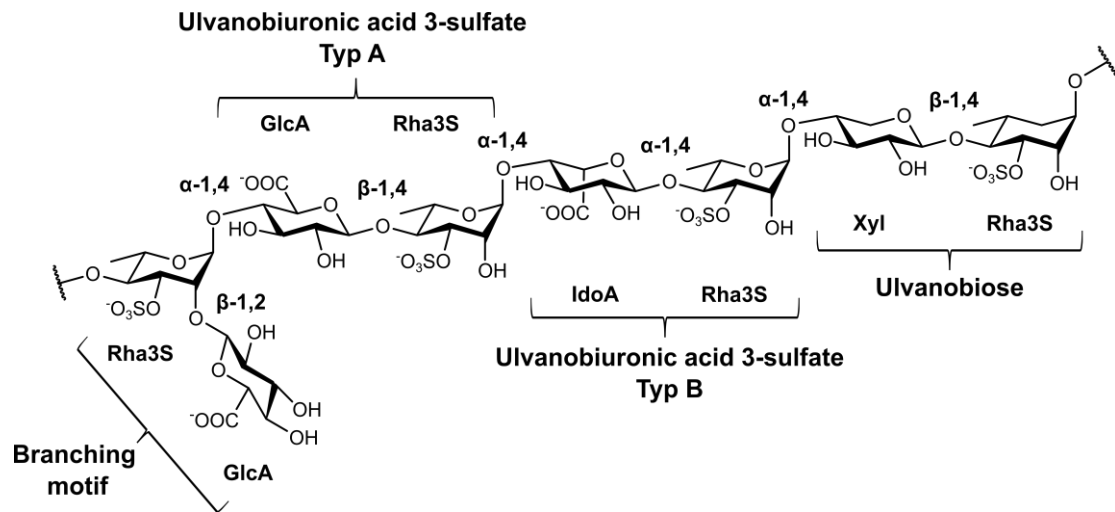
The combination of anthropological eutrophication of marine environments with naturally occurring geographic and hydrodynamic conditions can result in excessive proliferations of certain opportunistic macroalgae.<sup>[69,70]</sup> These massive macroalgal blooms are dominated by few specific genera which possess advantageous biological features such as an efficient photosynthesis, a rapid growth rate and a high capacity for nutrient uptake.<sup>[70,71]</sup> The worldwide occurring blooms dominated by the species of the genus *Ulva* (Chlorophyta) are termed green tides and cause severe ecological and economic consequences.<sup>[70–72]</sup> Public awareness and media coverage of green tides surged most likely as result of the 2008 Olympic Games in China, where the sudden appearance of a 30 km-long bloom and the beaching of millions of tons of algae at the sailing venue almost prevented the sailing disciplines from being held.<sup>[69,71]</sup> A massive emergency clean-up operation involving more than 10,000 people was essential in order to save the sailing competition.<sup>[69,71]</sup> The costs of approximately 290 million Euro for clean-up and resulting damages of aquacultures demonstrated the economic impact of one green tide.<sup>[69,71]</sup> Decay of non-removed algal mass also causes detrimental effects, harmful odors and smothering morass piles on the shore lead to a decreasing beach quality, which severely affects the tourism and daily life of the coastal region.<sup>[71,73,74]</sup> Local communities are therefore confronted with the challenge of choosing between the costs of removing and disposing the algal mass and the potential losses due to reduced tourism and aquaculture damages.<sup>[71]</sup>

New processes for sustainable applications of algal biomasses are currently the focus of numerous investigations and changing the status of algae from being waste towards a promising biorefinery feedstock.<sup>[75–80]</sup> For instance, the utilization of brown algae biomass for the production of biofuel has already been demonstrated.<sup>[80]</sup> Hydrolysates of macroalgae of the genus *Ulva* are suitable for a wide variety of applications, such as fermentations for the production of valuable components like rare sugars or bioethanol.<sup>[75–78,81–84]</sup> In addition, *Ulva* spp. offers an excellent nutritional content and can be employed as supplement in aquacultures systems or in food applications.<sup>[85,86]</sup> One of the most predominant components of *Ulva* spp. represents the cell-wall polysaccharide ulvan, which can account for up to 30% of the algal dry mass.<sup>[87]</sup>

#### **1.3.1 The marine polysaccharide ulvan**

The anionic water-soluble polysaccharide ulvan consists predominantly of sulfated rhamnose, xylose and uronic acids (glucuronic acid and iduronic acid) (Fig. 1).<sup>[87–90]</sup> The main repeating units in ulvan represent two disaccharides, which are designated as ulvanobiuronic acid 3-sulfate type A and B.<sup>[87–90]</sup> The more frequently occurring type A consists of  $\beta$ -D-glucuronic

acid (GlcA) linked to  $\alpha$ -L-rhamnose-3-sulfate (Rha3S) by a  $\beta$ -1,4-glycosidic bond.<sup>[87–90]</sup> In contrast, type B is composed of  $\alpha$ -L-iduronic acid (IdoA) which is bound to Rha3S via an  $\alpha$ -1,4-glycosidic bond.<sup>[87–90]</sup>



**Figure 1: Structure of ulvan.** The main chain of ulvan consists of the monosaccharides  $\alpha$ -L-rhamnose 3-sulfate (Rha3S),  $\beta$ -D-xylose (Xyl),  $\beta$ -D-glucuronic acid (GlcA) and  $\alpha$ -L-iduronic acid (IdoA). Ulvan consists of two main repeating units named ulvanobiuronic acid 3-sulfate type A and B, in which GlcA is  $\beta$ -1,4-linked and IdoA is  $\alpha$ -1,4-linked to Rha3S. Minor branching motifs, which consists of a single GlcA unit, can occur. A minor recurring motif is ulvanobiose, where Xyl is  $\beta$ -1,4-linked to Rha3S. The xylose can be sulfated at the O2 position (not shown).<sup>[87–92]</sup>

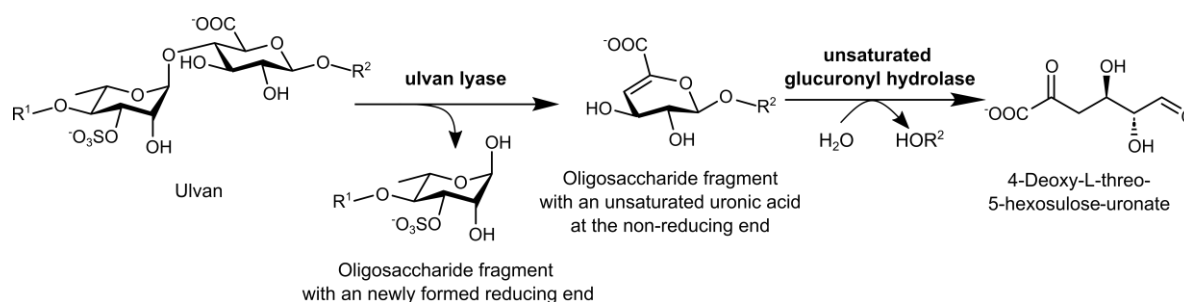
An additional minor repeating unit can occur in the ulvan backbone which is called ulvanobiose, in which  $\beta$ -D-xylose (Xyl) replaces the uronic acids in the previously mentioned motifs.<sup>[87,88,90]</sup> Increased complexity of the ulvan structure arises from the occurrence of continuous GlcA units within the main chain as well as the potential sulfatation of Xyl at the O2 position in the ulvanobiose.<sup>[87–92]</sup> The ulvan structure is further complicated by the presence of small branches, which are based on a single GlcA unit that is linked to the O2 of Rha3S by a  $\beta$ -1,2-glycosidic bond.<sup>[87–90,92]</sup>

### 1.3.1.1 Saccharification of ulvan by a bacterial enzyme cascade

Utilization of ulvan and its oligosaccharides, which are also increasingly demanded in the pharmaceutical and food industries due to their health-promoting properties,<sup>[93–97]</sup> has long been restricted by insufficient knowledge of a saccharification process. However, marine bacteria of the phylum *Bacteroidetes* and *Gammaproteobacteria* provided the ideal prerequisite for the discovery and characterization of suitable enzymes for ulvan degradation due to their CAZyme repertoire,<sup>[98–103]</sup> which consequently culminated in a complete ulvan saccharification pathway.<sup>[63]</sup>

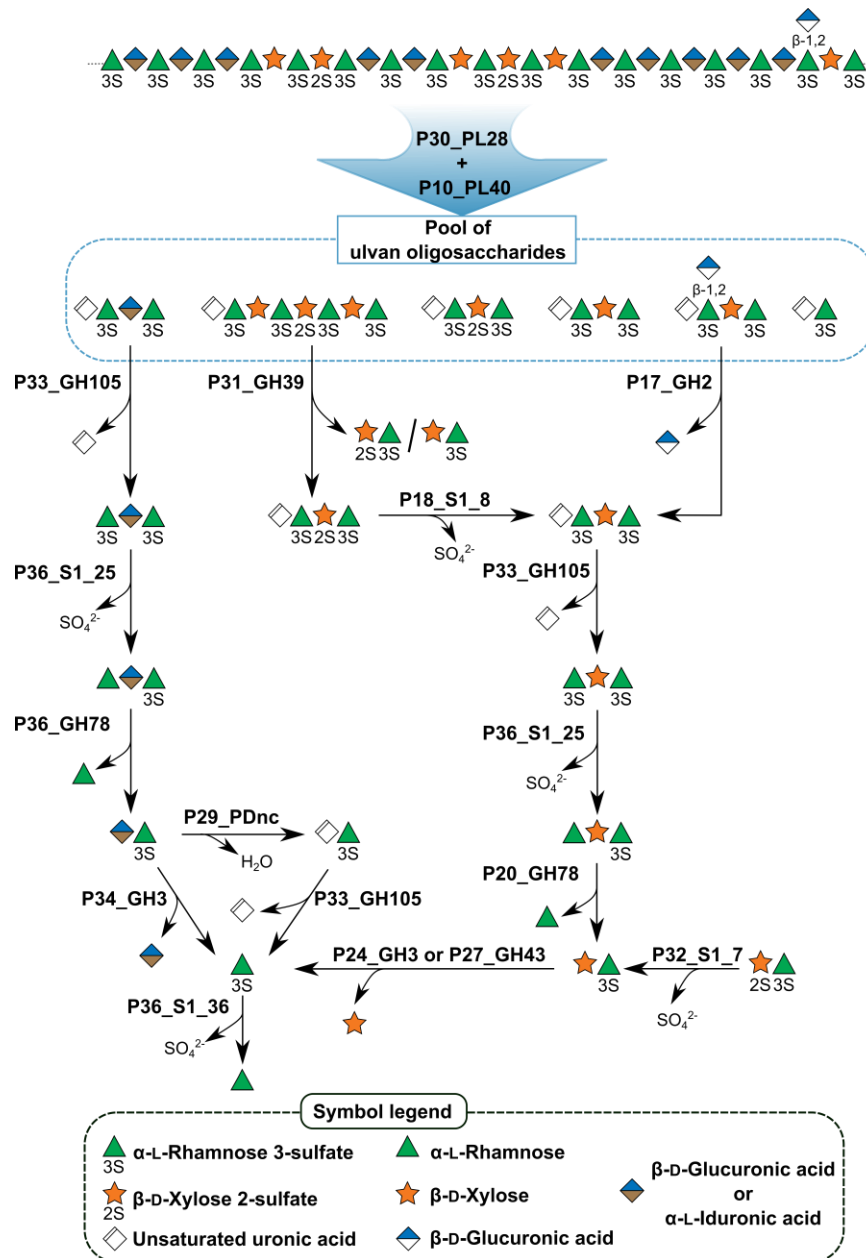
Initial ulvan depolymerization is catalyzed by PLs instead of GHs.<sup>[100–103]</sup> Ulvan lyases, which belong to PL families 24, 25, 28 and 40,<sup>[63,100–103]</sup> catalyze the glycosidic bond cleavage between Rha3S and uronic acids by a  $\beta$ -elimination mechanism, that yields an unsaturated uronic acid residue at the newly formed non-reducing end (Fig. 2).<sup>[44,45]</sup> The catalytic  $\beta$ -elimination mechanism consists of three steps and initiates with metal ion- or amino acid-

assisted neutralization of the negative charge on the carboxyl group of the uronic acid.<sup>[44,45,101–103]</sup> The neutralization renders the C5 proton susceptible for an attack by a base, which occurs in the second step.<sup>[44,45,101–103]</sup> The donation of a proton by an acid to the leaving group, which produces a reducing end at one fragment and the unsaturated uronic acid at the new non-reducing end of a second fragment, represents the last step.<sup>[44,45,100–103]</sup> In ulvan lyases, the neutralization of the negative charge is predominantly performed by arginine or glutamine residues.<sup>[100–103]</sup> Examples of amino acid residues which act as bases in the catalytic mechanism of ulvan lyases represent histidine, tyrosine and lysine, while histidine and tyrosine residues can also behave as acids.<sup>[100–103]</sup> Furthermore, it was proven that bivalent metal ions contribute to the structural integrity of the ulvan lyase and is thus required for enzyme stability and activity.<sup>[100–103]</sup> Ulvan lyases are rapidly inhibited by their reaction products,<sup>[91]</sup> thus fast depolymerization of formed oligosaccharides by additional CAZymes is required for effective polysaccharide degradation. The second step of ulvan depolymerization is generally performed by unsaturated glucuronyl hydrolases of the GH88 and/or GH105 family, which catalyze the cleavage of the unsaturated uronic acid residue from the non-reducing end of the oligosaccharide (Fig. 2) by a hydration mechanism.<sup>[43,99,104]</sup> The released unsaturated uronic acid residue spontaneously rearranges from the cyclic form to the linear 4-deoxy-L-threo-5-hexosulose-uronate.<sup>[99]</sup>



**Figure 2: The first two steps in ulvan degradation are catalyzed by an ulvan lyase and an unsaturated glucuronyl hydrolase.** Initial cleavage of ulvan involves PL-catalyzed  $\beta$ -elimination, which produces two oligosaccharide fragments, one containing a normal reducing end and the other carrying an unsaturated uronic acid residue at the non-reducing end. This unsaturated uronic acid is subsequently cleaved from the oligosaccharide by an unsaturated glucuronyl hydrolase and rearranges as a linear 4-deoxy-L-threo-5-hexosulose-uronate. R<sup>1</sup> and R<sup>2</sup> represent additional sugars of the ulvan backbone and can have varying degrees of depolymerizations and compositions.<sup>[44,45,99,100]</sup>

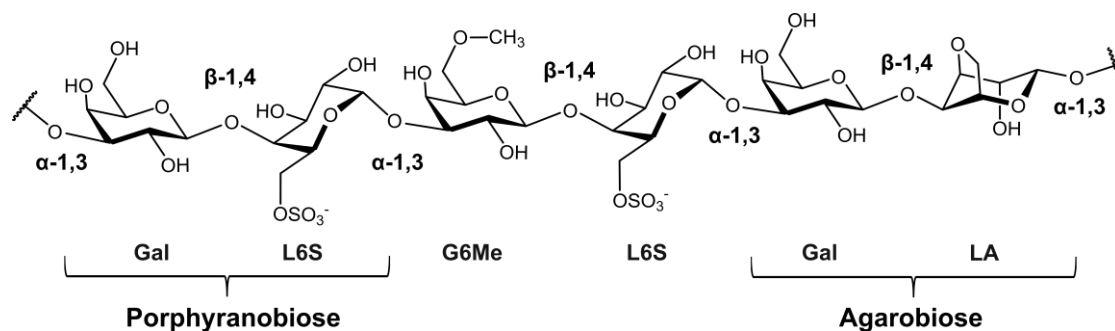
In addition to these two initial enzyme activities, further CAZymes and also sulfatases are required for complete saccharification. The basis for further research was the discovery of an ulvan-specific PUL in *Formosa agariphila* KMM 3901<sup>T</sup> (*F. agariphila*), which contains 39 genes that encode for enzymes involved in the ulvan breakdown and in the utilization of ulvan-derived monosaccharides.<sup>[63]</sup> The biochemical characterization of 12 enzymes from this PUL by Reisky *et al.* resulted in the elucidation of an enzyme cascade that enables the sequential degradation of ulvan to the level of monosaccharides (Fig. 3).<sup>[63]</sup> This cascade was afterwards further extended by the discovery of an oligosaccharide dehydratase, which facilitates the degradation of uronic acid-containing disaccharides.<sup>[105]</sup>



**Figure 3: Schematic illustration of the enzymatic cascade of *F. agariphila* for the saccharification of ulvan.** Initial ulvan depolymerization is catalyzed by two endo-acting ulvan lyases (P30\_PL28 and P10\_PL40) and results in a pool of diverse oligosaccharides. Depending on the composition and structure of the generated oligosaccharides, different CAZymes catalyze the next step in the degradation cascade. For instance, an endo-acting  $\alpha$ -1,4-L-rhamnosidase (P31\_GH39) can cleave larger oligosaccharides, that were resistant to further degradation by ulvan lyases, into dimers containing xylose and smaller oligosaccharides. Possible GlcA-branching moieties will be cleaved off by a  $\beta$ -glucuronidase (P17\_GH2). One of the most crucial functions is performed by the unsaturated glucuronyl hydrolases (P1\_GH88 or P33\_GH105), which catalyze the hydrolysis of formed unsaturated uronic acid units from oligosaccharides and thereby enable further degradation by other CAZymes. GH-inhibiting sulfatations are removed during the cascade by formyl-glycine-dependent sulfatases (P18\_S1\_7, P32\_S1\_7 and P36\_S1\_25). P36 is a multimodular enzyme which contains, in addition to the sulfatase module, a GH module that possesses  $\alpha$ -L-rhamnosidase activity (P36\_GH78) and cleaves previously desulfated rhamnose from oligosaccharides. Similarly, rhamnose can also be released from xylose-containing oligosaccharides by an additional  $\alpha$ -L-rhamnosidase (P20\_GH78). Xylose units are released from oligosaccharides by  $\beta$ -xylosidases (P24\_GH3 or P27\_GH43). Two degradation pathways are available for disaccharides consisting of uronic acid and Rha3S. The uronic acid unit can be converted into an unsaturated uronic acid by the elimination of water, catalyzed by a dehydratase (P29\_PDnc), which is subsequently cleaved off by the P33\_GH105. Alternatively, the uronic acid moiety can also be released by a promiscuous  $\beta$ -glucuronidase/ $\alpha$ -iduronidase (P34\_GH3). The enzymes of the ulvanolytic PUL from *F. agariphila* KMM 3901<sup>T</sup> were numbered by Reisky *et al.* (P1-P39), the same numbering was adopted for better comparison. The figure is derived and adapted from a review article<sup>[10]</sup> and summarizes the results from the Reisky *et al.*<sup>[63]</sup> as well as the Bäumgen and Dutschei *et al.*<sup>[105]</sup> studies.

## 1.4 Porphyran a marine red algal polysaccharide

Porphyran is a sulfated galactan, which represents the main cell wall polysaccharide of red algae of the genus *Porphyra*.<sup>[106,107]</sup> The linear backbone of porphyran consists of D- and L-galactose residues alternately linked by  $\beta$ -1,4 and  $\alpha$ -1,3 glycosidic bonds (Fig. 4).<sup>[107–109]</sup> The main repeating unit in porphyran represents a disaccharide, which is termed porphyranobiose and consists of 3-linked  $\beta$ -D-galactose (Gal) and 4-linked  $\alpha$ -L-galactose-6-sulfate (L6S).<sup>[107,109]</sup> Occasionally, agarobiose moieties occur within native porphyran, where 4-linked 3,6-anhydro- $\alpha$ -L-galactose (LA) replaces L6S.<sup>[107,109]</sup> Agarobiose, which is the main recurring unit in agarose, may also appear as small blocks in the form of neo-agarotetraose in porphyran.<sup>[107]</sup> Naturally occurring porphyran thus displays a hybrid structure, containing both porphyranobiose and agarobiose building blocks.<sup>[62,107,109]</sup> In addition, O-methylation of D-galactose represents a common modification, which leads to the presence of up to 28% of the methoxy sugar 6-O-methyl-D-galactose (G6Me) within the porphyran chain.<sup>[106,108]</sup> Furthermore, comparison of porphyran from various *Porphyra* spp. revealed that the structural composition of the polysaccharide can vary between organisms and is also influenced by environmental and seasonal fluctuations.<sup>[106]</sup>



**Figure 4: Structure of porphyran.** The porphyran backbone consists mainly of the alternating monosaccharide units 3-linked- $\beta$ -D-galactose (Gal) and 4-linked- $\alpha$ -L-galactose-6-sulfate (L6S) or 4-linked 3,6-anhydro- $\alpha$ -L-galactose (LA) which form porphyranobiose or agarobiose building blocks. In addition, O-methylation of D-galactose results in the presence of the methoxy sugar 6-O-methyl-D-galactose (G6Me).<sup>[106–109]</sup>

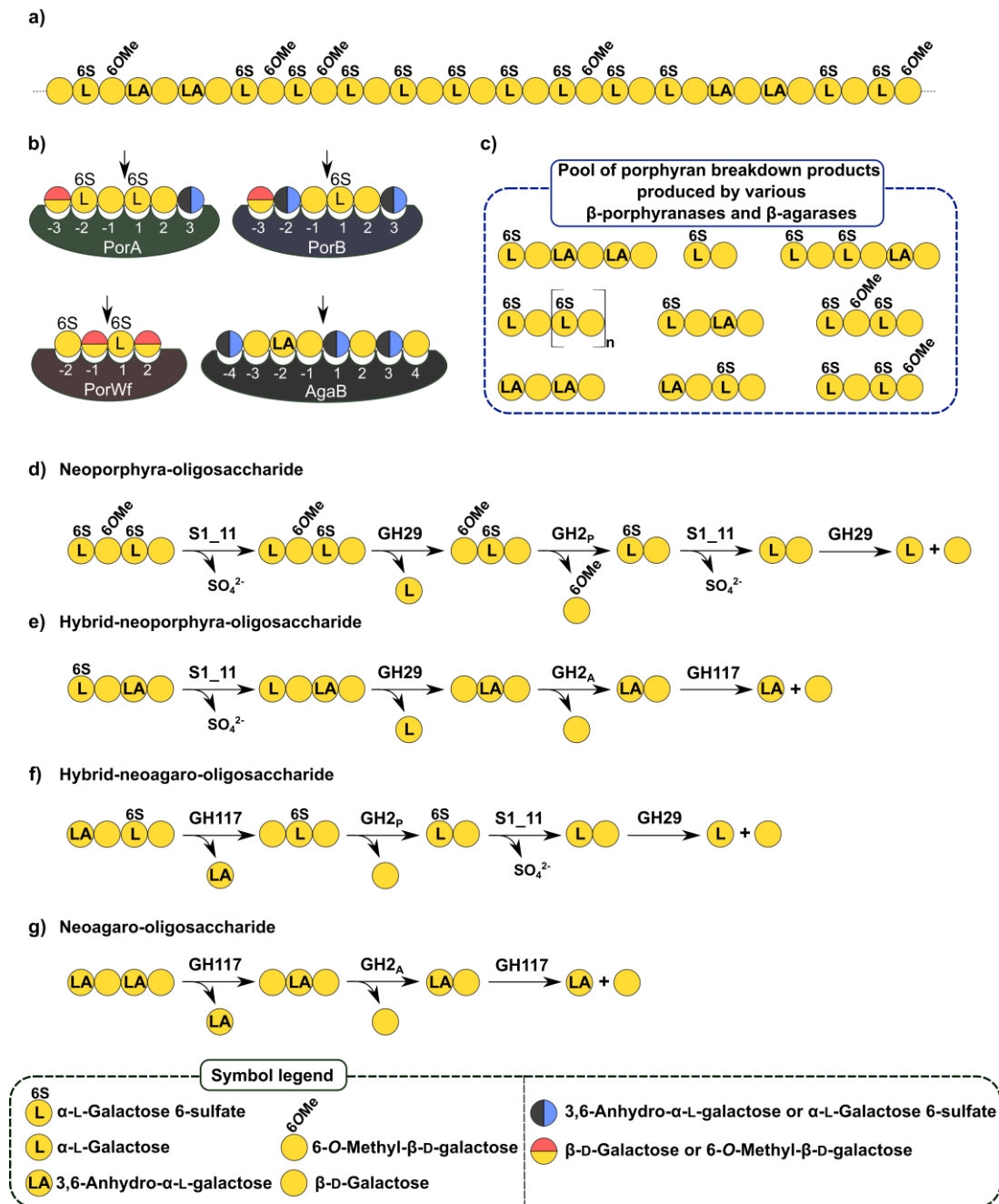
### 1.4.1 Enzymatic porphyran degradation

Various CAZymes are required for efficient porphyran breakdown due to its complex structure and hybrid nature (Fig. 5a).<sup>[62]</sup> The initial step in the enzymatic porphyran degradation is catalyzed by  $\beta$ -porphyranases, which have been discovered first in the marine flavobacterium *Zobellia galactanivorans* Dsij<sup>T</sup> (*Z. galactanivorans*).<sup>[109,110]</sup> These  $\beta$ -porphyranases, referred as PorA and PorB, are members of the GH family 16 and catalyze the cleavage of the  $\beta$ -1,4-glycosidic bond between two adjacent neoporphyranoiose (L6S-Gal-L6S-Gal) units leading to the release of the disaccharide (L6S-Gal) as their main product.<sup>[109,110]</sup> Several other marine  $\beta$ -porphyranases of the GH16 family, for instance from the flavobacterium *Wenyinzhuangia fucanilytica* (*W. fucanilytica*) or the red algae *Chondrus crispus* have been investigated and characterized.<sup>[111,112]</sup> Differences in observed substrate specificities, such as the tolerance of



LA units in -2 subsite of PorB<sup>[109,110]</sup> or the acceptance of G6Me moieties in the -1 and +2 subsites of the  $\beta$ -porphyranase from *W. fucanilytica* (Fig. 5b),<sup>[111]</sup> are based on structural variations in their binding pockets<sup>[109–111]</sup> and can be interpreted as an evolutionary adaptation to the hybrid character of the marine carbohydrate.<sup>[109]</sup> Furthermore, transcriptomics studies revealed that in the presence of porphyran as a sole carbon source,  $\beta$ -agarases which catalyze the cleavage of the  $\beta$ -1,4-glycosidic bond between two adjoining neoagarobiose moieties (LA-Gal-LA-Gal) are also expressed in *Z. galactanivorans*.<sup>[109]</sup> Expression of agarolytic enzymes in the presence of porphyran and their involvement in porphyran degradation can be attributed to the hybrid structure of native porphyran, which requires synergistic actions of agarose- and porphyran-active enzymes for complete depolymerization.<sup>[62,109]</sup>

Porphyran is considered as one of the most consumed algal polysaccharides, due to the fact of being a main ingredient of specific sushi dishes.<sup>[110,113]</sup> Dietary uptake of environmental microorganisms associated with algae contributed most likely to the acquisition of the marine polysaccharide degradation ability in human gut microbiota.<sup>[110]</sup> For instance, gut metagenome analyses revealed that certain human gut bacteria such as *Bacteroides plebeius* (*B. plebeius*) acquired the genes for a porphyran-utilization locus possibly through horizontal gene transfer from an ancestral marine bacterium and is thus capable of growing on porphyran.<sup>[62,110,114]</sup> Additional insights into enzymatic porphyran degradation were therefore obtained by the characterization of a novel  $\beta$ -porphyranase of the GH86 family and elucidation of an exo-based porphyran depolymerization cycle by *B. plebeius*.<sup>[62,114]</sup> Porphyran depolymerization in *B. plebeius* is initialized by endo-acting  $\beta$ -porphyranases of the GH86 and GH16 families and results in the formation of a wide variety of oligosaccharides (Fig 5c).<sup>[62,114]</sup> The GH86  $\beta$ -porphyranase catalyzes the cleavage of the  $\beta$ -1,4-glycosidic bond and produces predominantly larger oligosaccharides with the shortest product detected to be a tetra-oligosaccharide.<sup>[62,114]</sup> The following exo-based porphyran degradation cycle (Fig 5d) commences with the desulfation of a terminal L6S at the non-reducing end, which is catalyzed by an exo-6-sulfate L-galactose sulfatase.<sup>[62]</sup> Subsequently, hydrolysis of the  $\alpha$ -1,3-glycosidic bond between the previously desulfated L-galactose and D-galactose is achieved by an exo- $\alpha$ -L-galactosidase of the GH29 family.<sup>[62]</sup> Release of D-galactose from the non-reducing end by hydrolysis of the  $\beta$ -1,4 bond is then catalyzed by a  $\beta$ -galactosidase possessing an exo- $\beta$ -D-porphyrano-oligosaccharide hydrolase activity.<sup>[62]</sup> The depolymerization cycle may then restart with the desulfation reaction.<sup>[62]</sup> Variations of this degradation pathway (Fig. 5e-g) might occur due to the appearance of LA units or smaller agarose blocks within the porphyran chain, the degradation of these components can be catalyzed by exo-acting agarolytic enzymes.<sup>[62,115]</sup> Recent studies demonstrated that the exo-acting porphyran degradation cycle in *B. plebeius* also features enzymes which are capable to degrade oligosaccharide variants containing G6Me moieties.<sup>[116]</sup>



**Figure 5: Basic understanding of enzymatic porphyran degradation.** **a)** Schematic structure of a porphyran chain. **b)** Schematic models demonstrating the subsite substrate specificities of selected  $\beta$ -porphyranases and a  $\beta$ -agarase from *Z. galactanivorans* (PorA, PorB, AgaB)<sup>[109]</sup> as well as the  $\beta$ -porphyranase from *W. fucanilytica* (PorWf).<sup>[111]</sup> Based on substrate specificity and the structural composition of porphyran,  $\beta$ -agarases such as AgaB can cleave certain  $\beta$ -1,4-glycosidic bonds within porphyran.<sup>[109]</sup> Subsite pockets are numbered according to the nomenclature of Davies *et al.* with negative numbers indicating the direction towards the non-reducing end and positive numbers to the reducing end.<sup>[42]</sup> The black arrow indicates the  $\beta$ -1,4-glycosidic bond which is hydrolyzed by the enzyme. **c)** Depending on the substrate specificity of the  $\beta$ -porphyranases and  $\beta$ -agarases, completely different porphyran depolymerization products are formed. The presented oligosaccharides constitute only a selection and do not represent all products. **d)** The exo-acting porphyran depolymerization cycle from *B. plebeius* yields monosaccharides. The cycle starts with the desulfation of a terminal L6S by an exo-acting 6-sulfate L-galactosyl sulfatase (S1\_11). Cleavage of the desulfated  $\alpha$ -L-galactose by an exo- $\alpha$ -L-galactosidase of the GH29 family occurs next. Subsequent hydrolysis of the  $\beta$ -1,4-glycosidic bond with release of  $\beta$ -D-galactose or G6Me is carried out by a  $\beta$ -galactosidase (GH2<sub>p</sub>) possessing exo- $\beta$ -D-porphyrin-oligosaccharide hydrolase activity. The cycle may then restart with the desulfation of L6S. Degradation of **e)** hybrid neoporphyrin-oligosaccharides, **f)** hybrid neoagarin-oligosaccharides and **g)** neoagarin-oligosaccharides by variations of the exo-based porphyran depolymerization cycle relies on synergistic actions of porphyranolytic and agarolytic enzymes. The GH117 enzyme exhibits exo- $\alpha$ -1,3-L-neoagarin-oligosaccharide hydrolase activity and cleaves LA units from the non-reducing end.<sup>[117]</sup> GH2<sub>A</sub> represents a  $\beta$ -galactosidase possessing exo- $\beta$ -D-agarin-oligosaccharide hydrolase activity. The figure is derived and adapted from the Hehemann *et al.*<sup>[109]</sup>, Zhang *et al.*<sup>[111]</sup>, Robb *et al.*<sup>[62]</sup> and Mathieu *et al.*<sup>[118]</sup> studies.

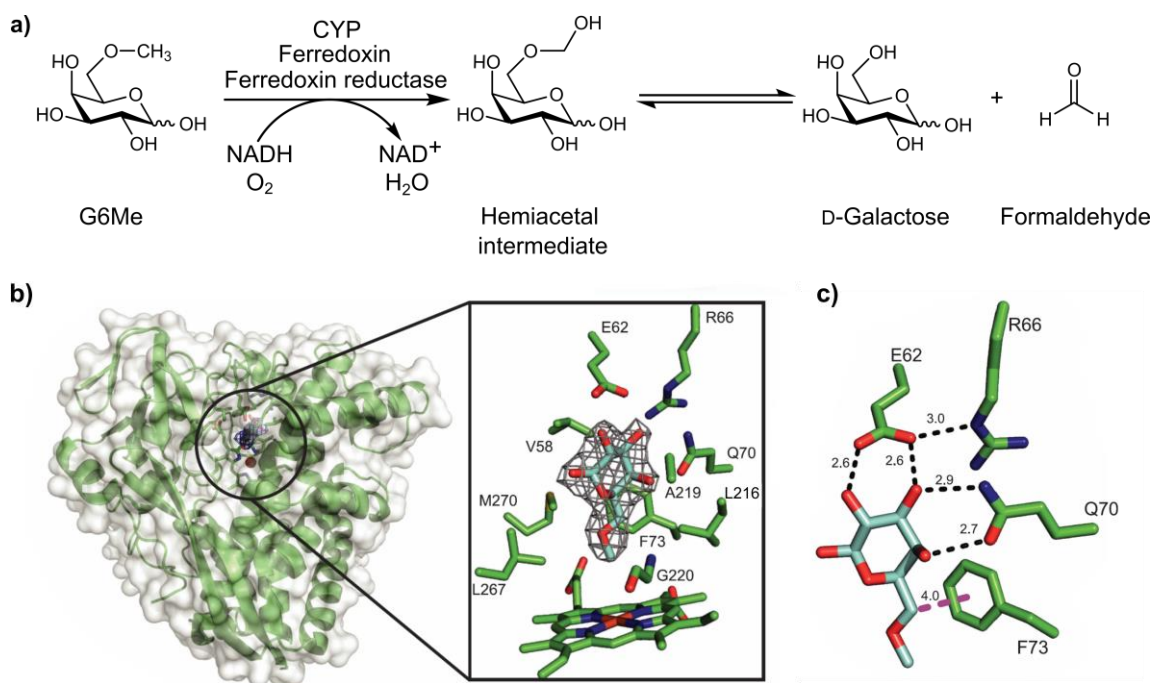
A completely biochemically characterized degradation pathway of  $\beta$ -porphyranase-produced disaccharides to the level of monosaccharides has not been described for *Z. galactanivorans*. However, there are reports of putative sulfatase genes being present in PUL structures of *Z. galactanivorans*, suggesting their involvement in the desulfation of L6S.<sup>[110]</sup> In theory, an  $\alpha$ -galactosidase might subsequently cleave the  $\alpha$ -1,3-glycosidic bond, releasing  $\alpha$ -L-galactose and  $\beta$ -D-galactose.<sup>[10]</sup> Eventually, a similar degradation pathway as described for *B. plebeius* might exist in *Z. galactanivorans*.

#### 1.4.1.1 Oxidative demethylation of G6Me by cytochrome P450 monooxygenases

The presence of the methoxy sugar G6Me within the porphyran chain can pose a challenge for (marine) microbes in terms of effective polysaccharide degradation and metabolism of the sugar.<sup>[54,109]</sup> Effective binding of some glycoside hydrolases can be inhibited by the impossibility of accommodating G6Me in certain subsites of the enzyme, resulting in reduced degradation efficiency or incomplete breakdown.<sup>[62,109]</sup> For instance, PorA from *Z. galactanivorans* is unable to degrade the tetrasaccharide L6S-G6Me-L6S-Gal due to the presence of G6Me.<sup>[109]</sup> Furthermore, experiments involving *B. plebeius* suggested that a complete porphyran conversion into monosaccharides cannot be achieved if the employed enzymes of the depolymerization cascade are not capable to accommodate G6Me in their structure.<sup>[62]</sup> Resistance towards enzymatic degradation caused by the presence of methyl ether groups might therefore also be a reasonable explanation why numerous O-methylated sugars can be found in seawater as part of high molecular mass dissolved organic matter.<sup>[54,119,120]</sup> Besides the potential inhibition of glycoside hydrolase binding,<sup>[109]</sup> the stability of the methyl ether bond represents a potent obstacle for the metabolic utilization of G6Me.<sup>[54]</sup> Demethylation of G6Me is therefore assumed to be required before the sugar can enter cellular glycolytic pathways.<sup>[54]</sup>

In general, oxidative demethylations can be catalyzed by oxidoreductases such as cytochrome P450 monooxygenases (CYPs).<sup>[121]</sup> CYPs are heme-containing enzymes capable of catalyzing numerous oxidative reactions including hydroxylation of non-activated C-H bonds, epoxidations, dealkylations and C-C bond cleavage.<sup>[121–123]</sup> In the most common hydroxylation reaction catalyzed by CYPs, one single oxygen atom of molecular O<sub>2</sub> is incorporated into a C-H bond of the substrate, while the remaining oxygen atom is reduced to water.<sup>[121–123]</sup> The reaction requires two electrons, which are consecutively shuttled from reduced nicotinamide adenine dinucleotide (NADH) or nicotinamide adenine dinucleotide phosphate (NADPH) via redox partners to the monooxygenase.<sup>[121–124]</sup> Evidence for the feasible regioselective demethylation of chemically permethylated sugars was demonstrated first by an engineered cytochrome P450 monooxygenase from *Bacillus megaterium*.<sup>[125]</sup> Recently, Reisky *et al.* succeeded in discovering and characterizing CYPs associated with marine carbohydrate degradation and thereby revealing the oxidative demethylation of G6Me.<sup>[54,126]</sup> A brief summary of the finding of these studies is now provided. Systematic genome analyses of marine bacteria

revealed that certain members of *Bacteroidetes*, *Gammaproteobacteria* and *Planctomycetes* contain three genes which were located in close proximity to genes for putative agarolytic or porphyranolytic CAZymes and encodes for a CYP and its redox partners ferredoxin and ferredoxin reductase.<sup>[54]</sup> In order to verify a suspected participation in a demethylation reaction, the CYP from *Z. galactanivorans* Dsjj<sup>T</sup> as well as the CYP and their redox partners ferredoxin and ferredoxin reductase from the Flavobacterium *F. agariphila* KMM 3901<sup>T</sup> were heterologously expressed, purified and the biological function investigated.<sup>[54]</sup> In combination with the redox partners from *F. agariphila* and NADH as electron donor, both CYPs were able to catalyze the oxidative demethylation of G6Me into equimolar amounts of formaldehyde and D-galactose (Fig. 6a).<sup>[54]</sup> Further investigations revealed that the redox partners were not interchangeable with those from other P450 monooxygenase systems and that G6Me was the only accepted substrate among 40 components tested.<sup>[54]</sup> The high substrate specificity towards G6Me could be explained by the elucidation of the crystal structure of the CYP from *Z. galactanivorans* (Fig. 6b) and the discovery of specific amino acids involved in binding and orientation of G6Me within the active site (Fig. 6c).<sup>[126]</sup>



**Figure 6: CYP-catalyzed oxidative demethylation of G6Me.** **a)** Oxidative demethylation involves the insertion of a single oxygen atom from molecular  $O_2$  into the C-H bond of the methyl group, thereby forming an unstable hemiacetal intermediate that spontaneously decomposes to yield equimolar amounts of D-galactose and formaldehyde.<sup>[54,121–123,125]</sup> The second oxygen atom is reduced to water during the reaction. Two electrons are successively required for the catalytic cycle, which are transferred from NADH to the heme iron of the monooxygenase via the redox partners ferredoxin reductase and ferredoxin. **b)** Crystal structure of CYP from *Z. galactanivorans* containing G6Me as substrate (protein data bank accession code: 6G5O).<sup>[126]</sup> The heme ligand is located deep inside the core of the fold and is covalently bound to the apoprotein via the thiolate of a cysteine residue. The active site is located directly above the heme ligand. **c)** The orientation of G6Me by the amino acids of the active site ensures that the methoxy group points directly to the iron center of the heme ligand. The highly specialized active site is adapted to G6Me, consequently no other methylated sugars could be converted by the CYP.<sup>[54,126]</sup> Hydrogen bonds are shown as black dotted lines while a C-H $\cdots$  $\pi$  interaction is displayed as purple dotted line. Distances are given in Å. Figure **b)** and **c)** were derived from the Robb *et al.* study.<sup>[126]</sup>

## 1.5 Alcohol dehydrogenases

Reisky *et al.* also demonstrated that *Z. galactanivorans* and *F. agariphila* possess a gene which encodes for a class 3 zinc-dependent alcohol dehydrogenase (ADH) and that this is located in direct proximity to the genes that encode for the key enzymes of the oxidative demethylation of G6Me.<sup>[54]</sup> In general, ADHs fall into the enzyme class of oxidoreductases and catalyze the reversible oxidation of an alcohol to the corresponding aldehyde or ketone employing the oxidized nicotinamide adenine dinucleotide (NAD<sup>+</sup>) or nicotinamide adenine dinucleotide phosphate (NADP<sup>+</sup>) cofactor.<sup>[127,128]</sup> Zinc-dependent ADHs represent a large family of ADHs<sup>[129]</sup> that can perform various biological functions such as polyol dehydrogenases that catalyze the conversion between sugar and sugar alcohol<sup>[130]</sup> or glutathione-dependent formaldehyde dehydrogenases that play a significant role in formaldehyde detoxification.<sup>[131]</sup> This also reveals the variety of potential substrates that may be converted by the ADH, which depends on the size of their substrate-binding domain.<sup>[129,132]</sup> Typical structural characteristics of zinc-dependent ADHs include the Rossmann fold<sup>[133]</sup> and the presence of a catalytic zinc ion in the active site of the enzyme as well as a structural zinc ion that supports stability of an external loop structure.<sup>[134]</sup>

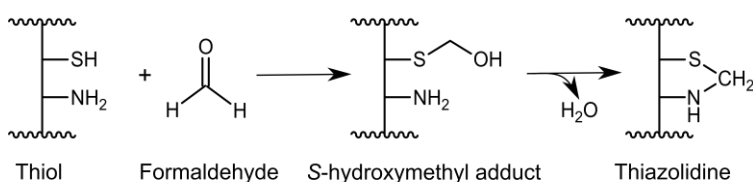
## 1.6 Formaldehyde: a cytotoxic metabolite

Formaldehyde is the smallest aldehyde and is produced as by-product in a variety of enzymatic reactions, such as the oxidative demethylation which can be catalyzed by CYPs,<sup>[54,135–137]</sup> Rieske non-heme iron-dependent oxygenases<sup>[138–141]</sup> and Fe(II)- $\alpha$ -ketoglutarate-dependent hydroxylases<sup>[142,143]</sup>. Oxidative *O*- and *N*-dealkylation reactions are found ubiquitously in nature and play significant roles in the metabolism and biosynthesis of alkaloids,<sup>[135,139,142,144,145]</sup> the resistance of plants against herbicides,<sup>[146]</sup> in DNA and RNA damage repair,<sup>[143,147–150]</sup> in epigenetic regulations<sup>[151,152]</sup> and in the bacterial degradation of the plant cell wall heteropolymer lignin<sup>[136–138,141,153]</sup> as well as the marine polysaccharide porphyran.<sup>[54]</sup> In addition, formaldehyde represents the central metabolite of methylotrophic bacteria,<sup>[154]</sup> which are abundant in nature and can occur in aquatic habitats,<sup>[155–158]</sup> soils<sup>[159–161]</sup> as well as the phyllo- and rhizosphere of plants.<sup>[162–165]</sup> Methylotrophic bacteria utilize reduced C1 hydrocarbons such as methane,<sup>[166,167]</sup> methanol,<sup>[163,168,169]</sup> methylamine<sup>[170–172]</sup> and methanethiol<sup>[173]</sup> for their growth and energy metabolism, which they initially oxidize to formaldehyde before converting it into cell mass or carbon dioxide.<sup>[154,166,174]</sup>

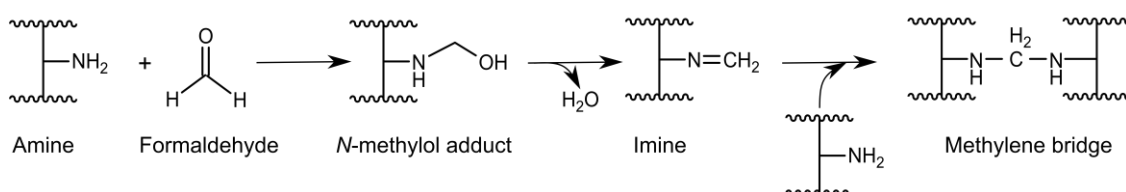
Formaldehyde formation has harmful consequences for the organism due to its electrophilic properties, which makes it susceptible to chemical attacks by nucleophiles such as free amino- and thiol groups of proteinogenic amino acids or nucleotides (Fig. 7).<sup>[175–177]</sup> The nucleophilic addition of a thiol to the polarized carbon atom of formaldehyde leads to a hemithioacetal, which can rapidly cyclize with an adjacent amine to form a thiazolidine adduct.<sup>[175,178]</sup> In contrast,

the nucleophilic addition of an amine to formaldehyde produces an *N*-methylol adduct, which can subsequently condense into an imine.<sup>[175,179]</sup> Generation of a cross-link in form of a methylene bridge may occur in a second reaction by the addition of a second nucleophilic amine to the imine.<sup>[175,179]</sup>

#### Reaction with thiols



#### Reaction with amines



**Figure 7: Reactions of formaldehyde with thiol or amino groups can lead to the formation of S- and N-hydroxymethylated adducts, thiazolidines and methylene bridges.** The figure was derived and adapted from the Chen *et al.* review article.<sup>[175]</sup>

Experiments concerning reactions between proteinogenic amino acids and formaldehyde revealed that the formation of hydroxymethylated, cyclized and cross-linked products occurs and that cysteines efficiently form stable thiazolidines.<sup>[176]</sup> In addition, the influence of formaldehyde on peptides and proteins was also investigated, reactions involving the *N*-terminal amino acids as well as the side chains of arginine, cysteine, histidine and lysine have been observed.<sup>[180,181]</sup> Furthermore, the formation of inter-protein and intra-protein cross-links are possible in the presence of formaldehyde.<sup>[180–182]</sup> Recent mass spectroscopy-based studies on protein-protein cross-links revealed that there may be a linkage mechanism alternative to the methylene bridge.<sup>[182]</sup> This cross-linking is speculated to be based on the dimerization of two formaldehyde-modified amino acid chains.<sup>[182]</sup> However, the precise structure of this linkage remains to be elucidated.<sup>[182]</sup> By modifying amino acids participating in enzymatic catalysis, formaldehyde can also have a detrimental effect on enzyme activities.<sup>[183]</sup>

The exocyclic nitrogen of adenine, guanine and cytosine as well as the endocyclic nitrogen of thymine and uracil are capable of reacting with formaldehyde to form *N*-hydroxymethylated adducts.<sup>[177]</sup> At the same time, the formation of inter- and intra-strand DNA crosslinks can be observed in the presence of formaldehyde.<sup>[184]</sup>

Formaldehyde-induced cross-link formation between amino acids and nucleotides have been identified and play an essential role in the generation of DNA-protein crosslinks (DPCs).<sup>[185,186]</sup> Primary genotoxic effects of formaldehyde might arise from the formation of DPCs.<sup>[186]</sup> Due to their bulkiness, DPCs represent a blockade for enzymes that participate in DNA replication

and transcription.<sup>[187,188]</sup> For example, it was shown that DNA polymerases cannot overcome DPCs and thereby terminate DNA synthesis.<sup>[188]</sup> Similar observations of DPC blocking were reported for bacterial helicases, where an inhibition of DNA strand separation was observable depending on the DPC size.<sup>[189,190]</sup> Simultaneously, studies with the T7 RNA polymerase demonstrated that blocking by DPCs can result in highly error-prone transcriptions.<sup>[187]</sup> In summary, formaldehyde causes mutagenic and cytotoxic effects, therefore organisms require suitable detoxification mechanisms to prevent accumulation of formaldehyde.

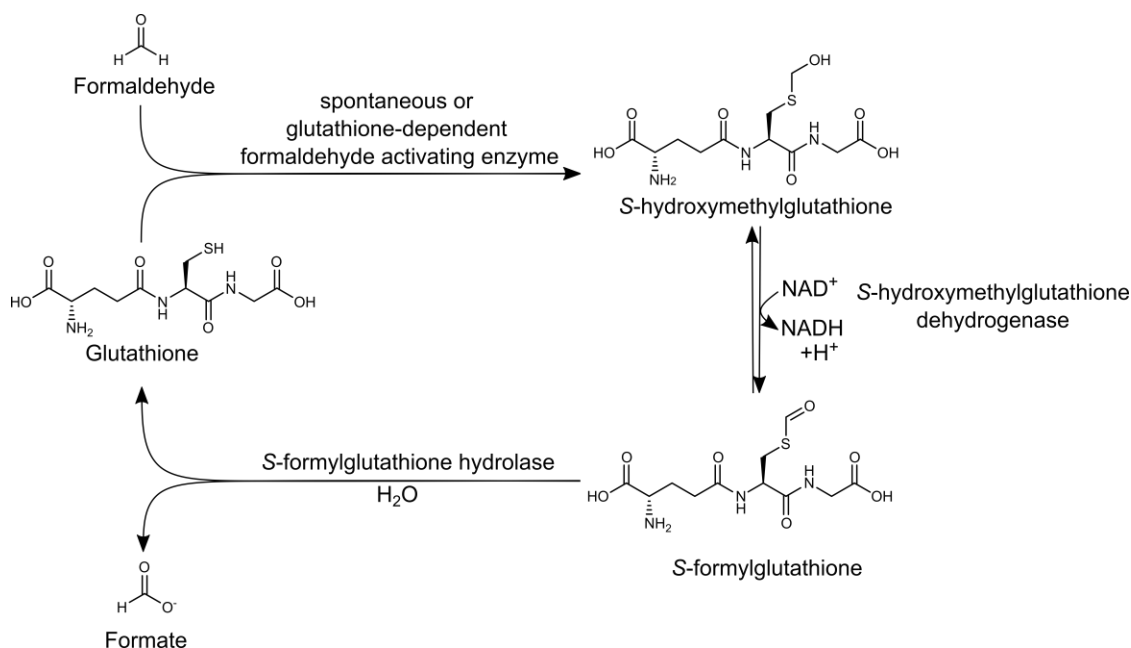
### 1.6.1 Detoxification of formaldehyde through different metabolic pathways

In order to cope with the severe toxicity of formaldehyde, microorganism harbor various formaldehyde detoxification pathways.<sup>[154,175,191,192]</sup> The discovery of these pathways was primarily studied involving methylotrophic bacteria,<sup>[154,191]</sup> however identical pathways were also discovered in non-methylotrophic organisms.<sup>[175,192]</sup> For instance, formaldehyde detoxification has also been reviewed in the context of host-adapted bacterial pathogens, considering that certain formaldehyde sources, such as the heme degradation,<sup>[193]</sup> may occur at the host-pathogen interface and thus pose a potential challenge for the growth and metabolism of the pathogen.<sup>[175]</sup> Formaldehyde detoxification can proceed via either dissimilatory or assimilatory pathways.<sup>[154,175,191,192]</sup> During assimilation, formaldehyde is incorporated in central metabolic pathways via several enzymatic steps and can thereby contribute towards biomass production.<sup>[154,175,191,192]</sup> In contrast, formaldehyde oxidation to formate occurs via dissimilatory routes.<sup>[154,175,191,192]</sup> Formate is subsequently oxidized to carbon dioxide by formate dehydrogenases and is accompanied by the generation of reducing equivalents.<sup>[194,195]</sup> The following sections provide a summary of the main formaldehyde detoxification pathways.

#### 1.6.1.1 Formaldehyde dissimilation via thiol-dependent pathways

One of the best characterized formaldehyde detoxification mechanism is based on a thiol cofactor serving as initial formaldehyde trap. The most common thiol cofactor utilized in the detoxification of formaldehyde is the tripeptide glutathione (GSH,  $\gamma$ -L-glutamyl-L-cysteinyl-glycine), which is widely distributed within prokaryotic and eukaryotic life forms.<sup>[175,196]</sup> Thiol-dependent detoxification initiates with a spontaneous reaction between the sulfhydryl group of GSH and formaldehyde, resulting in the formation of S-hydroxymethylglutathione (Fig. 8).<sup>[197-199]</sup> Additionally, enzymes capable of stimulating this spontaneous reaction have also been discovered.<sup>[200,201]</sup> For instance, the zinc- and glutathione-dependent formaldehyde-activating enzyme from *Paracoccus denitrificans* is suspected to accelerate the spontaneous reaction by functioning as a GSH carrier and promoting co-localization with formaldehyde inside the cell.<sup>[200,201]</sup> The formed intermediate is then oxidized by a NAD<sup>+</sup>-dependent zinc-

containing class 3 ADH to the thioester *S*-formylglutathione,<sup>[131,202,203]</sup> which is subsequently cleaved by a *S*-formylglutathione hydrolase to GSH and formate.<sup>[204]</sup>

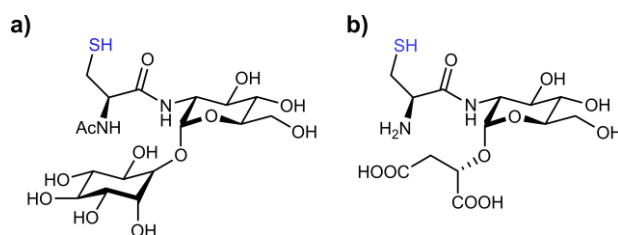


**Figure 8: Glutathione-dependent detoxification of formaldehyde yields formate.** *S*-hydroxymethylglutathione spontaneously formed from formaldehyde and glutathione<sup>[197–199]</sup> is oxidized to a thioester by a *S*-hydroxymethylglutathione dehydrogenase, which belongs to the zinc-dependent class 3 ADHs.<sup>[131,202,203]</sup> Regeneration of glutathione and generation of formate is then accomplished by the cleavage of the thioester, which is catalyzed by a *S*-formylglutathione hydrolase.<sup>[204]</sup>

*Actinomycetes* and other gram-positive microbes of the phylum *Firmicutes* contain alternative low-molecular-weight thiols, which they employ as cofactors in the detoxification of formaldehyde.<sup>[205–207]</sup> Mycothiol (2-(*N*-acetyl-L-cysteinyl)amido-2-deoxy- $\alpha$ -D-glucopyranosyl-1-D-*myo*-inositol) (MSH, Fig. 9a) was simultaneously isolated and structurally elucidated from *Streptomyces* spp. and *Mycobacteria bovis* nearly 30 years ago.<sup>[208–210]</sup> Participation of MSH in formaldehyde detoxification was demonstrated by the discovery of two MSH-dependent formaldehyde dehydrogenases from *Amycolatopsis methanolica* and *Rhodococcus erythropolis*.<sup>[211]</sup> Similar to their GSH-dependent counterpart, the MSH-dependent formaldehyde dehydrogenases belong to the zinc-containing ADHs and catalyze the formation of a *S*-formylthioester from the spontaneous adduct of mycothiol and formaldehyde.<sup>[207,211,212]</sup> In analogy to the GSH pathway, it is assumed that *S*-formylmycothiol is subsequently hydrolyzed to MSH and formate.<sup>[207]</sup>

Bacillithiol (2-(2-(*S*-L-cysteinyl)amino-2-deoxy- $\alpha$ -D-glucopyranosyloxy)-(2*S*)-butanedioic acid) (BSH, Fig. 9b) is an abundant thiol occurring for instance in *Bacilli*.<sup>[213,214]</sup> Analyses of the core pathways of formaldehyde detoxification in the methylotrophic organism *Bacillus methanolicus* MGA3 revealed that a BSH-dependent pathway was induced in the presence of formaldehyde stress.<sup>[205,215]</sup> Simultaneously, the presence of *S*-formylbacillithiol, the product of the BSH-dependent formaldehyde dehydrogenase catalyzed reaction, was detected in the cell lysate.<sup>[205,215]</sup>

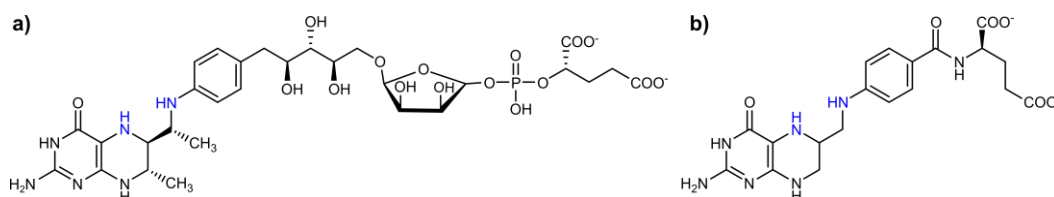




**Figure 9: Structure of a) mycothiol and b) bacillithiol.** Mycothiol is composed of *N*-acetylcysteine that is linked over an amide bond to glucosamine, which itself shares an  $\alpha$ -1,1-glycosidic bond with D-myo-inositol.<sup>[212]</sup> Bacillithiol is a glycoside consisting of L-cysteinyl-D-glucosamine and malic acid.<sup>[213]</sup> The blue-marked thiol groups are involved in formaldehyde detoxification.

### 1.6.1.2 Pterin-dependent formaldehyde dissimilation

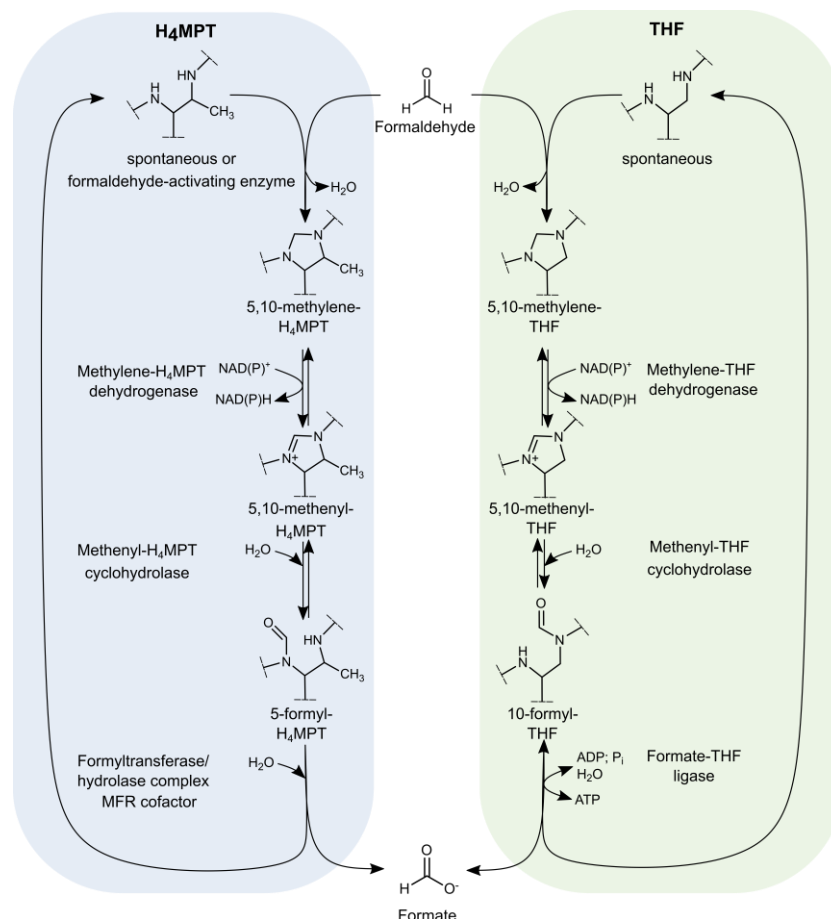
Oxidation of formaldehyde to formate in the presence of a pterin cofactor is another possibility of formaldehyde detoxification, which is based on an initial reaction between formaldehyde and the amino groups of the cofactor.<sup>[216,217]</sup> Two different pterin-dependent detoxification pathways exist in nature, which rely on either tetrahydrofolate (THF) or tetrahydromethanopterin (H<sub>4</sub>MPT) as cofactors.<sup>[154,175,191,192]</sup> THF and H<sub>4</sub>MPT share structural similarities in the pterin moiety, which differs merely in the presence of a methyl group at position seven in H<sub>4</sub>MPT.<sup>[217,218]</sup> However, major differences can be observed in the side chain structure of both cofactors (Fig. 10), which also impact the chemical properties of the substrate.<sup>[217,218]</sup>



**Figure 10: Structure of a) H<sub>4</sub>MPT and b) THF.** Both cofactors contain a pterin, a bicyclic *N*-heterocycle consisting of a pteridine ring substituted at position 2 with an amino group and at position 4 with a keto group.<sup>[218]</sup> In THF, the reduced pterin is linked to glutamate via *p*-aminobenzoate.<sup>[217]</sup> Whereas in H<sub>4</sub>MPT, the pterin is directly linked through a benzene ring to a methylene group of a ribitol moiety, which itself is bound to ribose-5-phosphate and thence to hydroxyglutamate.<sup>[217]</sup> The blue-marked amino groups are involved in formaldehyde detoxification.

The H<sub>4</sub>MPT-dependent route of formaldehyde detoxification (Fig. 11) starts with a spontaneous condensation reaction involving formaldehyde and H<sub>4</sub>MPT, resulting in the generation of 5,10-methylene-H<sub>4</sub>MPT.<sup>[216]</sup> Alternatively, this reaction can also be catalyzed by a formaldehyde-activating enzyme, leading to an increased rate of 5,10-methylene-H<sub>4</sub>MPT formation.<sup>[216,219]</sup> Oxidation to 5,10-methenyl-H<sub>4</sub>MPT takes place next, which is catalyzed by an NAD(P)-dependent methylene-H<sub>4</sub>MPT dehydrogenase.<sup>[220]</sup> The formation of 5-formyl-H<sub>4</sub>MPT is subsequently catalyzed by a methenyl-H<sub>4</sub>MPT cyclohydrolase.<sup>[221]</sup> Generation of formate and regeneration of H<sub>4</sub>MPT is then accomplished by two sequential reactions catalyzed by a formyltransferase/hydrolase complex involving a methanofuran or methylofuran cofactor.<sup>[222-225]</sup> The THF-dependent pathway (Fig. 11) begins also with a spontaneous reaction between formaldehyde and THF, leading to the formation of 5,10-methylene-THF.<sup>[217]</sup> Analogous to the H<sub>4</sub>MPT-dependent route, an oxidation and a hydrolysis occur, which produce 10-formyl-THF as product.<sup>[220,221,226]</sup> The last step is catalyzed by a formate-THF ligase, which

couples the conversion of ADP to ATP with the reversible oxidation of 10-formyl-THF to formate and THF.<sup>[227]</sup> Both pterin-dependent pathways can co-exist in one organism, exemplified by *Methylobacterium extorquens*, where they possess distinct functions regarding formaldehyde detoxification.<sup>[228,229]</sup> Research involving this  $\alpha$ -proteobacterium demonstrated that the formaldehyde oxidation is predominantly accomplished via the H<sub>4</sub>MPT pathway.<sup>[228,229]</sup> Whereas the THF pathway is utilized to initiate the assimilatory serine pathway, which requires 5,10-methylene-THF as precursor.<sup>[229,230]</sup> However, recent studies have indicated that the spontaneous reaction rate between THF and formaldehyde *in vivo* is low and therefore unlikely to provide an effective route for formaldehyde assimilation.<sup>[231]</sup> In *Methylobacterium extorquens*, the formation of 5,10-methenyl-THF can therefore also be generated by coupling the H<sub>4</sub>MPT and THF pathways.<sup>[229]</sup> Formaldehyde is initially oxidized to formate by the H<sub>4</sub>MPT pathway, which is then reduced to 5,10-methenyl-THF by the reverse THF pathway.<sup>[229]</sup> Nevertheless, formaldehyde assimilation solely by the spontaneous reaction may be favorable in specific conditions that prefer high biomass yield rather than rapid growth.<sup>[231]</sup>



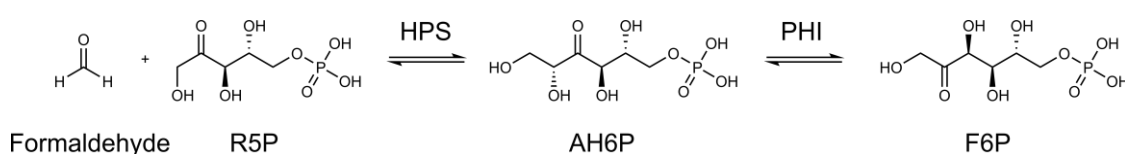
**Figure 11: Pterin-dependent formaldehyde detoxification results in the formation of formate.** Both pathways starts with a spontaneous reaction between the cofactors and formaldehyde.<sup>[216,217]</sup> This reaction can be accelerated for the H<sub>4</sub>MPT pathway by a formaldehyde-activating enzyme.<sup>[216,219]</sup> An oxidation and a hydrolysis reaction occur next in both pathways, which are catalyzed by a dehydrogenase and a cyclohydrolase.<sup>[220,221,226]</sup> The last step differs for both routes. In the H<sub>4</sub>MPT pathway the formation of formate and regeneration of the pterin cofactor is achieved by the formyltransferase/hydrolase complex in combination with a methanofuran or methylofuran cofactor (MFR).<sup>[222–225]</sup> Reversible oxidation of 5,10-methenyl-THF to formate and regeneration of the THF cofactor occurs in the THF pathway by the formate-THF ligase and is coupled to the conversion of ADP to ATP.<sup>[227]</sup>

### 1.6.1.3 Formaldehyde dissimilation through cofactor-independent pathways

Cofactor-independent pathways of formaldehyde detoxification also exist in nature, where formaldehyde is converted enzymically to formate in the absence of any previous reaction between formaldehyde and a cofactor.<sup>[191,192]</sup> For instance, the glutathione-independent formaldehyde dehydrogenases from *Methylococcus capsulatus* and *Pseudomonas aeruginosa* were able to catalyze the NAD<sup>+</sup>-dependent oxidation of formaldehyde to formate.<sup>[232–234]</sup> Furthermore, dye-linked formaldehyde dehydrogenases were also discovered, which are capable of the glutathione-independent oxidation of formaldehyde in the presence of a wide variety of electron acceptors.<sup>[235–237]</sup> Based on their relatively low activity, these dye-linked formaldehyde dehydrogenases are suspected to possess no primary function in formaldehyde detoxification, instead they might fulfil an auxiliary role and protect the organism in stress situations involving formaldehyde excess.<sup>[237,238]</sup> In addition to formaldehyde dehydrogenases, formaldehyde dismutases were also identified, which catalyze the disproportionation of hydrated formaldehyde into equimolar amounts of methanol and formate.<sup>[239–242]</sup>

### 1.6.1.4 Formaldehyde assimilation via the ribulose monophosphate pathway

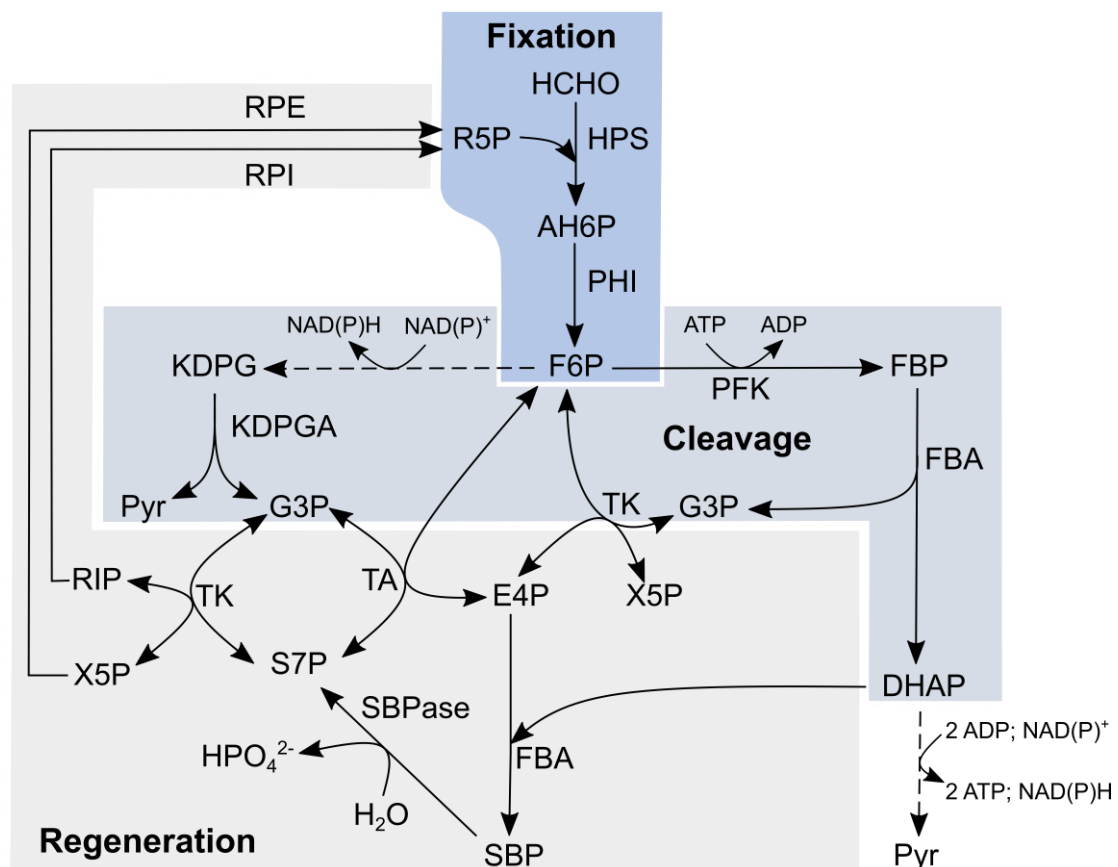
The ribulose monophosphate (RuMP) pathway is the most efficient route of formaldehyde assimilation in terms of ATP consumption and biomass yield.<sup>[243–245]</sup> The pathway can be divided into the parts: fixation, cleavage and regeneration.<sup>[246]</sup> Formaldehyde fixation is catalyzed by the two key enzymes 3-hexulose-6-phosphate synthase (HPS) and 6-phospho-3-hexuloisomerase (PHI).<sup>[174]</sup> The first step of fixation (Fig. 12) involves the HPS-catalyzed aldol reaction between formaldehyde and D-ribulose-5-phosphate (R5P) resulting in the intermediate D-arabino-3-hexulose-6-phosphate (AH6P), which is subsequently isomerized by PHI to D-fructose-6-phosphate (F6P).<sup>[174]</sup>



**Figure 12: The key reaction of the RuMP pathway is catalyzed by HPS and PHI.** HPS catalyzes the aldol reaction between formaldehyde and D-ribulose-5-phosphate (R5P), resulting in the formation of D-arabino-3-hexulose-6-phosphate (AH6P) as intermediate, which is then isomerized to D-fructose-6-phosphate by PHI.<sup>[174]</sup>

While the fixation reaction is performed identical in all organism, variations can occur in cleavage and regeneration parts (Fig. 13).<sup>[246–248]</sup> F6P is consumed in the cleavage part to generate pyruvate and triose phosphates such as dihydroxyacetone phosphate or glyceraldehyde-3-phosphate which then can be metabolized in the glycolysis or the Entner-Doudoroff pathway.<sup>[243,246–249]</sup> Regeneration of R5P is the last part of the RuMP pathway and is catalyzed by various enzymes of the pentose phosphate pathway.<sup>[243,246–249]</sup> Certain archaea

which lack a complete pentose phosphate pathway can also catalyze the reverse reaction, producing R5P and formaldehyde from F6P via HPS and PHI.<sup>[250]</sup> Some organisms, such as *Bacillus methanolicus* MGA3, also possess a dissimilatory variant of the RuMP pathway. In this alternative route, the generated F6P is isomerized to glucose-6-phosphate and subsequently oxidized to 6-phospho-glucono-1,5 lactone by a glucose-6-phosphate dehydrogenase.<sup>[215,251]</sup> Once hydrolyzed by a 6-phospho-gluconolactonase, the formed 6-phosphogluconate is decarboxylated by a 6-phospho-gluconate dehydrogenase to regenerate R5P.<sup>[215,251]</sup>



**Figure 13: Assimilation of formaldehyde via the RuMP pathway.** Formaldehyde fixation initiates via an aldol reaction between D-ribulose-5-phosphate (R5P) and formaldehyde, which is catalyzed by a 3-hexulose-6-phosphate synthetase (HPS).<sup>[174]</sup> The formed D-arabino-3-hexulose-6-phosphate (AH6P) intermediate is subsequently isomerized by the 6-phospho-3-hexulose-6-phosphate isomerase (PHI) to D-fructose-6-phosphate (F6P).<sup>[174]</sup> Cleavage of F6P into triose phosphates and/or pyruvate can proceed via two alternative pathways in which a fructose-1,6-bisphosphate aldolase (FBA) or a 2-keto-3-deoxy-6-phosphogluconate aldolase (KPDGA) catalyze the essential cleavage reactions. In the FBA pathway, F6P is initially phosphorylated to fructose-1,6-bisphosphate (FBP) by a phosphofructokinase (PFK) using ATP, which is then cleaved by FBA to generate dihydroxyacetone phosphate (DHAP) and glyceraldehyde-3-phosphate (G3P). In the KPDGA pathway, F6P is first converted by multiple enzymes to 2-keto-3-deoxy-6-phosphogluconate (KDPG), which is subsequently cleaved by KPDGA to G3P and pyruvate (Pyr). Regeneration of R5P can occur via two routes involving either a transaldolase (TA) or a sedoheptulose-1,7-bisphosphatase (SBPase). The TA catalyzes the transfer of a dihydroxyacetone group from F6P to erythrose-4-phosphates (E4P), which results in the formation of sedoheptulose-7-phosphates (S7P) and G3P. S7P can also be generated by the aldol reaction between DHAP and E4P, which is catalyzed by FBA, followed by a dephosphorylation by a SBPase. S7P and G3P are then converted by a transketolase (TK) to xylulose-5-phosphate (X5P) and ribose-5-phosphate (RIP). The final step involves the conversion of X5P to R5P via a ribulose-5-phosphate-3-epimerase (RPE) or the isomerization of RIP to R5P by a ribose-5-phosphate isomerase (RPI). Generated DHAP can also be utilized for the production of ATP and reduction equivalents by the channeling into glycolysis. Reactions involving the participation of several enzymes are indicated by dotted arrows. The figure is derived and adapted from the Zhang *et al.*<sup>[247]</sup> review article and is based on the references <sup>[174,243,246–248]</sup>.

#### 1.6.1.4.1 Formaldehyde induces gene expression of HPS and PHI

The gene organization and regulatory mechanism of HPS and PHI are highly diverse in methylotrophic bacteria and archaea.<sup>[252]</sup> One of the best studied mechanism for gene regulation of HPS and PHI in non-methylotrophic microbes is the formaldehyde-responsive transcription activator HxIR.<sup>[252–255]</sup> Expression of the *hxlA* and *hxlB* genes in *Bacillus subtilis* (*B. subtilis*), which are organized as *hxlAB* operon and encode for PHI and HPS respectively, can be induced by formaldehyde in dependence of HxIR.<sup>[253,254]</sup> Recent studies revealed that HxIR recognizes formaldehyde via an intra-helical crosslink formation, which caused a conformational change in form of *N*-terminal helix flipping and thus increased affinity for DNA binding.<sup>[255]</sup>

#### 1.6.1.4.2 HPS and PHI are the unique key enzymes of the RuMP pathway

HPS belongs to the enzyme class of aldolases, which catalyze the C-C bond formation between an enolizable carbonyl component, the donor substrate and an electrophilic acceptor.<sup>[256]</sup> Enolization of the donor generates a nucleophilic carbon atom which is capable of attacking an electrophilic carbonyl function of the acceptor.<sup>[256]</sup> Aldolases can be divided into different classes based on their mechanism of donor activation.<sup>[256]</sup> Class 1 aldolases activate the donor substrate by forming an enamine intermediate involving a lysine residue.<sup>[256]</sup> In contrast, activation of class 2 aldolases involves an enediolate formation, promoted by a bivalent metal cofactor.<sup>[256]</sup> Additionally, pyridoxal-5'-phosphate (PLP)-dependent aldolases activate the donor by the generation of a quinoid aldimine intermediate.<sup>[256]</sup> Biochemical characterizations of various HPS from methylotrophic microbes showed that a bivalent metal ion like magnesium or manganese is required for enzyme activity and stability.<sup>[257,258]</sup> Furthermore, the crystal structure of the HPS from *Mycobacterium gastri* MB19 revealed that the active site contained a magnesium ion.<sup>[259]</sup> Consequently, HPS belong to class 2 aldolases.<sup>[256]</sup> Based on the structure and site-directed mutagenesis, it was demonstrated that a conserved histidine residue is crucial for HPS activity.<sup>[259]</sup> This histidine is probable involved in the proton abstraction from the 1-hydroxymethyl group of R5P and thus provides the initial step of enediolate formation.<sup>[259]</sup> HPS was designated to be a member of the orotidine 5'-monophosphate decarboxylase (OMPDC) suprafamily based on the presence of a D-x-K-x-x-D motif.<sup>[259–261]</sup> Members of this family, such as the 3-keto-L-gulonate 6-phosphate decarboxylase (KGPDC), display the classical ( $\beta/\alpha$ )<sub>8</sub> barrel fold and catalyze a variety of reactions.<sup>[260,261]</sup> For instance, KGDPC catalyzes the Mg<sup>2+</sup>-dependent decarboxylation of 3-keto-L-gulonate 6-phosphate to L-xylulose 5-phosphate in a catabolic pathway of L-ascorbate in *Escherichia coli* K12.<sup>[262]</sup> Investigations concerning promiscuity within the OMPDC suprafamily revealed that the HPS from *Methylomonas aminofaciens* can also efficiently catalyze the KGPDC reaction.<sup>[260]</sup> In addition to formaldehyde, other aliphatic aldehydes such as glycolaldehyde or propionaldehyde can be converted by HPS in the presence of R5P as donor substrate.<sup>[257,263]</sup>

PHI is a member of the enzyme class of intramolecular oxidoreductases, which is a subgroup of isomerases and catalyzes the oxidation and reduction of distinct parts of the same molecule, leading to geometric or structural changes within the molecule.<sup>[264]</sup> The enzymology of PHI is scarcely understood, since the substrate AH6P is unstable and thus the activity of PHI is commonly determined in combination with the HPS-catalyzed reaction.<sup>[174]</sup>

### **1.6.1.5 Alternative pathways for formaldehyde assimilation**

In addition to the RuMP pathway, two alternative pathways have been identified which can be employed for formaldehyde assimilation.<sup>[154,192,247]</sup> In the serine cycle, formaldehyde is involved in the generation of acetyl coenzyme A.<sup>[192,247]</sup> The key enzyme for this pathway is a PLP-dependent serine hydroxymethyltransferase, which catalyzes the reversible transfer of a carbon unit from 5,10-methylene-THF to glycine and thereby the formation of serine and THF.<sup>[265]</sup> Serine is subsequently converted to acetyl coenzyme A and the glycine precursor glyoxylate via several enzymes.<sup>[230,266–268]</sup> In methylotrophic yeasts, formaldehyde assimilation proceeds via the dihydroxyacetone pathway, which is also known as xylulose monophosphate pathway.<sup>[269,270]</sup> In this pathway, a dihydroxyacetone synthase catalyzes the transfer of a glycolaldehyde group from xylulose-5-phosphate to formaldehyde, producing dihydroxyacetone and glyceraldehyde-3-phosphate.<sup>[269,271]</sup> Following the phosphorylation of the dihydroxyacetone by a dihydroxyacetone kinase, the produced dihydroxyacetone phosphate is converted with glyceraldehyde-3-phosphate to form fructose-1,6-bisphosphate and subsequently fructose-6-phosphate.<sup>[270]</sup> Xylulose-5-phosphate is regenerated via similar routes as those observed in the RuMP pathway.<sup>[270]</sup>

## 2. Aim of the thesis

Marine algae contribute significantly towards the carbon cycle by sequestering carbon dioxide in form of polysaccharides.<sup>[4,5]</sup> These complex carbohydrates represent a suitable carbon source for certain marine heterotrophic bacteria.<sup>[17,21]</sup> A bacterial phylum considered to be specialists in marine polysaccharide degradation represent the *Bacteroidetes*, which possess an enormous repertoire of diverse CAZymes and can thus catalyze the depolymerization of carbohydrates to the level of metabolizable monosaccharides.<sup>[18,19,21]</sup> The bacterial utilization of sugars additionally requires enzyme cascades, which are responsible for channeling the monosaccharides into appropriate carbon or energy pathways as well as the removal of potentially toxic metabolites. For instance, the oxidative demethylation of the methoxy sugar G6Me by a CYP and its redox partners is an essential prerequisite in porphyran degradation that enables the effective depolymerization by certain GHs as well as the metabolism of this monosaccharide moiety by the microbe.<sup>[54,109]</sup> However, this reaction generates significant quantities of formaldehyde,<sup>[54]</sup> which is cytotoxic for the organism due to its electrophilic properties.<sup>[175]</sup> Marine bacteria capable of efficient porphyran utilization must therefore possess suitable formaldehyde detoxification pathways. One part of this dissertation aimed therefore at identifying potential formaldehyde detoxification pathways in marine *Bacteroidetes*. In addition, the main objective was to verify whether these formaldehyde detoxification pathways can also play an essential role during porphyran breakdown, since this represents a potential source of formaldehyde via the oxidative demethylation reaction.

The identification of novel enzymes involved in the carbohydrate degradation contributes to a better understanding of the carbon cycle. Consequently, an additional aim of this dissertation was the biochemical characterization of alcohol dehydrogenases whose genes were located in close proximity to the genes that encoded for the key enzymes of the oxidative demethylation in the marine *Flavobacteriia* *Z. galactanivorans* and *F. agariphila*.<sup>[54]</sup> It was thus hypothesized that these alcohol dehydrogenases may possess a role in porphyran degradation.

Furthermore, the discovery of pathways involved in the detoxification of toxic intermediates and the characterization of novel enzymes or enzyme cascades involved in the degradation of polysaccharides are important requirements for a prospective industrial application of marine carbohydrates. The last aim of this thesis was the establishment of the groundwork for a potential biotechnological process based on the green algae polysaccharide ulvan as possible feedstock. For this purpose, a biotechnologically important microorganism capable of growing on ulvan-derived monosaccharides or oligosaccharides as sole carbon source should be identified. The development of this identified microbe into a self-sufficient strain that can grow on ulvan as sole carbon source should subsequently be achieved by introducing ulvanolytic CAZymes from the ulvan saccharification cascade of *F. agariphila*.<sup>[63]</sup>

### 3. Results & Discussion

#### 3.1 Connecting porphyran degradation to formaldehyde detoxification

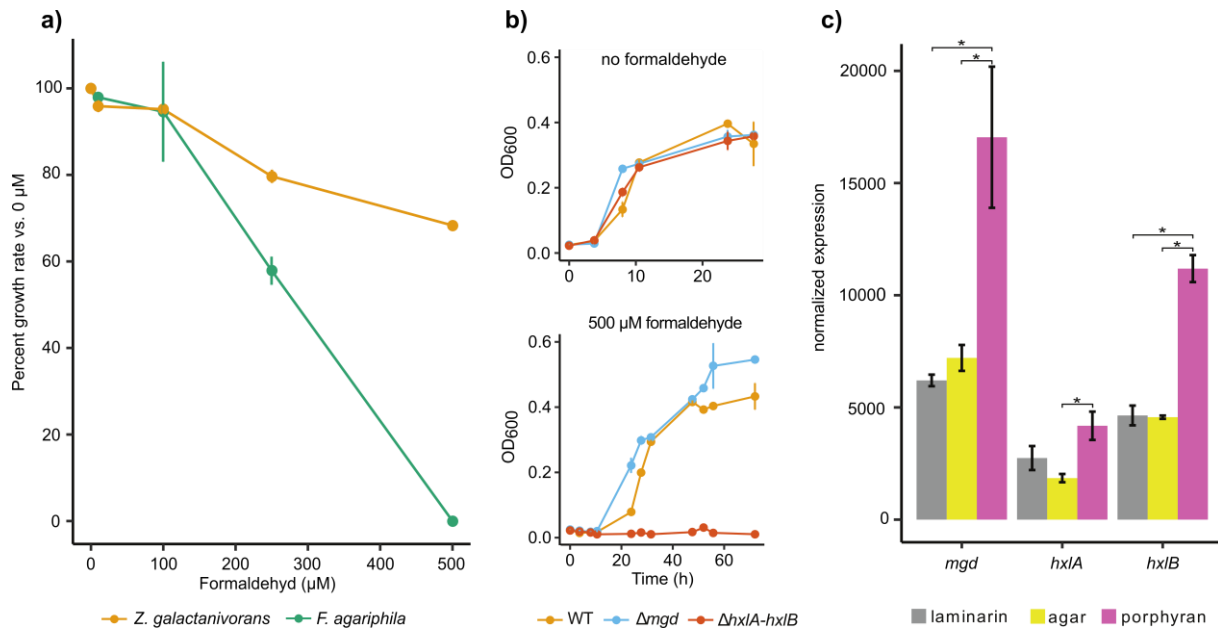
Oxidative demethylation of the methoxy sugar G6Me during porphyran degradation enables metabolization of the monosaccharide and may additionally facilitate CAZyme-catalyzed depolymerization of larger oligosaccharides, thus providing a crucial role in the microbial utilization of this marine carbohydrate.<sup>[54,109]</sup> However, the generation of formaldehyde by the oxidative demethylation reaction<sup>[54]</sup> creates a potential risk for the organism, as formaldehyde is a cytotoxic metabolite due to its highly reactive electrophilic nature.<sup>[175]</sup> Marine bacteria capable of porphyran degradation and G6Me utilization should therefore possess suitable detoxification pathways for formaldehyde. In this study, we therefore focused on elucidating a potential formaldehyde detoxification pathway which participates in the subsequent detoxification of formaldehyde following the oxidative demethylation of G6Me. The main focus of the study relies on the marine *Flavobacteriia* *F. agariphila* KMM3901<sup>T</sup> and *Z. galactanivorans* Dsij<sup>T</sup>, since both microbes are capable of performing the oxidative demethylation reaction.<sup>[54]</sup>

In order to gain a better understanding over the formaldehyde resistance of both *Flavobacteriia*, their growth was evaluated in the presence of various formaldehyde concentrations. While both organisms displayed an almost unchanged growth behavior at concentrations  $\leq 100$   $\mu\text{M}$  formaldehyde, reduced or no growth was noticeable at higher formaldehyde concentrations (Fig. 14a). Additionally, a significant difference in formaldehyde resistance was observed, while *Z. galactanivorans* could still grow in the presence of 500  $\mu\text{M}$  formaldehyde, no growth was observable for *F. agariphila* at this concentration. With the aim of providing a potential explanation for the increased formaldehyde resistance of *Z. galactanivorans*, the genomes of both organisms were analyzed for genes encoding for enzymes from well-known formaldehyde degradation pathways. This revealed that both microbes harbor annotated genes for enzymes involved in the serine and pterin-dependent pathways. However, since the assimilatory serine pathway and the dissimilatory THF-dependent pathway are based on the spontaneous reaction between THF and formaldehyde<sup>[217]</sup> which is assumed to proceed slowly *in vivo*,<sup>[231]</sup> those pathways are most likely improbable to act as major routes in formaldehyde detoxification. Eventually, these pathways may provide a back-up or auxiliary role in emergency situations that may arise from formaldehyde excess. Furthermore, *Z. galactanivorans* possessed the genes encoding for a 3-hexulose-6-phosphate synthase (HPS) and 6-phospho-3-hexuloisomerase (PHI), which represent the key enzymes of the RuMP pathway. Considering that this pathway is recognized as one of the most efficient ways of formaldehyde assimilation in terms of ATP consumption and biomass yield,<sup>[243–245]</sup> it was reasonable to assume that the presence of the genes could lead to an enhanced formaldehyde



resistance in *Z. galactanivorans*. In order to prove that the increased resistance towards formaldehyde is caused by the enzymes HPS and PHI, a *hxIA-hxIB* gene knockout strain of *Z. galactanivorans* was created. The resulting knock-out strain was unable to grow in the presence of 500  $\mu\text{M}$  formaldehyde, whereas the wild-type (WT) and a control knock-out strain lacking the CYP-encoding gene ( $\Delta mgd$ ) were able to grow normally (Fig. 14b). Consequently, knockout of the *hxIA* and *hxIB* genes resulted in a formaldehyde-sensitive strain that displayed normal growth behavior in the absence of formaldehyde. The result was thus comparable to the observations from He *et al.*, which demonstrated that a knockout of the central glutathione-dependent formaldehyde detoxification pathway in *Escherichia coli* (*E. coli*) also resulted in a formaldehyde-sensitive strain that was unable to grow on 500  $\mu\text{M}$  formaldehyde.<sup>[272]</sup> The knockout thus supported the assumption that the RuMP pathway occupies a pivotal role in the formaldehyde resistance and detoxification of *Z. galactanivorans*.

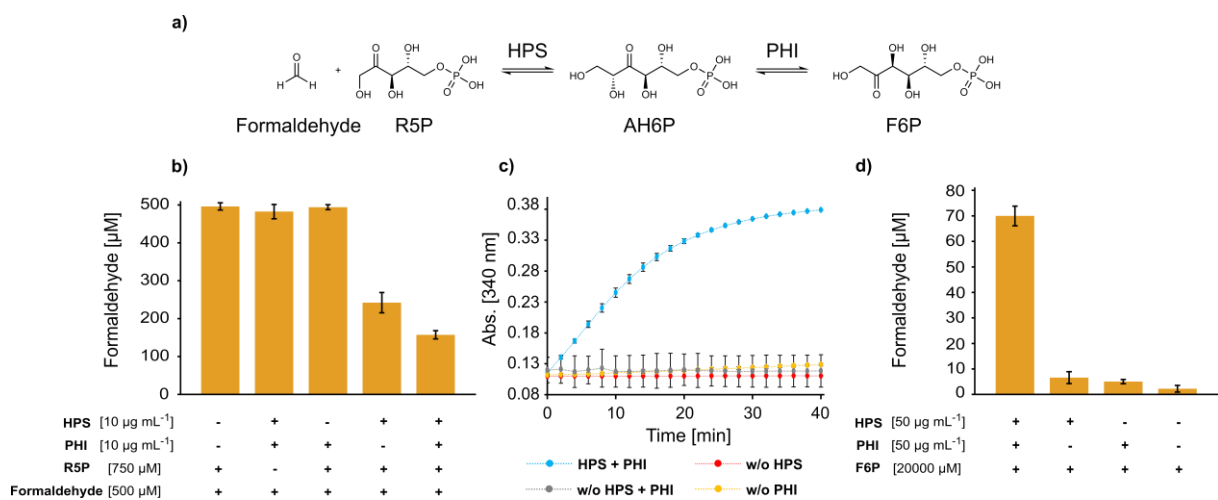
For establishing a connection between porphyrin degradation and formaldehyde detoxification, it was essential to prove that the genes encoding for HPS and PHI were also upregulated in the presence of porphyrin, considering that this carbohydrate is the origin of formed formaldehyde due to the oxidative demethylation of G6Me. For evaluation of gene regulation, *Z. galactanivorans* was grown with the marine polysaccharides laminarin, agar or porphyrin as a sole carbon source. These gene regulation and knock-out studies were performed by the project partners at Roscoff (France). The  $\beta$ -glucan laminarin was chosen as a control considering that it is the most abundant polysaccharide in the marine ecosystem<sup>[273]</sup> and agar was selected as control since the carbohydrate backbone shares some similarities with porphyrin<sup>[107]</sup> and may contain G6Me.<sup>[274]</sup> The genes encoding for the CYP (*mgd*), HPS (*hxIA*), and PHI (*hxIB*) were upregulated in the presence of porphyrin compared to laminarin and agar (Fig. 14c). The upregulation of *mgd* in the presence of porphyrin suggests that there is a potential formaldehyde source, while at the same time, the upregulation of *hxIA* and *hxIB* indicates that detoxification of formaldehyde via the RuMP pathway can occur. In analogy to the mechanism of the formaldehyde-responsive transcription activator HxlR from *B. subtilis*, the upregulation of the *hxIA* and *hxIB* genes in *Z. galactanivorans* is most likely regulated by the presence of formaldehyde and a transcriptional regulator.<sup>[253–255]</sup> In fact, the *hxIA* and *hxIB* genes of *Z. galactanivorans* are organized in a similar way as those of *B. subtilis*.<sup>[253,254]</sup> However, instead of the *hxlR* gene, *Z. galactanivorans* possesses an AraC-type transcriptional regulator gene, which is located in close proximity to the *hxIA-hxIB* genes. AraC family regulators generally act as gene expression activators after undergoing a conformational change upon ligand binding and can regulate cellular functions such as a stress response or carbon metabolism.<sup>[275–278]</sup> The increased upregulation of the *hxIB* gene compared to the *hxIA* gene suggests that both genes may be regulated differently, therefore it would be interesting in the future to identify how the transcriptional activator regulates both genes.



**Figure 14: The formaldehyde resistance of *Z. galactanivorans* depends crucially on genes that encode for the key enzymes of the RuMP pathway, which are upregulated in the presence of porphyran.** a) Increasing formaldehyde concentrations impair the growth of *F. agariphila* and *Z. galactanivorans*. The growth rate obtained in the absence of formaldehyde was taken as 100% for each bacterial strain. b) Growth curve of wild-type (WT),  $\Delta\text{mgd}$  (CYP) and  $\Delta\text{hxlA-hxlB}$  (HPS and PHI) mutant strains of *Z. galactanivorans* growing in ZoBell 2216 medium containing no or 500  $\mu\text{M}$  formaldehyde. c) Gene expression of *mgd* (CYP), *hxlA* (HPS) and *hxlB* (PHI) of *Z. galactanivorans* when grown with laminarin, agar or porphyran as sole carbon source. The influence of substrate on gene expression was examined by one-way ANOVA on log-transformed data, followed by a post-hoc Tukey test (\*,  $P < 0.05$ ). Expression data from the publicly available GEO dataset GSE99940. For a) – c) values are shown as mean  $\pm$  standard error of the mean ( $n=3$ ). The knock-out and the growth studies were performed by the project partners at Roscoff (France). The figure is derived from Article I.

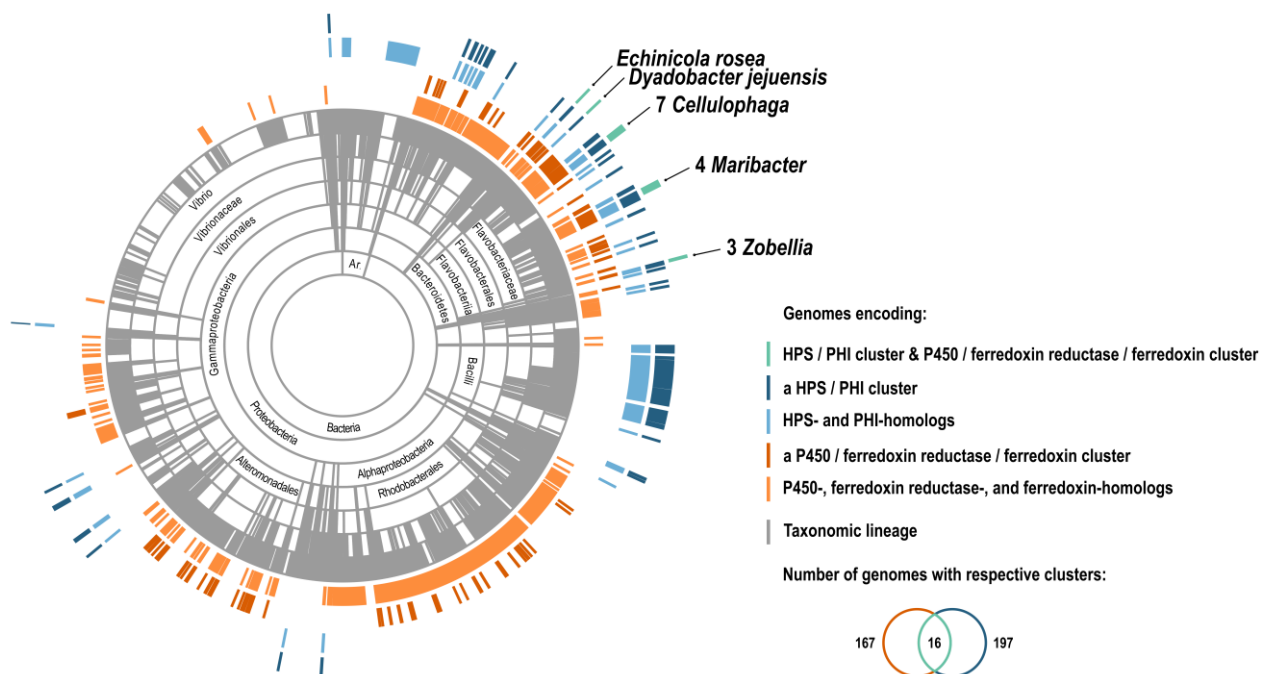
For verification whether the genes encode for enzymes that actually catalyze the key reactions of the RuMP pathway (Fig. 15a), we separately expressed them in *E. coli* and subsequently purified both enzymes. During the purification an irreversible denaturation of HPS was observed if no additional magnesium ions were present in the purification buffer. The HPS from *Z. galactanivorans* thus displayed similar requirements for bivalent metal ions as the 3-hexulose-6-phosphate synthases from the methylotrophic organisms *Methylococcus capsulatus* and *Mycobacterium gastri* MB19.<sup>[257,258]</sup> Activity of both enzymes was then determined using the Nash assay<sup>[279]</sup> for detecting an enzyme-catalyzed reduction in the formaldehyde concentration as well as a coupled enzyme assay for detecting F6P.<sup>[280]</sup> In the presence of R5P, a decrease in the formaldehyde concentration (Fig. 15b) and the formation of F6P was observed for the reaction mixture that contained both enzymes (Fig. 15c). Approximately 340  $\mu\text{M}$  of the initial formaldehyde concentration of 500  $\mu\text{M}$  was removed from the solution after 5 min incubation at 30°C, which corresponds to a conversion of 68.5%. In contrast, in the control reactions lacking R5P as well as in the absence of either HPS or both enzymes, no formaldehyde was incorporated and thus no F6P was formed (Fig. 15b and c). For the reaction mixture that contained HPS but not PHI, a reduction in formaldehyde was also observed, which is plausible regarding the fact that HPS catalyzes the reaction of R5P to AH6P independently of PHI (Fig. 15b). The difference in formaldehyde removal between the reaction

mix containing both enzymes compared with the mix excluding PHI was slightly, this finding is presumably based on the fact that the rate of the sequential reactions is limited by the HPS-catalyzed reaction.<sup>[174]</sup> The formation of an intermediate rather than F6P by HPS is confirmed indirectly by the enzyme coupled assay, since no absorbance increase was observed in the absence of PHI in the reaction mix (Fig. 15c). In order to test if both enzymes from *Z. galactanivorans* can also catalyze the reverse reaction, biocatalysis with F6P as substrate were performed. The formation of 70  $\mu\text{M}$  formaldehyde was detected in the presence of both enzymes and 20 mM F6P as substrate after 10 min incubation (Fig. 15d). The high substrate concentration was essential to shift the equilibrium towards formaldehyde formation, making this unfavorable reaction possible *in vitro* but most unlikely to occur *in vivo*. These observations are reasonable considering that the key reactions of the RuMP pathway are employed for the formaldehyde detoxification in the bacterial domain of life.<sup>[154,191,192]</sup> The results are therefore consistent and comparable with the findings of Ferenci *et al.*, which demonstrated that the equilibrium of the key reactions is in favor of F6P formation in *Methylococcus capsulatus*.<sup>[258]</sup> In summary, the biochemical results proved that *Z. galactanivorans* possesses the enzymatic repertoire for catalyzing the key reactions of the RuMP pathway.



**Figure 15: HPS and PHI from *Z. galactanivorans* catalyze the key reaction of the RuMP pathway.** a) The key reaction of the RuMP pathway consists of the HPS-catalyzed aldol reaction involving R5P and formaldehyde as well as the PHI-catalyzed isomerization of the formed AH6P intermediate to F6P. b) Biocatalysis verifying the enzyme-catalyzed detoxification of formaldehyde. Conditions: a protein concentration of  $10 \mu\text{g mL}^{-1}$  for HPS and PHI were employed. For substrates,  $500 \mu\text{M}$  formaldehyde and  $750 \mu\text{M}$  D-ribose-5-phosphate disodium salt were used. Reactions were performed in a  $50 \text{ mM}$  sodium phosphate buffer pH 7.5 supplemented with  $5 \text{ mM}$   $\text{MgCl}_2$  for 5 min, at an incubation temperature of  $30^\circ\text{C}$ . The formaldehyde concentration was then determined using the Nash assay<sup>[279]</sup>. c) Detection of F6P via coupled enzyme assay: generated F6P is initially converted by a phosphoglucose isomerase to D-glucose-6-phosphate, which is then oxidized by glucose-6-phosphate dehydrogenase under  $\text{NADP}^+$  consumption to D-glucono-1,5-lactone-6-phosphate.<sup>[280]</sup> Formation of NADPH was detected by an absorbance measurement. Same conditions as described for b) were used, with the exception that a  $50 \text{ mM}$  Tris-HCl buffer pH 7.5 containing  $5 \text{ mM}$   $\text{MgCl}_2$  was employed to prevent inhibition of the assay enzymes. Additionally,  $5 \text{ U mL}^{-1}$  for both commercially available assay enzymes and  $0.5 \text{ mM}$   $\text{NADP}^+$  were employed. d) HPS and PHI can also catalyze the reverse reaction and thus the formation of formaldehyde. Conditions: a protein concentration of  $50 \mu\text{g mL}^{-1}$  was used for HPS and PHI and  $20 \text{ mM}$  was employed for F6P. The reaction was performed in a  $50 \text{ mM}$  sodium phosphate buffer containing  $5 \text{ mM}$   $\text{MgCl}_2$  at  $30^\circ\text{C}$  for 10 min. The formaldehyde concentration was then determined using the Nash reagent. For b) - d) mean values are shown, error bars present  $\pm$  standard deviation ( $n=3$ ). The figure is derived and adapted from Article I.

With the aim of obtaining a deeper understanding of the distribution of the RuMP pathway in the marine ecosystem, we queried approximately 5500 marine bacterial genomes in the MarDB and MarRef databases for the key enzymes HPS and PHI. Overall, 197 genomes contained an HPS and PHI gene pair, which corresponds to ~3.58% of all genomes analyzed (Fig. 16). Since we were also interested in the connection between oxidative demethylation of G6Me and the formaldehyde detoxification via RuMP pathway, we also screened the 197 genomes for the *Z. galactanivorans*-like clusters consisting of CYP, ferredoxin reductase and ferredoxin. Among the 197 genomes, only 16 genomes contained the genetic prerequisite for the oxidative demethylation reaction. Furthermore, these genomes also harbored CAZymes of the GH86 and GH117 families, enabling these microbes also to degrade porphyran and agar.<sup>[114,117]</sup> This finding provided additional support for the hypothesis that the RuMP pathway is involved in the detoxification of formaldehyde, which is generated during the breakdown of marine carbohydrates. However, considering that the combination of genes encoding for the RuMP pathway and oxidative demethylation was distributed among only 16 genomes, it can be assumed that this combination is rather an exception than the rule for marine prokaryotes. Noteworthy, the best hits belonged to bacterial genera that are commonly isolated on the surface of macroalgae, indicating that formaldehyde detoxification based on the RuMP pathway is predominantly specific for marine bacteria growing on multicellular algae, reminiscent of the methylotrophic bacteria of the phyllosphere.<sup>[163]</sup>



**Figure 16: Taxonomic distribution of the RuMP pathway in marine prokaryotes.** The best hits were found for some *Maribacter*, *Cellulophaga*, *Zobellia* and *Arenibacter* strains. The colored outer rings indicate the occurrence of the HPS/PHI pairs (dark blue) and the gentriplet containing CYP, ferredoxin reductase and ferredoxin (dark orange). Genomes that encode homologous sequences are represented separately (lighter colors). The intersection of genomes which encode for both clusters is depicted in green. The figure is derived from Article I.

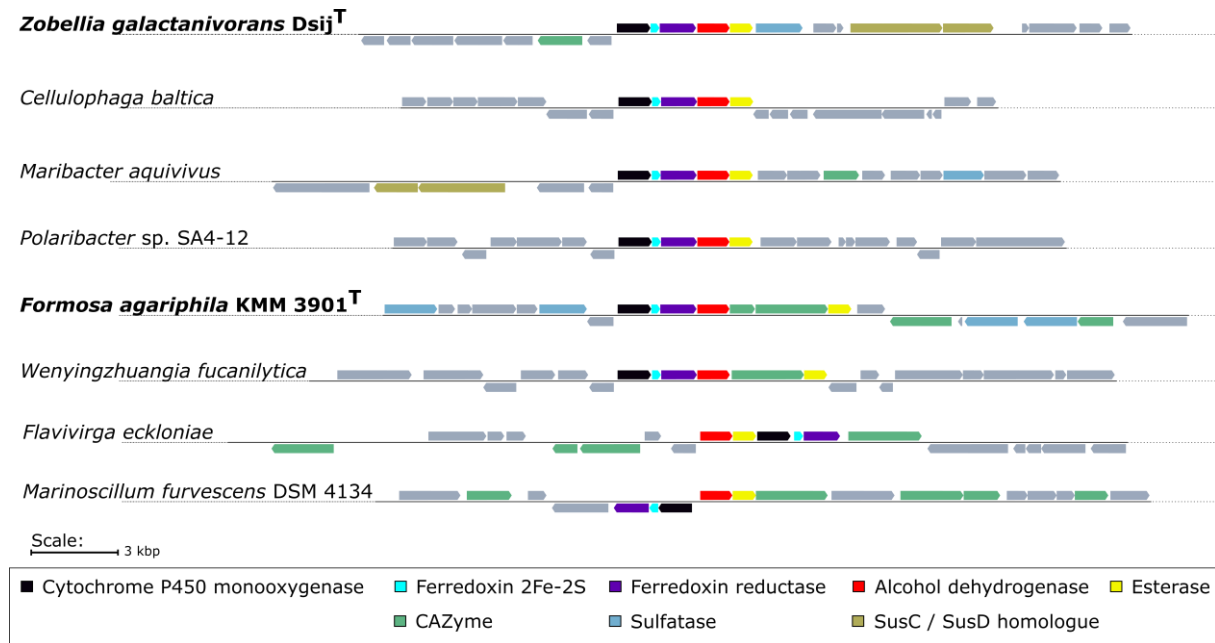
In conclusion, we have demonstrated in this work that *Z. galactanivorans* possesses a higher formaldehyde resistance than *F. agariphila* and that this was attributable to the existence of the RuMP pathway. We also demonstrated that in the presence of porphyran, genes encoding for the CYP and the key enzymes of the RuMP pathway were upregulated, which indicated that there is a possible formaldehyde source via oxidative demethylation of G6Me and at the same time a possibility for its subsequent detoxification via the RuMP pathway. This finding enabled us to provide evidence for a connection between porphyran degradation and formaldehyde detoxification. Furthermore, by verifying the activity of the key enzymes we were able to demonstrate that these enzymes are indeed responsible for formaldehyde resistance and fixation and thus the presence of the RuMP pathway as potential formaldehyde detoxification pathway in *Z. galactanivorans*. This article represents also one of the first studies that contextualizes the RuMP pathway to marine carbohydrate degradation.

### 3.2 Alcohol dehydrogenases involved in G6Me utilization by marine bacteria

Marine bacteria require various enzymes with diverse functions for the saccharification of porphyran and the utilization of the produced monosaccharides.<sup>[54,109]</sup> Discovering novel enzymes involved in these processes contributes to a deeper understanding of the complex carbon cycle and enables an industrial application of marine carbohydrates. While discovering the oxidative demethylation of G6Me, Reisky *et al.* also reported the presence of two genes that encode for a zinc-dependent alcohol dehydrogenase (ADH) and an esterase, which were located in close proximity to the gentriplet consisting of CYP, ferredoxin reductase and ferredoxin.<sup>[54]</sup> Considering that certain dehydrogenases can fulfil an auxiliary role in carbohydrate degradation and appear in the CAZy database in some AA families,<sup>[281–283]</sup> we aimed to elucidate the physiological function of these marine ADHs. For this purpose, we selected the ADHs from *Z. galactanivorans* (ZoADH) and *F. agariphila* (FoADH) as main research objects for this study.

In order to gain a general idea of the biological function of these ADHs as well as their distribution in marine bacteria, the MarDB and MarRef databases were queried for ADHs with similar sequences to ZoADH and FoADH and a sequence similarity network. The sequences of FoADH and ZoADH were present in a cluster that predominantly contained sequences annotated as zinc-dependent ADHs, histidine kinases, ADH GroES-like domains and few glutathione-dependent formaldehyde dehydrogenases/ADHs, which provided a first indication for a potential participation in formaldehyde detoxification. The subsequent genome neighborhood analysis revealed that several marine bacteria capable of porphyran degradation harbor the ADH gene, which occur in similar genomic arrangements consisting of genes encoding for an esterase, the ADH, the CYP and its redox partners (Fig. 17). In most organisms these genes are arranged as a cluster. In some cases, such as in *F. agariphila*, two

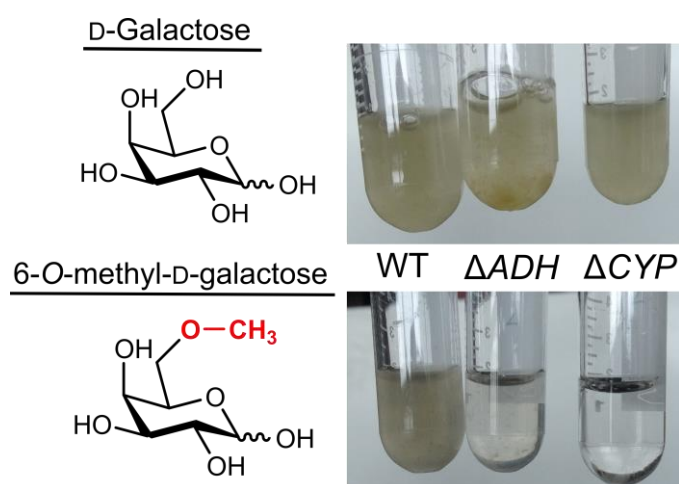
genes encoding for CAZymes of the GH2 and GH16 family are located between the ADH and esterase gene, which presumably contain a function in porphyrin depolymerization. Considering that the ADH gene appears to be conserved in porphyrin-degrading marine *Flavobacteriia* and consistently occurs adjacent to genes encoding for the key enzymes for the oxidative demethylation of G6Me and CAZymes, we hypothesized that the ADH catalyzes a specific function in polysaccharide utilization or a subsequent reaction.



**Figure 17: Genome neighborhood analysis revealed that the ADH gene is consistently located in direct proximity to genes encoding for the oxidative demethylation enzymes and CAZymes.** The ADH gene clusters with genes encoding for the CYP, ferredoxin reductase, ferredoxin and an esterase. In some organisms, such as *F. agariphila* or *W. fucanilytica*, variations of this cluster appear which additionally contain CAZymes. Furthermore, some genome arrangements, for instance those of *Flavivirga ecklonica* or *Marinoscillum furvescens* DSM 4134, contain the ADH gene cluster, in which the genes are arranged in reverse order or in the opposite direction. Other genes which not participate in carbohydrate breakdown or uptake/binding have been greyed out. The illustrated genomic arrangements represent only a minor selection and originate from Article II.

For the identification of the biological function as well as for verification of the ecological relevance of this ADH for the organisms, a knockout of the ADH gene in *Z. galactanivorans* was performed and the effect on growth was subsequently evaluated for different carbon sources. For the growth studies, the wild-type (WT) of *Z. galactanivorans* and the CYP gene knockout strain from Article I were utilized as controls. An impaired growth was observable for the ADH and CYP knockout strains when G6Me was employed as the sole carbon source, whereas the WT strain displayed normal growth (Fig. 18). In addition, all three strains exhibited regular growth when D-galactose was used as the carbon source. Based on the knockout and the results from the growth studies, we were able to confirm the hypothesis of Reisky *et al.* that the CYP-catalyzed reaction is essential for the metabolization of G6Me<sup>[54]</sup> and deduced that the ADH possesses a vital function involving either the oxidative demethylation or a subsequent reaction. The oxidative demethylation reaction yields equimolar amounts of D-galactose and formaldehyde as products,<sup>[54]</sup> which suggest that the ADH might fulfil a

function in the metabolism of one of these compounds. Since normal growth for the  $\Delta ADH$  strain was observed in the presence of D-galactose, a function in the galactose metabolism could be excluded. We therefore hypothesized that the diminished growth of the  $\Delta ADH$  strain might result from an insufficient removal of cytotoxic formaldehyde, which would indicate that the ADH has a major role in formaldehyde detoxification. This hypothesis was further supported by combining the results from the sequence similarity network and genome neighborhood analysis, which indicated a potential thiol-dependent formaldehyde detoxification pathway based on an ADH and an esterase. The presence of this dissimilatory detoxification mechanism would also clarify how *F. agariphila*, which otherwise possesses only THF-based detoxification pathways,<sup>[284]</sup> removes huge amounts of formed formaldehyde. However, this hypothesis would imply that the RuMP pathway in *Z. galactanivorans* is insufficient to catalyze a complete removal of formaldehyde and that a second pathway is required for formaldehyde detoxification. Perhaps, the poor growth of the  $\Delta ADH$  strain could be based on the presence of the RuMP pathway in *Z. galactanivorans*, which still allows slow grow in the presence of elevated formaldehyde concentrations.<sup>[284]</sup>



**Figure 18: ADH gene knockout in *Z. galactanivorans* adversely affects growth on G6Me.** Various *Z. galactanivorans* strains (wild-type (WT), gene knockout of CYP ( $\Delta CYP$ ) and gene knockout of ADH ( $\Delta ADH$ )) were incubated in minimal medium enriched with D-galactose or G6Me for 3 days at RT. The knock-out and the growth studies were performed by the project partners at Roscoff (France). The figure is derived from Article II.

Following expression in *E. coli* and purification of the enzymes, we initially examined the activities of the ADHs towards various alcohols and aldehydes to gain a preliminary understanding of their substrate range. Both enzymes exhibited a similar substrate specificity and preferentially converted aromatic aldehydes in the presence of NADH as cofactor. The highest specific activity of 64.1 U mg<sup>-1</sup> for FoADH and 54.9 U mg<sup>-1</sup> for ZoADH was found for the reduction of pyridine-3-carbaldehyde. Substrates containing a furan or thiophene ring, such as furfural and thiophene-3-carbaldehyde, were also preferentially converted in addition to compounds carrying a benzene ring. For the alcohol oxidation in the presence of NAD<sup>+</sup>, activities that are two orders of magnitude lower compared to the aldehyde reduction were

observed for both enzymes. These findings indicate that these ADHs can generally fulfill an aldehyde detoxifying role in the marine microbes. Both enzymes displayed a substrate specificity that resembled to some extent those of GSH-dependent formaldehyde dehydrogenases from prokaryotic and eukaryotic organisms.<sup>[131,202,203,285,286]</sup> For instance, FoADH and ZoADH also lacked also the activity for the oxidation of short-chain aliphatic alcohols such as methanol or ethanol.<sup>[202,203]</sup> A crucial difference is the conversion of aromatic alcohols/aldehydes, which represent unusual substrates for prokaryotic GSH-dependent formaldehyde dehydrogenases that generally convert long-chained aliphatic alcohols and hydroxylated fatty acids.<sup>[131,203]</sup> Since activity was observed especially for compounds containing a ring structure, various sugars were also considered as potential substrates for both ADHs. However, no activity was found for the oxidation and reduction of G6Me,  $\beta$ -galactose and other monosaccharides. In order to provide an explanation for the observed substrate specificity, crystallization of both ADHs and X-ray crystallographic studies were performed in collaboration with Prof. Dr. Ki Hyun Nam. The crystal structures of FoADH and ZoADH in complex with the essential NAD<sup>+</sup> cofactor have been determined with a resolution of 2.5 and 2.1 Å, respectively. The monomeric structure of both ADHs consists of a catalytic and a cofactor-binding domain, which are separated by a cleft containing a deep pocket that accommodates NAD<sup>+</sup> and the substrate. Characteristics of zinc-dependent ADHs including the typical Rossmann fold<sup>[133]</sup> as well as the occurrence of two zinc-binding sites, which harbor either a catalytic or a structural zinc ion,<sup>[134]</sup> were observed in both structures. The substrate specificity of both ADHs can be explained to some extent by the narrow active site which is required to accommodate the substrate, the catalytic zinc-binding site and the nicotinamide of NAD<sup>+</sup>, as well as possible interactions between the aromatic ring of the substrate and the hydrophobic surface of the enzymes. In addition, a complete biochemical characterization of both ADHs enabled the determination of the temperature and pH optima, the thermostability as well as the influence of sodium chloride, metal ions and solvents on the enzyme activities.

After demonstrating the activity of the ADHs towards various components, we wanted to verify whether the ADHs can catalyze the detoxification of formaldehyde in the presence of a thiol cofactor. Following the spontaneous reaction between the thiol cofactor and formaldehyde, the ADH should oxidize the formed S-hydroxymethyl adduct under NAD<sup>+</sup> reduction yielding a thioester. Unexpectedly, no NADH formation could be detected spectrophotometrically in the presence of GSH, MSH and BSH as thiol cofactor and formaldehyde. In order to rule out a possible inhibition by formaldehyde, the influence of formaldehyde on the enzyme activity was also checked. Both enzymes displayed no activity loss after one-hour incubation with 1 mM formaldehyde, an inhibition was therefore excluded. Since no ADH-catalyzed oxidation reaction was observed in the presence of thiol cofactors from well-known formaldehyde detoxification pathways,<sup>[202,211,215]</sup> we additionally tested other thiols as possible cofactors,



which either occur frequently in nature such as ergothioneine and cysteine<sup>[287]</sup> or contain an aromatic structure based on the substrate specificities of the ADHs. However, no activity could be observed for these cofactors either. Furthermore, no formaldehyde dismutase or formaldehyde dehydrogenase activity could be detected. These results were unexpected for us, since all previous findings indicated a formaldehyde detoxifying function for these ADHs. Nevertheless, a role in formaldehyde detoxification cannot be excluded entirely. Studies with GSH- and MSH-dependent formaldehyde dehydrogenases demonstrated that an exchange of the thiol cofactor with other thiols was impossible and that exactly one specific thiol is required for formaldehyde detoxification activity of the enzyme.<sup>[211,288]</sup> In addition, a recent study by Hiras *et al.* described the discovery of *N*-methyl-bacillithiol in the green sulfur bacterium *Chlorobaculum tepidum* as novel thiol and revealed that BSH derivatives are widely distributed in bacteria, including *Bacteroidetes*.<sup>[289,290]</sup> It is thus possible that these marine *Flavobacteriia* possess an unidentified thiol which, after a spontaneous reaction with formaldehyde, represents a substrate for the ADH. However, based on the observed substrate specificities as well as the crystal structures, it can be assumed that this thiol cannot be a sterically demanding compound like MSH or BSH.

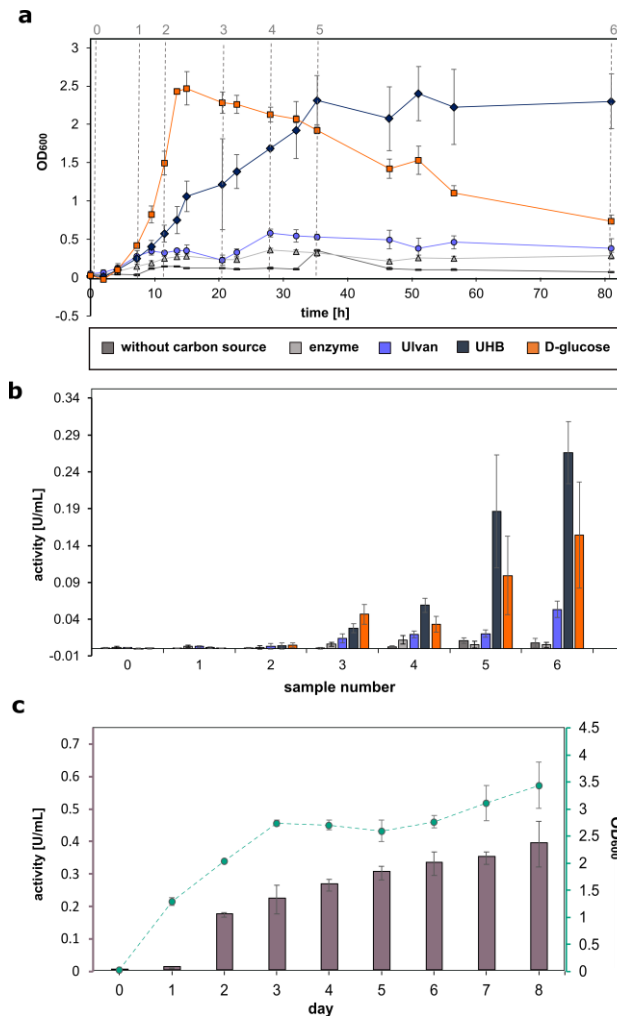
In summary, we were able to provide a complete biochemical characterization as well as the crystallization and elucidation of the crystal structures of two ADHs from the marine *Flavobacteriia* *F. agariphila* and *Z. galactanivorans*. Furthermore, we could demonstrate via sequence similarity network and genome neighborhood analysis that these ADHs seem to be conserved in marine porphyran-degrading *Flavobacteriia* and that the ADH gene exist in a gene cluster encoding the enzymes for the oxidative demethylation of G6Me and an esterase. We were able to prove the ecological relevance of the ADH for the utilization of G6Me by a gene knockout in *Z. galactanivorans* and subsequent growth studies. Although we could not fully elucidate the biological function of the ADHs, we demonstrated that the ADHs can preferentially detoxify aromatic aldehydes and that they were not involved in the metabolism of  $\beta$ -galactose or in literature-known formaldehyde detoxification pathways. However, a function in formaldehyde detoxification in combination with an unidentified thiol cofactor cannot be excluded. The results also strongly indicate that a combination of the CYP- and ADH-catalyzed reactions is essential for an efficient microbial utilization of G6Me. Therefore, it is necessary to consider these observations for a possible biotechnological application of porphyran with microbial organisms. Our research demonstrated the involvement and importance of ADHs in the utilization of the marine polysaccharide porphyran and provides a basis for further research.

### 3.3 Application of ulvan as feedstock for a biotechnologically relevant strain

The application of marine algae as a renewable biorefinery feedstock offers numerous advantages, including faster growth rates than terrestrial plants and the avoidance of arable land and fresh water.<sup>[75]</sup> Meanwhile, massive algal blooms such as the green tides cause a large accumulation of algal biomass,<sup>[71,72]</sup> which in most cases is considered as waste. Developing novel biotechnological processes to convert this cheap and abundant biomass into valuable products is therefore of general interest. The successful elucidation of a complete saccharification process of the marine polysaccharide ulvan,<sup>[63]</sup> which accounts for up to 30% of the algal dry mass of the green tide-dominating *Ulva* spp.<sup>[87]</sup> allows the potential utilization of this carbohydrate as a feedstock for biotechnological processes. In this study, we thus aimed to develop the basis for a novel bioprocess based on the application of ulvan-derived hydrolysates as an alternative carbon source for biotechnologically relevant microbial strains.

In order to identify an important industrial strain capable of growing on ulvan hydrolysate or ulvan-derived monosaccharides, we initially screened 10 different microorganisms including *E. coli*, *Saccharomyces cerevisiae* and *Bacillus* spp. for their ability to grow on these carbon sources. For the generation of suitable monosaccharide mixtures, we employed the CAZymes of the ulvan degradation cascade from *F. agariphila* KMM 3901<sup>T</sup> based on the Reisky *et al.* study.<sup>[63]</sup> The best performing strain in these growth studies was *Bacillus licheniformis* (*B. licheniformis*) DSM13, which was able to grow on the individual monomers as well as the ulvan-derived hydrolysate containing L-Rhamnose, Xyl, GlcA and 5-dehydro-4-deoxy-D-gluconate. However, the organism was unable to grow on ulvan as sole carbon source. The discovery of *B. licheniformis* DSM13 as suitable strain for a potential bioprocess with ulvan-derived monosaccharides was thus the prerequisite for further investigations.

Our next step was to verify whether it is feasible to utilize the ulvan hydrolysate as feedstock for a production process with *B. licheniformis* DSM13. For this purpose, we exemplarily quantified the activity of proteases during cultivations with ulvan-derived monosaccharides or D-glucose as sole carbon sources. We could demonstrate that the growth of *B. licheniformis* DSM13 with ulvan-derived monosaccharides proceeds slower compared to the cultivation with D-glucose (Fig. 19a), nevertheless comparable maximum optical densities could be achieved with both carbon sources. However, a prolonged stationary phase was observable with ulvan-derived monosaccharides compared to D-glucose. An increase in protease activity over time was detected for both cultivations (Fig. 19b), however since the prolonged growth phase yielded in more biomass, protease production was improved in the cultivation with ulvan-derived monosaccharides.



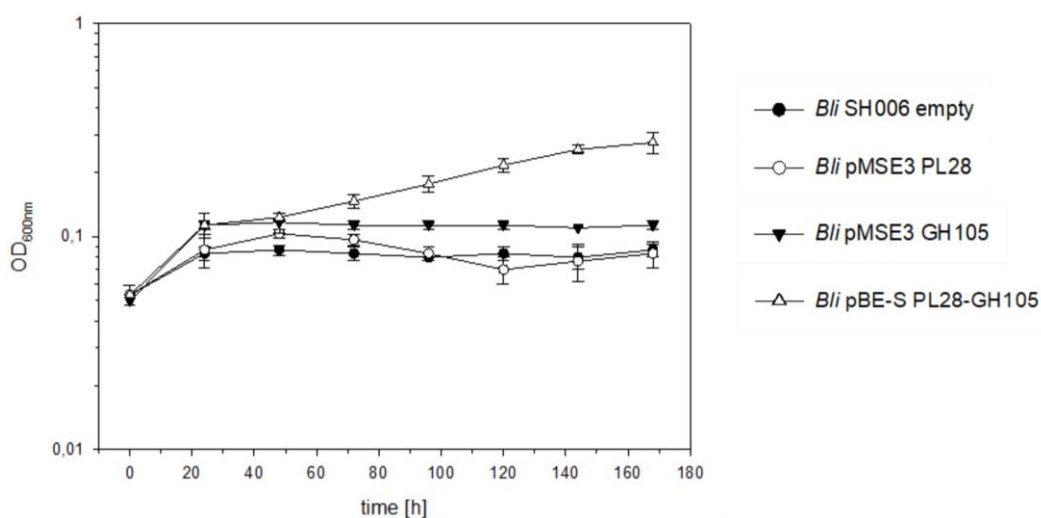
**Figure 19: Production of proteases with *B. licheniformis* DSM13 grown with different carbon sources.** **a)** *B. licheniformis* DSM13 was cultivated in M9 mineral medium supplemented with ulvan, ulvan-derived monosaccharides (UHB) or glucose for 80 h. Cultures cultivated in the absence of the supplied carbon source and with or without the ulvan hydrolyzing enzymes served as controls. Dotted lines indicate time points for **b)** the determination of protease activity. **c)** Growth of *B. licheniformis* DSM13 on ulvan-derived monosaccharides over 8 days with determined protease activity, which was determined via the protease-specific AAPF assay.<sup>[291]</sup> The figure is derived from Article III.

After demonstrating that ulvan-derived monosaccharides can be used for the production of proteases in *B. licheniformis* DSM13, we decided to test if ulvan-derived oligosaccharides can also serve as potential carbon source. By analyzing the growth on 12 different ulvan hydrolysates, which varied in depolymerization level and composition, it was possible to prove that *B. licheniformis* DSM13 can grow on ulvan-derived oligosaccharides. In addition, these growth studies allowed us to determine the degree of ulvan degradation required for growth, which also indicted missing enzymatic activities in *B. licheniformis* DSM13 that would enable growth on higher ulvan polymerization levels or even ulvan. High optical densities of *B. licheniformis* DSM13 after 24 h cultivation was already observed in the presence of ulvan hydrolysate, which was generated with the ulvan lyase P30\_P28 and the unsaturated glucuronyl hydrolase P33\_GH105 from *F. agariphila*.<sup>[63]</sup> In contrast, ulvan hydrolysate prepared via further ulvan depolymerization steps, including desulfation via sulfatases, could not further improve the growth of *B. licheniformis* DSM13. From these observations we were able to draw

two conclusions. Firstly, that the initial ulvan degradation consisting of ulvan lyase and unsaturated glucuronyl hydrolase is sufficient enough to provide a suitable level of ulvan depolymerization for the growth of *B. licheniformis* DSM13 and that these enzyme activities are probably missing in the organism. Secondly, that *B. licheniformis* DSM13 must possess putative CAZymes in order to utilize and metabolize ulvan oligosaccharides. A proteogenomic analysis of *B. licheniformis* DSM13 in the presence of different carbon sources including ulvan, ulvan-derived hydrolysates, rhamnose and glucose was additionally conducted to confirm these conclusions. In combination with a computational analysis, we were able to identify numerous putative CAZymes in *B. licheniformis* DSM13 that might be involved in the utilization of ulvan-derived oligosaccharides. For instance, certain GH families such as GH1 or GH3 have been identified by the proteogenomic and computational analysis that can exhibit xylosidase activity<sup>[292]</sup> and may catalyze the cleavage<sup>[292]</sup> of xylose moieties from oligosaccharides. Furthermore, enzymes that might be involved in the possible metabolism of monosaccharides were identified and detected. For example, a 4-deoxy-L-threo-5-hexosulose-uronate ketol-isomerase was one of the most abundant proteins in cells grown with the ulvan hydrolysates produced by ulvan lyase and GH105,<sup>[63,99,100]</sup> suggesting the potential metabolism of cleaved unsaturated uronic acids.<sup>[293]</sup> We also identified three proteins whose genes were annotated as sulfatases. Considering that sulfated rhamnose and xylose occur in ulvan, we aimed to investigate a possible involvement of these sulfatases in the breakdown of ulvan-derived oligosaccharides by *B. licheniformis* DSM13. However, based on an amino acid sequence alignment we were able to demonstrate that the sequences of the sulfatases shared high similarities to previously characterized lipoteichoic acid synthases and that numerous sequence features such as a cleavage motif, the active site threonine residue and a consensus sequence for substrate binding were present.<sup>[294–296]</sup> We therefore assumed that the gene annotation was incorrect and that the genes encode for lipoteichoic acid synthases, which have been annotated several times as sulfatases and also share high structural similarities to human and prokaryotic sulfatases.<sup>[294–296]</sup> Nevertheless, after expression of the genes in *E. coli* and purification of the enzymes, we also checked for potential sulfatase activity on ulvan-derived oligosaccharides, however no activity could be detected. It therefore remains unsolved how *B. licheniformis* DSM13 copes with sulfated sugar molecules.

Our previous observation that *B. licheniformis* DSM13 cannot grow on ulvan was also explained by both analyses; the organism does not possess PLs of the families 24, 25, 28 as well as 40 and consequently should be incapable of performing the initial ulvan depolymerization.<sup>[63,100–103]</sup> In addition, we were able to demonstrate that the microbe contains two genes that encode for GH105, however these proteins have not been detected in the proteome analysis, indicating a different enzyme activity. In summary, we were able to show that *B. licheniformis* DSM13 does not possess enzymes that catalyze the first two reactions in

ulvan degradation, which also confirmed the growth results with ulvan-derived oligosaccharides. Since only two enzymes were missing to enable growth on ulvan as sole carbon source, the last goal was to create a self-sufficient *Bacillus* strain capable of secreting the required enzymes (PL28 and GH105) for initial ulvan depolymerization.<sup>[63]</sup> We first selected *B. subtilis* JK138, which contains a similar CAZyme repertoire as *B. licheniformis*,<sup>[297,298]</sup> and *B. licheniformis* MW3, a derivative of *B. licheniformis* DSM13 strain which is more genetically accessible,<sup>[299]</sup> as possible expression hosts. After switching from the *B. licheniformis* MW3 strain to the protease-deficient *B. licheniformis* SH006 strain to avoid proteolytic degradation of the GH105 enzyme, and an overall optimization of protein secretion, we were able to establish the single functional expression of the PL28 gene as well as GH105 gene in *B. subtilis* and *B. licheniformis*. For the creation of a self-sufficient *B. licheniformis* SH006 strain, the co-expression of both genes was established next. After generating the co-expression vector pBE-S PL28-GH105, demonstrating the successful co-expression and detecting the activities of both enzymes, we finally decided to demonstrate that the *B. licheniformis* strain equipped with this vector is capable to grow on ulvan as a sole carbon source. Compared to the control strains, which were able to express either PL28, the GH105 or neither of the CAZymes, slow growth on ulvan was only observed for the *B. licheniformis* strain co-expressing and secreting both ulvanolytic enzymes (Fig. 20). We were thus successful in establishing a self-sufficient *Bacillus* strain for the utilization of ulvan as a sole carbon source.



**Figure 20: The self-sufficient *B. licheniformis* strain (*Bli* pBE-S PL28-GH105) enables the application of ulvan as sole carbon source.** The *B. licheniformis* SH006 strain (*Bli* SH006 empty), the *B. licheniformis* SH006 strain which can express the PL28 (*Bli* pMSE3 PL28) and the *B. licheniformis* SH006 strain expressing the GH105 (*Bli* pMSE3 GH105) were used as controls. All strains were grown in M9 minimal media supplemented with ulvan at an incubation temperature of 30°C for 7 days. The figure is derived and adapted from Article III.

In conclusion, we identified in this study that the industrially important strain *B. licheniformis* DSM13 was able to grow on different ulvan-derived monosaccharides and oligosaccharides. Furthermore, we could prove that these carbon sources can also be employed for a production process. This might actually have an industrial relevance, since *B. licheniformis* represents a

bacterial cell factory for the production of the serine protease subtilisin, which is widely employed in detergents.<sup>[300,301]</sup> By combining growth studies, proteomic and computational analyses, we were able to show that *B. licheniformis* DSM13 lacks the essential CAZymes involved in catalyzing the initial steps of ulvan degradation. Finally, a self-sufficient *B. licheniformis* strain capable of growing on ulvan as sole carbon source was created by heterologous co-expression of the PL28 and GH105 that originated from the marine flavobacterium *F. agariphila* KMM 3901<sup>T</sup>.<sup>[63,100]</sup> Consequently, this study contributes to a potential application of abundant algal biomass as an alternative feedstock and provides the groundwork for an establishment of a large-scale bioprocess.

## 4. Summary

The degradation of marine carbohydrates by *Bacteroidetes* represents an extremely complex research field, as the depolymerization of polysaccharides, the utilization of monosaccharides and the removal of toxic metabolites require various enzyme machineries that must act synergistically. However, the majority of scientific attention is concentrated on the elucidation of potential CAZymes and enzyme cascades involved in the breakdown of carbohydrates. This dissertation addressed to some extent the rather overlooked topics such as the involvement of enzymes and metabolic pathways in the utilization of monosaccharides and the detoxification of cytotoxic intermediates. For instance, marine *Bacteroidetes* which degrade porphyrin and utilize the methoxy sugar G6Me must be able to detoxify formaldehyde in order to prevent the detrimental effects of formaldehyde. We demonstrate in **Article I** that marine *Flavobacteriia* harbor diverse formaldehyde detoxification pathways and may therefore cope differently with cytotoxic formaldehyde concentrations. Furthermore, it was revealed that certain marine microbes possess the RuMP pathway and that this formaldehyde detoxifying route can be responsible for the removal of formaldehyde, which is produced by the oxidative demethylation of G6Me during the degradation of porphyrin.<sup>[54]</sup> The biochemical characterization of two ADHs from *Z. galactanivorans* and *F. agariphila* is described in **Article II**. These ADHs are apparently conserved in marine porphyrin-degrading *Flavobacteriia* and occupy an essential function in the microbial utilization of the methoxy sugar G6Me and thus also in porphyrin degradation by marine *Bacteroidetes*. Consequently, **Articles I** and **II** provide novel insights in form of newly-characterized enzymes and metabolic pathways involved in the utilization of porphyrin by marine *Bacteroidetes* and thereby deepen the knowledge of the carbon cycle.

In addition to the elucidation of relevant CAZymes and whole saccharification cascades involved in the marine carbohydrate degradation, a possible application of this acquired knowledge for future industrial processes represent a major aim for the valorization of abundant and sustainable algal biomass. Consequently, one part of this dissertation dealt with the possible utilization of the algal polysaccharide ulvan, which can be derived from green tide-forming macroalgae.<sup>[71,87]</sup> The identification of *B. licheniformis* as a biotechnologically important strain capable of utilizing ulvan-derived hydrolysates as a sole carbon source is described in **Article III**. Since it would be beneficial for a prospective industrial process to utilize the polysaccharide instead of hydrolysate, a self-sufficient strain that can grow on ulvan as a sole carbon source was generated by incorporating two ulvanolytic CAZymes from *F. agariphila*<sup>[63,100]</sup> in *B. licheniformis*. **Article III** thus proposes the basis for enabling ulvan as a potential feedstock for an industrial process.

## 5. References

- [1] S. Das, P. S. Lyla, S. A. Khan, *Curr. Sci.* **2006**, *90*, 1325–1335.
- [2] M. J. Garson, *Nat. Prod. Rep.* **1988**, *6*, 143–170.
- [3] K. Beetul, A. Gopeechund, D. Kaullysing, S. Mattan-Moorgawa, D. Puchooa, R. Bhagooli, in *Algae - Organisms for Imminent Biotechnology*, **2016**, pp. 237–376.
- [4] C. B. Field, M. J. Behrenfeld, J. T. Randerson, P. Falkowski, *Science*. **1998**, *281*, 237–240.
- [5] C. Arnosti, M. Wietz, T. Brinkhoff, J. H. Hehemann, D. Probandt, L. Zeugner, R. Amann, *Annu. Rev. Mar. Sci.* **2021**, *13*, 81–108.
- [6] K. D. Hoagland, J. R. Rosowski, M. R. Gretz, S. C. Roemer, *J. Phycol.* **1993**, *29*, 537–566.
- [7] M. Mühlenbruch, H. P. Grossart, F. Eigemann, M. Voss, *Environ. Microbiol.* **2018**, *20*, 2671–2685.
- [8] S. Kraan, in *Algae Based Polymers, Blends, and Composites: Chemistry, Biotechnology and Materials Science*, **2012**, pp. 489–532.
- [9] Z. A. Popper, G. Michel, C. Hervé, D. S. Domozych, W. G. T. Willats, M. G. Tuohy, B. Kloareg, D. B. Stengel, *Annu. Rev. Plant Biol.* **2011**, *62*, 567–590.
- [10] M. Baumgen, T. Dutschei, U. T. Bornscheuer, *ChemBioChem* **2021**, *22*, 2247–2256.
- [11] R. S. Aquino, A. M. Landeira-Fernandez, A. P. Valente, L. R. Andrade, P. A. S. Mourão, *Glycobiology* **2005**, *15*, 11–20.
- [12] W. Helbert, *Front. Mar. Sci.* **2017**, *4*, 6.
- [13] J. L. Olsen, P. Rouzé, B. Verhelst, Y. C. Lin, T. Bayer, J. Collen, E. Dattolo, E. De Paoli, S. Dittami, F. Maumus, G. Michel, A. Kersting, C. Lauritano, R. Lohaus, M. Töpel, T. Tonon, K. Vanneste, M. Amirebrahimi, J. Brakel, C. Boström, M. Chovatia, J. Grimwood, J. W. Jenkins, A. Jueterbock, A. Mraz, W. T. Stam, H. Tice, E. Bornberg-Bauer, P. J. Green, G. A. Pearson, G. Procaccini, C. M. Duarte, J. Schmutz, T. B. H. Reusch, Y. Van De Peer, *Nature* **2016**, *530*, 331–335.
- [14] H. Teeling, B. M. Fuchs, C. M. Bennke, K. Krüger, M. Chafee, L. Kappelmann, G. Reintjes, J. Waldmann, C. Quast, F. O. Glöckner, J. Lucas, A. Wichels, G. Gerdts, K. H. Wiltshire, R. I. Amann, *Elife* **2016**, *5*, e11888.
- [15] G. Giljan, C. Arnosti, I. V. Kirstein, R. Amann, B. M. Fuchs, *Environ. Microbiol.* **2022**, *24*, 2333–2347.
- [16] C. Arnosti, *Annu. Rev. Mar. Sci.* **2011**, *3*, 401–425.
- [17] J. M. Grondin, K. Tamura, G. Déjean, D. W. Abbott, H. Brumer, *J. Bacteriol.* **2017**, *199*, e00860-16.
- [18] F. Thomas, J. H. Hehemann, E. Rebuffet, M. Czjzek, G. Michel, *Front. Microbiol.* **2011**, *2*, 93.
- [19] L. S. McKee, S. L. La Rosa, B. Westereng, V. G. Eijssink, P. B. Pope, J. Larsbrink, *Environ. Microbiol. Rep.* **2021**, *13*, 559–581.
- [20] A. Buchan, G. R. LeCleir, C. A. Gulvik, J. M. González, *Nat. Rev. Microbiol.* **2014**, *12*, 686–698.
- [21] H. Teeling, B. M. Fuchs, D. Becher, C. Klockow, A. Gardebrecht, C. M. Bennke, M. Kassabgy, S. Huang, A. J. Mann, J. Waldmann, M. Weber, A. Klindworth, A. Otto, J. Lange, J. Bernhardt, C. Reinsch, M. Hecker, J. Peplies, F. D. Bockelmann, U. Callies, G. Gerdts, A. Wichels, K. H. Wiltshire, F. O. Glöckner, T. Schweder, R. Amann, *Science*. **2012**, *336*, 608–611.
- [22] M. Brunet, F. de Bettignies, N. Le Duff, G. Tanguy, D. Davout, C. Leblanc, A. Gobet, F. Thomas, *Environ. Microbiol.* **2021**, *23*, 1638–1655.
- [23] J. Zhang, J. Shi, S. Gao, Y. Huo, J. Cui, H. Shen, G. Liu, P. He, *PLoS One* **2019**, *14*, e0210460.
- [24] L. A. Arteaga, E. Boss, M. J. Behrenfeld, T. K. Westberry, J. L. Sarmiento, *Nat. Commun.* **2020**, *11*, 5364.
- [25] Y. Dai, S. Yang, D. Zhao, C. Hu, W. Xu, D. M. Anderson, Y. Li, X. P. Song, D. G. Boyce, L. Gibson, C. Zheng, L. Feng, *Nature* **2023**, *615*, 280–284.
- [26] T. Staufenger, V. Thiel, J. Wiese, J. F. Imhoff, *FEMS Microbiol. Ecol.* **2008**, *64*, 65–77.
- [27] S. Salaün, N. Kervarec, P. Potin, D. Haras, M. Piotto, S. La Barre, *Talanta* **2010**, *80*, 1758–1770.
- [28] N. Terrapon, V. Lombard, H. J. Gilbert, B. Henrissat, *Bioinformatics* **2015**, *31*, 647–655.
- [29] E. C. Martens, N. M. Koropatkin, T. J. Smith, J. I. Gordon, *J. Biol. Chem.* **2009**, *284*, 24673–24677.
- [30] L. Kappelmann, K. Krüger, J. H. Hehemann, J. Harder, S. Markert, F. Unfried, D. Becher, N. Shapiro, T. Schweder, R. I. Amann, H. Teeling, *ISME J.* **2019**, *13*, 76–91.
- [31] A. J. Glenwright, K. R. Pothula, S. P. Bhamidimarri, D. S. Chorev, A. Baslé, S. J. Firbank, H. Zheng, C. V. Robinson, M. Winterhalter, U. Kleinekathöfer, D. N. Bolam, B. Van Den Berg, *Nature* **2017**, *541*, 407–411.
- [32] G. Reintjes, C. Arnosti, B. Fuchs, R. Amann, *ISME J.* **2019**, *13*, 1119–1132.
- [33] G. Giljan, S. Brown, C. C. Lloyd, S. Ghobrial, R. Amann, C. Arnosti, *ISME Commun.* **2023**, *3*, 11.



- [34] G. Reintjes, C. Arnosti, B. M. Fuchs, R. Amann, *ISME J.* **2017**, *11*, 1640–1650.
- [35] B. I. Cantarel, P. M. Coutinho, C. Rancurel, T. Bernard, V. Lombard, B. Henrissat, *Nucleic Acids Res.* **2009**, *37*, 233–238.
- [36] A. Levasseur, E. Drula, V. Lombard, P. M. Coutinho, B. Henrissat, *Biotechnol. Biofuels* **2013**, *6*, 41.
- [37] A. Giordano, G. Andreotti, A. Tramice, A. Trincone, *Biotechnol. J.* **2006**, *1*, 511–530.
- [38] L. L. Lairson, B. Henrissat, G. J. Davies, S. G. Withers, *Annu. Rev. Biochem.* **2008**, *77*, 521–555.
- [39] G. J. Davies, K. S. Wilson, B. Henrissat, *Biochem. J.* **1997**, *321*, 557–559.
- [40] J. D. McCarter, G. Stephen Withers, *Curr. Opin. Struct. Biol.* **1994**, *4*, 885–892.
- [41] D. E. Koshland, *Biol. Rev.* **1953**, *28*, 416–436.
- [42] G. Davies, B. Henrissat, *Structure* **1995**, *3*, 853–859.
- [43] S. A. K. Jongkees, S. G. Withers, *Acc. Chem. Res.* **2014**, *47*, 226–235.
- [44] M. L. Garron, M. Cygler, *Glycobiology* **2010**, *20*, 1547–1573.
- [45] M. L. Garron, M. Cygler, *Curr. Opin. Struct. Biol.* **2014**, *28*, 87–95.
- [46] D. N. Bolam, A. Ciruela, S. McQueen-Mason, P. Simpson, M. P. Williamson, J. E. Rixon, A. B. Boraston, G. P. Hazlewood, H. J. Gilbert, *Biochem. J.* **1998**, *331*, 775–781.
- [47] A. B. Boraston, D. N. Bolam, H. J. Gilbert, G. J. Davies, *Biochem. J.* **2004**, *382*, 769–781.
- [48] R. L. J. Melcher, M. Neumann, J. P. Fuenzalida Werner, F. Gröhn, B. M. Moerschbacher, *Sci. Rep.* **2017**, *7*, 44115.
- [49] Y. Wang, R. Tang, J. Tao, X. Wang, B. Zheng, Y. Feng, *J. Biol. Chem.* **2012**, *287*, 29568–29578.
- [50] G. Vaaje-Kolstad, B. Westereng, S. J. Horn, Z. Liu, H. Zhai, M. Sørlie, V. G. H. Eijsink, *Science*. **2010**, *330*, 219–222.
- [51] B. Bissaro, Å. K. Røhr, G. Müller, P. Chylenski, M. Skaugen, Z. Forsberg, S. J. Horn, G. Vaaje-Kolstad, V. G. H. Eijsink, *Nat. Chem. Biol.* **2017**, *13*, 1123–1128.
- [52] W. T. Beeson, C. M. Phillips, J. H. D. Cate, M. A. Marletta, *J. Am. Chem. Soc.* **2012**, *134*, 890–892.
- [53] P. Chylenski, B. Bissaro, M. Sørlie, Å. K. Røhr, A. Várnai, S. J. Horn, V. G. H. Eijsink, *ACS Catal.* **2019**, *9*, 4970–4991.
- [54] L. Reisky, H. C. Büchschütz, J. Engel, T. Song, T. Schweder, J. H. Hehemann, U. T. Bornscheuer, *Nat. Chem. Biol.* **2018**, *14*, 342–344.
- [55] M. J. Selig, W. S. Adney, M. E. Himmel, S. R. Decker, *Cellulose* **2009**, *16*, 711–722.
- [56] S. A. Hettiarachchi, Y. K. Kwon, Y. Lee, E. Jo, T. Y. Eom, Y. H. Kang, D. H. Kang, M. De Zoysa, S. D. Marasinghe, C. Oh, *Microb. Cell Fact.* **2019**, *18*, 122.
- [57] T. Dutschei, I. Beidler, D. Bartosik, J. M. Seeßelberg, M. Teune, M. Baumgen, S. Q. Ferreira, J. Heldmann, F. Nagel, J. Krull, L. Berndt, K. Methling, M. Hein, D. Becher, P. Langer, M. Delcea, M. Lalk, M. Lammers, M. Höhne, J. H. Hehemann, T. Schweder, U. T. Bornscheuer, *Environ. Microbiol.* **2023**, 1–15.
- [58] L. P. Christov, B. A. Prior, *Enzyme Microb. Technol.* **1993**, *15*, 460–475.
- [59] M. Amendariz-Ruiz, J. A. Rodriguez-Gonzalez, R. M. Camacho-Ruiz, J. C. Mateos-Diaz, in *Methods in Molecular Biology*, **2018**, pp. 39–68.
- [60] J. H. Hehemann, L. Van Truong, F. Unfried, N. Welsch, J. Kabisch, S. E. Heiden, S. Junker, D. Becher, A. Thürmer, R. Daniel, R. Amann, T. Schweder, *Environ. Microbiol.* **2017**, *19*, 2320–2333.
- [61] A. G. Hettle, C. J. Vickers, A. B. Boraston, *Front. Plant Sci.* **2022**, *13*, 837636.
- [62] C. S. Robb, J. K. Hobbs, B. Pluvinage, G. Reintjes, L. Klassen, S. Monteith, G. Giljan, C. Amundsen, C. Vickers, A. G. Hettle, R. Hills, Nitin, X. Xing, T. Montana, W. F. Zandberg, D. W. Abbott, A. B. Boraston, *Nat. Chem. Biol.* **2022**, *18*, 501–510.
- [63] L. Reisky, A. Préchoux, M. K. Zühlke, M. Baumgen, C. S. Robb, N. Gerlach, T. Roret, C. Stanetty, R. Larocque, G. Michel, T. Song, S. Markert, F. Unfried, M. D. Mihovilovic, A. Trautwein-Schult, D. Becher, T. Schweder, U. T. Bornscheuer, J. H. Hehemann, *Nat. Chem. Biol.* **2019**, *15*, 803–812.
- [64] E. Ficko-Blean, A. Préchoux, F. Thomas, T. Rochat, R. Larocque, Y. Zhu, M. Stam, S. Génicot, M. Jam, A. Calteau, B. Viart, D. Ropartz, D. Pérez-Pascual, G. Correc, M. Matard-Mann, K. A. Stubbs, H. Rogniaux, A. Jeudy, T. Barbeyron, C. Médigue, M. Czjzek, D. Vallenet, M. J. McBride, E. Duchaud, G. Michel, *Nat. Commun.* **2017**, *8*, 1685.
- [65] T. Barbeyron, L. Brillet-Guéguen, W. Carré, C. Carrière, C. Caron, M. Czjzek, M. Hoebeke, G. Michel, *PLoS One* **2016**, *11*, e0164846.
- [66] S. R. Hanson, M. D. Best, C. H. Wong, *Angew. Chemie - Int. Ed.* **2004**, *43*, 5736–5763.
- [67] O. Berteau, A. Guillot, A. Benjdia, S. Rabot, *J. Biol. Chem.* **2006**, *281*, 22464–22470.
- [68] M. J. Appel, C. R. Bertozzi, *ACS Chem. Biol.* **2015**, *10*, 72–84.
- [69] D. Liu, J. K. Keesing, P. He, Z. Wang, Y. Shi, Y. Wang, *Estuar. Coast. Shelf Sci.* **2013**, *129*, 2–10.

- [70] M. Teichberg, S. E. Fox, Y. S. Olsen, I. Valiela, P. Martinetto, O. Iribarne, E. Y. Muto, M. A. V. Petti, T. N. Corbisier, M. Soto-Jiménez, F. Páez-Osuna, P. Castro, H. Freitas, A. Zitelli, M. Cardinaletti, D. Tagliapietra, *Glob. Chang. Biol.* **2010**, *16*, 2624–2637.
- [71] V. Smetacek, A. Zingone, *Nature* **2013**, *504*, 84–88.
- [72] N. Ye, X. Zhang, Y. Mao, C. Liang, D. Xu, J. Zou, Z. Zhuang, Q. Wang, *Ecol. Res.* **2011**, *26*, 477–485.
- [73] R. H. Charlier, P. Morand, C. W. Finkl, *Int. J. Environ. Stud.* **2008**, *65*, 191–208.
- [74] Y. Zhang, P. He, H. Li, G. Li, J. Liu, F. Jiao, J. Zhang, Y. Huo, X. Shi, R. Su, N. Ye, D. Liu, R. Yu, Z. Wang, M. Zhou, N. Jiao, *Natl. Sci. Rev.* **2019**, *6*, 825–838.
- [75] S. Shibasaki, M. Ueda, *Microorganisms* **2023**, *11*, 1499.
- [76] D. Greetham, J. M. Adams, C. Du, *Sci. Rep.* **2020**, *10*, 9728.
- [77] A. Bayu, M. F. Warsito, M. Y. Putra, S. Karnjanakom, G. Guan, *Carbon Resour. Convers.* **2021**, *4*, 150–163.
- [78] I. Podolean, S. M. Coman, C. Bucur, C. Teodorescu, S. Kikionis, E. Ioannou, V. Roussis, A. Primo, H. Garcia, V. I. Parvulescu, *Catal. Today* **2022**, *383*, 345–357.
- [79] M. T. Cesário, M. M. R. da Fonseca, M. M. Marques, M. C. M. D. de Almeida, *Biotechnol. Adv.* **2018**, *36*, 798–817.
- [80] A. J. Wargacki, E. Leonard, M. N. Win, D. D. Regitsky, C. N. S. Santos, P. B. Kim, S. R. Cooper, R. M. Raisner, A. Herman, A. B. Sivitz, A. Lakshmanaswamy, Y. Kashiyama, D. Baker, Y. Yoshikuni, *Science* **2012**, *335*, 308–313.
- [81] M. Diallo, A. D. Simons, H. van der Wal, F. Collas, S. W. M. K. Bwee Houweling-Tan, A. M. López-Contrerasa, *Appl. Environ. Microbiol.* **2019**, *85*, e02656-18.
- [82] R. Jiang, Y. Linzon, E. Vitkin, Z. Yakhini, A. Chudnovsky, A. Golberg, *Sci. Rep.* **2016**, *6*, 27761.
- [83] L. Korzen, I. N. Pulidindi, A. Israel, A. Abelson, A. Gedanken, *RSC Adv.* **2015**, *5*, 16223–16229.
- [84] H. Dominguez, E. P. Loret, *Mar. Drugs* **2019**, *17*, 357.
- [85] H. M. E. M. S, R. Baskaran, *Algal Res.* **2023**, *71*, 103069.
- [86] S. Laramore, R. Baptiste, P. S. Wills, M. D. Hanisak, *J. Appl. Phycol.* **2018**, *30*, 3603–3610.
- [87] M. Lahaye, A. Robic, *Biomacromolecules* **2007**, *8*, 1765–1774.
- [88] M. Lahaye, E. A. C. Cimadevilla, R. Kuhlenskamp, B. Quemener, V. Lognoné, P. Dion, *J. Appl. Phycol.* **1999**, *11*, 1–7.
- [89] M. Lahaye, B. Ray, *Carbohydr. Res.* **1996**, *283*, 161–173.
- [90] J. T. Kidgell, M. Magnusson, R. de Nys, C. R. K. Glasson, *Algal Res.* **2019**, *39*, 101422.
- [91] M. Lahaye, M. Brunel, E. Bonnin, *Carbohydr. Res.* **1997**, *304*, 325–333.
- [92] M. Lahaye, B. Ray, *Carbohydr. Res.* **1995**, *274*, 313–318.
- [93] K. M. Barakat, M. M. Ismail, H. E. Abou El Hassayeb, N. A. El Sersy, M. E. Elshobary, *Rend. Lincei. Sci. Fis. Nat.* **2022**, *33*, 829–841.
- [94] L. Wang, X. Wang, H. Wu, R. Liu, *Mar. Drugs* **2014**, *12*, 4984–5020
- [95] Y. H. R. Hung, G. W. Chen, C. L. Pan, H. T. V. Lin, *Fermentation* **2021**, *7*, 160.
- [96] J. Venkatesan, S. Anil, S. K. Kim, M. S. Shim, *Polymers (Basel)*. **2016**, *8*, 30.
- [97] F. Chiellini, A. Morelli, in *Biomaterials - Physics and Chemistry*, **2011**, pp. 75–98.
- [98] T. Tang, S. Cao, B. Zhu, Q. Li, *Algal Res.* **2021**, *60*, 102477.
- [99] P. N. Collén, A. Jeudy, J. F. Sassi, A. Groisillier, M. Czjzek, P. M. Coutinho, W. Helbert, *J. Biol. Chem.* **2014**, *289*, 6199–6211.
- [100] L. Reisky, C. Stanetty, M. D. Mihovilovic, T. Schweder, J. H. Hehemann, U. T. Bornscheuer, *Appl. Microbiol. Biotechnol.* **2018**, *102*, 6987–6996.
- [101] T. Ulaganathan, M. T. Boniecki, E. Foran, V. Buravenkov, N. Mizrachi, E. Banin, W. Helbert, M. Cygler, *ACS Chem. Biol.* **2017**, *12*, 1269–1280.
- [102] T. Ulaganathan, E. Banin, W. Helbert, M. Cygler, *J. Biol. Chem.* **2018**, *293*, 11564–11573.
- [103] T. Ulaganathan, W. Helbert, M. Kopel, E. Banin, M. Cygler, *J. Biol. Chem.* **2018**, *293*, 4026–4036.
- [104] S. A. K. Jongkees, S. G. Withers, *J. Am. Chem. Soc.* **2011**, *133*, 19334–19337.
- [105] M. Baumgen, T. Dutschei, D. Bartosik, C. Suster, L. Reisky, N. Gerlach, C. Stanetty, M. D. Mihovilovic, T. Schweder, J.-H. Hehemann, U. T. Bornscheuer, *J. Biol. Chem.* **2021**, *297*, 101210.
- [106] D. A. Rees, E. Conway, *Biochem. J.* **1962**, *84*, 411–416.
- [107] G. Correc, J. H. Hehemann, M. Czjzek, W. Helbert, *Carbohydr. Polym.* **2011**, *83*, 277–283.
- [108] N. S. Anderson, D. . Rees, *J. Chem. Soc.* **1965**, 5880–5887.
- [109] J. H. Hehemann, G. Correc, F. Thomas, T. Bernard, T. Barbeyron, M. Jam, W. Helbert, G. Michel, M. Czjzek, *J. Biol. Chem.* **2012**, *287*, 30571–30584.
- [110] J. H. Hehemann, G. Correc, T. Barbeyron, W. Helbert, M. Czjzek, G. Michel, *Nature* **2010**, *464*, 908–912.
- [111] Y. Zhang, Y. Chang, J. Shen, X. Mei, C. Xue, *J. Agric. Food Chem.* **2020**, *68*, 7032–7039.
- [112] G. Manat, M. Fanuel, D. Jouanneau, M. Jam, J. Mac-Bear, H. Rogniaux, T. Mora, R. Larocque,

- A. Lipinska, M. Czjzek, D. Ropartz, E. Ficko-Blean, *J. Biol. Chem.* **2022**, *298*, 102707.
- [113] T. Bito, F. Teng, F. Watanabe, *J. Agric. Food Chem.* **2017**, *65*, 10685–10692.
- [114] J. H. Hehemann, A. G. Kelly, N. A. Pudlo, E. C. Martens, A. B. Boraston, *Proc. Natl. Acad. Sci. U. S. A.* **2012**, *109*, 19786–19791.
- [115] B. Pluvinaud, J. M. Grondin, C. Amundsen, L. Klassen, P. E. Moote, Y. Xiao, D. Thomas, N. A. Pudlo, A. Anele, E. C. Martens, G. D. Inglis, R. E. R. Uwiera, A. B. Boraston, D. W. Abbott, *Nat. Commun.* **2018**, *9*, 1043.
- [116] S. Mathieu, M. Touvrey, L. Poulet, T. S. Sophie Drouillard, Ulaganathan, L. Ségurel, M. Cygler, W. Helbert, *bioRxiv Biochem.* **2023**, 1–39.
- [117] E. Rebuffet, A. Groisillier, A. Thompson, A. Jeudy, T. Barbeyron, M. Czjzek, G. Michel, *Environ. Microbiol.* **2011**, *13*, 1253–1270.
- [118] G. Heß, P. Haiss, D. Wistuba, H.-U. Siehl, S. Berger, D. Sicker, K.-P. Zeller, *Chemie unserer Zeit* **2016**, *50*, 34–43.
- [119] C. Panagiotopoulos, D. J. Repeta, L. Mathieu, J. F. Rontani, R. Sempéré, *Mar. Chem.* **2013**, *154*, 34–45.
- [120] C. Panagiotopoulos, D. J. Repeta, C. G. Johnson, *Org. Geochem.* **2007**, *38*, 884–896.
- [121] V. B. Urlacher, M. Girhard, *Trends Biotechnol.* **2019**, *37*, 882–897.
- [122] V. B. Urlacher, R. Bernhardt, *BioSpektrum* **2019**, *25*, 715–718.
- [123] V. B. Urlacher, M. Girhard, *Trends Biotechnol.* **2012**, *30*, 26–36.
- [124] F. Hannemann, A. Bichet, K. M. Ewen, R. Bernhardt, *Biochim. Biophys. Acta* **2007**, *1770*, 330–344.
- [125] J. C. Lewis, S. Bastian, C. S. Bennett, Y. Fu, Y. Mitsuda, M. M. Chen, W. A. Greenberg, C. H. Wong, F. H. Arnold, *Proc. Natl. Acad. Sci. U. S. A.* **2009**, *106*, 16550–16555.
- [126] C. S. Robb, L. Reisky, U. T. Bornscheuer, J. H. Hehemann, *Biochem. J.* **2018**, *475*, 3875–3886.
- [127] Y. G. Zheng, H. H. Yin, D. F. Yu, X. Chen, X. L. Tang, X. J. Zhang, Y. P. Xue, Y. J. Wang, Z. Q. Liu, *Appl. Microbiol. Biotechnol.* **2017**, *101*, 987–1001.
- [128] M. M. Musa, R. S. Phillips, *Catal. Sci. Technol.* **2011**, *1*, 1311–1323.
- [129] F. L. Sirota, S. Maurer-Stroh, Z. Li, F. Eisenhaber, B. Eisenhaber, *Front. Bioeng. Biotechnol.* **2021**, *9*, 701120.
- [130] F. Lu, W. Xu, W. Zhang, C. Guang, W. Mu, *Appl. Microbiol. Biotechnol.* **2019**, *103*, 6473–6481.
- [131] W. G. Gutheil, B. Holmquist, B. L. Vallee, *Biochemistry* **1992**, *31*, 475–481.
- [132] B. Persson, J. Hedlund, H. Jörnvall, *Cell. Mol. Life Sci.* **2008**, *65*, 3879–3894.
- [133] S. T. Rao, M. G. Rossmann, *J. Mol. Biol.* **1973**, *76*, 241–256.
- [134] K. A. McCall, C. Huang, C. A. Fierke, *J. Nutr.* **2000**, *130*, 1437S–1446S.
- [135] B. Siminszky, L. Gavilano, S. W. Bowen, R. E. Dewey, *Proc. Natl. Acad. Sci. U. S. A.* **2005**, *102*, 14919–14924.
- [136] S. J. B. Mallinson, M. M. Machovina, R. L. Silveira, M. Garcia-Borràs, N. Gallup, C. W. Johnson, M. D. Allen, M. S. Skaf, M. F. Crowley, E. L. Neidle, K. N. Houk, G. T. Beckham, J. L. Dubois, J. E. McGeehan, *Nat. Commun.* **2018**, *9*, 2487.
- [137] M. E. Wolf, D. J. Hitchen, J. L. DuBois, J. E. McGeehan, L. D. Eltis, *Curr. Opin. Biotechnol.* **2022**, *73*, 43–50.
- [138] A. Bleem, E. Kuatsjah, G. N. Presley, D. J. Hitchen, M. Zahn, D. C. Garcia, W. E. Michener, G. König, K. Tornesakis, M. N. Allemann, R. J. Giannone, J. E. McGeehan, G. T. Beckham, J. K. Michener, *Chem Catal.* **2022**, *2*, 1989–2011.
- [139] R. M. Summers, T. M. Louie, C. L. Yu, L. Gakhar, K. C. Louie, M. Subramanian, *J. Bacteriol.* **2012**, *194*, 2041–2049.
- [140] S. M. Barry, G. L. Challis, *ACS Catal.* **2013**, *3*, 2362–2370.
- [141] E. Lanfranchi, M. Trajković, K. Barta, J. G. de Vries, D. B. Janssen, *ChemBioChem* **2019**, *20*, 118–125.
- [142] J. M. Hagel, P. J. Facchini, *Nat. Chem. Biol.* **2010**, *6*, 273–275.
- [143] P. Falnes, R. F. Johansen, E. Seeberg, *Nature* **2002**, *419*, 178–182.
- [144] J. M. Hagel, P. J. Facchini, *Front. Physiol.* **2010**, *1*, 14.
- [145] S. C. Farrow, P. J. Facchini, *J. Biol. Chem.* **2013**, *288*, 28997–29012.
- [146] R. L. D'Ordine, T. J. Rydel, M. J. Storek, E. J. Sturman, F. Moshiri, R. K. Bartlett, G. R. Brown, R. J. Eilers, C. Dart, Y. Qi, S. Flasinski, S. J. Franklin, *J. Mol. Biol.* **2009**, *392*, 481–497.
- [147] P. A. Aas, M. Otterlei, P. Falnes, C. B. Vågbø, F. Skorpen, M. Akbari, O. Sundheim, M. Bjørås, G. Slupphaug, E. Seeberg, H. E. Krokan, *Nature* **2003**, *421*, 859–863.
- [148] Y. Mishina, C. He, *J. Inorg. Biochem.* **2006**, *100*, 670–678.
- [149] S. C. Trewick, T. F. Henshaw, R. P. Hausinger, T. Lindahl, B. Sedgwick, *Nature* **2002**, *419*, 174–178.
- [150] T. Gerken, C. A. Girard, Y. C. L. Tung, C. J. Webby, V. Saudek, K. S. Hewitson, G. S. H. Yeo, M. A. McDonough, S. Cunliffe, L. A. McNeill, J. Galvanovskis, P. Rorsman, P. Robins, X. Prieur,

- A. P. Coll, M. Ma, Z. Jovanovic, I. S. Farooqi, B. Sedgwick, I. Barroso, T. Lindahl, C. P. Ponting, F. M. Ashcroft, S. O'Rahilly, C. J. Schofield, *Science*. **2007**, *318*, 1469–1472.
- [151] Y. I. Tsukada, J. Fang, H. Erdjument-Bromage, M. E. Warren, C. H. Borchers, P. Tempst, Y. Zhang, *Nature* **2006**, *439*, 811–816.
- [152] Y. Shi, F. Lan, C. Matson, P. Mulligan, J. R. Whetstine, P. A. Cole, R. A. Casero, Y. Shi, *Cell* **2004**, *119*, 941–953.
- [153] E. Erickson, A. Bleem, E. Kuatsjah, A. Z. Werner, J. L. DuBois, J. E. McGeehan, L. D. Eltis, G. T. Beckham, *Nat. Catal.* **2022**, *5*, 86–98.
- [154] H. Yurimoto, N. Kato, Y. Sakai, *Chem. Rec.* **2005**, *5*, 367–375.
- [155] J. C. Murreil, V. McGowan, D. L. N. Cardy, *Chemosphere* **1993**, *26*, 1–11.
- [156] J. L. Dixon, S. Sargeant, P. D. Nightingale, J. Colin Murrell, *ISME J.* **2013**, *7*, 568–580.
- [157] J. L. Dixon, R. Beale, P. D. Nightingale, *ISME J.* **2011**, *5*, 704–716.
- [158] J. D. Neufeld, H. Schäfer, M. J. Cox, R. Boden, I. R. McDonald, J. C. Murrell, *ISME J.* **2007**, *1*, 480–491.
- [159] S. Radajewski, G. Webster, D. S. Reay, S. A. Morris, P. Ineson, B. B. Nedwell, J. I. Prosser, J. C. Murrell, *Microbiology* **2002**, *148*, 2331–2342.
- [160] A. Stacheter, M. Noll, C. K. Lee, M. Selzer, B. Glowik, L. Ebertsch, R. Mertel, D. Schulz, N. Lampert, H. L. Drake, S. Kolb, *ISME J.* **2013**, *7*, 1051–1064.
- [161] A. T. Tveit, A. G. Hestnes, S. L. Robinson, A. Schintlmeister, S. N. Dedysh, N. Jehmlich, M. Von Bergen, C. Herbold, M. Wagner, A. Richter, M. M. Svenning, *Proc. Natl. Acad. Sci. U. S. A.* **2019**, *116*, 8515–8524.
- [162] S. Wellner, N. Ladders, P. Kämpfer, *Syst. Appl. Microbiol.* **2011**, *34*, 621–630.
- [163] J. A. Vorholt, *Nat. Rev. Microbiol.* **2012**, *10*, 828–840.
- [164] S. Kanukollu, R. Remus, A. M. Rücker, C. Buchen-Tschiskale, M. Hoffmann, S. Kolb, *Environ. Microbiomes* **2022**, *17*, 35.
- [165] M. Kumar, R. S. Tomar, H. Lade, D. Paul, *World J. Microbiol. Biotechnol.* **2016**, *32*, 120.
- [166] L. Chistoserdova, M. G. Kalyuzhnaya, M. E. Lidstrom, *Annu. Rev. Microbiol.* **2009**, *63*, 477–499.
- [167] M. O. Ross, A. C. Rosenzweig, *J. Biol. Inorg. Chem.* **2017**, *22*, 307–319.
- [168] T. K. Le, Y. J. Lee, G. H. Han, S. J. Yeom, *Front. Bioeng. Biotechnol.* **2021**, *9*, 787791.
- [169] J. T. Keltjens, A. Pol, J. Reimann, H. J. M. Op Den Camp, *Appl. Microbiol. Biotechnol.* **2014**, *98*, 6163–6183.
- [170] D. Wischer, D. Kumaresan, A. Johnston, M. El Khawand, J. Stephenson, A. M. Hillebrand-Voiculescu, Y. Chen, J. C. Murrell, *ISME J.* **2015**, *9*, 195–206.
- [171] M. Suleiman, K. Zecher, O. Yücel, N. Jagmann, B. Philipp, *Appl. Environ. Microbiol.* **2016**, *82*, 7113–7122.
- [172] P. R. Levering, J. P. van Dijken, M. Veenhuis, W. Harder, *Arch. Microbiol.* **1981**, *129*, 72–80.
- [173] Ö. Eyice, N. Myronova, A. Pol, O. Carrión, J. D. Todd, T. J. Smith, S. J. Gurman, A. Cuthbertson, S. Mazard, M. A. S. H. Mennink-Kersten, T. D. H. Bugg, K. K. Andersson, A. W. B. Johnston, H. J. M. Op Den Camp, H. Schäfer, *ISME J.* **2018**, *12*, 145–160.
- [174] N. Kato, H. Yurimoto, R. K. Thauer, *Biosci. Biotechnol. Biochem.* **2006**, *70*, 10–21.
- [175] N. H. Chen, K. Y. Djoko, F. J. Veyrier, A. G. McEwan, *Front. Microbiol.* **2016**, *7*, 257.
- [176] J. J. A. G. Kamps, R. J. Hopkinson, C. J. Schofield, T. D. W. Claridge, *Commun. Chem.* **2019**, *2*, 126.
- [177] S. Shishodia, D. Zhang, A. H. El-Sagheer, T. Brown, T. D. W. Claridge, C. J. Schofield, R. J. Hopkinson, *Org. Biomol. Chem.* **2018**, *16*, 4021–4032.
- [178] R. G. Kallen, *J. Am. Chem. Soc.* **1971**, *93*, 6236–6248.
- [179] C. Auerbach, M. Moutschen-Dahmen, J. Moutschen, *Mutat. Res.* **1977**, *39*, 317–361.
- [180] B. Metz, G. F. A. Kersten, P. Hoogerhout, H. F. Brugghe, H. A. M. Timmermans, A. De Jong, H. Meiring, J. Ten Hove, W. E. Hennink, D. J. A. Crommelin, W. Jiskoot, *J. Biol. Chem.* **2004**, *279*, 6235–6243.
- [181] B. Metz, G. F. A. Kersten, G. J. E. Baart, A. De Jong, H. Meiring, J. Ten Hove, M. J. Van Steenbergen, W. E. Hennink, D. J. A. Crommelin, W. Jiskoot, *Bioconjug. Chem.* **2006**, *17*, 815–822.
- [182] T. Tayri-Wilk, M. Slavin, J. Zamel, A. Blass, S. Cohen, A. Motzik, X. Sun, D. E. Shalev, O. Ram, N. Kalisman, *Nat. Commun.* **2020**, *11*, 3128.
- [183] T. John, E. Pires, S. S. Hester, E. Salah, R. J. Hopkinson, C. J. Schofield, *Commun. Chem.* **2023**, *6*, 12.
- [184] M. Kawanishi, T. Matsuda, T. Yagi, *Front. Environ. Sci.* **2014**, *2*, 36.
- [185] E. A. Hoffman, B. L. Frey, L. M. Smith, D. T. Auble, *J. Biol. Chem.* **2015**, *290*, 26404–26411.
- [186] K. Lu, W. Ye, L. Zhou, L. B. Collins, X. Chen, A. Gold, L. M. Ball, J. A. Swenberg, *J. Am. Chem. Soc.* **2010**, *132*, 3388–3399.
- [187] T. Nakano, R. Ouchi, J. Kawazoe, S. P. Pack, K. Makino, H. Ide, *J. Biol. Chem.* **2012**, *287*, 6562–

- 6572.
- [188] A. V. Yudkina, A. P. Dvornikova, D. O. Zharkov, *PLoS One* **2018**, *13*, e0198480.
- [189] A. Kumari, I. G. Minko, R. L. Smith, R. S. Lloyd, A. K. McCullough, *J. Biol. Chem.* **2010**, *285*, 21313–21322.
- [190] T. Nakano, M. Miyamoto-Matsubara, M. I. Shoukamy, A. M. H. Salem, S. P. Pack, Y. Ishimi, H. Ide, *J. Biol. Chem.* **2013**, *288*, 4649–4658.
- [191] J. A. Vorholt, *Arch. Microbiol.* **2002**, *178*, 239–249.
- [192] V. J. Klein, M. Irla, M. G. López, T. Brautaset, L. F. Brito, *Microorganisms* **2022**, *10*, 220.
- [193] T. Matsui, S. Nambu, Y. Ono, C. W. Goulding, K. Tsumoto, M. Ikeda-Saito, *Biochemistry* **2013**, *52*, 3025–3027.
- [194] L. B. Maia, J. J. G. Moura, I. Moura, *J. Biol. Inorg. Chem.* **2015**, *20*, 287–309.
- [195] V. O. Popov, V. S. Lamzin, *Biochem. J.* **1994**, *301*, 625–643.
- [196] S. C. Lu, *Biochim. Biophys. Acta* **2013**, *1830*, 3143–3153.
- [197] S. Naylor, R. P. Mason, J. K. M. Sanders, D. H. Williams, G. Moneti, *Biochem. J.* **1988**, *249*, 573–579.
- [198] P. C. Sanghani, C. L. Stone, B. D. Ray, E. V. Pindel, T. D. Hurley, W. F. Bosron, *Biochemistry* **2000**, *39*, 10720–10729.
- [199] R. J. Hopkinson, P. S. Barlow, C. J. Schofield, T. D. W. Claridge, *Org. Biomol. Chem.* **2010**, *8*, 4915–4920.
- [200] M. Goenrich, S. Bartoschek, C. H. Hagemeyer, C. Griesinger, J. A. Vorholt, *J. Biol. Chem.* **2002**, *277*, 3069–3072.
- [201] R. J. Hopkinson, I. K. H. Leung, T. J. Smart, N. R. Rose, L. Henry, T. D. W. Claridge, C. J. Schofield, *PLoS One* **2015**, *10*, 1371.
- [202] M. Koivusalo, M. Baumann, L. Uotila, *FEBS Lett.* **1989**, *257*, 105–109.
- [203] R. D. Barber, M. A. Rott, T. J. Donohue, *J. Bacteriol.* **1996**, *178*, 1386–1393.
- [204] C. F. Gonzalez, M. Proudfoot, G. Brown, Y. Korniyenko, H. Mori, A. V. Savchenko, A. F. Yakunin, *J. Biol. Chem.* **2006**, *281*, 14514–14522.
- [205] P. Chandrangu, V. Van Loi, H. Antelmann, J. D. Helmann, *Antioxidants Redox Signal.* **2018**, *28*, 445–462.
- [206] G. L. Newton, K. Arnold, M. S. Price, C. Sherrill, S. B. Delcardayre, Y. Aharonowitz, G. Cohen, J. Davies, R. C. Fahey, C. Davis, *J. Bacteriol.* **1996**, *178*, 1990–1995.
- [207] G. L. Newton, R. C. Fahey, *Arch. Microbiol.* **2002**, *178*, 388–394.
- [208] G. L. Newton, C. A. Bewley, T. J. Dwyer, R. Horn, Y. Aharonowitz, G. Cohen, J. Davies, D. J. Faulkner, R. C. Fahey, *Eur. J. Biochem.* **1995**, *230*, 821–825.
- [209] S. Sakuda, Y. Ze-Zhou, Y. Yamada, *Biosci. Biotechnol. Biochem.* **1994**, *58*, 1347–1348.
- [210] H. S. C. Spies, D. J. Steenkamp, *Eur. J. Biochem.* **1994**, *224*, 203–213.
- [211] M. Misset-Smits, P. W. van Ophem, S. Sakuda, J. A. Duine, *FEBS Lett.* **1997**, *409*, 221–222.
- [212] M. Rawat, Y. Av-Gay, *FEMS Microbiol. Rev.* **2007**, *31*, 278–292.
- [213] G. L. Newton, M. Rawat, J. J. La Clair, V. K. Jothivasan, T. Budiarto, C. J. Hamilton, A. Claiborne, J. D. Helmann, R. C. Fahey, *Nat. Chem. Biol.* **2009**, *5*, 625–627.
- [214] A. Gaballa, G. L. Newton, H. Antelmann, D. Parsonage, H. Upton, M. Rawat, A. Claiborne, R. C. Fahey, J. D. Helmann, *Proc. Natl. Acad. Sci. U. S. A.* **2010**, *107*, 6482–6486.
- [215] J. E. N. Müller, F. Meyer, B. Litsanov, P. Kiefer, J. A. Vorholt, *Mol. Microbiol.* **2015**, *98*, 1089–1100.
- [216] J. A. Vorholt, C. J. Marx, M. E. Lidstrom, R. K. Thauer, *J. Bacteriol.* **2000**, *182*, 6645–6650.
- [217] B. E. H. Maden, *Biochem. J.* **2000**, *350*, 609–629.
- [218] P. Basu, S. J. N. Burgmayer, *Coord. Chem. Rev.* **2011**, *255*, 1016–1038.
- [219] P. Acharya, M. Goenrich, C. H. Hagemeyer, U. Demmer, J. A. Vorholt, R. K. Thauer, U. Ermler, *J. Biol. Chem.* **2005**, *280*, 13712–13719.
- [220] J. A. Vorholt, L. Chistoserdova, M. E. Lidstrom, R. K. Thauer, *J. Bacteriol.* **1998**, *180*, 5351–5356.
- [221] B. K. Pomper, J. A. Vorholt, L. Chistoserdova, M. E. Lidstrom, R. K. Thauer, *Eur. J. Biochem.* **1999**, *261*, 475–480.
- [222] B. K. Pomper, O. Saurel, A. Milon, J. A. Vorholt, *FEBS Lett.* **2002**, *523*, 133–137.
- [223] B. K. Pomper, J. A. Vorholt, *Eur. J. Biochem.* **2001**, *269*, 4769–4775.
- [224] J. L. Hemmann, O. Saurel, A. M. Ochsner, B. K. Stodden, P. Kiefer, A. Milon, J. A. Vorholt, *J. Biol. Chem.* **2016**, *291*, 9042–9051.
- [225] J. L. Hemmann, T. Wagner, S. Shima, J. A. Vorholt, *Proc. Natl. Acad. Sci. U. S. A.* **2019**, *116*, 25583–25590.
- [226] S. Sah, U. Varshney, *Biochemistry* **2015**, *54*, 3504–3513.
- [227] C. J. Marx, M. Laukel, J. A. Vorholt, M. E. Lidstrom, *J. Bacteriol.* **2003**, *185*, 7169–7175.
- [228] C. J. Marx, L. Chistoserdova, M. E. Lidstrom, *J. Bacteriol.* **2003**, *185*, 7160–7168.
- [229] G. J. Crowther, G. Kosály, M. E. Lidstrom, *J. Bacteriol.* **2008**, *190*, 5057–5062.

- [230] H. Šmejkalová, T. J. Erb, G. Fuchs, *PLoS One* **2010**, *5*, e13001.
- [231] H. He, E. Noor, P. A. Ramos-Parra, L. E. García-Valencia, J. A. Patterson, R. I. D. de la Garza, A. D. Hanson, A. Bar-Even, *Metabolites* **2020**, *10*, 65.
- [232] D. I. Stirling, H. Dalton, *J. Gen. Microbiol.* **1978**, *107*, 19–29.
- [233] S. Tate, H. Dalton, *Microbiology* **1999**, *145*, 159–167.
- [234] W. Zhang, S. Chen, Y. Liao, D. Wang, J. Ding, Y. Wang, X. Ran, D. Lu, H. Zhu, *Protein Expr. Purif.* **2013**, *92*, 208–213.
- [235] C. R. Klein, F. P. Kessler, C. Perrei, J. Frank, J. A. Duine, A. C. Schwartz, *Biochem. J.* **1994**, *301*, 289–295.
- [236] J. A. Zahn, D. J. Bergmann, J. M. Boyd, R. C. Kunz, A. A. DiSpirito, *J. Bacteriol.* **2001**, *183*, 6832–6840.
- [237] I. W. Marison, M. M. Attwood, *J. Gen. Microbiol.* **1980**, *117*, 305–313.
- [238] A. C. Schwartz, G. Gockel, J. Groß, B. Moritz, H. E. Meyer, *Arch. Microbiol.* **2004**, *182*, 458–466.
- [239] H. Yonemitsu, Y. Kikuchi, *Biosci. Biotechnol. Biochem.* **2018**, *82*, 49–56.
- [240] S. Imoto, H. Yonemitsu, N. Totsui, N. Kishimoto, *Biosci. Biotechnol. Biochem.* **2020**, *84*, 1444–1450.
- [241] D. van der Waals, L. E. Heim, S. Vallazza, C. Gedig, J. Deska, M. H. G. Pechtl, *Chem. Eur. J.* **2016**, *22*, 11568–11573.
- [242] N. Kato, T. Yamagami, M. Shimao, C. Sakazawa, *Eur. J. Biochem.* **1986**, *156*, 59–64.
- [243] W. B. Whitaker, N. R. Sandoval, R. K. Bennett, A. G. Fast, E. T. Papoutsakis, *Curr. Opin. Biotechnol.* **2015**, *33*, 165–175.
- [244] T. Strøm, T. Ferenci, J. R. Quayle, *Biochem. J.* **1974**, *144*, 465–476.
- [245] I. Goldberg, J. S. Rock, A. Ben-Bassat, R. I. Mateles, *Biotechnol. Bioeng.* **1976**, *18*, 1657–1668.
- [246] J. R. Quayle, T. Ferenci, *Microbiol. Rev.* **1978**, *42*, 251–273.
- [247] W. Zhang, T. Zhang, S. Wu, M. Wu, F. Xin, W. Dong, J. Ma, M. Zhang, M. Jiang, *RSC Adv.* **2017**, *7*, 4083–4091.
- [248] J. E. N. Müller, F. Meyer, B. Litsanov, P. Kiefer, E. Potthoff, S. Heux, W. J. Quax, V. F. Wendisch, T. Brautaset, J. C. Portais, J. A. Vorholt, *Metab. Eng.* **2015**, *28*, 190–201.
- [249] F. W. Koopman, J. H. De Winde, H. J. Ruijsenaars, *Appl. Microbiol. Biotechnol.* **2009**, *83*, 705–713.
- [250] I. Orita, T. Sato, H. Yurimoto, N. Kato, H. Atomi, T. Imanaka, Y. Sakai, *J. Bacteriol.* **2006**, *188*, 4698–4704.
- [251] E. N. M. Jonas, B. Litsanov, M. Bortfeld-Miller, C. Trachsel, J. Grossmann, T. Brautaset, J. A. Vorholt, *Proteomics* **2014**, *14*, 725–737.
- [252] H. Yurimoto, N. Kato, Y. Sakai, *Appl. Environ. Microbiol.* **2009**, *84*, 407–416.
- [253] S. Sugimoto, *J. Bacterology* **1999**, *181*, 7154–7160.
- [254] H. Yurimoto, R. Hirai, N. Matsuno, H. Yasueda, N. Kato, Y. Sakai, *Mol. Microbiol.* **2005**, *57*, 511–519.
- [255] R. Zhu, G. Zhang, M. Jing, Y. Han, J. Li, J. Zhao, P. R. Chen, *Nat. Commun.* **2021**, *12*, 581.
- [256] S. Desmons, R. Fauré, S. Bontemps, *ACS Catal.* **2019**, 9575–9588.
- [257] K. Nobou, *Methods Enzymol.* **1990**, *188*, 397–401.
- [258] T. Ferenci, T. Strøm, J. R. Quayle, *Biochem. J.* **1974**, *144*, 477–486.
- [259] I. Orita, A. Kita, H. Yurimoto, N. Kato, Y. Sakai, K. Miki, *Proteins* **2010**, *78*, 3488–3492.
- [260] W. S. Yew, J. Akana, E. L. Wise, I. Rayment, J. A. Gerlt, *Biochemistry* **2005**, *44*, 1807–1815.
- [261] J. A. Gerlt, F. M. Raushel, *Curr. Opin. Chem. Biol.* **2003**, *7*, 252–264.
- [262] W. S. Yew, J. A. Gerlt, *J. Bacterology* **2002**, *184*, 302–306.
- [263] R. Beisswenge, G. Snatzke, J. Thieme, M.-R. Kula, *Tetrahedron Lett.* **1991**, *32*, 3159–3162.
- [264] A. G. McDonald, S. Boyce, K. F. Tipton, in *eLS*, **2005**, 1–11.
- [265] H. S. Fernandes, M. J. Joa, N. M. F. S. A. Cerqueira, *ACS Catal.* **2018**, *8*, 10096–10110.
- [266] H. L. Kornberg, H. A. Krebs, *Nature* **1957**, *179*, 988–991.
- [267] P. Kiefer, P. Christen, S. Massou, J. Portais, J. A. Vorholt, *Proc. Natl. Acad. Sci. U. S. A.* **2009**, *106*, 4846–4851.
- [268] H. Yu, J. C. Liao, *Nat. Commun.* **2018**, *9*, 3992.
- [269] J. P. van Dijken, W. Harder, A. J. Beardsmore, J. R. Quayle, *FEMS Microbiol. Lett.* **1978**, *4*, 97–102.
- [270] V. Wegat, J. T. Fabarius, V. Sieber, *Biotechnol. Biofuels Bioprod.* **2022**, *15*, 113.
- [271] N. Kato, T. Higuchi, C. Sakazawa, T. Nishizawa, Y. TANI, H. Yamada, *Biochim. Biophys. Acta* **1982**, *715*, 143–150.
- [272] H. He, C. Edlich-Muth, S. N. Lindner, A. Bar-Even, *ACS Synth. Biol.* **2018**, *7*, 1601–1611.
- [273] S. Becker, J. Tebben, S. Coffinet, K. Wiltshire, M. H. Iversen, T. Harder, K.-U. Hinrichs, J.-H. Hehemann, *Proc. Natl. Acad. Sci. U. S. A.* **2020**, *117*, 6599–6607.
- [274] A. Chiovitti, A. Bacic, D. J. Craik, G. T. Kraft, M. L. Liao, *Carbohydr. Res.* **2004**, *339*, 1459–1466.

- [275] A. Gallegos, R. Schleif, A. Bairoch, K. A. Y. Hofmann, J. L. Ramos, *Microbiol. Mol. Biol. Rev.* **1997**, *61*, 393–410.
- [276] D. Pletzer, G. Schweizer, H. Weingart, *J. Bacterology* **2014**, *196*, 3098–3110.
- [277] B. Sprusansky, B. Rezuchova, D. Homerova, J. Kormanec, *Microbiology* **2001**, *147*, 1291–1301.
- [278] K. Kotecka, A. Kawalek, K. Kobylecki, A. A. Bartosik, *Int. J. Mol. Sci.* **2021**, *22*, 5066.
- [279] T. Nash, *Biochem. J.* **1953**, *55*, 416–421.
- [280] H.-J. Hohorst, in *Methods of Enzymatic Analysis* **1965**, 134–138.
- [281] D. Kracher, R. Ludwig, *Die Bodenkultur J. L. Manag. Food Environ.* **2016**, *67*, 145–163.
- [282] L. Sützl, C. V. F. P. Laurent, A. T. Abrera, G. Schütz, R. Ludwig, D. Haltrich, *Appl. Microbiol. Biotechnol.* **2018**, *102*, 2477–2492.
- [283] K. Takeda, H. Matsumura, T. Ishida, M. Samejima, *PLoS One* **2015**, *10*, e0115722.
- [284] S. Brott, F. Thomas, M. Behrens, K. Methling, D. Bartosik, T. Dutschei, M. Lalk, G. Michel, T. Schweder, U. T. Bornscheuer, *ChemBioChem* **2022**, *23*, e202200269.
- [285] L. Uotila, M. Koivusalo, *J. Biol. Chem.* **1974**, *249*, 7653–7663.
- [286] H. Achkor, M. Diaz, M. R. Fernandez, J. A. Biosca, X. Pares, M. C. Martinez, *Plant Physiol.* **2003**, *132*, 2248–2255.
- [287] C. E. Hand, J. F. Honek, *J. Nat. Prod.* **2005**, *68*, 293–308.
- [288] H. Schütte, J. Flossdorf, H. Sahm, M.-R. Kula, *Eur. J. Biochem.* **1976**, *62*, 151–160.
- [289] J. Hiras, S. V Sharma, V. Raman, R. A. J. Tinson, M. Arbach, D. F. Rodrigues, J. Norambuena, C. J. Hamilton, T. E. Hanson, *MBio* **2018**, *9*, e01603-18.
- [290] G. L. Newton, M. Rawat, *MBio* **2019**, *10*, e02634-18.
- [291] Y. Kannan, Y. Koga, Y. Inoue, M. Haruki, M. Takagi, T. Imanaka, M. Morikawa, S. Kanaya, *Appl. Environ. Microbiol.* **2001**, *67*, 2445–2452.
- [292] Z. Zhang, M. Ge, Q. Guo, Y. Jiang, W. Jia, L. Gao, J. Hu, *J. Fungi* **2022**, *8*, 325.
- [293] Y. Maruyama, S. Oiki, R. Takase, B. Mikami, K. Murata, W. Hashimoto, *J. Biol. Chem.* **2015**, *290*, 6281–6292.
- [294] O. Rahman, L. G. Dover, I. C. Sutcliffe, *Trends Microbiol.* **2009**, *17*, 219–225.
- [295] I. Campeotto, M. G. Percy, J. T. Macdonald, A. Förster, P. S. Freemont, A. Gründling, *J. Biol. Chem.* **2014**, *289*, 28054–28069.
- [296] D. Lu, M. E. Wörmann, X. Zhang, O. Schneewind, A. Gründling, P. S. Freemont, *Proc. Natl. Acad. Sci. U. S. A.* **2009**, *106*, 1584–1589.
- [297] A. Sharma, T. Satyanarayana, *Genomics Insights* **2013**, *6*, 25–36.
- [298] B. Veith, C. Herzberg, S. Steckel, J. Feesche, K. H. Maurer, P. Ehrenreich, S. Bäumer, A. Henne, H. Liesegang, R. Merkl, A. Ehrenreich, G. Gottschalk, *J. Mol. Microbiol. Biotechnol.* **2004**, *7*, 204–211.
- [299] B. Waschkau, J. Waldeck, S. Wieland, R. Eichstädt, F. Meinhardt, *Appl. Microbiol. Biotechnol.* **2008**, *78*, 181–188.
- [300] A. B. van Putten, F. Spitzenberger, G. Kretzmer, B. Hitzmann, M. Dors, R. Simutis, K. Schügerl, *J. Biotechnol.* **1996**, *49*, 83–93.
- [301] J. A. Wells, D. A. Estell, *Trends Biochem. Sci.* **1988**, *13*, 291–297.

## Author Contributions

### **Article I      Connecting algal polysaccharide degradation to formaldehyde detoxification**

S. Brott, F. Thomas, M. Behrens, K. Methling, D. Bartosik, T. Dutschei, M. Lalk, G. Michel, T. Schweder and U. T. Bornscheuer, *ChemBioChem* **2022**, 23, e202200269.

M.G., T.S. and U.T.B. initiated the study and directed the project. F.T. conducted the growth studies and created the knock-out strains. S.B. and M.B. expressed and purified the enzymes and performed the biocatalysis. D.B. performed the computational analysis. K.M. and M.L. performed metabolite analysis, S.B. prepared the main manuscript, which was revised by F.T., T.D, M.G, T.S. and U.T.B. and approved by all authors.

### **Article II      Unique alcohol dehydrogenases involved in algal sugar utilization by marine bacteria**

S. Brott, K. H. Nam, F. Thomas, T. Dutschei, L. Reisky, M. Behrens, H. C. Grimm, G. Michel, T. Schweder and U. T. Bornscheuer, *Appl. Microbiol. Biotechnol.* **2023**, 107, 2363–2384.

M.G., T.S., and U.T.B. initiated the study and directed the project. F.T. conducted the growth studies and created the knock-out strain. K.H.N. performed the crystallization and structural analyses. T.D. performed the computational analysis. L. R. and H.C.G. performed the cloning and initial experiments on the enzyme function of FoADH. S.B. and M.B. expressed and purified the enzymes and performed further experiments on enzyme function and characterization. S.B. and K.H.N prepared the main manuscript, which was revised by F.T., T.D., H.C.G., L.R., M.G., T.S., and U.T.B. and was approved by all authors.

### **Article III      Metabolic engineering enables *Bacillus licheniformis* to grow on the marine polysaccharide ulvan**

T. Dutschei, M. K. Zühlke, N. Welsch, T. Eisenack, M. Hilkmann, J.Krull, C. Stühle, S. Brott, A. Dürwald, L. Reisky, J.-H. Hehemann, D. Becher, T. Schweder and U. T. Bornscheuer, *Microb. Cell Fact.* **2022**, 21, 207.

UTB, LR and TS designed the study, supervised its execution and co-wrote the manuscript. TD wrote the main manuscript with the support of MKZ and NW. TD performed the initial screening of organism and growth and activity assays, with TE and CS. The proteome analysis was performed by TE and MKZ. DB coordinated MS measurements. The computational analysis was performed by MKZ, AD and SB. JK performed the sugar monosaccharide composition analysis in the lab of JHH. SB expressed and purified the putative sulfatases and



performed the activity assays. NW developed the *Bacillus* host-vector system and the strain *Bacillus* design with MH. All authors read and approved the final manuscript

---

Stefan Brott

---

Prof. Dr. Uwe T. Bornscheuer



# Articles



# Article I



# Connecting Algal Polysaccharide Degradation to Formaldehyde Detoxification

Stefan Brott,<sup>[a]</sup> François Thomas,<sup>[b]</sup> Maike Behrens,<sup>[a]</sup> Karen Methling,<sup>[c]</sup> Daniel Bartosik,<sup>[d]</sup> Theresa Dutschei,<sup>[a]</sup> Michael Lalk,<sup>[c]</sup> Gurvan Michel,<sup>[b]</sup> Thomas Schweder,<sup>[d]</sup> and Uwe T. Bornscheuer<sup>\*[a]</sup>

Formaldehyde is a toxic metabolite that is formed in large quantities during bacterial utilization of the methoxy sugar 6-O-methyl-D-galactose, an abundant monosaccharide in the red algal polysaccharide porphyran. Marine bacteria capable of metabolizing porphyran must therefore possess suitable detoxification systems for formaldehyde. We demonstrate here that detoxification of formaldehyde in the marine Flavobacterium

*Zobellia galactanivorans* proceeds via the ribulose monophosphate pathway. Simultaneously, we show that the genes encoding the key enzymes of this pathway are important for maintaining high formaldehyde resistance. Additionally, these genes are upregulated in the presence of porphyran, allowing us to connect porphyran degradation to the detoxification of formaldehyde.

Marine algae are considered to be one of the most important primary producers in the marine ecosystem and one of the largest sources of marine carbohydrates.<sup>[1,2]</sup> Serving as energy storage and structural cell wall components, carbohydrates constitute up to 70% of algae dry mass.<sup>[3]</sup> Compared to their terrestrial counterparts, marine polysaccharides differ in the backbone structure and side-group modifications.<sup>[4]</sup> One bacterial phylum considered to be specialist in the degradation of high molecular weight organic matter such as marine carbohydrates are the Bacteroidetes.<sup>[5–7]</sup> Marine Bacteroidetes harbor gene clusters which are referred to as polysaccharide utilization loci (PULs) encoding carbohydrate-active enzymes (CAZymes) as well as specific proteins for the binding and uptake of sugar units.<sup>[5,8]</sup> Their tremendous repertoire of CAZymes allows them to depolymerize complex marine carbohydrates and utilize the

imported monosaccharides as a carbon and energy source.<sup>[4,8]</sup> Observations that Bacteroidetes are among the first responders after micro- and macroalgal blooms are related to their abilities of rapid growth on colonizable surfaces such as macroalgae as well as their CAZymes production.<sup>[9,10]</sup>

A model bacterium for the bioconversion of algal biomass is the marine Flavobacterium *Zobellia galactanivorans* Dsij<sup>T</sup>, which was originally isolated from the red alga *Delesseria sanguinea* near the coast of Roscoff (Brittany, France).<sup>[11]</sup> In-depth analysis of its complete genome and growth studies revealed that this microorganism possesses 50 PULs, is able to grow on numerous marine polysaccharides and utilizes them as a carbon source.<sup>[12,13]</sup> Extensive biochemical studies have elucidated essential CAZymes from *Z. galactanivorans* and their roles in the complex degradation pathways for alginate and laminarin from brown algae<sup>[14–19]</sup> as well as for carrageenan, agar and porphyran from red algae.<sup>[20–23]</sup> Porphyran is the common name of the agar from red algae of the genus *Porphyra* and is their main cell wall polysaccharide.<sup>[24]</sup> The porphyran backbone consists mainly of the alternating monosaccharide units 4-linked- $\alpha$ -L-galactose-6-sulfate (L6S) and 3-linked- $\beta$ -D-galactose (Gal) or 3,6-anhydro- $\alpha$ -L-galactose (LA) (Figure S1, Supporting Information).<sup>[25,26]</sup> In addition, O-methylation of D-galactose is a frequent modification that results in the presence of up to 28% of the methoxy sugar 6-O-methyl-D-galactose (G6Me) within the porphyran chain.<sup>[24,25,27]</sup>

Considering the stability of methyl ethers, it is reasonable to assume that G6Me must first be demethylated before it can enter the cellular metabolism. We recently have demonstrated that the oxidative demethylation of G6Me is catalyzed by a cytochrome P450 monooxygenase with the appropriate redox partners ferredoxin and ferredoxin reductase.<sup>[28]</sup> The crystal structure of the cytochrome P450 monooxygenase from *Z. galactanivorans* informed on the binding of G6Me as well as other mechanistic insights.<sup>[29]</sup> The products of this demethylation are D-galactose and formaldehyde in equimolar amounts.<sup>[28]</sup> However, formaldehyde formation leads to a

[a] S. Brott, M. Behrens, T. Dutschei, Prof. U. T. Bornscheuer  
Department of Biotechnology & Enzyme Catalysis  
Institute of Biochemistry, University of Greifswald  
Greifswald 17487 (Germany)  
E-mail: uwe.bornscheuer@uni-greifswald.de  
Homepage: <http://biotech.uni-greifswald.de>

[b] Prof. F. Thomas, Prof. G. Michel  
Laboratory of Integrative Biology of Marine Models (LBI2 M)  
Station Biologique de Roscoff (SBR)  
Sorbonne Université, CNRS  
29688 Roscoff, Bretagne (France)

[c] Dr. K. Methling, Prof. M. Lalk  
Department of Cellular Biochemistry & Metabolomics  
Institute of Biochemistry, University of Greifswald  
Greifswald 17487 (Germany)

[d] D. Bartosik, Prof. T. Schweder  
Department of Pharmaceutical Biotechnology  
Institute of Pharmacy, University of Greifswald  
Greifswald 17487 (Germany)

Supporting information for this article is available on the WWW under <https://doi.org/10.1002/cbic.202200269>

© 2022 The Authors. ChemBioChem published by Wiley-VCH GmbH. This is an open access article under the terms of the Creative Commons Attribution Non-Commercial NoDerivs License, which permits use and distribution in any medium, provided the original work is properly cited, the use is non-commercial and no modifications or adaptations are made.

problem for the organism, since formaldehyde is a toxic metabolite in cells due to its high reactivity as an electrophile.<sup>[30]</sup> The polarized carbonyl group of formaldehyde can be attacked by nucleophiles such as free amine or thiol groups of amino acids<sup>[31]</sup> and proteins<sup>[32]</sup> or nucleic acids,<sup>[33]</sup> resulting in protein and DNA damages and covalent cross-links.<sup>[34]</sup>

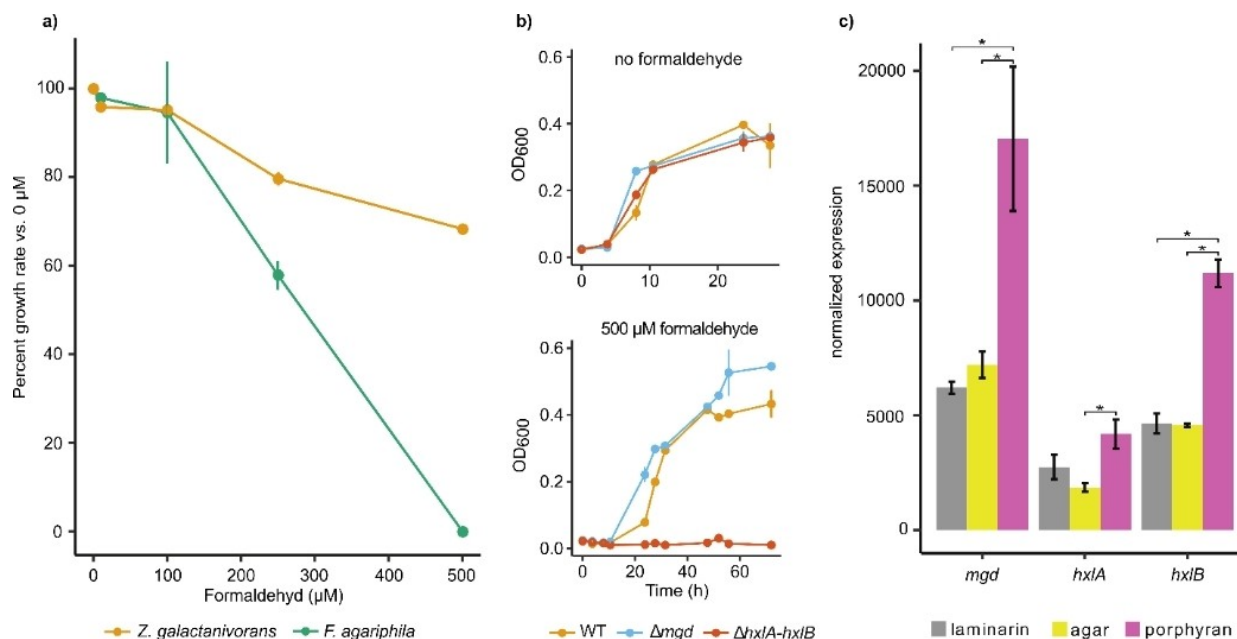
Marine bacteria capable of degrading porphyran and utilizing G6Me should therefore possess suitable detoxification pathways for formaldehyde. Focusing on the discovery of possible pathways of formaldehyde detoxification, we first searched through the genomes of the Flavobacteria *Z. galactanivorans* Dsij<sup>T</sup> and *Formosa agariphila* KMM 3901<sup>T</sup>,<sup>[35]</sup> which possess the cytochrome P450 monooxygenases and thus catalyze the oxidative demethylation of G6Me,<sup>[28]</sup> for genes encoding enzymes from well-known detoxification pathways. Both organisms harbor annotated genes for enzymes found in the serine and tetrahydrofolate pathways (Table S1, Supporting Information). However, unlike *F. agariphila*, *Z. galactanivorans* additionally carries the genes for the putative key enzymes of the ribulose monophosphate (RuMP) pathway. This putative RuMP pathway was proposed to be an advantageous adaptive trait for *Z. galactanivorans* to cope with the release of formaldehyde when degrading red algal cell walls.<sup>[12]</sup> Altogether, *F. agariphila* and *Z. galactanivorans* should provide different responses to the accumulation of formaldehyde. The RuMP pathway is the most efficient pathway of formaldehyde assimilation in terms of ATP consumption and biomass yield.<sup>[36–38]</sup> It can be divided into three parts: fixation, cleavage, and regeneration.<sup>[39]</sup> While the cleavage and regeneration part can take place via different routes and are catalyzed by common enzymes of the central carbon cycle, the fixation of formaldehyde takes place via two unique key enzymes: a 3-hexulose-6-phosphate synthase (HPS) and a 6-phospho-3-hexuloisomerase (PHI).<sup>[39,40]</sup> HPS, a member of the class 2 aldolases,<sup>[41]</sup> catalyzes the Mg<sup>2+</sup>-dependent aldol reaction between formaldehyde and D-ribulose-5-phosphate (R5P) to give the intermediate D-arabino-3-hexulose-6-phosphate (AH6P), which is then isomerized by PHI to D-fructose-6-phosphate (F6P) (Figure 2, top).<sup>[40]</sup> F6P is consumed in the cleavage part to generate triose phosphates such as glyceraldehyde-3-phosphate or dihydroxyacetone phosphate which then can be metabolized in the glycolysis or the Entner-Doudoroff pathway.<sup>[39,42]</sup> Furthermore, R5P is regenerated from F6P by reactions occurring in the pentose-phosphate cycle.<sup>[40]</sup> It has been demonstrated that the RuMP pathway can play an important role in the degradation of methoxylated lignin monomers by non-methylotrophic bacteria.<sup>[44]</sup> However, most knowledge about the RuMP pathway originates from methylotrophic bacteria that grow on reduced C1 components such as methane or methanol, which they oxidize to formaldehyde.<sup>[40]</sup> In addition to these components, numerous methylated sugars are present in the marine ecosystem<sup>[43]</sup> and are thus a potential source of formaldehyde. However, the RuMP pathway has not yet been investigated in the context of marine carbohydrate degradation, we therefore aimed to investigate whether this pathway plays a role in the degradation of porphyran by Bacterioidetes.

We reasoned that the presence of the RuMP pathway in *Z. galactanivorans* should lead to an increased resistance to formaldehyde compared to *F. agariphila*. To test this hypothesis, we cultivated each organism in the presence of increasing formaldehyde concentrations. For *F. agariphila* a significant decrease in growth rate was observed at formaldehyde concentrations greater than 100 μM, while no growth was seen at 500 μM (Figure 1a). In contrast, the presence of formaldehyde concentrations up to 500 μM revealed just minor effects on the growth of *Z. galactanivorans*. However, no growth was detected in the presence of a formaldehyde concentration of 1,000 μM (Figure S2, Supporting Information). In order to prove that the increased resistance towards formaldehyde is caused by the enzymes HPS and PHI, *hxIA* and *hxIB* gene knockout strains of *Z. galactanivorans* were created and the influence of formaldehyde on their growth was investigated again. In the presence of 500 μM formaldehyde, the  $\Delta$ *hxIA-hxIB* strain was unable to grow, whereas the wild-type (WT) and a control knock-out strain lacking the P450 monooxygenase encoding gene ( $\Delta$ *mgd*) were able to grow normally (Figure 1b). Knockout of the *hxIA* and *hxIB* genes thus resulted in a formaldehyde-sensitive strain, which displayed normal growth behavior in the absence of formaldehyde. Both findings supported our assumption that these genes were responsible for the detoxification of formaldehyde.

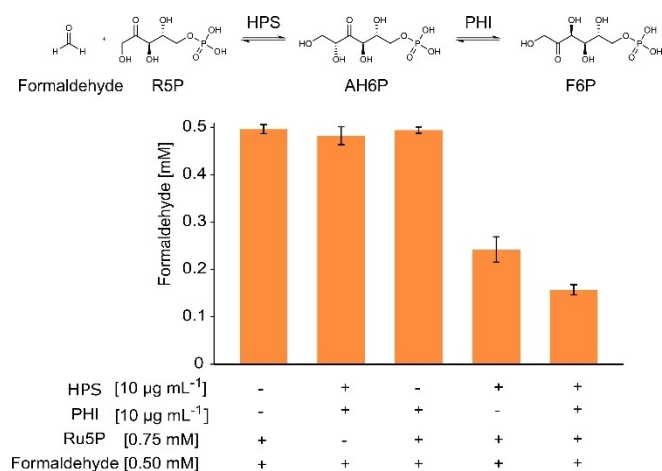
After demonstrating their role for formaldehyde resistance, we were interested to know whether the genes encoding HPS and PHI were also upregulated in the presence of porphyran, considering that this is the origin of formed formaldehyde due to the oxidative demethylation of G6Me. In order to evaluate gene regulation, *Z. galactanivorans* was grown with the marine carbohydrates laminarin, agar or porphyran as a sole carbon source. The β-glucan laminarin was selected as a control considering that it is the most abundant polysaccharide in the marine ecosystem<sup>[45]</sup> and agar was chosen as control because it may contain G6Me.<sup>[46]</sup> The genes encoding the P450 monooxygenase (*mgd*), HPS (*hxIA*), and PHI (*hxIB*) were upregulated in the presence of porphyran compared to laminarin and agar (Figure 1c). No upregulation in the presence of agar was observed, a possible explanation for this is the absence of G6Me in agar. Upregulation of *mgd* in the presence of porphyran indicates that there is a possible source of formaldehyde, while at the same time, the upregulation of *hxIA* and *hxIB* suggests that formaldehyde detoxification via the RuMP pathway can occur.

Following this demonstration that the genes of HPS and PHI were upregulated in the presence of porphyran, we wanted to verify whether they encode enzymes that catalyze the key reactions of the RuMP pathway. Therefore, we expressed the enzymes in *Escherichia coli* and purified them (Figure S3, Supporting Information). In order to determine the activity of the enzymes, the R5P-dependent disappearance of formaldehyde was determined using the Nash reagent<sup>[47]</sup> and the formation of F6P was monitored by an enzyme-coupled assay.<sup>[48]</sup> In the presence of D-ribulose-5-phosphate, a decrease in the formaldehyde concentration (Figure 2) and the formation of F6P (Figure S4, Supporting Information) was observed for the





**Figure 1.** The genes encoding for the key enzymes of the RuMP pathway are crucial for formaldehyde resistance of *Z. galactanivorans* and are upregulated in the presence of porphyran. a) Effect of increasing concentrations of formaldehyde on the growth of *F. agariphila* and *Z. galactanivorans*. For each bacterial strain, the growth rate obtained in the absence of formaldehyde was taken as 100%. b) Growth curve of WT,  $\Delta mgd$  (cytochrome P450 monooxygenase) and  $\Delta hxlA-hxlB$  (HPS and PHI) mutant strains of *Z. galactanivorans* in ZoBell 2216 medium containing no or 500  $\mu\text{M}$  formaldehyde. c) Expression of genes encoding cytochrome P450 monooxygenase (*mgd*), 3-hexulose-6-phosphate synthase (*hxlA*) and 6-phospho-3-hexulose isomerase (*hxlB*) in *Z. galactanivorans* grown with laminarin, agar or porphyran as sole carbon source. The effect of substrate on gene expression was tested by one-way ANOVA on log-transformed data, followed by a post-hoc Tukey test (\*,  $P < 0.05$ ). Expression data from the publicly available GEO dataset GSE99940. For a)–c) Values are mean  $\pm$  s.e.m (n = 3).

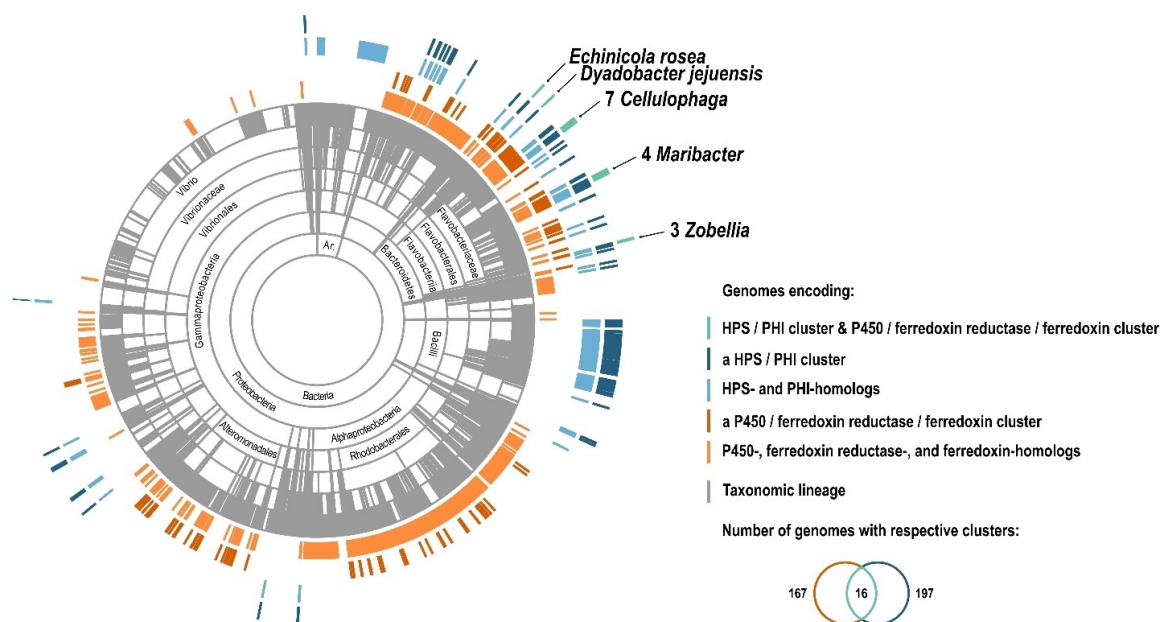


**Figure 2.** HPS and PHI catalyze the incorporation of formaldehyde to produce fructose-6-phosphate. A protein concentration of 10  $\mu\text{g mL}^{-1}$  for HPS and PHI were used in the biocatalysis. For substrates, 0.75 mM D-ribulose-5-phosphate disodium salt and 0.5 mM formaldehyde were used. The reactions were performed in a 50 mM sodium phosphate buffer pH 7.5 supplemented with 5 mM  $\text{MgCl}_2$  for 5 min, at an incubation temperature of 30 °C and an agitation of 1,000 rpm. The formaldehyde concentration was then determined using the Nash reagent. Mean values are shown, error bars present  $\pm$  s.d. (n = 3).

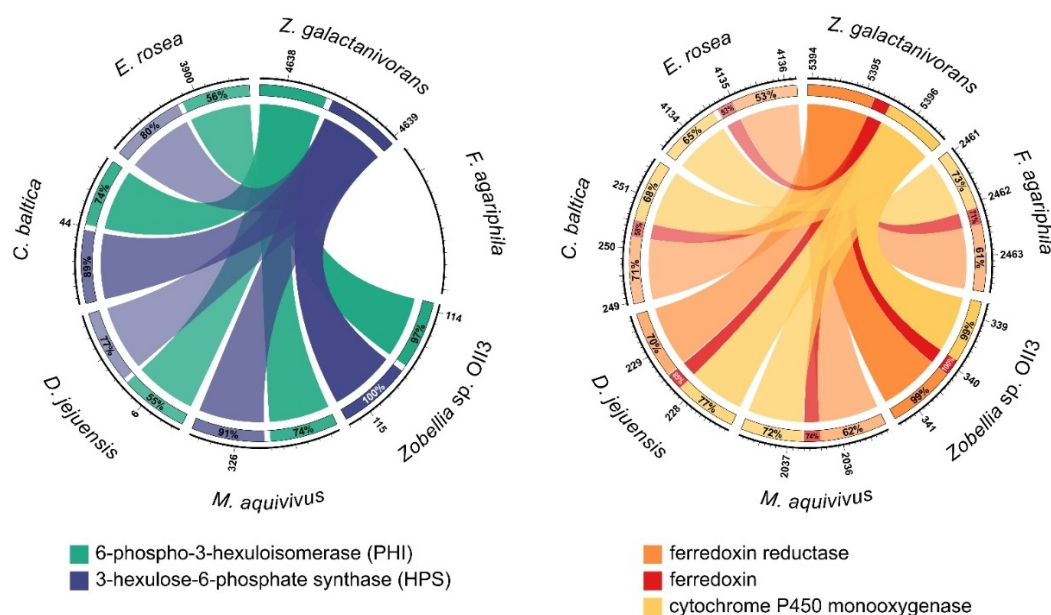
reaction mixture that contained both enzymes. After 5 min incubation at 30 °C, approximately 0.34 mM of the initial formaldehyde concentration of 0.5 mM was removed from the solution, which corresponds to a conversion of 68.5%. Mean-

while, in the control reactions without D-ribulose-5-phosphate and in the absence of either HPS or both enzymes no incorporation of formaldehyde and thus no formation of F6P was observed. For the reaction mixture containing HPS but not PHI, a decrease in formaldehyde could also be detected, which is reasonable considering that HPS catalyzes the reaction of R5P to AH6P independently of PHI. Moreover, the enzymes were able to catalyze the reverse reaction, since very low formation of formaldehyde was observed when F6P was used at a substrate concentration of 20 mM (Figure S5, Supporting Information). In conclusion, *Z. galactanivorans* harbors the active key enzymes of the RuMP pathway.

Since we could prove that *Z. galactanivorans* utilizes the RuMP pathway for formaldehyde detoxification, we were interested in the distribution of this pathway in marine ecosystems. We therefore queried approximately 5,500 marine bacterial genomes from the MarDB and MarRef databases for the key enzymes of the RuMP pathway and identified 197 genomes (equivalent to ~3.58%) encoding HPS- and PHI- gene pairs (Figure 3). Among the 197 genomes, only 16 contain similar cytochrome P450 monooxygenase, ferredoxin reductase, and ferredoxin encoding clusters like *Z. galactanivorans* (Figure 3). The key enzymes of the RuMP pathway as well as the enzymes of the cytochrome P450 cluster were highly similar to those of *Z. galactanivorans*, which is exemplarily shown for five selected reference genomes, including *Cellulophaga*, *Maribacter*, and *Zobellia* in Figure 4.



**Figure 3.** Taxonomic distribution of the RuMP pathway in marine prokaryotes. The colored outer rings indicate the occurrence of the HPS/PHI pairs (dark blue) and the P450 cluster (dark orange). Genomes that encode homologous sequences are shown independently (lighter colors). The intersection of genomes encoding both clusters is shown in green.



**Figure 4.** Key enzymes of the RuMP pathway and the enzymes of the P450 cluster from *Zobellia galactanivorans* are highly similar to those in five selected reference genomes of other marine taxa. The similarity is indicated by the opacity of each link as well as the given percentage within each coding sequence (CDS). The outer scale shows the genomic region of the CDS in kbp.

In addition, these 16 bacterial genomes also featured CAZymes belonging to the GH86 and GH117 families which can catalyze the degradation of agar and porphyran. This supports the hypothesis that the RuMP pathway may be responsible for the detoxification of formaldehyde, which is produced during the degradation of marine carbohydrates and thus may provide growth advantages for these marine bacteria over others.

Besides the marine strains with genomically clustered RuMP-based detoxification genes, we found 104 additional marine isolates where putative HPS and PHI homologs are distributed over the genomes. Interestingly the best hits are found for some *Zobellia*, a few *Maribacter*, and *Cellulophaga* as well as *Arenibacter* strains, which are bacterial genera commonly isolated at the surface of macroalgae.<sup>[49,50]</sup> This suggests that

marine RuMP-based detoxification is mainly specific to bacteria living on multicellular algae, reminiscent of methylotrophic bacteria of the phyllosphere.<sup>[51]</sup>

In summary, we demonstrated in this work that *Z. galactanivorans* exhibited higher resistance to formaldehyde than *F. agariphila* and that this was based on the presence of the RuMP pathway. Consequently, the knockout of the genes, encoding the key enzymes of this pathway, led to a formaldehyde-sensitive strain. We could also demonstrate that in the presence of porphyran the genes encoding the cytochrome P450 monooxygenase and the RuMP pathway were upregulated. This revealed that there is a potential source of formaldehyde through the oxidative demethylation of G6Me and simultaneously a possibility for its detoxification via the RuMP pathway. By verifying the enzyme activity of expressed and purified HPS and PHI, we could demonstrate that the genes encoding the enzymes are indeed responsible for the fixation of formaldehyde. As a result, we were able to provide evidence for a connection between porphyran degradation and formaldehyde detoxification. Genomic analyses in marine genome databases revealed that this pathway is the exception rather than the rule in marine microbes. It may thus provide growth advantages for some marine bacteria over others in the competition for marine polysaccharides.

## Acknowledgements

The authors thank Nolwen Le Duff for technical assistance with microbiology experiments. F.T. acknowledges support from the French government via the National Research Agency program ALGAVOR (ANR-18-CE02-0001). D.B. was supported by a scholarship from the Institute of Marine Biotechnology e.V. We thank the German Research Foundation (DFG) for funding through the Research Unit FOR2406 "Proteogenomics of Marine Polysaccharide Utilization" (POMPU) (grant# BO 1862/17-2 to U.T.B. and SCHW 595/10-2 to T.S.). Open Access funding enabled and organized by Projekt DEAL.

## Conflict of Interest

The authors declare no conflict of interest.

## Data Availability Statement

The data that support the findings of this study are available in the supplementary material of this article.

**Keywords:** Bacteroidetes · carbohydrates · CAZymes formaldehyde detoxification · RuMP pathway

- [1] D. Krause-Jensen, C. M. Duarte, *Nat. Geosci.* **2016**, *9*, 737–742.  
[2] C. Arnosti, M. Wietz, T. Brinkhoff, J. H. Hehemann, D. Probandt, L. Zeugner, R. Amann, *Annu. Rev. Mar. Sci.* **2021**, *13*, 81–108.

- [3] A. Usman, S. Khalid, A. Usman, Z. Hussain, Y. Wang, in *Algae Based Polymers, Blends and Compositions: Chemistry, Biotechnology and Material Sciences* (Eds.: K. M. Zia, M. Zuber, M. Ali), Elsevier, Amsterdam, **2017**, pp. 115–153.  
[4] M. Bäumgen, T. Dutschei, U. T. Bornscheuer, *ChemBioChem* **2021**, *22*, 2247–2256.  
[5] F. Thomas, J. H. Hehemann, E. Rebuffet, M. Czjzek, G. Michel, *Front. Microbiol.* **2011**, *2*, 93.  
[6] J. M. Grondin, K. Tamura, G. Déjean, D. W. Abbott, H. Brumer, *J. Bacteriol.* **2017**, *199*, 15.  
[7] R. Munoz, R. Rosselló-Móra, R. Amann, *Syst. Appl. Microbiol.* **2016**, *39*, 281–296.  
[8] P. Lapébie, V. Lombard, E. Drula, N. Terrapon, B. Henrissat, *Nat. Commun.* **2019**, *10*, 2043.  
[9] H. Teeling, B. M. Fuchs, D. Becher, C. Klockow, A. Gardebrecht, C. M. Bennke, M. Kassabgy, S. Huang, A. J. Mann, J. Waldmann, M. Weber, A. Klindworth, A. Otto, J. Lange, J. Bernhardt, C. Reinsch, M. Hecker, J. Peplies, F. D. Bockelmann, U. Callies, G. Gerdt, A. Wichels, K. H. Wiltshire, F. O. Glöckner, T. Schweder, R. Amann, *Science* **2012**, *336*, 608–611.  
[10] M. Brunet, F. de Bettignies, N. Le Duff, G. Tanguy, D. Davoult, C. Leblanc, A. Gobet, F. Thomas, *Environ. Microbiol.* **2021**, *23*, 1638–1655.  
[11] T. Barbeyron, S. L'Haridon, E. Corre, B. Kloareg, P. Potin, *Int. J. Syst. Evol. Microbiol.* **2001**, *51*, 985–997.  
[12] T. Barbeyron, F. Thomas, V. Barbe, H. Teeling, C. Schenowitz, C. Dossat, A. Goesmann, C. Leblanc, F. O. Glöckner, M. Czjzek, R. Amann, G. Michel, *Environ. Microbiol.* **2016**, *18*, 4610–4627.  
[13] F. Thomas, P. Bordron, D. Eveillard, G. Michel, *Front. Microbiol.* **2017**, *8*, 1808.  
[14] F. Thomas, T. Barbeyron, T. Tonon, S. Génicot, M. Czjzek, G. Michel, *Environ. Microbiol.* **2012**, *14*, 2379–2394.  
[15] F. Thomas, L. C. E. Lundqvist, M. Jam, A. Jeudy, T. Barbeyron, C. Sandström, G. Michel, M. Czjzek, *J. Biol. Chem.* **2013**, *288*, 23021–23037.  
[16] M. Dudek, A. Dieudonné, D. Jouanneau, T. Rochat, G. Michel, B. Sarels, F. Thomas, *Nucleic Acids Res.* **2020**, *48*, 7786–7800.  
[17] D. Jouanneau, L. J. Klau, R. Larocque, A. Jaffrenou, G. Duval, N. Le Duff, T. Roret, A. Jeudy, F. L. Aachmann, M. Czjzek, F. Thomas, *Glycobiology* **2021**, *31*, 1364–1377.  
[18] A. Labourel, M. Jam, A. Jeudy, J. Hehemann, M. Czjzek, G. Michel, *J. Biol. Chem.* **2014**, *289*, 2027–2042.  
[19] A. Labourel, M. Jam, L. Legentil, B. Sylla, J. H. Hehemann, V. Ferrières, M. Czjzek, G. Michel, *Acta Crystallogr. Sect. D* **2015**, *71*, 173–184.  
[20] E. Ficko-Blean, D. Duffieux, É. Rebuffet, R. Larocque, A. Groisillier, G. Michel, M. Czjzek, *Acta Crystallogr.* **2015**, *71*, 209–223.  
[21] E. Ficko-Blean, A. Préchoux, F. Thomas, T. Rochat, R. Larocque, Y. Zhu, M. Stam, S. Génicot, M. Jam, A. Calteau, B. Viart, D. Ropartz, D. Pérez-Pascual, G. Correc, M. Matard-Mann, K. A. Stubbs, H. Rogniaux, A. Jeudy, T. Barbeyron, C. Médigue, M. Czjzek, D. Vallenet, M. J. McBride, E. Ducaud, G. Michel, *Nat. Commun.* **2017**, *8*, 1685.  
[22] J. H. Hehemann, G. Correc, F. Thomas, T. Bernard, T. Barbeyron, M. Jam, W. Helbert, G. Michel, M. Czjzek, *J. Biol. Chem.* **2012**, *287*, 30571–30584.  
[23] E. Rebuffet, A. Groisillier, A. Thompson, A. Jeudy, T. Barbeyron, M. Czjzek, G. Michel, *Environ. Microbiol.* **2011**, *13*, 1253–1270.  
[24] D. A. Rees, E. Conway, *Biochem. J.* **1962**, *84*, 411–416.  
[25] N. S. Anderson, D. A. Rees, *J. Chem. Soc.* **1965**, 5880–5887.  
[26] G. Correc, J. H. Hehemann, M. Czjzek, W. Helbert, *Carbohydr. Polym.* **2011**, *83*, 277–283.  
[27] D. Ropartz, A. Giuliani, M. Fanuel, C. Hervé, M. Czjzek, H. Rogniaux, *Anal. Chim. Acta* **2016**, *933*, 1–9.  
[28] L. Reisky, H. C. Büchschütz, J. Engel, T. Song, T. Schweder, J. H. Hehemann, U. T. Bornscheuer, *Nat. Chem. Biol.* **2018**, *14*, 342–344.  
[29] C. S. Robb, L. Reisky, U. T. Bornscheuer, J. H. Hehemann, *Biochem. J.* **2018**, *475*, 3875–3886.  
[30] N. H. Chen, K. Y. Djoko, F. J. Veyrier, A. G. McEwan, *Front. Microbiol.* **2016**, *7*, 257.  
[31] J. J. A. G. Kamps, R. J. Hopkinson, C. J. Schofield, T. D. W. Claridge, *Commun. Chem.* **2019**, *2*, 126.  
[32] T. Tayri-Wilk, M. Slavin, J. Zamel, A. Blass, S. Cohen, A. Motzik, X. Sun, D. E. Shalev, O. Ram, N. Kalisman, *Nat. Commun.* **2020**, *11*, 3128.  
[33] S. Shishodia, D. Zhang, A. H. El-Sagheer, T. Brown, T. D. W. Claridge, C. J. Schofield, R. J. Hopkinson, *Org. Biomol. Chem.* **2018**, *16*, 4021–4032.  
[34] K. Lu, W. Ye, L. Zhou, L. B. Collins, X. Chen, A. Gold, L. M. Ball, J. A. Swenberg, *J. Am. Chem. Soc.* **2010**, *132*, 3388–3399.

- [35] A. J. Mann, R. L. Hahnke, S. Huang, J. Werner, P. Xing, T. Barbeyron, B. Huettel, K. Stüber, R. Reinhardt, J. Harder, F. O. Glöckner, R. I. Amann, H. Teeling, *Appl. Environ. Microbiol.* **2013**, *79*, 6813–6822.
- [36] T. Strom, T. Ferenci, J. R. Quayle, *Biochem. J.* **1974**, *144*, 465–476.
- [37] I. Goldberg, J. S. Rock, A. Ben-Bassat, R. I. Mateles, *Biotechnol. Bioeng.* **1976**, *18*, 1657–1668.
- [38] W. B. Whitaker, N. R. Sandoval, R. K. Bennett, A. G. Fast, E. T. Papoutsakis, *Curr. Opin. Biotechnol.* **2015**, *33*, 165–175.
- [39] J. E. N. Müller, F. Meyer, B. Litsanov, P. Kiefer, E. Potthoff, S. Heux, W. J. Quax, V. F. Wendisch, T. Brautaset, J. C. Portais, J. A. Vorholt, *Metab. Eng.* **2015**, *28*, 190–201.
- [40] N. Kato, H. Yurimoto, R. K. Thauer, *Biosci. Biotechnol. Biochem.* **2006**, *70*, 10–21.
- [41] S. Desmons, R. Fauré, S. Bontemps, *ACS Catal.* **2019**, *9*, 9575–9588.
- [42] H. He, C. Edlich-Muth, S. N. Lindner, A. Bar-Even, *ACS Synth. Biol.* **2018**, *7*, 1601–1611.
- [43] C. Panagiotopoulos, D. J. Repeta, L. Mathieu, J. F. Rontani, R. Sempéré, *Mar. Chem.* **2013**, *154*, 34–45.
- [44] R. Mitsui, Y. Kusano, H. Yurimoto, Y. Sakai, N. Kato, M. Tanaka, *Appl. Environ. Microbiol.* **2003**, *69*, 6128–6132.
- [45] S. Becker, J. Tebben, S. Coffinet, K. Wiltshire, M. H. Iversen, T. Harder, K. U. Hinrichs, J. H. Hehemann, *Proc. Natl. Acad. Sci. USA* **2020**, *117*, 6599–6607.
- [46] A. Chiovitti, A. Bacic, D. J. Craik, G. T. Kraft, M. L. Liao, *Carbohydr. Res.* **2004**, *339*, 1459–1466.
- [47] T. Nash, *Biochem. J.* **1953**, *55*, 416–421.
- [48] H.-J. Hohorst, *Methods Enzym. Anal.* **1965**, 134–138.
- [49] M. Martin, D. Portetelle, G. Michel, M. Vandenbol, *Appl. Microbiol. Biotechnol.* **2014**, *98*, 2917–2935.
- [50] M. Martin, T. Barbeyron, R. Martin, D. Portetelle, G. Michel, M. Vandenbol, *Front. Microbiol.* **2015**, *6*, 1487.
- [51] J. A. Vorholt, *Nat. Rev. Microbiol.* **2012**, *10*, 828–840.

---

Manuscript received: May 10, 2022

Accepted manuscript online: May 13, 2022

Version of record online: May 30, 2022

# ChemBioChem

Supporting Information

## **Connecting Algal Polysaccharide Degradation to Formaldehyde Detoxification**

Stefan Brott, François Thomas, Maike Behrens, Karen Methling, Daniel Bartosik, Theresa Dutschei, Michael Lalk, Gurvan Michel, Thomas Schweder, and Uwe T. Bornscheuer\*

## Supporting Information

## Table of Contents

Experimental Procedures.....	2
Figure S1: Structure of porphyrin.....	5
Figure S2: Effect of increasing concentrations of formaldehyde on the growth of <i>F. agariphila</i> and <i>Z. galactanivorans</i> .....	5
Figure S3: SDS-PAGE of purified proteins.....	6
Figure S4: Coupled enzyme assay for the detection of F6P formation.....	6
Figure S5: Formaldehyde formation in the reverse reaction.....	7
Table S1: Annotated genes for <i>F. agariphila</i> and <i>Z. galactanivorans</i> from known formaldehyde detoxification pathways.....	8
Table S2: Primers used in this study.....	8
Table S3: Bacterial strains and plasmids used in this study.....	9
References.....	9
Author Contribution.....	10

## Experimental Procedures

### Reagents

D-Ribulose-5-phosphate and D-fructose-6-phosphate were purchased as disodium salts from Sigma Aldrich. The 37% formaldehyde solution was also purchased from Sigma Aldrich. All other chemicals were purchased at the highest purity from Sigma-Aldrich, Carl Roth, Alfa Aesar or Acros.

### Gene deletions in *Z. galactanivorans*

Deletion mutants of genes encoding a cytochrome P450 monooxygenase (ZGAL\_4677) and both, a putative 3-hexulose-6-phosphate synthase (ZGAL\_3942, HxlA) and a 6-phospho-3-hexulose isomerase (ZGAL\_3941, HxlB) were constructed using a *sacB* system described previously.<sup>[1]</sup> All primers and strains are listed in **Tables S2** and **S3**. To delete *zgal\_4677*, a 2,049 bp fragment including the first 36 bp of *zgal\_4677* and 2,013 bp of upstream sequence was amplified using primers OFT0046 and OFT0048 on genomic DNA from *Z. galactanivorans* Dsij<sup>T</sup>. The fragment was digested with BamHI and XbaI and ligated into pYT313 that had been digested with the same enzymes, to generate pFT14. A 2,222 bp fragment including the final 57 bp of *zgal\_4677* and 2,165 bp of downstream sequence was amplified using primers OFT0047 and OFT0049. The fragment was cloned into XbaI and PstI sites of pFT2 to generate the *zgal\_4677* deletion construct pFT15. To delete *zgal\_3941* and *zgal\_3942*, a 2,013 bp fragment including the first 27 bp of *zgal\_3941* and 1,986 bp of upstream sequence was amplified using primers OFT0052 and OFT0054. The fragment was digested with XbaI and Sall and ligated into pYT313 that had been digested with the same enzymes, to generate pFT16. A 1,491 bp fragment including the final 27 bp of *zgal\_3942* and 1,464 bp of downstream sequence was amplified using primers OFT0053 and OFT0055. The fragment was cloned into Sall and PstI sites of pFT16 to generate the *zgal\_3941-3942* deletion construct pFT17. Plasmids pFT15 and pFT17 were introduced individually into the wild-type *Z. galactanivorans* Dsij<sup>T</sup> by conjugation from *E. coli* S17-1. Conjugants with plasmids integrated in the genome were isolated on Cytophaga-agar containing 50 µg mL<sup>-1</sup> erythromycin. Single erythromycin-resistant colonies were grown overnight at 30 °C in Cytophaga medium without antibiotics. Cells that lost the plasmid through a second recombination were selected on Cytophaga-agar containing 5% sucrose. Isolated colonies were checked for erythromycin sensitivity. Deletions were confirmed by PCR and sequencing on isolated colonies using primer pairs OFT0050- OFT0051 to identify the *zgal\_4677* deletion mutant (mZG\_0084), and primers OFT0056-OFT0057 to identify the *zgal\_3941-3942* deletion mutant (mZG\_0082).

### Bacterial growth

*F. agariphila* KMM 3901<sup>T</sup> and *Z. galactanivorans* Dsij<sup>T</sup> strains were routinely grown from glycerol stocks in Zobell 2216E medium at 25 °C. Their resistance to formaldehyde was tested by inoculating them (initial OD<sub>600</sub> 0.05) in 50 mL flasks containing 5 mL Zobell 2216E medium with increasing initial formaldehyde concentration (10 µM – 1 mM). To test the effect of gene deletions, *Z. galactanivorans* WT, mZG0082 ( $\Delta$ *zgal\_3941-3942*) and mZG0084 ( $\Delta$ *zgal\_4677*) strains were grown in 5 mL Zobell 2216E medium with or without 500 µM formaldehyde. All tests were performed in triplicates and growth was followed by monitoring OD<sub>600</sub> on 180 µL of culture using a microplate spectrophotometer (Spark Tecan, Männedorf, Switzerland).

### Gene expression analysis

Expression data were retrieved from a previously published study<sup>[2]</sup> with a publicly available GEO dataset GSE99940. Briefly, *Z. galactanivorans* Dsij<sup>T</sup> was grown in marine minimum medium with 2 g L<sup>-1</sup> laminarin, agar or porphyrin as a sole carbon source. After 48 h, RNA was retrieved from cells for cDNA synthesis and analyzed on a custom microarray. The effect of substrate on gene expression was tested by one-way ANOVA on normalized and log-transformed data, followed by a post-hoc Tukey test.

### **Cloning and expression in *E. coli***

Synthetic genes, codon optimized for expression in *E. coli*, encoding HPS and PHI from *Z. galactanivorans*, were synthesized and cloned into the pET-51b vector by BioCat GmbH (Heidelberg, Germany). The constructs encoded the recombinant proteins as fusions to a cleavable N-terminal Strep-tag for affinity purification. Chemically competent *E. coli* BL21 (DE3) cells were transformed with the plasmids harboring HPS or PHI and were spread on lysogeny broth (LB) agar plates containing 100 µg mL<sup>-1</sup> ampicillin. The agar plates were incubated overnight at 37 °C. One colony was picked and used to inoculate 5 mL LB medium which contained 100 µg mL<sup>-1</sup> ampicillin and was then incubated at 37 °C and 180 rpm overnight. For overexpression the cultivation was performed with 200 mL LB medium containing 100 µg mL<sup>-1</sup> ampicillin in a 1 L flask. The LB medium was inoculated with the overnight culture so that a starting optical density (OD<sub>600</sub>) of 0.05 was obtained. Cells were then incubated at 37 °C and 180 rpm until an OD<sub>600</sub> of 1 was reached. Expression of target enzymes was then induced by the addition of 1 mM isopropyl-β-D-thiogalactopyranoside (IPTG). For the expression of HPS, 1 mM MgCl<sub>2</sub> was supplemented simultaneously and the cultivation was then continued at 25 °C and 180 rpm overnight. For PHI, cultivation was subsequently continued at 20 °C and 180 rpm overnight after the addition of IPTG. Cells were harvested by centrifugation at 10,000 x g and 4 °C for 30 min, washed with 50 mM sodium phosphate buffer pH 7.5, and subsequently stored at -20 °C until cell disruption.

### **Purification**

For cell disruption, the cell pellet was resuspended in 10 mL of lysis buffer (100 mM TRIS-HCl buffer (pH 8.0) containing 500 mM NaCl, 5 mM MgCl<sub>2</sub>, 0.1% Triton-X-100, and 1 mM phenylmethylsulfonyl fluoride). Cell disruption on ice was performed using a Sonoplus HD 2070 ultrasonic homogenizer (Bandelin electronic GmbH & Co. KG, Berlin, Germany) with the program: 2 × 3 min, 50% power, 50% cycle time. Cell debris was subsequently removed by centrifugation at 10,000 x g and 4 °C for 30 min. Purification utilizing gravity flow columns was performed using 10 mL of the Strep-Tactin® Sepharose® 50% suspension (IBA Lifesciences GmbH, Göttingen, Germany) as column material. After equilibration of the column with the wash buffer (100 mM TRIS-HCl buffer (pH 8.0), which contained 500 mM NaCl, 5 mM MgCl<sub>2</sub> and 0.1% Triton-X-100), the clarified lysate was applied. Unbound proteins were then removed from the column by excessive washing with the wash buffer. Elution of the target enzymes was then performed with the elution buffer 100 mM TRIS-HCl buffer (pH 8.0), which contained 2.5 mM D-desthiobiotin in addition to 500 mM NaCl and 5 mM MgCl<sub>2</sub>. Elution fractions were pooled and concentrated using a Vivaspin 6 centrifugal concentrator with a 10 kDa molecular weight cut-off (Sartorius AG, Göttingen, Germany). PD-10 desalting columns (Cytiva Europe GmbH, Freiburg, Germany) were then used to desalt the sample and exchange the elution buffer to a 50 mM sodium phosphate buffer pH 7.5 supplemented with 5 mM MgCl<sub>2</sub>.

### **Sodium dodecyl sulfate-polyacrylamide gel electrophoresis**

Sodium dodecyl sulfate-polyacrylamide gel electrophoresis (SDS-PAGE) was performed to verify the purity of the target enzymes. 20 µL protein sample was mixed with 5 µL of a 5-fold stock of SDS sample buffer (100 mM TRIS-HCl buffer (pH 6.8) containing 4% w/v SDS, 20% v/v glycerol, 2% (v/v) β-mercaptoethanol, 25 mM EDTA and 0.04% w/v bromophenol blue) and denatured by incubation at 95 °C for 10 min. For the SDS-PAGE a 12.5% acrylamide gel (separating gel) and a 4.0% loading gel were used. Electrophoresis was carried out at 200 V. Proteins were stained with Coomassie Blue (PhastGel® Blue R, Sigma Aldrich, Taufkirchen, Germany). As reference the Pierce™ Unstained protein molecular weight marker (Thermo Scientific, Waltham, MA, USA) was used.

### **Determination of protein concentration**

Protein concentrations were determined using the Pierce™ BCA Protein Assay Kit (Thermo Fisher Scientific, Waltham, MA, USA).

### **Enzyme assays**

Activity of HPS was assayed by the D-ribulose-5-phosphate-dependent disappearance of formaldehyde and by the formation of F6P. A protein concentration of 10 µg mL<sup>-1</sup> for HPS and PHI were used in the biocatalysis. As substrates, 0.75 mM D-ribulose-5-phosphate disodium salt and 0.5 mM formaldehyde were used. The reaction volume was 0.2 mL and the reactions were performed in a 50 mM sodium phosphate buffer (pH 7.5) supplemented with 5 mM MgCl<sub>2</sub> for 5 min at an incubation temperature of 30 °C and an agitation of 1000 rpm. The formaldehyde concentration was then determined using the Nash reagent.<sup>[3]</sup>

In the reverse reaction a protein concentration of 50 µg mL<sup>-1</sup> for each enzyme and 20 mM D-fructose-6-phosphate disodium salt as substrate were used. The reaction volume was 0.2 mL and the reactions were performed in a 50 mM sodium phosphate buffer pH 7.5 supplemented with 5 mM MgCl<sub>2</sub> for 10 minutes at an incubation temperature of 30 °C and an agitation of 1000 rpm. Formaldehyde formation was then detected using the Nash reagent.<sup>[3]</sup>

Additionally, F6P formation was detected by coupling HPS and PHI with the phosphoglucose isomerase (PGI) from yeast (Roche Holding AG, Basel, Switzerland) and the glucose-6-phosphate dehydrogenase (G6pDHG) from baker's yeast Type XV (Sigma Aldrich, St. Louis, MO, USA).<sup>[4]</sup> A protein concentration of 10 µg mL<sup>-1</sup> was used for HPS and PHI, and 5 U mL<sup>-1</sup> were used for PGI and G6pDHG. For substrates, 0.75 mM D-ribulose-5-phosphate disodium salt, 0.5 mM formaldehyde and 0.5 mM NADP<sup>+</sup> were used. The reaction was carried out in a 50 mM TRIS-HCl buffer (pH 7.5) containing 5 mM MgCl<sub>2</sub> at 30 °C. The absorbance at 340 nm was measured every 2 min using the Infinite® M200 pro microplate reader (Tecan Group Ltd., Männedorf, Switzerland).



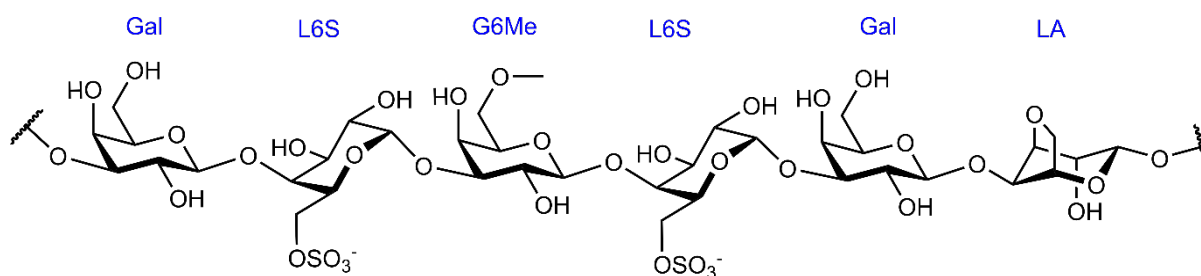
### Formaldehyde quantification

For the determination of the formaldehyde concentration, 0.2 mL freshly prepared Nash reagent<sup>[3]</sup> was added immediately to the reaction mixture, this mix was then immediately incubated at 50 °C at an agitation of 1,000 rpm for 10 min. After centrifugation at 17,000 x *g* for 2 min to remove precipitated proteins, the mixture was transferred to a microtiter plate and absorbance was measured at 420 nm. The formaldehyde concentration was then determined by a formaldehyde standard curve, which was prepared in parallel to the reaction mixture.

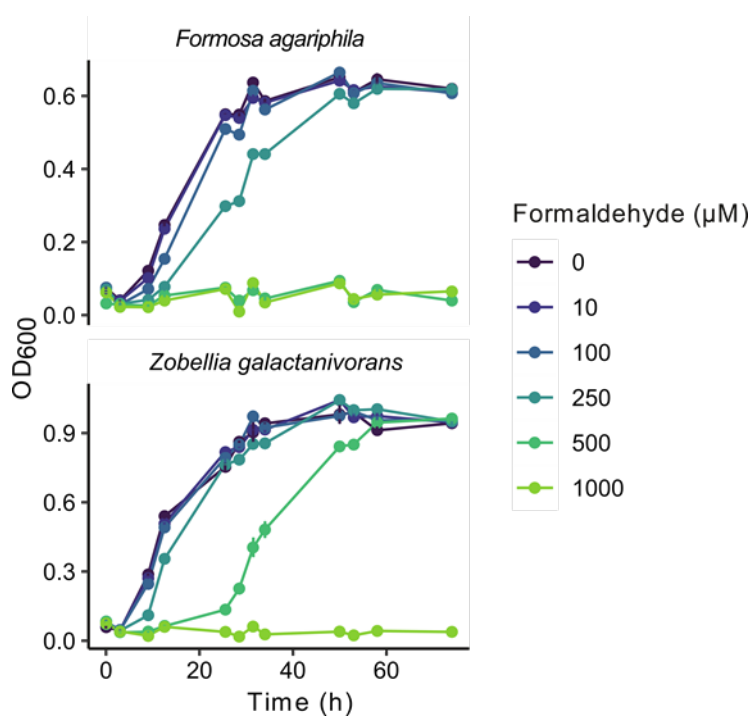
### Computational analysis

RefSeq assemblies of genomes deposited in MarRef (v1.5) and MarDB (v1.5)<sup>[5]</sup> were downloaded from NCBI<sup>[6]</sup> to create a target database. Translated coding sequences were compared to TIGRFAM profiles TIGR03127.1 (6-phospho-3-hexuloisomerase) and TIGR03128.1 (3-hexulose-6-phosphate synthase) as well as to PFAM models PF07992.17 together with PF14759.9 (to aim for ferredoxin reductase homologs, ZOBGAL\_RS21970), PF00111.30 (for putative ferredoxins, ZOBGAL\_RS21975) and PF00067.25 (for putative cytochrome P450 monooxygenases, ZOBGAL\_RS21980) using the hmmscan function of HMMER v3.3.2<sup>[7]</sup> with model-specific noise cutoff threshold (--cut\_nc). Results were then compared to *Z. galactanivorans* Dsij<sup>T</sup> sequences ZOBGAL\_RS18540 (HPS), ZOBGAL\_RS18545 (PHI), ZOBGAL\_RS21970, ZOBGAL\_RS21975, and ZOBGAL\_RS21980 using Protein-Protein BLAST v2.11.0+<sup>[8]</sup> with default settings. Circos was used to visualize similarity on protein level<sup>[9]</sup>.

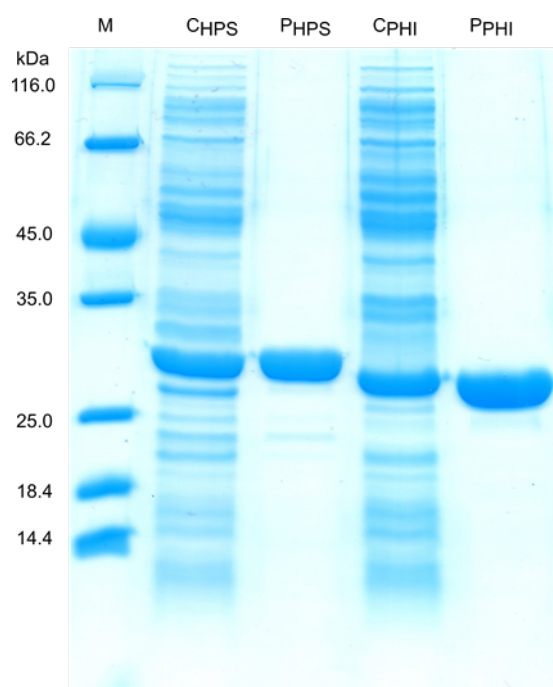
## Supporting Figures



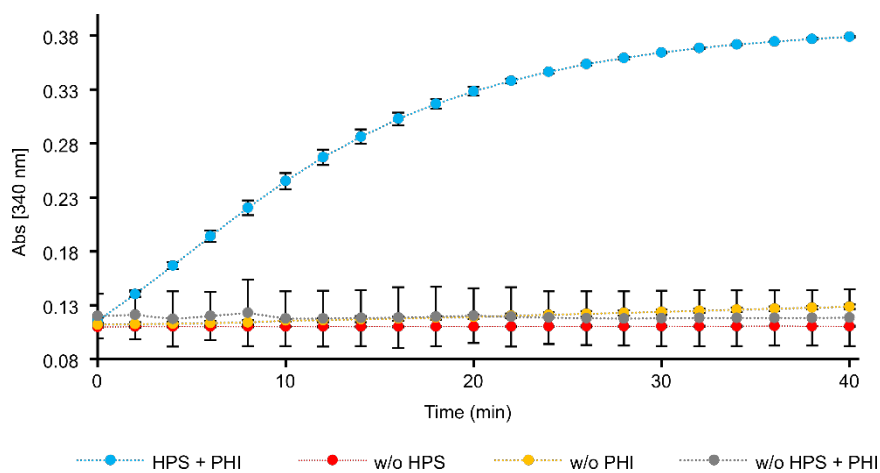
**Figure S1: Structure of porphyran.** The porphyran backbone consists of chains composed mainly of the alternating monosaccharide units 4-linked- $\alpha$ -L-galactose-6-sulfate (L6S) and 3-linked- $\beta$ -D-galactose (Gal) or 3,6-anhydro- $\alpha$ -L-galactose (LA). In addition, O-methylation of D-galactose results in the presence of the methoxy sugar 6-O-methyl-D-galactose (G6Me).



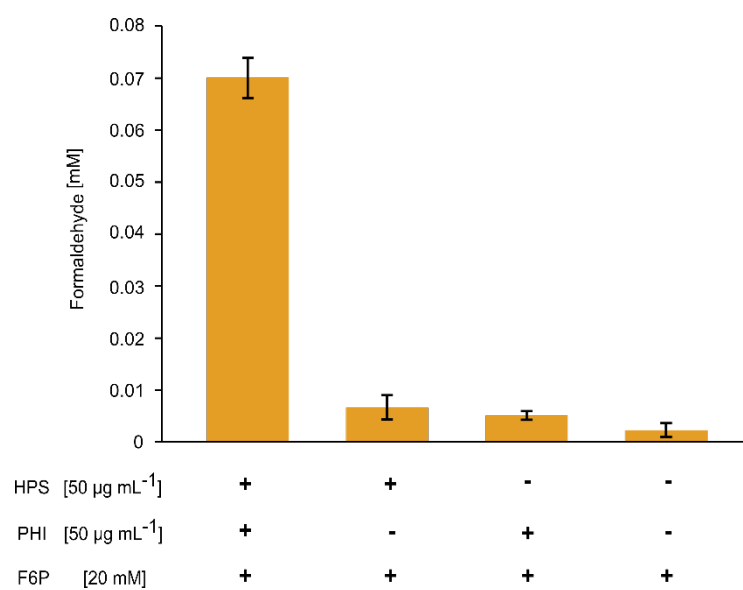
**Figure S2: Effect of increasing concentrations of formaldehyde on the growth of *F. agariphila* and *Z. galactanivorans*.** Growth was performed with Zobell 2216E medium with increasing initial formaldehyde concentration at 25 °C. Values are mean  $\pm$  s.e.m. (n = 3).



**Figure S3: SDS-PAGE of purified proteins.** The purified proteins (P) and the crude cell extract (C) were separated on a 12.5% gel and stained with Coomassie blue. 7.5  $\mu\text{g}$  of the proteins were loaded onto the gel. As reference (M) the Pierce™ Unstained protein molecular weight marker (Thermo Scientific, Waltham, MA, USA) was used. The experiment was repeated independently with similar results.



**Figure S4: Coupled enzyme assay for the detection of F6P formation.** Formed F6P is converted by PGI to glucose-6-phosphate, which is then oxidized by G6pDHG under  $\text{NADP}^+$  consumption to D-glucono-1,5-lactone-6-phosphate. A protein concentration of  $10 \mu\text{g mL}^{-1}$  was used for HPS and PHI, and  $5 \text{ U mL}^{-1}$  was used for PGI and G6pDHG. For substrates,  $0.75 \text{ mM}$  D-ribulose-5-phosphate,  $0.5 \text{ mM}$  formaldehyde and  $0.5 \text{ mM}$   $\text{NADP}^+$  were used. The reaction was carried out in a  $50 \text{ mM}$  TRIS-HCl buffer (pH 7.5) containing  $5 \text{ mM}$   $\text{MgCl}_2$  at  $30 \text{ }^\circ\text{C}$ . The absorbance at  $340 \text{ nm}$  was measured every 2 min using the Infinite® M200 pro microplate reader. Mean values are shown, error bars present  $\pm$  s.d. ( $n = 3$ ).



**Figure S5: Formaldehyde formation in the reverse reaction.** A protein concentration of 50  $\mu\text{g mL}^{-1}$  for each enzyme and 20 mM D-fructose-6-phosphate as substrate were used. The reaction volume was 0.2 mL and the reactions were performed in a 50 mM sodium phosphate buffer pH 7.5 supplemented with 5 mM  $\text{MgCl}_2$  for 10 min at an incubation temperature of 30 °C and an agitation of 1,000 rpm. Mean values are shown, error bars present  $\pm$  s.d. (n = 3).

## Supporting Tables

**Table S1: Annotated genes found in the NCBI database for *F. agariphila* KMM3901<sup>T</sup> and *Z. galactanivorans* Dsij<sup>T</sup>, which encode enzymes involved in known formaldehyde detoxification pathways.** The accession number is given for each gene.

Annotated enzyme activity	<i>F. agariphila</i> KMM3901 <sup>T</sup>	<i>Z. galactanivorans</i> Dsij <sup>T</sup>
3-Hexulose-6-phosphate synthase	-	WP_013995270.1
6-Phospho-3-hexuloisomerase	-	WP_013995269.1
Serine hydroxymethyltransferase	WP_038533459.1	WP_013996064.1
Bifunctional methylenetetrahydrofolate dehydrogenase/methenyltetrahydrofolate cyclohydrolase	WP_038527446.1	WP_013993916.1
Formyltetrahydrofolate deformylase	WP_038527618.1	WP_215931961.1

**Table S2: Primers used in this study.**

Primers	Sequence and Description
OFT0046	5' TTTTTTGGATCC <sup>TCCTTATAGTCGGGTATATCAAGG</sup> 3'; forward primer used in construction of pFT14; BamHI site underlined
OFT0047	5' GAGTTGACCACAGAACCATAACC 3'; reverse primer used in construction of pFT15; PstI site downstream in amplified fragment
OFT0048	5' TTTTTTCTAGATTTTCAAACGGGTCTGGAAGC 3'; reverse primer used in construction of pFT14; XbaI site underlined
OFT0049	5' TTTTTTCTAGACAGCGTAAAGTAGGTTTTCATAAC 3'; forward primer used in construction of pFT15; XbaI site underlined
OFT0050	5' GGCTCTAATATGGGTTGCATCCG 3'; forward primer to confirm deletion of <i>zgal_4677</i>
OFT0051	5' ATATCGGTCTCTATCTCACTGGC 3'; reverse primer to confirm deletion of <i>zgal_4677</i>
OFT0052	5' TTTTTTCTAGAAGTTGGCATTGAAAGCTGTAGG 3'; forward primer used in construction of pFT16; XbaI site underlined
OFT0053	5' TTTTTTCTGCAGCAGAAGTAAAAATCCAATGACTTTTAGC 3'; reverse primer used in construction of pFT17; PstI site underlined
OFT0054	5' TTTTTTGTCGACCTTGCTTTCATCAAGTATGTTCTCC 3'; reverse primer used in construction of pFT16; Sall site underlined
OFT0055	5' TTTTTTGTCGACGAGCTAAAGGAATTATTGGAAGCC 3'; forward primer used in construction of pFT17; Sall site underlined
OFT0056	5' CGGACGAGGGGTTAAATAGCC 3'; forward primer to confirm deletion of <i>zgal_3941-3942</i>
OFT0057	5' TTCGTCTTTTGAATTATGAGGAGGC 3'; reverse primer to confirm deletion of <i>zgal_3941-3942</i>

**Table S3: Bacterial strains and plasmids used in this study.**

	Description <sup>a</sup>	Ref.
<b><i>E. coli</i> strains</b>		
NEB5α	Strain used for general cloning Genotype: <i>fhuA2 (argF-lacZ)U169 phoA glnV44 80 (lacZ)M15 gyrA96 recA1 relA1 endA1 thi-1 hsdR17</i>	New England Biolabs (Ipswich, MA, USA)
S17-1 λ pir	Strain used for conjugation with <i>Z. galactanivorans</i> Genotype: <i>λpir hsdR pro thi</i> ; chromosomal integrated RP4-2 Tc::Mu Km::Tn7	[10]
<b>Marine strains</b>		
<i>F. agariphila</i> KMM 3901 <sup>T</sup>	wild type <i>F. agariphila</i> strain	[11]
<i>Z. galactanivorans</i> Dsij <sup>T</sup> (DSM 12802)	wild type <i>Z. galactanivorans</i> strain	[12]
mZG0082	Δ <i>zgal_3941-3942</i> in <i>Z. galactanivorans</i> Dsij <sup>T</sup>	This study
mZG0084	Δ <i>zgal_4677</i> in <i>Z. galactanivorans</i> Dsij <sup>T</sup>	This study
<b>Plasmids</b>		
pYT313	Suicide vector carrying <i>sacB</i> under <i>F. johnsoniae ompA</i> promoter; Ap <sup>r</sup> (Em <sup>r</sup> )	[1]
pFT14	2,049 bp region upstream of <i>Z. galactanivorans zgal_4677</i> amplified with primers OFT0046 and OFT0048 and cloned into BamHI and XbaI sites of pYT313; Ap <sup>r</sup> (Em <sup>r</sup> )	This study
pFT15	Construct used to delete <i>Z. galactanivorans zgal_4677</i> ; 2,222 bp region downstream of <i>zgal_4677</i> amplified with primers OFT0047 and OFT0049 and cloned into PstI and XbaI sites of pFT14; Ap <sup>r</sup> (Em <sup>r</sup> )	This study
pFT16	2,013 bp region upstream of <i>Z. galactanivorans zgal_3941</i> amplified with primers OFT0052 and OFT0054 and cloned into XbaI and Sall sites of pYT313; Ap <sup>r</sup> (Em <sup>r</sup> )	This study
pFT17	Construct used to delete <i>Z. galactanivorans zgal_3941-3942</i> ; 1,491 bp region downstream of <i>zgal_3942</i> amplified with primers OFT0053 and OFT0055 and cloned into PstI and Sall sites of pFT16; Ap <sup>r</sup> (Em <sup>r</sup> )	This study

<sup>a</sup>Antibiotic resistance phenotypes: ampicillin, Ap<sup>r</sup>; erythromycin, Em<sup>r</sup>. Antibiotic resistance phenotypes are those expressed in *E. coli*. The antibiotic resistance phenotypes given in parentheses are those expressed in *Z. galactanivorans* but not in *E. coli*.

## References

- [1] Y. Zhu, F. Thomas, R. Larocque, N. Li, D. Duffieux, L. Cladière, F. Souchaud, G. Michel, M. J. McBride, *Environ. Microbiol.* **2017**, *19*, 2164–2181.
- [2] F. Thomas, P. Bordron, D. Eveillard, G. Michel, *Front. Microbiol.* **2017**, *8*, 1808.
- [3] T. Nash, *Biochem. J.* **1953**, *55*, 416–421.
- [4] H.-J. Hohorst, *Methods Enzym. Anal.* **1965**, 134–138.
- [5] T. Klemetsen, I. A. Raknes, J. Fu, A. Agafonov, S. V. Balasundaram, G. Tartari, E. Robertsen, N. P. Willassen, *Nucleic Acids Res.* **2018**, *46*, D693–D699.
- [6] E. W. Sayers, J. Beck, J. R. Brister, E. E. Bolton, K. Canese, D. C. Comeau, K. Funk, A. Ketter, S. Kim, A. Kimchi, P. A. Kitts, A. Kuznetsov, S. Lathrop, Z. Lu, K. McGarvey, T. L. Madden, T. D. Murphy, N. O'Leary, L. Phan, V. A. Schneider, F. Thibaud-Nissen, B. W. Trawick, K. D. Pruitt, J. Ostell, *Nucleic Acids Res.* **2020**, *48*, D9–D16.
- [7] R. D. Finn, J. Clements, S. R. Eddy, *Nucleic Acids Res.* **2011**, *39*, 29–37.
- [8] B. B. Salgaonkar, M. Kabilan, J. M. Braganca, *World J. Microbiol. Biotechnol.* **2011**, *27*, 403–410.
- [9] M. Krzywinski, J. Schein, I. Birol, J. Connors, R. Gascoyne, D. Horsman, S. J. Jones, M. A. Marra, *Genome Res.* **2009**, *19*, 1639–1645.
- [10] V. de Lorenzo, K. N. Timmis, *Methods Enzymol.* **1994**, *235*, 386–405.
- [11] A. J. Mann, R. L. Hahnke, S. Huang, J. Werner, P. Xing, T. Barbeyron, B. Huettel, K. Stüber, R. Reinhardt, J. Harder, F. O. Glöckner, R. I. Amann, H. Teeling, *Appl. Environ. Microbiol.* **2013**, *79*, 6813–6822.
- [12] T. Barbeyron, S. L'Haridon, E. Corre, B. Kloareg, P. Potin, *Int. J. Syst. Evol. Microbiol.* **2001**, *51*, 985–997.

## Author Contributions

M.G., T.S. and U.T.B. initiated the study and directed the project. F.T. conducted the growth studies and created the knock-out strains. S.B. and M.B. expressed and purified the enzymes and performed the biocatalysis. D.B. performed the computational analysis. K.M. and M.L. performed metabolite analysis, S.B. prepared the main manuscript, which was revised by F.T., T.D, M.G, T.S. and U.T.B. and approved by all authors.

# Article II







# Unique alcohol dehydrogenases involved in algal sugar utilization by marine bacteria

Stefan Brott<sup>1</sup> · Ki Hyun Nam<sup>2</sup> · François Thomas<sup>3</sup> · Theresa Dutschei<sup>1</sup> · Lukas Reisky<sup>1</sup> · Maike Behrens<sup>1</sup> · Hanna C. Grimm<sup>1</sup> · Gurvan Michel<sup>3</sup> · Thomas Schweder<sup>4</sup> · Uwe T. Bornscheuer<sup>1</sup>

Received: 25 October 2022 / Revised: 20 February 2023 / Accepted: 21 February 2023  
© The Author(s) 2023

## Abstract

Marine algae produce complex polysaccharides, which can be degraded by marine heterotrophic bacteria utilizing carbohydrate-active enzymes. The red algal polysaccharide porphyran contains the methoxy sugar 6-*O*-methyl-*D*-galactose (G6Me). In the degradation of porphyran, oxidative demethylation of this monosaccharide towards *D*-galactose and formaldehyde occurs, which is catalyzed by a cytochrome P450 monooxygenase and its redox partners. In direct proximity to the genes encoding for the key enzymes of this oxidative demethylation, genes encoding for zinc-dependent alcohol dehydrogenases (ADHs) were identified, which seem to be conserved in porphyran utilizing marine *Flavobacteriia*. Considering the fact that dehydrogenases could play an auxiliary role in carbohydrate degradation, we aimed to elucidate the physiological role of these marine ADHs. Although our results reveal that the ADHs are not involved in formaldehyde detoxification, a knockout of the ADH gene causes a dramatic growth defect of *Zobellia galactanivorans* with G6Me as a substrate. This indicates that the ADH is required for G6Me utilization. Complete biochemical characterizations of the ADHs from *Formosa agariphila* KMM 3901<sup>T</sup> (FoADH) and *Z. galactanivorans* Dsij<sup>T</sup> (ZoADH) were performed, and the substrate screening revealed that these enzymes preferentially convert aromatic aldehydes. Additionally, we elucidated the crystal structures of FoADH and ZoADH in complex with NAD<sup>+</sup> and showed that the strict substrate specificity of these new auxiliary enzymes is based on a narrow active site.

## Key points

- Knockout of the ADH-encoding gene revealed its role in 6-*O*-methyl-*D*-galactose utilization, suggesting a new auxiliary activity in marine carbohydrate degradation.
- Complete enzyme characterization indicated no function in a subsequent reaction of the oxidative demethylation, such as formaldehyde detoxification.
- These marine ADHs preferentially convert aromatic compounds, and their strict substrate specificity is based on a narrow active site.

**Keywords** Alcohol dehydrogenase · Porphyran · CAZyme · Bacteroidetes · *Zobellia galactanivorans* · Auxiliary activity

✉ Uwe T. Bornscheuer  
uwe.bornscheuer@uni-greifswald.de

<sup>1</sup> Department of Biotechnology & Enzyme Catalysis, Institute of Biochemistry, University of Greifswald, 17487 Greifswald, Germany

<sup>2</sup> Department of Life Science, Pohang University of Science and Technology, Pohang 37673, South Korea

<sup>3</sup> Laboratory of Integrative Biology of Marine Models (LBI2M), Station Biologique de Roscoff (SBR), Sorbonne Université, CNRS 29688, Roscoff, Bretagne, France

<sup>4</sup> Department of Pharmaceutical Biotechnology, Institute of Pharmacy, University of Greifswald, 17487 Greifswald, Germany

## Introduction

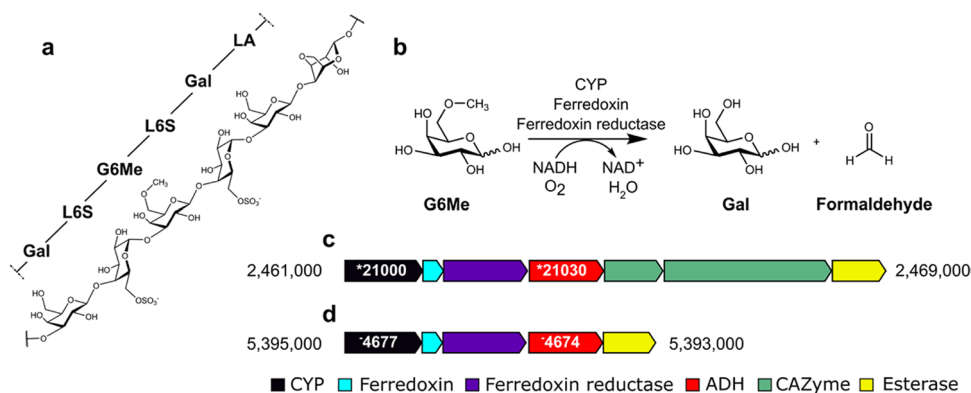
Marine algae represent one of the most crucial primary producers within the marine carbon cycle and contribute to approximately 50% of the total global primary production (Field 1998). For instance, macroalgae sequester approximately 173 GT of carbon dioxide/year (Krause-Jensen and Duarte 2016) and accumulate the excess carbon in the form of carbohydrates, which they utilize as cell wall constituents or for energy storage (Arnosti et al. 2021). Degradation of these marine polysaccharides can be extremely complicated due to their complexity and the occurrence of side chain

modifications like sulfations, methylations, or acetylations (Bäumgen et al. 2021a). It was shown that complex enzymatic cascades are required for the breakdown of a single algal polysaccharide (Reisky et al. 2019; Sichert et al. 2020). Members of the bacterial phylum *Bacteroidetes* are considered specialists in the pivotal degradation of marine polysaccharides (Thomas et al. 2011a) and are observed as first responders after micro- and macroalgal blooms (Teeling et al. 2012; Brunet et al. 2021). They contain specific gene clusters referred to as polysaccharide utilization loci (PULs) (Grondin et al. 2017), which encode for carbohydrate-active enzymes (CAZymes) that catalyze the breakdown of the carbohydrates (Lapébie et al. 2019), as well as proteins essential for the binding and uptake of smaller sugar molecules (Bauer et al. 2006; Martens et al. 2009). Characterizing individual CAZymes helps elucidate the complete degradation pathways of marine carbohydrates and provides a deeper understanding of the global carbon cycle, which has been successfully performed, for instance, for ulvan from green algae (Reisky et al. 2019; Bäumgen et al. 2021b), fucoidan from brown algae (Sichert et al. 2020), and carrageenan from red algae (Ficko-Blean et al. 2017).

Recently, we have demonstrated that in the degradation process of the red algal galactan porphyran (Fig. 1a) by marine bacteria, oxidative demethylation of the methoxy sugar 6-*O*-methyl-*D*-galactose (G6Me) occurs (Reisky et al. 2018). This reaction, which is catalyzed by a cytochrome P450 monooxygenase (CYP) and its respective redox partners consisting of ferredoxin reductase and ferredoxin, leads to the formation of equimolar amounts of *D*-galactose and

formaldehyde (Fig. 1b) (Reisky et al. 2018). It was hypothesized that this reaction is crucial in terms of G6Me utilization as it removes the highly stable methyl ether, consequently generating an easily metabolizable compound (Reisky et al. 2018). The crystal structure of the CYP from *Zobellia galactanivorans* Dsij<sup>T</sup> provided additional information on the binding of G6Me as well as other mechanistic insights (Robb et al. 2018). In addition to the key enzymes for the oxidative demethylation of G6Me, glycoside hydrolases (GH2 and GH16), an esterase, and a putative zinc-dependent alcohol dehydrogenase (ADH) were also observed in the genomic context of the marine Flavobacterium *Formosa agariphila* KMM 3901<sup>T</sup> (Fig. 1c) (Reisky et al. 2018). A similar genomic context was also found in *Zobellia galactanivorans* Dsij<sup>T</sup> (Fig. 1d).

Considering the fact that dehydrogenases play only a minor auxiliary role in carbohydrate degradation and are poorly represented in the Carbohydrate-Active enZymes (CAZy) database, with some exceptions in the AA3, AA6, AA7, and AA12 families (Takeda et al. 2015; Kracher and Ludwig 2016; Sützl et al. 2018), it remains unclear which biological function this ADH provides for the organism. ADHs belong to the enzyme class of oxidoreductases and catalyze the reversible oxidation of an alcohol to the corresponding aldehyde or ketone employing the nicotinamide adenine dinucleotide (NAD<sup>+</sup>) or nicotinamide adenine dinucleotide phosphate (NADP<sup>+</sup>) cofactor. Depending on the size of the substrate-binding domain, it is possible for ADHs to possess a broad substrate scope; while some exhibit only activities for small aliphatic alcohols, others can convert sterically challenging cyclic components (Persson et al.



**Fig. 1** Porphyran contains 6-*O*-methyl-*D*-galactose, which can be metabolized by marine bacteria via oxidative demethylation. **a** Porphyran, the common name of the galactan of red algae of the genus *Porphyra*, consists of chains composed mainly of the alternating monosaccharide units 4-linked- $\alpha$ -L-galactose-6-sulfate (L6S) and 3-linked- $\beta$ -D-galactose (Gal) or 3,6-anhydro- $\alpha$ -L-galactose (LA). Furthermore, the *O*-methylation of *D*-galactose results in the formation of 6-*O*-methyl-*D*-galactose (G6Me). **b** The oxidative demethylation of G6Me is catalyzed by a cytochrome P450 monooxygenase in com-

bination with its redox partners ferredoxin and ferredoxin reductase, producing *D*-galactose and formaldehyde in equimolar amounts. **c** In *Formosa agariphila* KMM 3901<sup>T</sup> and **d** *Zobellia galactanivorans* Dsij<sup>T</sup>, genes encoding for the key enzymes of oxidative demethylation are located in close proximity to a gene encoding for zinc-dependent alcohol dehydrogenase. \*BN863\_, for example, \*21,030 refers to locus tag *BN863\_21030* for *F. agariphila* while  $\bar{z}gal$ , for example,  $\bar{z}gal_{4674}$  refers to locus tag *zgal\_4674* for *Z. galactanivorans*

2008; Sirota et al. 2021). A major family of ADHs includes the group of zinc-dependent ADHs, which exhibit a typical Rossmann fold (Rao and Rossmann 1973) and contain a catalytic zinc ion in the active site as well as additional non-catalytic zinc ion supporting the stability of an external loop structure (Hambidge et al. 2000). Various biological functions are observed within this family (Sirota et al. 2021), including polyol dehydrogenases catalyzing the conversion between sugar and sugar alcohol (Lu et al. 2019), cinnamyl alcohol dehydrogenases (Larroy et al. 2002; Pick et al. 2013), and glutathione-dependent formaldehyde dehydrogenases (Gutheil et al. 1992; Sanghani et al. 2000; Achkor et al. 2003), which play an important part in the detoxification of formaldehyde (Vorholt 2002). Additionally, ADHs provide numerous advantageous properties for organic synthesis, including high enantioselectivity and applicability under mild reaction conditions (Koesoema et al. 2020). Consequently, they are now employed in numerous biotechnological applications such as the preparation of chiral alcohols (Zhang et al. 2015), rare sugars (Lu et al. 2019), fine chemicals, as well as the synthesis of building blocks for various essential pharmaceuticals (Hall and Bommarius 2011; Zheng et al. 2017). Discovering and characterizing additional ADHs with unique biochemical properties is thus also desirable for potential industrial applications.

In this study, we aimed to elucidate the putative function of these ADHs, which are consistently located in close proximity to genes that are essential for the oxidative demethylation of G6Me of polysaccharide utilizing marine *Flavobacteriia*. We provide a detailed biochemical characterization as well as the crystal structures for the ADHs from *Formosa agariphila* KMM 3901<sup>T</sup> (FoADH) and *Zobellia galactanivorans* Dsij<sup>T</sup> (ZoADH). We propose the putative biological functions of these ADHs and demonstrate their importance for the utilization of G6Me via growth studies with a *Z. galactanivorans* knockout strain.

## Materials and methods

### Materials, strains, and plasmids

All chemicals and reagents used, unless otherwise specified, were purchased from Sigma-Aldrich (St. Louis, MO, USA), Thermo Fisher Scientific (Waltham, MA, USA), Th. Geyer (Berlin, Germany), ABCR GmbH (Karlsruhe, Germany), Honeywell Fluka<sup>TM</sup> (Morristown, NJ, USA), Carl Roth GmbH (Karlsruhe, Germany), chemPUR GmbH (Karlsruhe, Germany), TCI Deutschland GmbH (Eschborn, Germany), and Cayman Chemical Company (Ann Arbor, MI, USA). Porphyrin and G6Me were obtained from Biosynth Carbosynth (Staad, Switzerland). Primers were obtained from Invitrogen (Waltham, MA, USA). Phage-resistant

*Escherichia coli* (*E. coli*) BL21 (genotype: *fhuA2* [lon] *ompT gal* ( $\lambda$  *DE3*) [*dcm*]  $\Delta$ *hsdS*  $\lambda$  *DE3*= $\lambda$  *sBamHI*o  $\Delta$ *EcoRI*-B int::(*lacI*::*PlacUV5*::*T7 gene1*) *i21*  $\Delta$ *nin5*) was obtained from New England Biolabs (Ipswich, MA, USA). The conjugative strain *E. coli* S17-1  $\lambda$  *pir* (genotype *λpir hsdR pro thi*; chromosomal integrated RP4-2 Tc::Mu Km::Tn7) (de Lorenzo and Timmis 1994) was grown from in-house glycerol stocks. A construct for the expression of the FoADH (GenBank accession number: OP548117) from *F. agariphila* KMM 3901<sup>T</sup> was prepared using the FastCloning strategy (Li et al. 2011) with genomic DNA as a template for the amplification of the insert. *F. agariphila* KMM 3901<sup>T</sup> (collection number DSM-15362) was obtained from the DSMZ (Braunschweig, Germany). The pET28a vector was amplified with the 5-GCG GCC GCA CTC GAG CA-3' and 5-CAT ATG GCT GCC GCG C-3' oligonucleotides, while the insert was amplified with the 5'-CAC AGC AGC GGC CTG GTG CCG CGC GGC AGC CAT ATG TCC ATA ATT TCA AAA TGC GCT ATT G-3' and 5'-CAG TGG TGG TGG TGG TGC TCG AGT GCG GCC GCT TAA AAA ATA ATT ACA CCC TTT GCA TTC-3' oligonucleotides. A synthetic gene, codon optimized for expression in *E. coli*, encoding the ZoADH (GenBank accession number: OP548118) from *Z. galactanivorans* Dsij<sup>T</sup>, was synthesized and cloned into a pET28a vector by BioCat GmbH (Heidelberg, Germany). The constructs encode the recombinant protein as fusion to a N-terminal Strep-tag for affinity purification.

### Computational analysis for FoADH and ZoADH

Sequences of FoADH (Uniprot ID: T2KM87) and ZoADH (Uniprot ID: G0L712) were blasted against the MarDB and MarRef databases using the Marine Metagenomic Portal (Klemetsen et al. 2018; Priyam et al. 2019) with the  $-e$  value of  $1e^{-5}$  and maximal target sequences of 1000. The automated fasta hit table of both blasts was fused and used for the generation of a sequence similarity network (Zallot et al. 2019). An alignment score of 150 was chosen for the refinement and generation of a genome neighborhood analysis of ten genes down- and upstream of the ADH genes (Zallot et al. 2019). Resulting diagrams were visualized via Cytoscape (Paul Shannon et al. 2003), and genome neighborhood diagrams were generated from the online server. Only shared sequences of the MarDB/MarRef database with the UniProtKB databases could be incorporated into the genome neighborhood analysis.

### ADH knockout in *Z. galactanivorans* and growth studies

The deletion mutant of the ADH gene *zgal\_4674* in *Z. galactanivorans* Dsij<sup>T</sup> (collection number DSM-12802)

was constructed using a *sacB* system (Zhu et al. 2017), as previously described for the deletion variant of the CYP gene (Brott et al. 2022). Briefly, to delete *zgal\_4674*, a 2448-bp fragment including the last 43 bp of *zgal\_4674* and 2405 bp of the downstream sequence was amplified using primers OFT0041 and OFT0043 on genomic DNA from *Z. galactanivorans* Dsij<sup>T</sup>. The fragment was digested with *Bam*HI and *Xba*I and ligated into pYT313, which had been digested with the same enzymes, to generate pFT12. A 2077-bp fragment including the first 29 bp of *zgal\_4674* and 2048 bp of the upstream sequence was amplified using primers OFT0040 and OFT0042. The fragment was cloned into *Xba*I and *Sal*I sites of pFT12 to generate the *zgal\_4674* deletion construct pFT13. Conjugative transfer of pFT13 from *E. coli* S17-1 into the wild-type *Z. galactanivorans* Dsij<sup>T</sup> and second recombination steps were carried out as described previously (Zhu et al. 2017). Deletions were confirmed by PCR and sequencing on isolated colonies using primer pairs OFT0044–OFT0045 to identify the *zgal\_4674* deletion mutant (mZG\_0080). Primers employed are displayed in Table S1 in the Supplementary Information (SI). For growth studies, precultures of three *Z. galactanivorans* strains (wild-type, knockout ADH, and knockout CYP) were prepared in the Zobell 2216E medium (Zobell 1941). The 3-day precultures were then rinsed twice with a sterile saline solution. Marine minimal medium (Thomas et al. 2011b) amended with D-galactose or G6Me (4 g L<sup>-1</sup>) was then inoculated so that an initial optical density (OD<sub>600</sub>) of 0.05 was achieved. Appropriate cultures were incubated for 3 days at room temperature.

### Enzyme production and purification

Chemically competent *E. coli* BL21 (DE3) cells were transformed with the plasmids harboring FoADH or ZoADH and were spread on lysogeny broth (LB) agar plates containing 50 µg mL<sup>-1</sup> kanamycin. The agar plates were incubated overnight at 37 °C. One colony was picked and used to inoculate 5 mL LB medium which contained 50 µg mL<sup>-1</sup> kanamycin and was then incubated at 37 °C and 180 rpm overnight. For overexpression, the cultivation was performed in a terrific broth (TB) medium containing 50 µg mL<sup>-1</sup> kanamycin. The TB medium was inoculated with the overnight culture so that a starting OD<sub>600</sub> of 0.05 was obtained. Cells were then incubated at 37 °C and 180 rpm until an OD<sub>600</sub> of 0.8 was reached. Expression of target enzymes was induced by the addition of 1 mM isopropyl-β-D-thiogalactopyranoside (IPTG). The cultivation was performed at 25 °C and 180 rpm overnight. Cells were harvested by centrifugation at 10,000×g and 4 °C for 1 h, washed with 50 mM sodium phosphate buffer (NaPi) pH 7.5, and subsequently stored at -20 °C until cell disruption. The purification procedures of FoADH and ZoADH for crystallization and enzyme

assays are identical. Cells were resuspended in 50 mM Tris–HCl buffer pH 8.0 containing 200 mM NaCl. Following cell lysis by ultra-sonication (2×3 min, 50% power, 50% cycle), cell debris was removed by centrifugation at 10,000×g, at 4 °C for 20 min. The clarified supernatant was loaded on a gravity flow column containing Strep-Tactin XT Sepharose<sup>®</sup> 50% suspension (IBA-Lifesciences GmbH, Göttingen, Germany) as column material. The column was washed with 100 mM Tris–HCl buffer pH 8.0 containing 150 mM NaCl in order to remove unbound and undesirable proteins. The target enzymes were then eluted with the same buffer containing an additional 50 mM of biotin. Elution fractions were pooled and concentrated using a Vivaspin 6 centrifugal concentrator with a 10 kDa molecular weight cut-off (Sartorius AG, Göttingen, Germany). Size exclusion chromatography was subsequently performed via the Äkta<sup>™</sup> pure chromatography system (Cytiva Europe GmbH, Germany). The concentrated enzyme solution was applied to a HiPrep<sup>™</sup> 16/60 Sephacryl<sup>®</sup> S-200 HR column (Cytiva Europe GmbH, Freiburg, Germany) that was previously equilibrated with 10 mM Tris–HCl buffer pH 8.0 containing 200 mM NaCl. Elution fractions were collected, and the purity was verified by sodium dodecyl sulfate–polyacrylamide gel electrophoresis (SDS-PAGE). Pure fractions were combined and concentrated as mentioned above. The enzyme solution was stored at 4 °C for crystallization. For application in enzyme assays, a PD-10 desalting column (Cytiva Europe GmbH, Freiburg, Germany) was employed to desalt the protein sample and exchange the buffer.

### SDS-PAGE and determination of protein content

SDS-PAGE was performed to verify the purity of the target enzymes. Twenty microliters of protein sample was mixed with 5 µL of a fivefold stock of SDS sample buffer (100 mM Tris–HCl buffer at pH 6.8 containing 4% (w/v) SDS, 20% (v/v) glycerol, 2% (v/v) β-mercaptoethanol, 25 mM ethylenediaminetetraacetic acid (EDTA), and 0.04% (w/v) bromophenol blue) and denatured at 99 °C for 15 min. For the SDS-PAGE, a 12.5% acrylamide gel (separating gel) and a 4.0% loading gel were used. Electrophoresis was carried out at 200 V. Proteins were stained with Coomassie Blue (PhastGel<sup>®</sup> Blue R). As a reference, the Pierce<sup>™</sup> Unstained Protein Molecular Weight Marker (Thermo Fisher Scientific, Waltham, MA, USA) was used. Protein concentrations were determined using the Pierce<sup>™</sup> BCA Protein Assay Kit (Thermo Fisher Scientific, Waltham, MA, USA) with bovine serum albumin as a protein standard.

### Crystallization

Purified FoADH (25 mg mL<sup>-1</sup>) and ZoADH (25 mg mL<sup>-1</sup>) were incubated with 20 mM NAD<sup>+</sup> overnight. An initial

crystallization screen was performed using the sitting drop vapor-diffusion method at 22 °C. The droplets contained 0.2 µL of protein and 0.2 µL of reservoir solution. Microcrystals of FoADH were obtained from a reservoir solution containing 0.1 M Tris–HCl at pH 7.5, 0.2 M KCl, and 22% (w/v) polyethylene glycol 3350. Microcrystals of ZoADH were obtained from a reservoir solution containing 0.1 M Tris–HCl at pH 7.5, 0.2 M KCl, and 20% (w/v) polyethylene glycol 3350. Further crystal optimization was performed by scale-up of the droplets containing 2 µL of protein and 2 µL of reservoir solution, using the hanging drop vapor-diffusion method at 22 °C. Suitable FoADH and ZoADH crystals for X-ray diffraction were obtained from 0.1 M Tris–HCl at pH 7.5, 0.2 M KCl, and 20–22% (w/v) polyethylene glycol 3350 within 1 day.

### Data collection

X-ray diffraction data were collected at beamline 11C at Pohang Light Source II (PLS-II, Pohang, South Korea) with a Pilatus 6 M detector (Dectris, Switzerland). The FoADH crystals were equilibrated in a cryoprotectant buffer containing reservoir buffer plus 20% (v/v) ethylene glycol. ZoADH crystals were equilibrated in a cryoprotectant buffer containing reservoir buffer plus 20% (v/v) glycerol. The crystal was mounted on the goniometer and cooled under a nitrogen gas stream at 100 K. The diffraction data were indexed, integrated, and scaled using the HKL2000 program (Otwinowski and Minor 1997). A data collection statistic is given in Table S2.

### Structure determination

The electron density maps of FoADH and ZoADH were obtained via the molecular replacement method using the MOLREP program (Vagin and Teplyakov 2010). The crystal structure of an ADH from *Artemisia annua* (PDB code: 6LJH, unpublished) was used as a search model for both FoADH and ZoADH. Model building and refinement were performed with the COOT program (Emsley and Cowtan 2004) and phenix.refinement in PHENIX (Liebschner et al. 2019), respectively. The geometry of the final models was evaluated with MolProbity (Williams et al. 2018). Structural figures were generated with PyMOL ([www.pymol.org](http://www.pymol.org)). Structure-based sequence alignments were generated using Clustal-Omega (Sievers et al. 2011) and ESPript (Gouet et al. 1999). Tetrameric interfaces of ADHs were analyzed by PDBePISA (Krissinel and Henrick 2007). The interaction between ADHs and ligands was analyzed using PLIP (Salentin et al. 2015). The structure factor and coordinates are deposited in the Protein Data Bank under PDB codes 8H2A (FoADH-NAD) and 8H2B (ZoADH-NAD).

### Enzyme activity determination and substrate screening

For determining the enzyme activity of the ADHs, the absorbance maximum of NADH at 340 nm was utilized. The absorbance at 340 nm was measured every minute over a 10-min period using a microplate spectrophotometer (BioTek Synergy H1, Agilent Technologies, Santa Clara, CA, USA), and the slope over time was used to determine activities or relative activities. One unit of activity is defined as the oxidation or formation of 1 µmol of NADH/min. For the calculation of activity, the molar absorption coefficient of NADH was determined via a standard curve that covered the range of 0 to 0.5 mM. For the initial substrate screening, several alcohols/aldehydes/ketones were employed at a final concentration of 10 mM. For increased substrate solubility, these reactions contained 3.5% (v/v) dimethyl sulfoxide (DMSO). The total volume for all reactions was 0.2 mL. The oxidation and reduction were both conducted at an incubation temperature of 70 °C. Reduction of aldehydes was performed in the presence of a 50 mM succinate buffer at pH 6.5, while oxidation reactions were assayed in the presence of a 50 mM NaPi buffer at pH 8.5. The final enzyme concentrations used to provide a linear absorbance increase or decrease ranged from 20 to 100 µg mL<sup>-1</sup> for the oxidation reactions and from 0.25 to 2.5 µg mL<sup>-1</sup> for the reduction reactions. The reaction was initialized by the addition of 0.5 mM NAD<sup>+</sup> or NADH. For the measurement with sugar substrates, a reduced reaction temperature of 40 °C and an increased measuring time of 30 min were chosen. Various sugars were used at a final substrate concentration of 30 mM. A concentration of 0.2% (w/v) was used for porphyrin. Oxidation and reduction reactions were performed in the identical buffers as used for substrate screening, and the final enzyme concentration was 0.1 mg mL<sup>-1</sup>. The reaction was initialized by the addition of 0.5 mM NAD<sup>+</sup> or NADH. For the determination of cofactor utilization, the oxidation of 10 mM benzyl alcohol was performed in the presence of different NAD<sup>+</sup> or NADP<sup>+</sup> concentrations ranging from 0 to 5 mM in 50 mM HEPES buffer at pH 8.5 at 25 °C and a final enzyme concentration of 0.1 mg mL<sup>-1</sup>. For the determination of the kinetic parameters, a final protein content of 0.1 mg mL<sup>-1</sup> (corresponding to a protein concentration of 2.44 µM) was used for the oxidation reactions. When determining  $K_m$  and  $V_{max}$  values for NAD<sup>+</sup>, 15 mM benzyl alcohol was used as the final substrate concentration, while a final cofactor concentration of 5 mM NAD<sup>+</sup> was used for the measurement of benzyl alcohol. The oxidation reactions were carried out in 50 mM NaPi buffer at pH 8.5 and at a reaction temperature of 70 °C. A final protein content of 5 µg mL<sup>-1</sup> was used in the reduction reaction (corresponding to a protein

concentration of 0.012  $\mu\text{M}$ ). For the determination of the kinetic parameters for NADH, 2.5 mM pyridine-3-carbaldehyde was used as the final substrate concentration, while a final cofactor concentration of 0.5 mM NADH was used for the determination of the kinetic parameters for pyridine-3-carbaldehyde. The reduction reactions were carried out in 50 mM succinate buffer at pH 6.5 and at 70 °C. In order to test for thiol-dependent formaldehyde detoxification, different thiols were evaluated as potential cofactors. For this reaction, the thiol cofactor and formaldehyde were used in a 1:1 ratio at a final concentration of 0.5 mM. The measurement was performed in the 50 mM NaPi buffer at pH 8.5 at 70 °C with a final enzyme concentration of 0.2 mg mL<sup>-1</sup>. The reaction was started by the addition of 0.5 mM NAD<sup>+</sup>. The ADH-catalyzed disproportionation of formaldehyde into methanol and formate was monitored by a pH change utilizing the phenol red assay (Martínez-Martínez et al. 2018). This measurement was performed on a microtiter plate, and the reaction volume was 0.2 mL. Five millimolars of formaldehyde was used as a substrate, 0.5 mM NAD<sup>+</sup> as a cosubstrate, and 0.1 mg mL<sup>-1</sup> as the final enzyme concentration. The pH indicator phenol red was used at a final concentration of 91  $\mu\text{M}$ . The reaction was performed in a 5 mM HEPES buffer at pH 8.5 at 40 °C. Absorbance at 560 nm was measured every minute for 20 min.

### Influence of pH and buffer components

To determine the pH optimum of the enzymes, the oxidation and reduction reactions were both investigated in the presence of varying pH values. All buffers had a concentration of 50 mM. A citrate buffer was used in the pH range of 5 to 6, a NaPi buffer in the range of 6 to 8.5, a CHES buffer in the range of 8.5 to 10, and a CAPS buffer in the range of 10 to 12.5. The assay conditions for the oxidation reaction were as follows: 200  $\mu\text{L}$  reaction volume, 10 mM benzyl alcohol, and 0.5 mM NAD<sup>+</sup> was used as substrate. The reaction was started by the addition of 0.1 mg mL<sup>-1</sup> ADH. For the reduction reaction, instead of benzyl alcohol and NAD<sup>+</sup>, 10 mM benzaldehyde and 0.5 mM NADH were used. Since benzaldehyde was less soluble in the buffer than benzyl alcohol, both reactions contained 3.5% (v/v) DMSO in order to achieve better comparability. The reaction was carried out at 25 °C in the respective buffers. To examine the influence of buffer components on enzyme activity, different buffers with a concentration of 50 mM were used. The buffers had a pH of 6.5 for the reduction reaction, whereas it was 8.5 for the oxidation reaction. The reaction was carried out under the same conditions as those for the pH optimum. Relative activities were determined as described above.

### Influence of temperature and thermostability

The temperature optimum was determined by conducting the oxidation reaction at different temperatures in the range between 20 and 90 °C. For this, the reaction mixture without enzyme was preheated to the desired temperature in a reaction tube by using a heating block (Eppendorf ThermoMixer<sup>®</sup>C, Eppendorf SE, Hamburg, Germany) for at least 45 min. The reaction mixture had a volume of 200  $\mu\text{L}$ . Thirty millimolars of benzyl alcohol and 0.5 mM of NAD<sup>+</sup> were employed as substrates, and the reaction was carried out at different temperatures ranging from 20 to 90 °C in a 50 mM NaPi buffer at pH 7.5. The reaction was initiated by the addition of an enzyme with a final concentration of 0.1 mg mL<sup>-1</sup>. For the thermostability determination, the purified ADH (1 mg mL<sup>-1</sup>) was incubated in 50 mM NaPi buffer at pH 7.5 for 1 or 4 h in a gradient thermal cycler (FlexCycler<sup>2</sup>, Analytik Jena, Jena, Germany) at various temperatures ranging from 20 to 80 °C. Residual activity was then determined as described above and compared with a control that was incubated on ice. The assay conditions were as follows: the reaction volume was 200  $\mu\text{L}$ , the final enzyme concentration was 0.1 mg mL<sup>-1</sup>, the substrate was 10 mM benzyl alcohol, and the reaction was performed at 40 °C in 50 mM NaPi buffer at pH 7.5. The reaction was initiated by the addition of 0.5 mM NAD<sup>+</sup>.

### Influence of sodium chloride

The determination of NaCl influence on enzyme activity was performed by carrying out the oxidation reaction in the presence of different NaCl concentrations varying from 0 to 800 mM. The relative activities were determined as described above and were compared with the control, where no additional NaCl was present. Assay conditions were as follows: the reaction volume was 200  $\mu\text{L}$ , the substrate was 10 mM benzyl alcohol, the final enzyme concentration was 0.1 mg mL<sup>-1</sup>, and the NaCl concentration was between 0 and 800 mM. The reaction was carried out at 25 °C in a 50 mM NaPi buffer at pH 8.5 or in a 50 mM tricine buffer at pH 8.5 and started by the addition of 0.5 mM NAD<sup>+</sup>.

### Influence of metal ions and other small molecules

For the determination of the influence of various metal ions on enzyme activity, the ADHs with a concentration of 1 mg mL<sup>-1</sup> were incubated with either 1 or 10 mM metal ions at RT for 1 h before activity measurement. A sample without additional metal ions served as a control. For the activity measurement, the standard assay was used under the following conditions: the reaction mixture had a total volume of 200  $\mu\text{L}$ , a substrate of 10 mM benzyl alcohol was used, a final enzyme concentration of 0.1 mg mL<sup>-1</sup>

was employed, and the reaction was performed in 50 mM HEPES buffer at pH 8.5 at 25 °C. The reaction was initiated by the addition of 0.5 mM NAD<sup>+</sup>. In order to determine the effect of EDTA, dithiothreitol (DTT), and 2-mercaptoethanol (2-ME) on enzyme activity, the ADHs were incubated at a protein concentration of 1 mg mL<sup>-1</sup> with these components at concentrations of 1, 10, or 25 mM for 1 h at RT before activity determination. Higher concentrations of up to 100 mM were additionally tested for EDTA. The untreated enzyme served as a control. The activity measurement was performed as described for the influence of metal ions.

### Influence of solvents and formaldehyde

To evaluate the influence of selected water-miscible solvents on the activity of both ADHs, the oxidation reaction was conducted in the presence of 5, 10, and 20% (v/v) solvent and compared with a control containing no additional solvent. The relative activity was determined as described above. The total reaction volume was 0.2 mL, and 0.1 mg mL<sup>-1</sup> of the enzyme was used as the final enzyme concentration. The reactions were performed in 50 mM NaPi buffer at 25 °C. Ten millimolars of benzyl alcohol was employed as a substrate, and the reactions were started by adding 0.5 mM NAD<sup>+</sup>. The enzymes were incubated at a concentration of 1 mg mL<sup>-1</sup> with different concentrations of formaldehyde varying from 0 to 50 mM for 1 h at RT prior to activity measurement to evaluate the effect of formaldehyde on enzyme activity. Relative activity was determined as described above. For the activity measurement, the same conditions were used for the influence of solvent.

## Results

### Distribution and gene neighborhood analysis

In order to obtain an overview regarding the distribution and function of these ADHs in marine bacteria, we queried the MarDB and MarRef databases for ADHs with similar sequences to FoADH and ZoADH and constructed a sequence similarity network based on an alignment score of 150 and a sequence identity of 63.14%. This analysis revealed six main clusters, which we define here as clusters containing at least 34 sequences, with FoADH and ZoADH included in main cluster 2 (Fig. S1). This main cluster primarily contained sequences that were annotated as zinc-dependent ADHs, histidine kinases, ADH GroES-like domains, and some glutathione-dependent formaldehyde dehydrogenases/ADHs. However, glutathione-dependent and mycothiol-dependent formaldehyde dehydrogenases were identified predominantly in clusters 1 and 4, respectively. Based on main cluster 2, we performed a genome

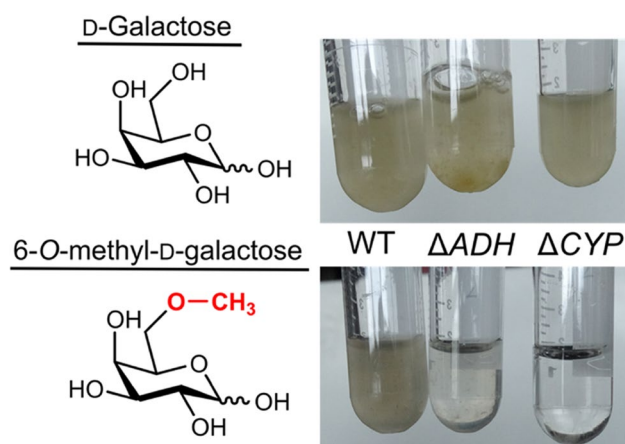
neighborhood analysis to obtain a general sense of which genes are located in close proximity to the ADH gene. Similar genomic arrangements consisting of CYP, redox partners, an esterase, and the ADH can be identified in several marine bacteria that are capable of degrading marine polysaccharides (Fig. S2), including members of the genera *Polaribacter*, *Maribacter*, and *Arenibacter*. Minor differences in gene arrangement can be observed among some organisms such as *F. agariphila* or *Algibacter lectus*, where genes encoding for CAZymes (GH2 and GH16) are located between the ADH and the esterase gene. Additionally, some genes encoding for sulfatases and SusC/SusD homologs, which are responsible for the binding and transport of sugar molecules (Martens et al. 2009), are located up- and downstream of the ADH gene. Considering that the ADH gene consistently appears in the proximity of the genes, which encode for CAZymes and key enzymes for the oxidative demethylation of G6Me, it is conceivable that the ADH possesses a specific function in carbohydrate utilization or a subsequent reaction.

### Knockout of the ADH encoding gene in *Z. galactanivorans* and growth studies

In an attempt to elucidate the biological relevance of the ADHs for the organisms, a knockout of the gene that encodes for the ADH in *Z. galactanivorans* was performed, followed by growth experiments. The controls employed for these growth studies were the wild-type (WT) and an additional knockout strain of *Z. galactanivorans* in which the CYP gene was deleted. When G6Me was employed as the sole carbon source, impaired growth was observed for the ADH and CYP knockout strains, while the WT exhibited normal growth (Fig. 2). In contrast, regular growth was observable for all three strains in a control, which contained D-galactose as sole carbon source. Consequently, the ADH possessed an impact on the G6Me utilization of *Z. galactanivorans*.

### Functional overexpression and purification of the ADHs

Since we could demonstrate the biological significance of the ADH for the utilization of G6Me by the gene knockout in *Z. galactanivorans*, our next aim was to identify the enzyme function. We, therefore, cloned the gene encoding for the ADH from *F. agariphila* into a pET28a vector. For the ADH from *Z. galactanivorans*, a synthetic gene was ordered in the pET28a vector. Both enzymes were successfully overexpressed and purified (Fig. S3), which established the basis to elucidate the putative biological functions of these ADHs by performing biochemical and structural biological characterizations.



**Fig. 2** Knockout of the ADH gene in *Z. galactanivorans* leads to impaired growth on G6Me. Different *Z. galactanivorans* strains (wild type (WT), gene knockout ADH ( $\Delta ADH$ ), and gene knockout CYP ( $\Delta CYP$ )) were incubated in minimal medium amended with D-galactose or G6Me for 3 days at RT

### Substrate spectrum of the ADHs

In order to obtain a preliminary understanding of the substrate spectrum of these ADHs, their ability for alcohol oxidation as well as the reduction of various aldehydes and ketones were examined. Both enzymes converted predominantly aromatic substrates (Tables 1 and 2). The highest specific activity of  $64.1 \text{ U mg}^{-1}$  for FoADH and  $54.9 \text{ U mg}^{-1}$  for ZoADH was observed for the reduction of pyridine-3-carbaldehyde. In addition to compounds containing a benzene ring, substrates harboring a furan or thiophene ring, such as furfural and thiophene-3-carbaldehyde, were also preferentially converted. Positions of additional substituents at the benzene ring influenced the activity. A difference in the specific activities for the constitutional isomers of terephthalaldehyde and tolualdehyde was observed for both enzymes. In particular, substrates that possessed an additional substituent in *ortho*-position were converted significantly less efficiently. In addition, the length of the aldehyde substituent at the benzene ring also affected the activity. For instance, hydrocinnamaldehyde was converted by both enzymes, whereas for phenylacetaldehyde, no activity was observable. In contrast to benzaldehyde, the structurally similar acetophenone could not be oxidized. Thus, both ADHs were unable to convert ketones to secondary alcohols. In comparison to the reduction reaction, significantly reduced specific activities were noticed for the oxidation reactions (Table 2). Simultaneously, lower  $K_m$  values in the range of 0.6 to 0.8 mM could be determined for pyridine-3-carbaldehyde compared to the  $K_m$  values of 3.6 and 5.3 mM for benzyl alcohol (Fig. S4). The highest specific activity of  $490 \text{ mU mg}^{-1}$  for FoADH and  $290 \text{ mU mg}^{-1}$  for ZoADH has been observed

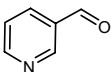
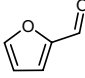
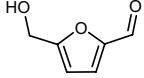
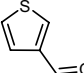
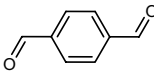
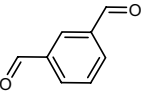
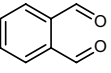
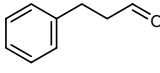
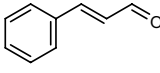
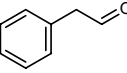
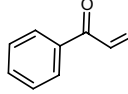
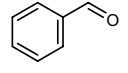
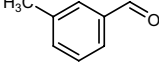
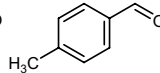
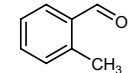
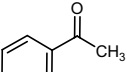
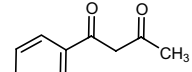
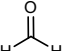
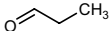

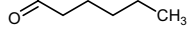
for 2,5-bis(hydroxymethyl)furan. Both ADHs lacked any activity for smaller aliphatic alcohols such as methanol and ethanol. Since the ADHs exhibited predominantly activities for substrates containing a ring structure, several sugars were also considered possible substrates. However, no activity was observed for the oxidation or reduction of galactose, G6Me, and additional monosaccharides and disaccharides (Table S3). Additionally, the marine carbohydrate porphyran was also evaluated as a potential substrate; however, no activity was detected either. As mentioned earlier in the “Introduction,” ADHs require either  $\text{NAD}^+$  or  $\text{NADP}^+$  as a cofactor for their enzymatic activity. In order to identify the preferred cofactor for both ADHs, the oxidation of benzyl alcohol was conducted in the presence of varying  $\text{NAD}^+$  and  $\text{NADP}^+$  concentrations. Both ADHs utilize  $\text{NAD}^+$  as a cofactor, whereas in the presence of up to 5 mM  $\text{NADP}^+$ , no activity for the oxidation reaction was observed.

### Testing for formaldehyde detoxification activity

Since the activity was neither observed for galactose nor for G6Me, we hypothesized that the ADHs may participate in formaldehyde detoxification, considering that formaldehyde is formed as a by-product in the oxidative demethylation reaction. Members of the zinc-dependent ADHs may catalyze the glutathione-dependent formaldehyde detoxification; therefore, various thiols were considered potential cofactors. Thiol-dependent detoxification of formaldehyde proceeds via a spontaneous reaction between the sulfhydryl group of the thiol cofactor and the carbon atom of formaldehyde, resulting in the formation of an alcohol (Fig. 3a) (Chen et al. 2016). Subsequently, this alcohol can be oxidized by the ADH to a thioester, which is then converted by an esterase to formate and the starting thiol cofactor (Gonzalez et al. 2006). Based on the results of our genome neighborhood analysis, where we have also demonstrated that a gene encoding for an esterase is located in the vicinity of the ADH gene, it is quite possible that thiol-dependent detoxification of formaldehyde can proceed via both enzymes. In addition to glutathione, mainly mycothiol (Misset-Smits et al. 1997; Newton and Fahey 2002) and bacillithiol (Newton et al. 2009; Chandransu et al. 2018) are well-known cofactors in formaldehyde detoxification (Fig. 3b). However, no activity was detected for these thiols. Furthermore, common thiols abundant in nature such as cysteine, coenzyme A, and L-ergothioneine (Hand and Honek 2005) were also investigated as cofactors. Nevertheless, no activity was observed for these substrates in combination with formaldehyde either. Considering that the ADHs mainly exhibited activity for aromatic substrates, aromatic thiols such as 2-mercaptoimidazole or



**Table 1** Initial substrate screening of the ADH in the reduction direction revealed that it preferentially converts aromatic aldehydes

Abbr.	Substrates	Specific activity [U/mg]		
		FoADH	ZoADH	
1	Pyridine-3-carbaldehyde	64.09 ± 2.39	54.85 ± 4.34	
2	Furfural	47.77 ± 1.19	44.78 ± 2.07	
3	5-(Hydroxymethyl)furfural	44.81 ± 2.16	38.29 ± 2.47	
4	Thiophene-3-carbaldehyde	37.45 ± 4.19	29.32 ± 2.59	
5	Terephthalaldehyde	30.05 ± 3.60	27.34 ± 4.68	
6	Isophthalaldehyde	26.71 ± 1.47	36.94 ± 3.68	
7	Phthalaldehyde	n.d. <sup>a)</sup>	n.d.	
8	Hydrocinnamaldehyde	26.00 ± 2.23	30.13 ± 2.32	
9	Cinnamaldehyde <sup>b)</sup>	12.57 ± 0.90	11.20 ± 0.11	
10	Phenylacetaldehyde	n.d.	n.d.	
11	Phenylglyoxal	n.d.	n.d.	
12	Benzaldehyde	5.14 ± 0.09	12.49 ± 0.73	
13	<i>m</i> -Tolualdehyde	6.30 ± 1.06	7.32 ± 0.32	
14	<i>p</i> -Tolualdehyde	4.71 ± 0.32	5.60 ± 0.44	
15	<i>o</i> -Tolualdehyde	0.04 ± 0.01	0.04 ± 0.01	
16	Acetophenone	n.d.	n.d.	
17	Benzoylacetone	n.d.	n.d.	
18	Formaldehyde	n.d.	n.d.	
19	Propionaldehyde	1.58 ± 0.10	0.92 ± 0.36	
20	Butyraldehyde	3.62 ± 1.04	4.02 ± 0.48	
21	Caproaldehyde	7.07 ± 0.64	6.62 ± 0.30	

Substrates were employed at a final concentration of 10 mM. For NADH, a concentration of 0.5 mM was used. The reaction contained 3.5% (v/v) DMSO. The reaction was conducted in a 50 mM succinate buffer at pH 6.5 at an incubation temperature of 70 °C. All measurements were performed in triplicates; the mean and the standard deviation are given

*n.d.*, not detected

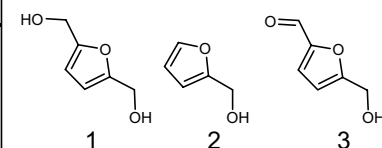
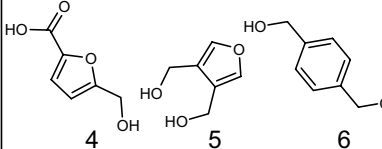
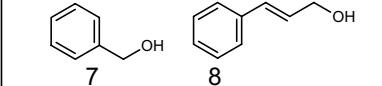
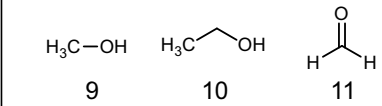
<sup>a)</sup>Due to a high background absorption of the compound, a substrate concentration of 1 mM was employed

4-mercaptophenol were considered possible substrates as well. However, even with these compounds, no oxidation reaction was detected. Furthermore, neither enzyme exhibited activity for the oxidation or reduction of formaldehyde in the presence of only NAD<sup>+</sup> or NADH as cofactors. In addition, a disproportionation reaction of formaldehyde into methanol and formate catalyzed by the ADH was also checked. However, no activity could be detected. Consequently, the ADHs possessed no activities for the substrate or for the products of the oxidative demethylation of G6Me. To provide additional insights into these ADHs, we performed further biochemical characterizations of both enzymes.

### Influence of pH and buffer components on enzyme activity

In order to determine the optimal pH for the enzymatic reaction, several buffers were investigated in the pH range from 5.5 to 12.5. A similar pH optimum was observed for both enzymes (Fig. 4). The reduction reaction was most efficiently catalyzed at pH 6.5, while oxidation was found to be most efficient at pH 8.5 (Fig. 4a, b, d–e). At pH 5 and at 12.5, no activity was detected for either enzyme; precipitation was noticed at pH 5 while employing higher protein concentrations. Since a considerable difference in activity was observed between NaPi and CHES buffer at pH 8.5,

**Table 2** Both ADHs possess minor, specific activities for the oxidation of alcohols

Abbr.	Substrate	Specific activity [mU/mg]		
		FoADH	ZoADH	
1	2,5-Bis(hydroxymethyl)furan	490 ± 50	290 ± 90	
2	Furfuryl alcohol	310 ± 10	194 ± 51	
3	5-(Hydroxymethyl)furfural	n.d. <sup>a)</sup>	n.d.	
4	5-(Hydroxymethyl)furan-2-carboxylic acid	n.d.	n.d.	
5	3,4-Bis(hydroxymethyl)furan	n.d.	n.d.	
6	1,4-Benzenedimethanol	86 ± 1.5	51 ± 3.0	
7	Benzyl alcohol	81 ± 0.7	53 ± 0.1	
8	Cinnamyl alcohol <sup>b)</sup>	11 ± 3.1	6 ± 2.9	
9	Methanol	n.d.	n.d.	
10	Ethanol	n.d.	n.d.	
11	Formaldehyde	n.d.	n.d.	

Formaldehyde was also tested in a possible oxidation reaction to exclude thiol-independent formaldehyde dehydrogenase activity. Substrates were employed at a final concentration of 10 mM. For NAD<sup>+</sup>, a concentration of 0.5 mM was used. The reaction contained 3.5% (v/v) DMSO. The reaction was conducted in a 50 mM NaPi buffer at pH 8.5 at an incubation temperature of 70 °C. All measurements were performed in triplicates; the mean and the standard deviation are given *n.d.*, not detected

<sup>a)</sup>Due to a high background absorption of the compound, a substrate concentration of 1 mM was employed

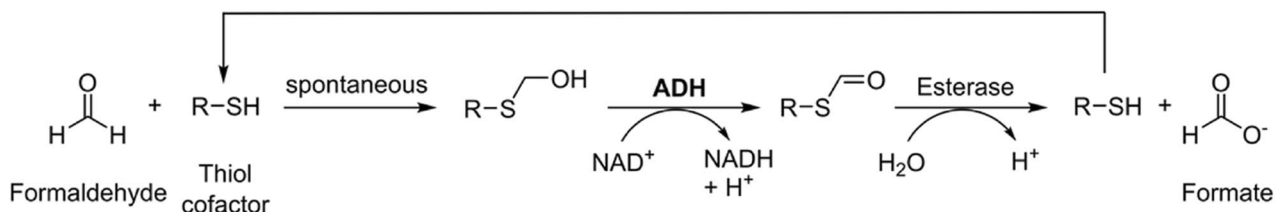
other buffers were also evaluated at pH 6.5 (Fig. 4c) and 8.5 (Fig. 4f) to investigate the influence of buffer components on the activity. For the oxidation reaction at pH 8.5, it was shown that by employing a Tris-HCl buffer, an approximately 60 to 80% increased activity was obtained compared to the activity in the NaPi buffer. In contrast, a significant activity decrease of 95% was observed for both enzymes in the presence of a borate-NaOH buffer. For the reduction reaction at pH 6.5, a slight increase in activity of ~8 to 16% could be detected using citrate and succinate buffer compared to the NaPi buffer, with the highest activity found for the succinate buffer.

### Influence of temperature and enzyme thermostability

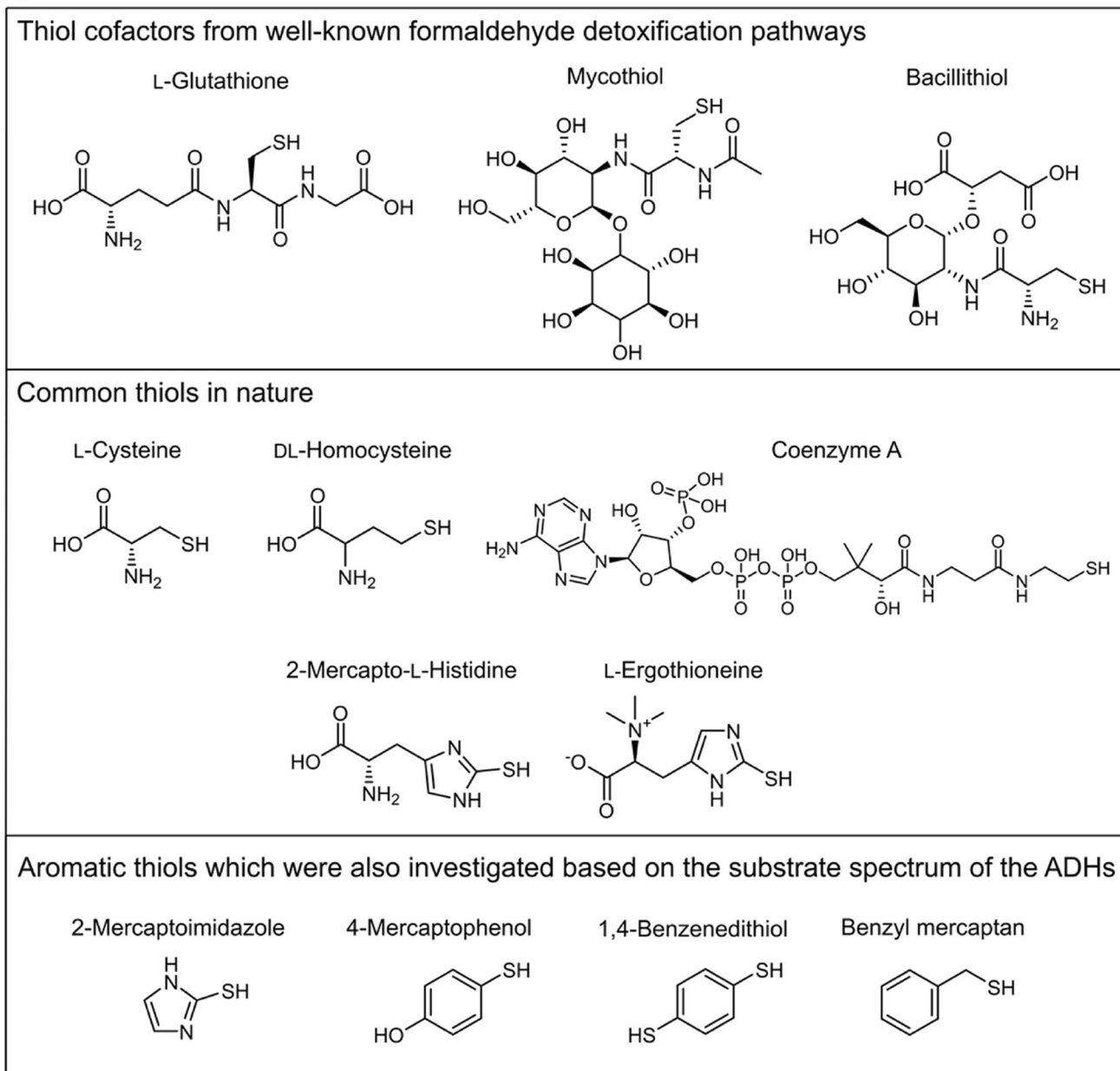
In addition to the pH value, the temperature influence is essential for enzymatic activity. At the same time, elevated temperatures promote substrate solubility and thus the application of higher concentrations, which may also shift the reaction equilibrium towards product formation (Unsworth et al. 2007). Therefore, the impact of temperature in the range between 20 and 90 °C was investigated for both enzymes. The ADHs possessed a similar temperature profile, where activity increased with rising temperature, reaching an optimum between 65 to 75 °C (Fig. 5a). However, at higher temperatures, the activity

decreased rapidly, whereas at room temperature, only a relative activity of about 18% for FoADH and 10% for ZoADH was observed. The measurement for the temperature optimum was performed for 10 min to ensure that any influence of thermostability would not affect the results. The thermostability of enzymes is an important parameter for biocatalysis since many industrial processes operate at higher temperatures for longer time periods, leading to increased product yields. The thermostability of the ADHs was therefore evaluated next by incubating the enzymes for 1 or 4 h at various temperatures ranging from 20 to 80 °C followed by determination of residual activity. After 1 h incubation at 59 °C as well as lower temperatures, no decrease in activity was detected for FoADH compared to a control incubated on ice (Fig. 5b). Residual activity only diminished at higher incubation temperatures, and residual activity of roughly 20% was still observed for 80 °C. In contrast, after 4 h incubation, almost no residual activity was observed at this temperature. Nevertheless, even after this extended incubation period, a high remaining activity of approximately ≤ 85% was detected for the temperature range of 20 to 59 °C. ZoADH exhibited a similar behavior in thermostability as FoADH; however, an initial activity decrease of 20% was observed for the 1 h incubation already at 57 °C (Fig. 5c). A severe activity loss of almost 95 to 100% was observed for ZoADH when incubated for 4 h at temperatures > 73 °C.

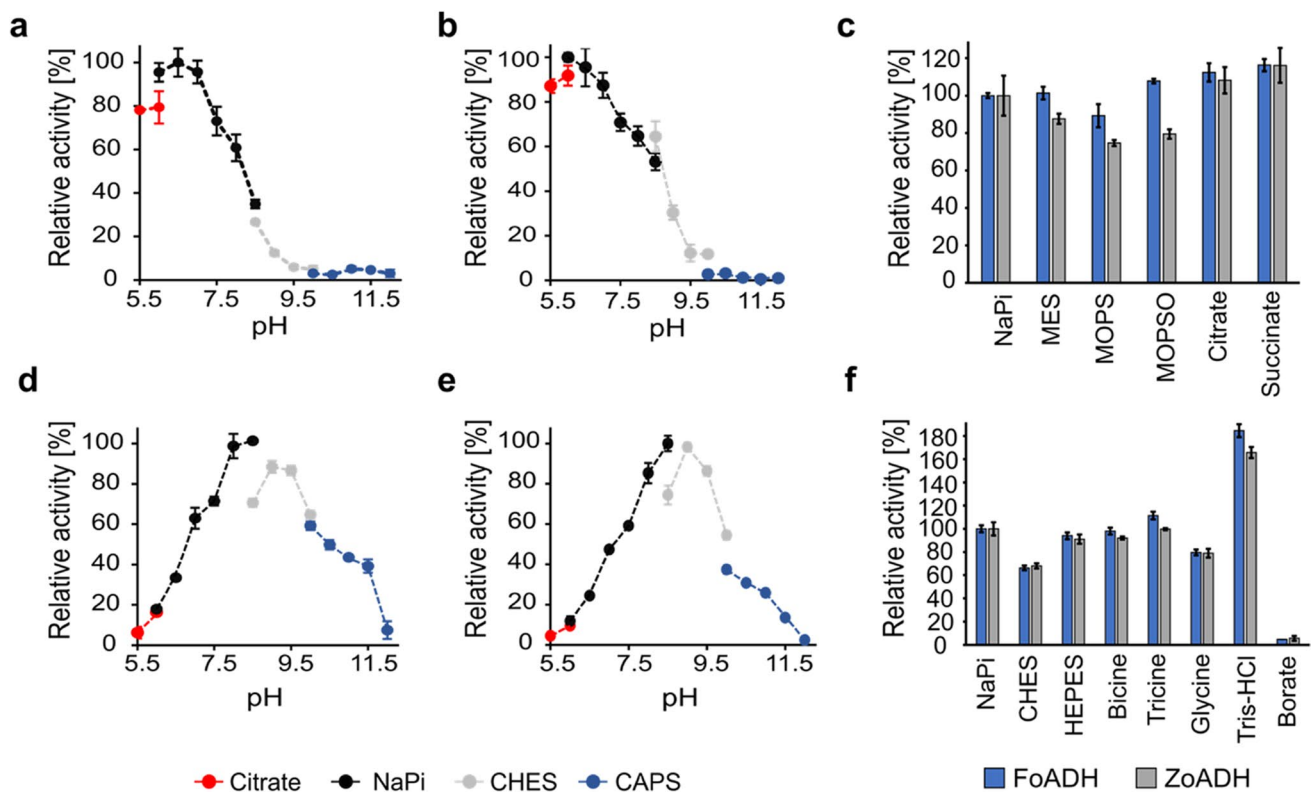
**a**



**b**



**Fig. 3** Thiol-dependent detoxification of formaldehyde catalyzed by an ADH and an esterase. **a** Principle of thiol-dependent detoxification of formaldehyde and **b** investigated thiols



**Fig. 4** Influence of pH and buffer components on the ADH activity. pH optimum for the reduction reaction of **a** FoADH and **b** ZoADH as well as the pH optimum for the oxidation reaction catalyzed by **d** FoADH and **e** ZoADH. **c** Reduction of benzaldehyde and **f** oxidation of benzyl alcohol by the ADHs at the respective pH optima using various buffers. A pH of 6.5 was employed for the reduction reaction and a pH of 8.5 for the oxidation reaction; all buffers had a concentration of 50 mM. Since some buffers including bicine, tricine, Tris, MOPSO, and HEPES contain hydroxyl groups, a falsified activity due to the turnover of these substances was excluded by a measurement without additional substrate. However, no activity was observed for

any buffer component. All measurements (**a-f**) were performed under the following conditions: a final substrate concentration of 10 mM benzyl alcohol or benzaldehyde, 3.5% (v/v) DMSO, and 0.5 mM NAD<sup>+</sup> or NADH was used. The reaction was started by the addition of ADH at a final enzyme concentration of 0.1 mg mL<sup>-1</sup>. The measurement was performed at 25 °C in the respective buffers with concentrations of 50 mM. The maximum relative activity (100%) corresponds to the measurements in the 50 mM NaPi buffers at pH 6.5 for reduction and pH 8.5 for oxidation reactions. All measurements were performed in triplicates; the mean is given, and the error bars indicate the standard deviation

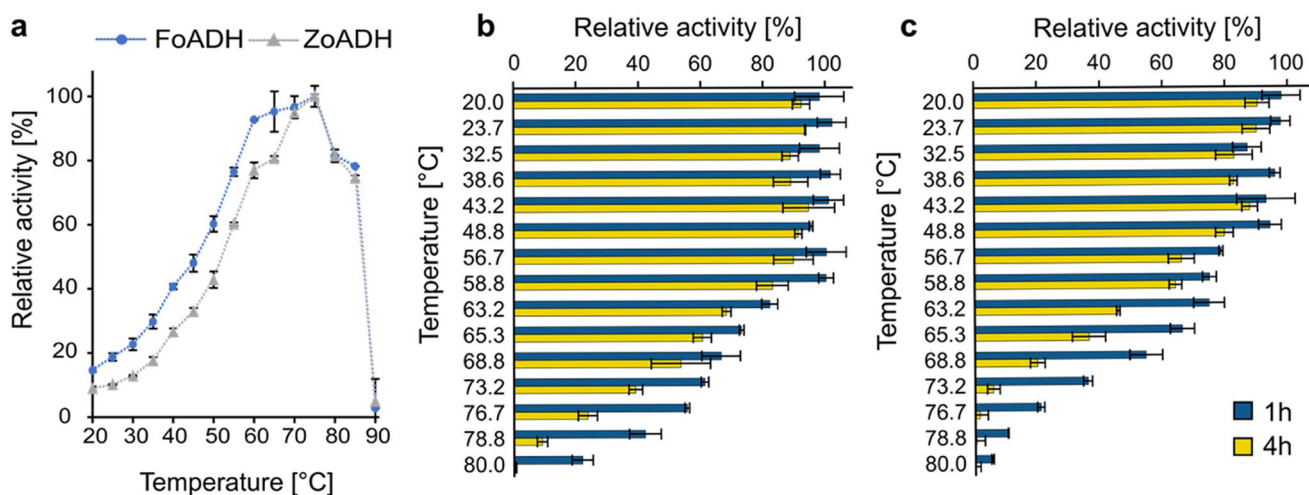
### Influence of sodium chloride

Enzymes originating from marine organisms may possess habitat-related characteristics such as an increased salt tolerance (Trincone 2011). Considering that both enzymes originate from marine bacteria, the influence of NaCl on the enzyme activity was tested. For this purpose, the relative activities for the oxidation reaction were determined in the presence of different NaCl concentrations ranging from 0 to 800 mM in the NaPi and tricine buffer, respectively. Both ADHs displayed similar behavior in the presence of rising NaCl concentrations (Fig. S5). An increase in the relative activity of approximately 10% was observed in the range from 0 to 150 mM NaCl for FoADH using the tricine buffer. In contrast, only a minor increase in activity was observed for the NaCl concentration of 100 mM in the NaPi buffer. A difference in the NaCl influence depending on the selected buffer was also noticed for ZoADH, with a higher effect

in the tricine buffer. For ZoADH, an increase in the relative activity of 20% was also detected in the range of 0 to 200 mM NaCl. At NaCl concentrations  $\geq 400$  mM, a diminished relative activity was observed for both enzymes.

### Influence of metal ions and other small molecules

Both enzymes are annotated as zinc-dependent ADHs, which contain a catalytic zinc ion in the active site. An influence of various metal ions on the enzyme activity is thus possible and was therefore investigated next. For this purpose, the enzymes were incubated with different metal ions at concentrations of 1 or 10 mM for 1 h prior to activity measurement, and the relative activities were determined. High dependence on metal ions was observed for both ADHs, with nearly all ions assayed exhibiting a beneficial effect on enzyme activity (Table 3; Fig. S6). Particularly higher concentrations of Ni<sup>2+</sup>, Co<sup>2+</sup>, and Mn<sup>2+</sup> led to a 10- to



**Fig. 5** Temperature optimum and thermostability of the ADHs. **a** Influence of temperature on enzyme activity. The measurement was performed at various temperatures ranging from 20 to 80 °C for 10 min. The maximum relative activity (100%) corresponds to the measurement at 75 °C for both enzymes. Influence of temperature on enzyme stability for **b** FoADH and **c** ZoADH. The enzymes with a concentration of 1 mg mL<sup>-1</sup> were incubated at different temperatures between 20 and 80 °C for 1 or 4 h, followed by the determination of residual activity. The measurement was performed at 40 °C. The

14-fold increase in relative activity for both enzymes compared to the control, which contained no additional metal ion. In contrast, complete inhibition for both enzymes was only observed for Cu<sup>2+</sup>, Zn<sup>2+</sup>, and 10 mM Fe<sup>3+</sup>. Additionally, we analyzed whether the chelating agent EDTA, which is capable of complexing bivalent metal ions, affects the enzymatic activity. After 1 h incubation in the presence of 25 mM EDTA, a reduction in the relative activity for both enzymes was found, while an almost complete inhibition was observable at an EDTA concentration of 100 mM (Table 3; Fig. S7). The influence of DTT and 2-ME on activity was also investigated since these compounds can affect enzyme stability. DTT had a lesser impact on both enzymes than 2-ME. A major decline in the relative activity of over 70% was observed for both enzymes after 1 h incubation with 10 mM 2-ME (Table 3; Fig. S7). When compared to ZoADH, the effect of the reducing agents was more pronounced for the activity of FoADH.

### Influence of solvents and formaldehyde

The influence of water-miscible solvents on the enzyme activity of both ADHs was also investigated. Increasing the amount of solvent in the reaction led to a decrease in the relative activity for all tested solvents (Fig. S8). Compared to the other solvents, methanol and DMSO had the weakest negative effects on the enzyme activity, leading to a relative activity of still 50% in the presence of 10% (v/v) solvent. In

maximum relative activity (100%) corresponds to a control incubated on ice for 1 or 4 h. All measurements (a–c) were performed under the following conditions: a final substrate concentration of 10 mM benzyl alcohol and 0.5 mM NAD<sup>+</sup> was used. The reaction was started by the addition of ADH at a final enzyme concentration of 0.1 mg mL<sup>-1</sup>. The measurements were performed in a 50 mM NaPi buffer at pH 7.5. All measurements were performed in triplicates; the mean is given, and the error bars indicate the standard deviation

**Table 3** Influence of various substances on the enzyme activity of both ADHs

Chemical	Conc. (mM)	Relative activity (%)	
		FoADH	ZoADH
None	–	100 ± 1.3	100 ± 9.3
KCl	10	121 ± 1.9	154 ± 7.9
CaCl <sub>2</sub>	10	188 ± 6.3	306 ± 9.9
MgCl <sub>2</sub>	10	219 ± 7.2	328 ± 11.7
NiCl <sub>2</sub>	10	891 ± 13.8	1004 ± 6.6
CoCl <sub>2</sub>	10	1280 ± 38.1	1242 ± 25.4
MnCl <sub>2</sub>	10	1394 ± 58.5	973 ± 45.0
ZnCl <sub>2</sub>	10	n.d.	n.d.
CuCl <sub>2</sub>	10	n.d.	n.d.
FeCl <sub>3</sub>	10	n.d.	n.d.
EDTA	25	61 ± 1.9	61 ± 7.8
DTT	10	48 ± 4.6	85 ± 3.9
2-ME	10	19 ± 1.7	28 ± 4.1

The ADH was incubated with the respective component for 1 h at RT prior to measurement. The maximum relative activity (100%) corresponds to the measurement for the control, which contained no additives. All measurements were performed under following conditions: a final substrate concentration of 10 mM benzyl alcohol and 0.5 mM NAD<sup>+</sup> was used. The reaction was started by the addition of ADH at a final enzyme concentration of 0.1 mg mL<sup>-1</sup>. The measurements were performed in a 50 mM HEPES buffer at pH 8.5 at 25 °C. All measurements were performed in triplicates; the mean and the standard deviation are given

*n.d.*, not detected

addition, the presence of formaldehyde on the enzyme activity was examined, since formaldehyde is released during the oxidative demethylation of G6Me and the ADHs are most likely involved in this reaction. Therefore, the ADHs were incubated with a variety of formaldehyde concentrations in the range between 0 and 50 mM for 1 h at RT, and the relative activities were determined. In the presence of 0 to 1 mM formaldehyde, no reduction in activity was observed. An initial decrease in the relative activity of approximately 10–20% could be perceived in the presence of 2.5 mM formaldehyde (Fig. S9). At higher formaldehyde concentrations, a more severe activity decrease was found, while no activity was observed for both enzymes in the presence of 50 mM formaldehyde.

### Overall structures of FoADH and ZoADH

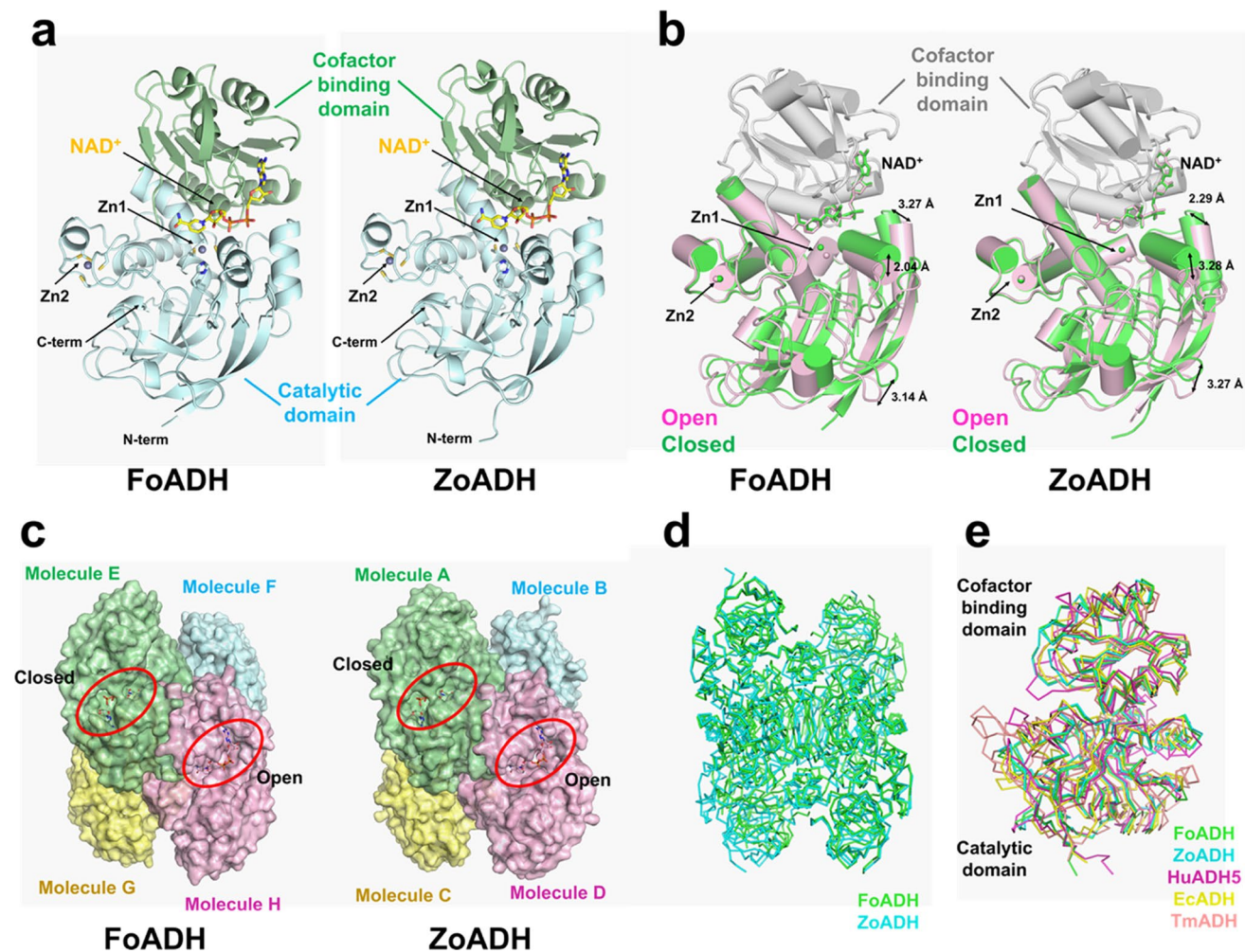
In order to gain a deeper understanding of the molecular function, we performed X-ray crystallography studies of FoADH and ZoADH. For the determination of the functional states of both ADHs, the essential  $\text{NAD}^+$  cofactor was added to purified FoADH and ZoADH proteins before crystallization. The crystal structures of FoADH and ZoADH in complex with  $\text{NAD}^+$  were determined at a resolution of 2.5 and 2.1 Å, respectively (Table S2). FoADH and ZoADH crystals belong to the space group monoclinic  $P2_1$  and orthorhombic  $P2_12_12_1$ , respectively, and contain four and eight molecules in the asymmetric unit, respectively (Fig. S10). The electron density map of FoADH and ZoADH clearly showed the almost entire polypeptide chain, except for a partially disordered fragment of the loop between the  $\beta 5$ - and  $\beta 6$ -strands (Gly111-His115 in both enzymes), which is involved in substrate binding and specificity. The monomer structures of FoADH and ZoADH comprise the catalytic domain (residues 1–149 and residues 283–326 for both enzymes) and the cofactor-binding domain (residues 150–282 for both enzymes) (Fig. 6a), which are separated by a cleft containing a deep pocket, which accommodates the substrate and the  $\text{NAD}^+$  cofactor. The catalytic domain contains two zinc-binding sites, Zn1 and Zn2, which are responsible for catalytic activity and structural stability, respectively. The cofactor binding domain adopts a typical Rossmann fold with the conserved sequence “GXGXXG.” FoADH and ZoADH had a 76.0% similarity in amino acid sequence (Fig. S11), and their monomer structures showed a similarity with a root-mean-square deviation (r.m.s.d.) of 0.350–0.772 Å (Table S4).

In FoADH, molecules A/B/C/D and E/F/G/H form a tetrameric formation (Fig. S10). In the superimposition of monomeric FoADH molecules, the A, B, C, E, and G molecules showed structural similarity (denoted as closed form) with a r.m.s.d. of 0.256–0.353 Å, whereas molecules

D and H (denoted as open form) showed the relatively high r.m.s.d. value of 0.457–0.626 Å when superimposed with molecules A, B, C, E, and G (Fig. 6b; Table S5). On the other hand, molecule F maintains the intermediate conformation between the closed and open conformations. When the cofactor binding domains of molecules A and H of FoADH were superimposed, the catalytic binding of molecule H was shifted by approximately 2.0–3.3 Å in the opposite direction of the substrate-binding cleft compared to molecule A (Fig. 6b).

In ZoADH, the superimposition of molecules A, B, and C exhibited a similar conformation (denoted as closed form) with a r.m.s.d. of 0.198–0.226 Å, whereas molecule D (denoted as open form) showed a relatively high r.m.s.d. value of 0.314–0.471 Å when superimposed with molecules A, B, and C (Fig. 6b; Table S6). Superposition of the cofactor binding domains of molecules A and D clearly revealed the conformational difference between the catalytic domains. The catalytic domain of molecule D is shifted about 2.2–3.3 Å to the outside of the substrate binding cleft of ZoADH compared to molecule A. Accordingly, in the structure of  $\text{NAD}^+$ -bound FoADH, molecules A/B/C and D represent closed and open conformations of the substrate binding site, respectively. Collectively, the crystal structures of  $\text{NAD}^+$ -bound ZoADH and FoADH contain open and closed conformations between catalytic and cofactor-binding domains (see below).

The crystal structures of FoADH and ZoADH showed the tetrameric formation via the arrangement of a dimer of dimers (Fig. 6c). In both ADHs, the  $\beta 17$ - and  $\beta 18$ -strands of the cofactor binding domains are stabilized by forming an antiparallel  $\beta$ -sheet with the  $\beta 17^*$  and  $\beta 18^*$  strands (asterisk indicates the second monomer), respectively (Figs. S12 and S13). For FoADH, the dimeric interface is stabilized by the main chain interactions of Ile297-Ile299\* (asterisk denotes the partner molecule) and Ile299-Ile297\* between the  $\beta 17$  strands and Tyr310-Tyr310\* between  $\beta 18$  strands (Fig. S12). In addition, numerous hydrogen and salt bridges were observed in the dimer interface with a buried surface area of 1654 Å<sup>2</sup> (Table S7). The dimer of dimers is stabilized by hydrogen interaction and the buried interface of dimers of dimers is 1193 Å<sup>2</sup> (Table S7). For ZoADH, the dimeric interface is stabilized by the main chain interactions of Ile298-Ile300\* and Ile300-Ile298\* between the  $\beta 17$  strand and Tyr311-Tyr311\* between the  $\beta 18$  strand (Fig. S13). Moreover, numerous hydrogen and salt bridges were observed at the dimer interface with a buried surface area of 1640 Å<sup>2</sup> (Table S8). The dimer of dimers is stabilized by hydrogen interactions and salt bridges and the buried interface of dimers of dimers is ~1205 Å<sup>2</sup> (Table S8). All active sites of the tetrameric ADH in the crystal were exposed to solvent (Fig. 6c). Superposition of tetrameric molecules of FoADH and ZoADH in the



**Fig. 6** Crystal structures of FoADH and ZoADH. **a** Monomer structures of ZoADH and FoADH. The catalytic and cofactor domains are indicated by cyan and green, respectively.  $\text{NAD}^+$  and zinc ions are indicated by a yellow stick and a gray sphere, respectively. **b** Superimposition of closed (green) and open conformation between catalytic and cofactor-binding domains of ZoADH and FoADH monomers. The superimposed cofactor-binding domain of ZoADH and FoADH are indicated as gray cartoons. **c** Tetrameric formation of ZoADH

and FoADH. **d** Superimposition of tetrameric formation of FoADH (green) and ZoADH (cyan). **e** Superimposition of monomer structures of FoADH (green) and ZoADH (cyan) with all-trans-retinol dehydrogenase ADH4 from *Homo sapiens* (pink, PDB code: 3COS), uncharacterized zinc-type alcohol dehydrogenase-like protein YdjJ from *E. coli* (wheat, 5vm2), and scyllo-inosose 3-dehydrogenase from *Thermotoga maritima* (3IP1, yellow)

asymmetric unit shows a r.m.s.d. of 0.327–0.888 Å for whole  $\text{C}\alpha$  atoms (Fig. 6d).

Structural homology search by DALI revealed that both FoADH and ZoADH share structural similarities to the class II alcohol dehydrogenase (ADH4) from humans (PDB code: 3COS, Z-score = 45.8 for FoADH and 45.3 for ZoADH, sequence identity = 32% for FoADH [357 $\alpha$  atoms] and 30% for ZoADH [357 $\alpha$  atoms]), an ADH from *E. coli* (PDB code: 5vm2, Z-score = 48.1 for FoADH and 38.1 for ZoADH, sequence identity = 28% for FoADH [329 $\alpha$  atoms] and 27% for ZoADH [328 $\alpha$  atoms]) as well as an ADH from *Thermotoga maritima* (PDB code: 3IP1, Z-score = 35.8 for FoADH and 36.8 for ZoADH, sequence identity = 25% for FoADH [328 $\alpha$  atoms] and 23% for ZoADH [332 $\alpha$  atoms]).

Although these structural homologous ADHs share low amino acid sequence similarities with less than 32% compared to FoADH and ZoADH, the active site residues involved in the  $\text{Zn}^{2+}$  and  $\text{NAD}^+$  binding are highly conserved (Fig. S11). In addition, the  $\text{NAD}^+$ -binding domain exhibits a typical Rossmann fold motif and has the classical conserved sequence “GXGXG” as in other ADHs, and the topologies of those ADHs are highly similar (Fig. S11). The overall topology of those homolog structures was similar to FoADH and ZoADH (Fig. S14). However, superimposition of those ADH structures revealed that there is a large difference in conformation between catalytic and cofactor-binding domains with a r.m.s.d. of 1.373–2.963 Å for FoADH and 1.376–2.191 for ZoADH (Fig. 6e), indicating that they

possess large distinct NAD<sup>+</sup> and substrate-binding clefts. Meanwhile, ADHs from *E. coli* and *T. maritima* also formed the tetrameric formation in crystal structures like FoADH and ZoADH (Fig. S14). These ADHs have a similar tetrameric assembly; however, the superimposition of the tetrameric ADHs showed that these tetrameric assemble have low similarity with a r.m.s.d. of 17.68–29.94 Å.

### NAD<sup>+</sup> and Zn<sup>2+</sup>-binding sites of FoADH and ZoADH

While NAD<sup>+</sup> is the required cofactor for alcohol oxidation, Zn<sup>2+</sup> interacts with the alcohol molecule in the active site. The electron density maps of a NAD<sup>+</sup> molecule and two zinc ions are clearly observed in a substrate-binding cleft of both FoADH and ZoADH (Fig. S15). The binding configuration of NAD<sup>+</sup> and the Zn<sup>2+</sup> ions of ZoADH and FoADH are highly similar (Fig. 7a). The adenine ring of NAD<sup>+</sup> is located in the hydrophobic pocket formed by hydrophobic interaction (Ile219, Leu245, Thr268, Ile270, and Leu273 for FoADH, Ile220, Leu246, Thr269, Ile271, and Leu274 for ZoADH). The adenine ribose appears to be in a C2'-endo conformation, and the O2' and O3'-hydroxyl group of ribose forms a hydrogen bond with the side chain of aspartate (Asp218 for FoADH and Asp219 for ZoADH). The pyrophosphate moiety of the NAD<sup>+</sup> interacts with the nitrogen atoms of the main chain of glycine-valine residue (Gly197-Val198 for FoADH and Gly198 and Val199 for ZoADH) that forms the loop between strand β5 and helix α4. The nicotinamide ribose is in a C2'-endo conformation, and hydrogen bonds are formed between the ribose O2'-hydroxyl group and threonine (Thr43 for FoADH and ZoADH). The nicotinamide ring is in the anti-conformation. The carboxamide nitrogen atom of the nicotinamide ring interacted with the main chain of proline (Pro313 for FoADH and Pro314 for ZoADH) and valine (Val290 for FoADH and Val291 for ZoADH). The carboxamide oxygen atom of the nicotinamide ring interacted with the main chain of tyrosine (Tyr315 for FoADH and Tyr316 for ZoADH). Therefore, in both FoADH and ZoADH, the NAD<sup>+</sup> molecules are stabilized by hydrophobic and hydrogen bond interactions.

In both FoADH and ZoADH, two zinc ions are commonly observed in the active site (Zn1 site) and in a loop between α2 and β7 (Zn2 site) (Fig. 7a; Fig. S15). The zinc ion at the Zn1 site is coordinated by conserved cysteine and histidine residues (Cys41, His58, and Cys169 for FoADH and Cys41, His58, and Cys170 for ZoADH) in the catalytic domain. The zinc ion at the Zn2 site is involved in the protein stability and is tetrahedrally coordinated by conserved cysteine residues (Cys88, Cys91, Cys94, and Cys102 for both enzymes) (Fig. S15). Their result indicated that ZoADH and FoADH showed high structural similarity for the NAD<sup>+</sup> and zinc-binding configuration.

Different structural conformations were observed between monomeric ADHs in the tetrameric formation of FoADH and ZoADH (Fig. 6b), indicating that they exhibit structurally different substrate binding clefts and active sites. In both results of superimposition of the active sites of FoADH and ZoADH, the positions of the NAD<sup>+</sup> and Zn2 sites were similar, whereas a significant difference was observed in the positions of the catalytic Zn1 sites (Fig. 7b). In FoADH and ZoADH, the maximum distances between metals from the Zn1 site were 2.57 and 2.60 Å, respectively, from the closed and open conformations of two domains of ADHs (Fig. 7b).

Since the substrate binds to the Zn1 site and a dehydrogenase reaction occurs through the interaction of NAD<sup>+</sup> with the hydroxyl group, the size of the space between NAD<sup>+</sup> and Zn1 is involved in substrate selectivity. The closest/longest distances between the Zn<sup>2+</sup> and C5 atoms of the nicotinamide ring of NAD<sup>+</sup> in FoADH and ZoADH were 3.21/4.91 Å and 3.46/5.49 Å, respectively (Fig. 7c). These different distances between Zn<sup>2+</sup> and NAD<sup>+</sup> were caused by the different closed and open conformations of FoADH and ZoADH.

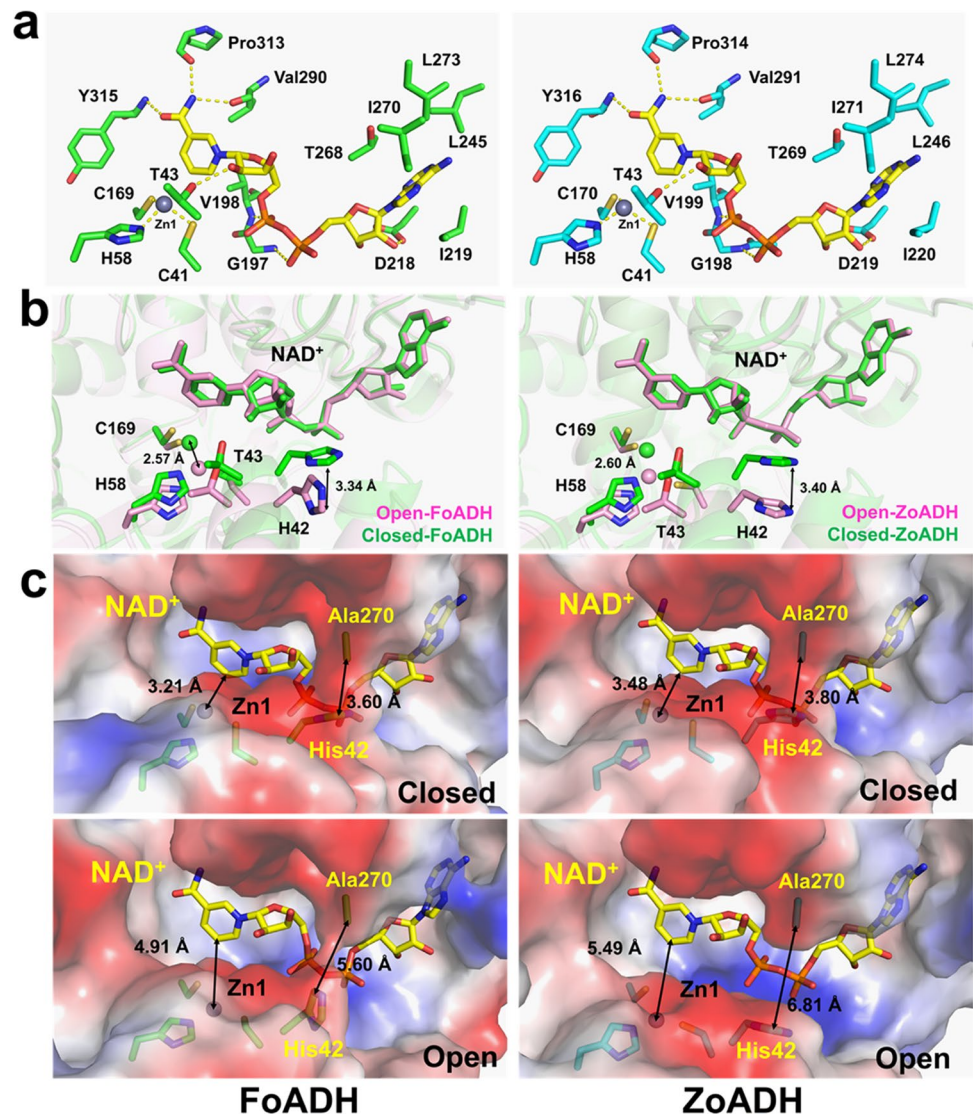
The electrostatic surfaces of FoADH and ZoADH showed that the substrate binding sites commonly exhibited a hydrophobic surface (Fig. 7c). The space of the substrate binding site of FoADH in closed and open conformations was approximately 3.4 × 4.2 Å and 3.9 × 5.4 Å, respectively (Fig. S15). In the closed and open conformations of FoADH, His42 and Ala270 are apart by 3.60 and 5.60 Å, respectively, showing the surface structures surrounding the NAD<sup>+</sup> (Fig. 7c). ZoADH also exhibits open and closed conformations similar to FoADH, but the distance of open conformation is relatively wide. The space of the substrate binding site of ZoADH in closed and open conformation was approximately 3.0 × 3.8 Å and 3.8 × 4.9 Å, respectively (Fig. S15). In the closed conformation of ZoADH, the catalytic domain and the cofactor domain are close to each other, especially His42 and Ala270 by a distance of 3.88 Å, indicating the surface structure surrounding the NAD<sup>+</sup> (Fig. 7c). On the other hand, in the open conformation of ZoADH, His42 and Ala270 are apart by 6.81 Å, and accordingly, the entire NAD<sup>+</sup> molecule in the surface structure is exposed to the solvent (Fig. 7c).

## Discussion

In the present work, FoADH from *F. agariphila* KMM 3901<sup>T</sup> and ZoADH from *Z. galactanivorans* Dsij<sup>T</sup> were characterized in detail to draw conclusions about their biological function. Three main conclusions regarding biological function can be derived from the knockout of the genes encoding for ZoADH and CYP in *Z. galactanivorans*



**Fig. 7** Active sites of FoADH and ZoADH. **a** Interaction of ZoADH and FoADH with NAD<sup>+</sup> and zinc ions at the Zn1 site. **b** Superimposition of the active sites of open and closed conformations of FoADH and ZoADH. **c** Comparison of electrostatic surface structures of open and closed conformations of FoADH and ZoADH



and subsequent growth studies on D-galactose and G6Me. First, we confirmed the hypothesis of Reisky et al. that in the absence of CYP-catalyzed oxidative demethylation, a G6Me utilization as the sole carbon source is infeasible for the organism (Reisky et al. 2018). Surprisingly, the knockout of the ZoADH gene also caused diminished growth of *Z. galactanivorans* in the presence of G6Me. Second, due to this observation, we can conclude a significant role of these ADHs in G6Me utilization in these marine bacteria. From an ecological perspective, this has additional importance for marine carbohydrate degraders. G6Me can occur up to 28% within the porphyrin chain (Rees and Conway 1962). Thus, reduced utilization of G6Me would represent a substantial potential loss as a carbon source for the organism. Third, since normal growth was

observed in the presence of D-galactose as the sole carbon source, a function in D-galactose metabolism can be excluded. This was also supported by the observation that both ADHs lacked activity for D-galactose. The ADHs are therefore probably involved in oxidative demethylation or a subsequent reaction. Since no activity was observed for G6Me, the substrate of oxidative demethylation could be excluded. Consequently, we hypothesized that the ADHs are involved in the detoxification of formaldehyde, which is a by-product of the oxidative demethylation reaction. This was also supported by the resistance of both ADHs to formaldehyde exposure. Formaldehyde is a toxic metabolite due to its properties as a highly reactive electrophile. It can react with free amino and thiol groups of proteins and nucleic acids, leading to protein and DNA damage as

well as cross-link formations (Chen et al. 2016; Shishodia et al. 2018; Tayri-Wilk et al. 2020). It has been shown that higher concentrations of formaldehyde can negatively affect the growth of *Z. galactanivorans* (Brott et al. 2022). Thus, reduced growth of the ADH knockout strain could be explained by the potential accumulation of formaldehyde. There are numerous metabolic pathways in which formaldehyde can be detoxified (Yurimoto et al. 2005; Klein et al. 2022). However, in the thiol-dependent formaldehyde detoxification, a zinc-dependent ADH and an esterase perform the key reactions (Sanghani et al. 2000; Gonzalez et al. 2006). Genome neighborhood analysis revealed that most marine bacteria that possess the ADH gene are located in close proximity to a gene encoding for an esterase in addition to the CYP gene. We, therefore, investigated whether the ADH catalyzed thiol-dependent detoxification of formaldehyde. However, with glutathione, mycothiol, and bacillithiol as thiol cofactors, no activity was detected for either ADH. These observations can be further explained by the crystal structures of both ADHs; sterically demanding compounds such as mycothiol or bacillithiol cannot fit into the narrow active site of these enzymes. These observations are also consistent with the results from the sequence similarity network, in which glutathione- and mycothiol-dependent formaldehyde dehydrogenases were predominantly present in different clusters (main clusters 1 and 4) than the ADHs (main cluster 2). Since no activity could be detected with literature-known cofactors, additional thiols were considered; however, no activity could be observed either. Thiol cofactors are still being discovered (Newton and Rawat 2019); perhaps marine organisms also possess an unidentified thiol, which can serve as a cofactor for this reaction. Since no activity was observed for formaldehyde without an additional thiol cofactor, the biological function of a thiol-independent formaldehyde dehydrogenase was excluded. In addition, some ADHs can possess dismutase activities (Trivić et al. 1999). A formaldehyde dismutase catalyzes the disproportionation of formaldehyde to methanol and formic acid in the presence of a covalently bound  $\text{NAD}^+$  (Yonemitsu and Kikuchi 2018). However, this reaction could not be detected. Both organisms harbor other metabolic pathways for the detoxification of formaldehyde (Brott et al. 2022). For instance, in *Z. galactanivorans*, the genes encoding the key enzymes of the ribulose monophosphate pathway are upregulated in the presence of porphyran (Brott et al. 2022), so an accumulation of formaldehyde is unlikely. Eventually, the ADHs might have a completely different biological function, such as the regeneration of NADH (Hilberath et al. 2021; Kokorin et al. 2021). In the oxidative demethylation reaction, NADH is oxidized to  $\text{NAD}^+$ , and a reduced growth in the ADH knockout strain due to cofactor depletion might be possible. NADH could be

regenerated by the oxidation of an unknown component or by the thiol-dependent formaldehyde detoxification pathway. However, it is doubtful that the loss of one single enzyme would cause such a tremendous effect on NADH/ $\text{NAD}^+$  homeostasis. Additionally, the ADHs displayed predominantly activity for the reduction of aldehydes under NADH consumption, so recycling of a cofactor is improbable.

Both ADHs possessed predominantly activity for aromatic substances, resulting in a substrate specificity resembling partially those of cinnamyl alcohol and/or benzyl alcohol dehydrogenases (Larroy et al. 2002; Willson et al. 2022). However, the highest activity was observed for pyridine-3-carbaldehyde and furan derivatives. Furfural is generally produced as a side product by pretreating lignocellulosic biomass for the production of bioethanol. Under acidic conditions and high temperatures, dehydration of pentoses and hexoses proceeds, leading to the formation of furfural or hydroxymethylfurfural. Furfural acts as an inhibitor in subsequent bioethanol-producing fermentations by bacteria by prolonging the lag phase of growth and thereby the fermentation time (Mariscal et al. 2016). Consequently, these marine bacteria possess ADHs that catalyze the potential removal of furfural, although the biological function may be different. The ADHs lacked activity for various sugar substrates, which excluded a polyol dehydrogenase activity. Activity for any other monosaccharides, disaccharides, or even oligosaccharides formed during porphyran degradation is unlikely as well, considering the substrate specificity of the enzymes based on the narrow active site. The data from biochemical characterizations are discussed in the SI.

We have determined the crystal structures of FoADH and ZoADH complexed with  $\text{NAD}^+$  and two zinc ions. These ADHs showed high structural similarity in terms of topology and assembly. On the one hand, these two ADHs showed similarities in topology with other ADHs from humans, *E. coli*, and *T. maritima*, but showed distinct conformation between the cofactor and catalytic domains of those ADHs. On the other hand, the crystal structures of FoADH and ZoADH showed open and closed conformations, indicating that the conformation between the two domains can change in the state where the substrate is not bound. These distinct conformations of FoADH and ZoADH represent different substrate binding pockets. When they exhibit an open conformation between the two domains of FoADH and ZoADH, they form a broadened substrate-binding pocket. Accordingly, in terms of substrate accessibility, we consider that substrate accessibility will be easier when FoADH and ZoADH have an open conformation.

During substrate recognition, when the converting functional group from the substrate approaches the Zn1 site on the substrate binding pocket of FoADH and ZoADH, the rest of the substrate is exposed to the nicotinamide of  $\text{NAD}^+$  or

the hydrophobic surface. Considering that the nicotinamide group of NAD<sup>+</sup> is involved in the oxidoreductase mechanism of the ADH, the substrate would prefer to be located on the hydrophobic surface rather than the nicotinamide group of NAD<sup>+</sup>. Accordingly, FoADH and ZoADH may prefer substrates having a hydrophobic body. Our biochemical studies showed that both enzymes prefer aromatic substrates. We expected that the aromatic ring of the substrate may be located on a hydrophobic surface nearby the substrate binding pocket of FoADH and ZoADH. In this case, the aromatic ring of the substrate could interact with the Phe136 residue in the hydrophobic surfaces of the enzymes. Based on the active site structures of both, ADH computational docking of a substrate will be able to provide an insight into the molecular mechanism and substrate specificity. However, from the results of this study, ZoADH and FoADH have various conformations between catalytic and cofactor binding domains in NAD<sup>+</sup> and two zinc ion-binding states, indicating the computational docking results could be different depending on the applied model structure. Also, based on our results, we concluded that the docking results may be different from biochemical experiments if the active sites of ZoADH and FoADH may have different conformations. Therefore, to better understand the substrate specificity, the crystal structures of ZoADH and FoADH in complex with the biological substrate will be needed in the future.

In summary, in this study, we determined the putative functions of conserved ADH from marine *Flavobacteriia*. Additionally, we provided the crystal structures of the enzymes of *F. agariphila* and *Z. galactanivorans*. Enzymatic studies revealed the preferential conversion of aromatic aldehydes. We revealed that these enzymes are not involved in formaldehyde detoxification or in the subsequent reaction of the oxidative demethylation of G6Me. Based on gene knock-outs, we demonstrated the essential role of these ADHs in the utilization of marine algal sugars. Our study indicates a potential auxiliary activity of these ADHs in the utilization of algal sugars by marine *Flavobacteriia*.

**Supplementary Information** The online version contains supplementary material available at <https://doi.org/10.1007/s00253-023-12447-x>.

**Author contribution** M.G., T.S., and U.T.B. initiated the study and directed the project. F.T. conducted the growth studies and created the knock-out strain. K.H.N. performed the crystallization and structural analyses. T.D. performed the computational analysis. L. R. and H.C.G. performed the cloning and initial experiments on the enzyme function of FoADH. S.B. and M.B. expressed and purified the enzymes and performed further experiments on enzyme function and characterization. S.B. and K.H.N. prepared the main manuscript, which was revised by F.T., T.D., H.C.G., L.R., M.G., T.S., and U.T.B. and was approved by all authors.

**Funding** Open Access funding enabled and organized by Projekt DEAL. François Thomas acknowledges support from the French government via the National Research Agency program ALGAVOR

(ANR-18-CE02-0001). We thank the German Research Foundation (DFG) for funding through the Research Unit FOR2406 “Proteogenomics of Marine Polysaccharide Utilization” (POMPU) (Grants No. BO 1862/17–1 and No. BO 1862/17–2 to U.T.B. and No. SCHW 595/10–2 to T.S.).

**Data availability** The datasets generated during and/or analyzed during the current study are available from the corresponding author upon reasonable request.

## Declarations

**Ethical approval** Not applicable.

**Conflict of interest** The authors declare no conflict of interest.

**Open Access** This article is licensed under a Creative Commons Attribution 4.0 International License, which permits use, sharing, adaptation, distribution and reproduction in any medium or format, as long as you give appropriate credit to the original author(s) and the source, provide a link to the Creative Commons licence, and indicate if changes were made. The images or other third party material in this article are included in the article's Creative Commons licence, unless indicated otherwise in a credit line to the material. If material is not included in the article's Creative Commons licence and your intended use is not permitted by statutory regulation or exceeds the permitted use, you will need to obtain permission directly from the copyright holder. To view a copy of this licence, visit <http://creativecommons.org/licenses/by/4.0/>.

## References

- Achkor H, Díaz M, Fernández MR, Biosca JA, Parés X, Martínez MC (2003) Enhanced formaldehyde detoxification by overexpression of glutathione-dependent formaldehyde dehydrogenase from *Arabidopsis*. *Plant Physiol* 132:2248–2255. <https://doi.org/10.1104/pp.103.022277>
- Arnosti C, Wietz M, Brinkhoff T, Hehemann JH, Probandt D, Zeugner L, Amann R (2021) The biogeochemistry of marine polysaccharides: sources, inventories, and bacterial drivers of the carbohydrate cycle. *Annu Rev Mar Sci* 13:81–108. <https://doi.org/10.1146/annurev-marine-032020-012810>
- Bauer M, Kube M, Teeling H, Richter M, Lombardot T, Allers E, Würdemann CA, Quast C, Kuhl H, Knaust F, Wobken D, Bischof K, Musmann M, Choudhuri JV, Meyer F, Reinhardt R, Amann RI, Glöckner FO (2006) Whole genome analysis of the marine Bacteroidetes “*Gramella forsetii*” reveals adaptations to degradation of polymeric organic matter. *Environ Microbiol* 8:2201–2213. <https://doi.org/10.1111/j.1462-2920.2006.01152.x>
- Bäumgen M, Dutschei T, Bartosik D, Suster C, Reisky L, Gerlach N, Stanetty C, Mihovilovic MD, Schweder T, Hehemann J-H, Bornscheuer UT (2021) A new carbohydrate-active oligosaccharide dehydratase is involved in the degradation of ulvan. *J Biol Chem* 297:101210. <https://doi.org/10.1016/j.jbc.2021.101210>
- Bäumgen M, Dutschei T, Bornscheuer UT (2021b) Marine polysaccharides: occurrence, enzymatic degradation and utilization. *ChemBioChem* 22:2247–2256. <https://doi.org/10.1002/cbic.202100078>
- Brott S, Thomas F, Behrens M, Methling K, Bartosik D, Dutschei T, Lalk M, Michel G, Schweder T, Bornscheuer UT (2022) Connecting algal polysaccharide degradation to formaldehyde detoxification. *ChemBioChem* 23:e202200269. <https://doi.org/10.1002/cbic.202200269>
- Brunet M, de Bettignies F, Le Duff N, Tanguy G, Davoult D, Leblanc C, Gobet A, Thomas F (2021) Accumulation of detached kelp

- biomass in a subtidal temperate coastal ecosystem induces succession of epiphytic and sediment bacterial communities. *Environ Microbiol* 23:1638–1655. <https://doi.org/10.1111/1462-2920.15389>
- Chandrangu P, Van LV, Antelmann H, Helmann JD (2018) The role of bacillithiol in Gram-Positive *Firmicutes*. *Antioxid Redox Signal* 28:445–462. <https://doi.org/10.1089/ars.2017.7057>
- Chen NH, Djoko KY, Veyrier FJ, McEwan AG (2016) Formaldehyde stress responses in bacterial pathogens. *Front Microbiol* 7:257. <https://doi.org/10.3389/fmicb.2016.00257>
- de Lorenzo V, Timmis KN (1994) Analysis and construction of stable phenotypes in gram-negative bacteria with Tn5- and Tn10-derived minitransposons. *Methods Enzymol* 235:386–405. [https://doi.org/10.1016/0076-6879\(94\)35157-0](https://doi.org/10.1016/0076-6879(94)35157-0)
- Emsley P, Cowtan K (2004) Coot: model-building tools for molecular graphics. *Acta Crystallogr D* 60:2126–2132. <https://doi.org/10.1107/S0907444904019158>
- Ficko-Blean E, Préchoux A, Thomas F, Rochat T, Larocque R, Zhu Y, Stam M, Génicot S, Jam M, Calteau A, Viart B, Ropartz D, Pérez-Pascual D, Correc G, Matard-Mann M, Stubbs KA, Rogniaux H, Jedy A, Barbeyron T, Médigue C, Czjzek M, Valenet D, McBride MJ, Duchaud E, Michel G (2017) Carrageenan catabolism is encoded by a complex regulon in marine heterotrophic bacteria. *Nat Commun* 8:1685. <https://doi.org/10.1038/s41467-017-01832-6>
- Field CB (1998) Primary production of the biosphere: integrating terrestrial and oceanic components. *Science* 281:237–240. <https://doi.org/10.1042/bst0040954>
- Gonzalez CF, Proudfoot M, Brown G, Korniyenko Y, Mori H, Savchenko AV, Yakunin AF (2006) Molecular basis of formaldehyde detoxification: characterization of two S-formylglutathione hydrolases from *Escherichia coli*, FrmB and YeiG. *J Biol Chem* 281:14514–14522. <https://doi.org/10.1074/jbc.M600996200>
- Gouet P, Courcelle E, Stuart DI, Métoz F (1999) ESPript: analysis of multiple sequence alignments in PostScript. *Bioinformatics* 15:305–308. <https://doi.org/10.1093/bioinformatics/15.4.305>
- Grondin JM, Tamura K, Déjean G, Abbott DW, Brumer H (2017) Polysaccharide utilization loci: fueling microbial communities. *J Bacteriol* 199:e00860–e916. <https://doi.org/10.1128/JB.00860-16>
- Gutheil WG, Holmquist B, Vallee BL (1992) Purification, characterization, and partial sequence of the glutathione-dependent formaldehyde dehydrogenase from *Escherichia coli*: a class III alcohol dehydrogenase. *Biochemistry* 31:475–481. <https://doi.org/10.1021/bi00117a025>
- Hall M, Bommaris AS (2011) Enantioenriched compounds via enzyme-catalyzed redox reactions. *Chem Rev* 111:4088–4110. <https://doi.org/10.1021/cr200013n>
- Hambidge M, Cousins RJ, Costello RB (2000) Zinc and health: current status and future directions: Introduction. *J Nutr* 130:1344S–1349S
- Hand CE, Honek JF (2005) Biological chemistry of naturally occurring thiols of microbial and marine origin. *J Nat Prod* 68:293–308. <https://doi.org/10.1021/np049685x>
- Hilberath T, Raffaele A, Windeln LM, Urlacher VB (2021) Evaluation of P450 monooxygenase activity in lyophilized recombinant *E. coli* cells compared to resting cells. *AMB Express* 11:162. <https://doi.org/10.1186/s13568-021-01319-0>
- Klein VJ, Irla M, López MG, Brautaset T, Brito LF (2022) Unraveling formaldehyde metabolism in bacteria: road towards synthetic methylotrophy. *Microorganisms* 10:220. <https://doi.org/10.3390/microorganisms10020220>
- Klemetsen T, Raknes IA, Fu J, Agafonov A, Balasundaram V, Tartari G, Robertsen E, Willassen NP (2018) The MAR databases: development and implementation of databases specific for marine metagenomics. *Nucleic Acids Res* 46:692–699. <https://doi.org/10.1093/nar/gkx1036>
- Koesoema AA, Standley DM, Senda T, Matsuda T (2020) Impact and relevance of alcohol dehydrogenase enantioselectivities on biotechnological applications. *Appl Microbiol Biotechnol* 104:2897–2909. <https://doi.org/10.1007/s00253-020-10440-2>
- Kokorin A, Parshin PD, Bakkes PJ, Pometun AA, Tishkov VI, Urlacher VB (2021) Genetic fusion of P450 BM3 and formate dehydrogenase towards self-sufficient biocatalysts with enhanced activity. *Sci Rep* 11:21706. <https://doi.org/10.1038/s41598-021-00957-5>
- Kracher D, Ludwig R (2016) Cellobiose dehydrogenase: an essential enzyme for lignocellulose degradation in nature - a review. *Die Bodenkultur J L Manag Food Environ* 67:145–163. <https://doi.org/10.1515/boku-2016-0013>
- Krause-Jensen D, Duarte CM (2016) Substantial role of macroalgae in marine carbon sequestration. *Nat Geosci* 9:737–742. <https://doi.org/10.1038/ngeo2790>
- Krissinel E, Henrick K (2007) Inference of macromolecular assemblies from crystalline state. *J Mol Biol* 372:774–797. <https://doi.org/10.1016/j.jmb.2007.05.022>
- Lapébie P, Lombard V, Drula E, Terrapon N, Henrissat B (2019) Bacteroidetes use thousands of enzyme combinations to break down glycans. *Nat Commun* 10:2043. <https://doi.org/10.1038/s41467-019-10068-5>
- Larroy C, Parés X, Biosca JA (2002) Characterization of a *Saccharomyces cerevisiae* NADP(H)-dependent alcohol dehydrogenase (ADHVII), a member of the cinnamyl alcohol dehydrogenase family. *Eur J Biochem* 269:5738–5745. <https://doi.org/10.1046/j.1432-1033.2002.03296.x>
- Li C, Wen A, Shen B, Lu J, Huang Y, Chang Y (2011) FastCloning: a highly simplified, purification-free, sequence- and ligation-independent PCR cloning method. *BMC Biotechnol* 11:92. <https://doi.org/10.1186/1472-6750-11-92>
- Liebschner D, Afonine PV, Baker ML, Bunkóczi G, Chen VB, Croll TI, Hintze B, Hung LW, Jain S, McCoy AJ, Moriarty NW, Oeffner RD, Poon BK, Prisant MG, Read RJ, Richardson JS, Richardson DC, Sammito MD, Sobolev OV, Stockwell DH, Terwilliger TC, Urzhumtsev AG, Videau LL, Williams CJ, Adams PD (2019) Macromolecular structure determination using X-rays, neutrons and electrons: recent developments in Phenix. *Acta Crystallogr D* 75:861–877. <https://doi.org/10.1107/S2059798319011471>
- Lu F, Xu W, Zhang W, Guang C, Mu W (2019) Polyol dehydrogenases: intermediate role in the bioconversion of rare sugars and alcohols. *Appl Microbiol Biotechnol* 103:6473–6481. <https://doi.org/10.1007/s00253-019-09980-z>
- Mariscal R, Mairales-Torres P, Ojeda M, Sádaba I, López Granados M (2016) Furfural: a renewable and versatile platform molecule for the synthesis of chemicals and fuels. *Energy Environ Sci* 9:1144–1189. <https://doi.org/10.1039/c5ee02666k>
- Martens EC, Koropatkin NM, Smith TJ, Gordon JI (2009) Complex glycan catabolism by the human gut microbiota: the Bacteroidetes sus-like paradigm. *J Biol Chem* 284:24673–24677. <https://doi.org/10.1074/jbc.R109.022848>
- Martínez-Martínez M, Coscolín C, Santiago G, Chow J, Stogios PJ, Bargiela R, Gertler C, Navarro-Fernández J, Bollinger A, Thies S, Méndez-García C, Popovic A, Brown G, Chernikova TN, García-Moyano A, Bjerga GEK, Pérez-García P, Hai T, Del Pozo MV, Stokke R, Steen IH, Cui H, Xu X, Nocek BP, Alcaide M, Distaso M, Mesa V, Peláez AI, Sánchez J, Buchholz PCF, Pleiss J, Fernández-Guerra A, Glöckner FO, Golyshina OV, Yakimov MM, Savchenko A, Jaeger KE, Yakunin AF, Streit WR, Golyshin PN, Guallar V, Ferrer M (2018) Determinants and prediction of esterase substrate promiscuity patterns. *ACS Chem Biol* 13:225–234. <https://doi.org/10.1021/acscchembio.7b00996>
- Misset-Smits M, Van Ophem PW, Sakuda S, Duine JA (1997) Mycothiol, 1-O-(2'-[N-acetyl-L-cysteinyl]amido-2'-deoxy- $\alpha$ -D-glucopyranosyl)-D-myo-inositol, is the factor of NAD/

- factor-dependent formaldehyde dehydrogenase. FEBS Lett 409:221–222. [https://doi.org/10.1016/S0014-5793\(97\)00510-3](https://doi.org/10.1016/S0014-5793(97)00510-3)
- Newton GL, Fahey RC (2002) Mycothiol biochemistry. Arch Microbiol 178:388–394. <https://doi.org/10.1007/s00203-002-0469-4>
- Newton GL, Rawat M (2019) N-methyl-bacillithiol, a novel thiol from anaerobic bacteria. Mbio 10:e02634-e2718. <https://doi.org/10.1128/mBio.02634-18>
- Newton GL, Rawat M, La Clair JJ, Jothivasan VK, Budiarto T, Hamilton CJ, Claiborne A, Helmann JD, Fahey RC (2009) Bacillithiol is an antioxidant thiol produced in Bacilli. Nat Chem Biol 5:625–627. <https://doi.org/10.1038/nchembio.189>
- Otwinowski Z, Minor W (1997) Processing of X-ray diffraction data collected in oscillation mode. In: Carter CW (ed) Macromolecular Crystallography Part A. Methods Enzymol 276:307–326. [https://doi.org/10.1016/S0076-6879\(97\)76066-X](https://doi.org/10.1016/S0076-6879(97)76066-X)
- Persson B, Hedlund J, Jörnvall H (2008) Medium- and short-chain dehydrogenase/reductase gene and protein families: the MDR superfamily. Cell Mol Life Sci 65:3879–3894. <https://doi.org/10.1007/s00018-008-8587-z>
- Pick A, Rühmann B, Schmid J, Sieber V (2013) Novel CAD-like enzymes from *Escherichia coli* K-12 as additional tools in chemical production. Appl Microbiol Biotechnol 97:5815–5824. <https://doi.org/10.1007/s00253-012-4474-5>
- Priyam A, Woodcroft BJ, Rai V, Moghul I, Munagala A, Ter F, Chowdhary H, Pieniak I, Maynard LJ, Gibbins MA, Moon HK, Davis-Richardson A, Uludag M, Watson-Haigh NS, Challis R, Nakamura H, Favreau E, Gómez EA, Pluskal T, Leonard G, Rumpf W, Wurm Y (2019) Sequenceserver: a modern graphical user interface for custom BLAST databases. Mol Biol Evol 36:2922–2924. <https://doi.org/10.1093/molbev/msz185>
- Rao ST, Rossmann MG (1973) Comparison of super-secondary structures in proteins. J Mol Biol 76:241–256. [https://doi.org/10.1016/0022-2836\(73\)90388-4](https://doi.org/10.1016/0022-2836(73)90388-4)
- Rees DA, Conway E (1962) The structure and biosynthesis of porphyrin: a comparison of some samples. Biochem J 84:411–416. <https://doi.org/10.1042/bj0840411>
- Reisky L, Büchenschütz HC, Engel J, Song T, Schweder T, Hehemann JH, Bornscheuer UT (2018) Oxidative demethylation of algal carbohydrates by cytochrome P450 monooxygenases brief-communication. Nat Chem Biol 14:342–344. <https://doi.org/10.1038/s41589-018-0005-8>
- Reisky L, Préchoux A, Zühlke MK, Bäumgen M, Robb CS, Gerlach N, Roret T, Stanetty C, Larocque R, Michel G, Song T, Markert S, Unfried F, Mihovilovic MD, Trautwein-Schult A, Becher D, Schweder T, Bornscheuer UT, Hehemann JH (2019) A marine bacterial enzymatic cascade degrades the algal polysaccharide ulvan. Nat Chem Biol 15:803–812. <https://doi.org/10.1038/s41589-019-0311-9>
- Robb CS, Reisky L, Bornscheuer UT, Hehemann JH (2018) Specificity and mechanism of carbohydrate demethylation by cytochrome P450 monooxygenases. Biochem J 475:3875–3886. <https://doi.org/10.1042/BCJ20180762>
- Salentin S, Schreiber S, Haupt VJ, Adasme MF, Schroeder M (2015) PLIP: fully automated protein-ligand interaction profiler. Nucleic Acids Res 43:W443–W447. <https://doi.org/10.1093/nar/gkv315>
- Sanghani PC, Stone CL, Ray BD, Pindel EV, Hurley TD, Bosron WF (2000) Kinetic mechanism of human glutathione-dependent formaldehyde dehydrogenase. Biochemistry 39:10720–10729. <https://doi.org/10.1021/bi9929711>
- Shannon P, Markiel A, Ozier O, Baliga NS, Wang JT, Ramage D, Amin N, Schwikowski B, Ideker T (2003) Cytoscape: a software environment for integrated models of biomolecular interaction networks. Genome Res 13:2498–2504. <https://doi.org/10.1101/gr.1239303.metabolite>
- Shishodia S, Zhang D, El-Sagheer AH, Brown T, Claridge TDW, Schofield CJ, Hopkinson RJ (2018) NMR analyses on N-hydroxymethylated nucleobases-implications for formaldehyde toxicity and nucleic acid demethylases. Org Biomol Chem 16:4021–4032. <https://doi.org/10.1039/c8ob00734a>
- Sichert A, Corzett CH, Schechter MS, Unfried F, Markert S, Becher D, Fernandez-Guerra A, Liebeke M, Schweder T, Polz MF, Hehemann JH (2020) Verrucomicrobia use hundreds of enzymes to digest the algal polysaccharide fucoidan. Nat Microbiol 5:1026–1039. <https://doi.org/10.1038/s41564-020-0720-2>
- Sievers F, Willm A, Dineen D, Gibson TJ, Karplus K, Li W, Lopez R, McWilliam H, Remmert M, Söding J, Thompson JD, Higgins DG (2011) Fast, scalable generation of high-quality protein multiple sequence alignments using Clustal Omega. Mol Syst Biol 7:539. <https://doi.org/10.1038/msb.2011.75>
- Sirota FL, Maurer-Stroh S, Li Z, Eisenhaber F, Eisenhaber B (2021) Functional classification of super-large families of enzymes based on substrate binding pocket residues for biocatalysis and enzyme engineering applications. Front Bioeng Biotechnol 9:701120. <https://doi.org/10.3389/fbioe.2021.701120>
- Sützl L, Laurent CVFP, Abrera AT, Schütz G, Ludwig R, Haltrich D (2018) Multiplicity of enzymatic functions in the CAZY AA3 family. Appl Microbiol Biotechnol 102:2477–2492. <https://doi.org/10.1007/s00253-018-8784-0>
- Takeda K, Matsumura H, Ishida T, Samejima M, Ohno H, Yoshida M, Igarashi K, Nakamura N (2015) Characterization of a novel PQQ-dependent quinoxinoprotein pyranose dehydrogenase from *Coprinopsis cinerea* classified into auxiliary activities family 12 in carbohydrate-active enzymes. PLoS One 10:e0115722. <https://doi.org/10.1371/journal.pone.0115722>
- Tayri-Wilk T, Slavin M, Zamel J, Blass A, Cohen S, Motzik A, Sun X, Shalev DE, Ram O, Kalisman N (2020) Mass spectrometry reveals the chemistry of formaldehyde cross-linking in structured proteins. Nat Commun 11:3128. <https://doi.org/10.1038/s41467-020-16935-w>
- Teeling H, Fuchs BM, Becher D, Klockow C, Gardebrecht A, Bennis CM, Kassabgy M, Huang S, Mann AJ, Waldmann J, Weber M, Klindworth A, Otto A, Lange J, Bernhardt J, Reinsch C, Hecker M, Peplies J, Bockelmann FD, Callies U, Gerdt G, Wichels A, Wiltshire KH, Glöckner FO, Schweder T, Amann R (2012) Substrate-controlled succession of marine bacterioplankton populations induced by a phytoplankton bloom. Science 336:608–611. <https://doi.org/10.1126/science.1218344>
- Thomas F, Hehemann JH, Rebuffet E, Czjzek M, Michel G (2011a) Environmental and gut Bacteroidetes: the food connection. Front Microbiol 2:93. <https://doi.org/10.3389/fmicb.2011.00093>
- Thomas F, Barbeyron T, Michel G (2011b) Evaluation of reference genes for real-time quantitative PCR in the marine flavobacterium *Zobellia galactanivorans*. J Microbiol Methods 84:61–66. <https://doi.org/10.1016/j.mimet.2010.10.016>
- Trincon A (2011) Marine biocatalysts: enzymatic features and applications. Mar Drugs 9:478–499. <https://doi.org/10.3390/md9040478>
- Trivić S, Leskova V, Winston GW (1999) Aldehyde dismutase activity of yeast alcohol dehydrogenase. Biotechnol Lett 21:231–234. <https://doi.org/10.1023/A:1005476115349>
- Unsworth LD, Van Der Oost J, Koutsopoulos S (2007) Hyperthermophilic enzymes - stability, activity and implementation strategies for high temperature applications. FEBS J 274:4044–4056. <https://doi.org/10.1111/j.1742-4658.2007.05954.x>
- Vagin A, Teplyakov A (2010) Molecular replacement with MOLREP. Acta Crystallogr D 66:22–25. <https://doi.org/10.1107/S0907444909042589>
- Vorholt JA (2002) Cofactor-dependent pathways of formaldehyde oxidation in methylotrophic bacteria. Arch Microbiol 178:239–249. <https://doi.org/10.1007/s00203-002-0450-2>

- Williams CJ, Headd JJ, Moriarty NW, Prisant MG, Videau LL, Deis LN, Verma V, Keedy DA, Hintze BJ, Chen VB, Jain S, Lewis SM, Arendall WB 3rd, Snoeyink J, Adams PD, Lovell SC, Richardson JS, Richardson DC (2018) MolProbity: more and better reference data for improved all-atom structure validation. *Protein Sci* 27:293–315. <https://doi.org/10.1002/pro.3330>
- Willson BJ, Herman R, Langer S, Thomas GH (2022) Improved furfural tolerance in *Escherichia coli* mediated by heterologous NADH-dependent benzyl alcohol dehydrogenases. *Biochem J* 479:1045–1058. <https://doi.org/10.1042/BCJ20210811>
- Yonemitsu H, Kikuchi Y (2018) Biodegradation of high concentrations of formaldehyde using *Escherichia coli* expressing the formaldehyde dismutase gene of *Methylobacterium sp.* FD1. *Biosci Biotechnol Biochem* 82:49–56. <https://doi.org/10.1080/09168451.2017.1397497>
- Yurimoto H, Kato N, Sakai Y (2005) Assimilation, dissimilation, and detoxification of formaldehyde, a central metabolic intermediate of methylotrophic metabolism. *Chem Rec* 5:367–375. <https://doi.org/10.1002/tcr.20056>
- Zallot R, Oberg N, Gerlt JA (2019) The EFI Web Resource for genomic enzymology tools: leveraging protein, genome, and metagenome databases to discover novel enzymes and metabolic pathways. *Biochemistry* 58:4169–4182. <https://doi.org/10.1021/acs.biochem.9b00735>
- Zhang R, Xu Y, Xiao R (2015) Redesigning alcohol dehydrogenases/reductases for more efficient biosynthesis of enantiopure isomers. *Biotechnol Adv* 33:1671–1684. <https://doi.org/10.1016/j.biotechadv.2015.08.002>
- Zheng YG, Yin HH, Yu DF, Chen X, Tang XL, Zhang XJ, Xue YP, Wang YJ, Liu ZQ (2017) Recent advances in biotechnological applications of alcohol dehydrogenases. *Appl Microbiol Biotechnol* 101:987–1001. <https://doi.org/10.1007/s00253-016-8083-6>
- Zhu Y, Thomas F, Larocque R, Li N, Duffieux D, Cladière L, Souchaud F, Michel G, McBride MJ (2017) Genetic analyses unravel the crucial role of a horizontally acquired alginate lyase for brown algal biomass degradation by *Zobellia galactanivorans*. *Environ Microbiol* 19:2164–2181. <https://doi.org/10.1111/1462-2920.13699>
- Zobell CE (1941) Studies on marine bacteria. I. The cultural requirements of heterotrophic aerobes. *J Mar Res* 4:41–75

**Publisher's note** Springer Nature remains neutral with regard to jurisdictional claims in published maps and institutional affiliations.

1 **Supporting Information**

2 **Unique alcohol dehydrogenases involved in algal sugar utilization by marine**  
3 **bacteria**

4  
5 Stefan Brott<sup>1</sup>, Ki Hyun Nam<sup>2</sup>, François Thomas<sup>3</sup>, Theresa Dutschei<sup>1</sup>, Lukas Reisky<sup>1</sup>, Maïke  
6 Behrens<sup>1</sup>, Hanna C. Grimm<sup>1</sup>, Gurvan Michel<sup>3</sup>, Thomas Schweder<sup>4</sup>, and Uwe T. Bornscheuer<sup>1\*</sup>

7  
8 <sup>1</sup>Department of Biotechnology & Enzyme Catalysis, Institute of Biochemistry, University of  
9 Greifswald, Greifswald 17487, Germany

10 <sup>2</sup>Department of Life Science, Pohang University of Science and Technology, Pohang 37673,  
11 South Korea

12 <sup>3</sup>Laboratory of Integrative Biology of Marine Models (LBI2M), Station Biologique de Roscoff  
13 (SBR), Sorbonne Université, CNRS 29688 Roscoff, Bretagne, France

14 <sup>4</sup>Department of Pharmaceutical Biotechnology, Institute of Pharmacy, University of Greifswald,  
15 Greifswald 17487, Germany

16 \*Corresponding author: E-mail: [uwe.bornscheuer@uni-greifswald.de](mailto:uwe.bornscheuer@uni-greifswald.de)

17	<b>Table of Contents</b>	
18	<b>Additional Discussion</b> .....	3
19	<b>Figures</b>	
20	<b>Fig. S1</b> Sequence similarity network from FoADH and ZoADH.....	4
21	<b>Fig. S2</b> Genome neighborhood diagram of main cluster 2.....	5
22	<b>Fig. S3</b> SDS-PAGE of purified proteins.....	6
23	<b>Fig. S4</b> Effect of NaCl on enzyme activity.....	6
24	<b>Fig. S5</b> Influence of different metal ions on enzyme activity.....	7
25	<b>Fig. S6</b> Influence of EDTA, DTT and 2-Mercaptoethanol on enzyme activity.....	7
26	<b>Fig. S7</b> Influence of water-miscible solvents on enzyme activity.....	8
27	<b>Fig. S8</b> Influence of formaldehyde on enzyme activity.....	8
28	<b>Fig. S9</b> Asymmetric units of both ADHs.....	9
29	<b>Fig. S10</b> Structure-based amino acid alignment of both ADHs.....	10
30	<b>Fig. S11</b> Dimeric interface of both ADH.....	11
31	<b>Fig. S12</b> Structural comparison of ZoADH and FoADH with structural homologs.....	12
32	<b>Fig. S13</b> Electron density maps.....	13
33	<b>Fig. S14</b> Substrate binding pocket of FoADH and ZoADH.....	14
34	<b>Tables</b>	
35	<b>Table S1</b> Primers used for knockout experiments.....	15
36	<b>Table S2</b> Data collection and refinement statistics.....	16
37	<b>Table S3</b> The ADHs lacked activity for various sugar substrates.....	17
38	<b>Table S4</b> Superimposition of monomer structures of FoADH and ZoADH.....	18
39	<b>Table S5</b> Superimposition of monomeric structures of FoADH.....	18
40	<b>Table S6</b> Superimposition of monomeric structures of ZoADH.....	18
41	<b>Table S7</b> Hydrogen bonds and salt bridges on the interface of FoADH.....	19
42	<b>Table S8</b> Hydrogen bonds and salt bridges on the interface of ZoADH.....	23
43	<b>References</b> .....	25
44		



## 45 **Additional Discussion**

46 The biochemical characteristics of both enzymes are almost identical. The pH optimum for the  
47 reduction and oxidation reactions are different, similar observations have also been reported  
48 for several other ADHs (Ying et al. 2014; Akal et al. 2019; Zhang et al. 2021). The optima in  
49 *Z. galactanivorans* also represent the pH range in which this organism prefers to grow  
50 (Barbeyron et al. 2001). Increased activity for the oxidation reaction was observed for both  
51 ADHs in the presence of Tris-HCl buffer. Most likely, this is caused by a potential subsequent  
52 reaction between formed aldehyde and the primary amine of Tris, which might shift the  
53 equilibrium towards product formation. Reactions between aldehydes and Tris are well known  
54 in literature (Bubb et al. 1995) and may possess an influence on the enzyme activity of ADHs  
55 (Trivić et al. 1998). In contrast, almost no activity was detected in the presence of borate buffer;  
56 similar observations were reported for an ADH from yeast, where borate performed a  
57 competitive inhibition with respect to NAD<sup>+</sup> (Smith and Johnson 1975).

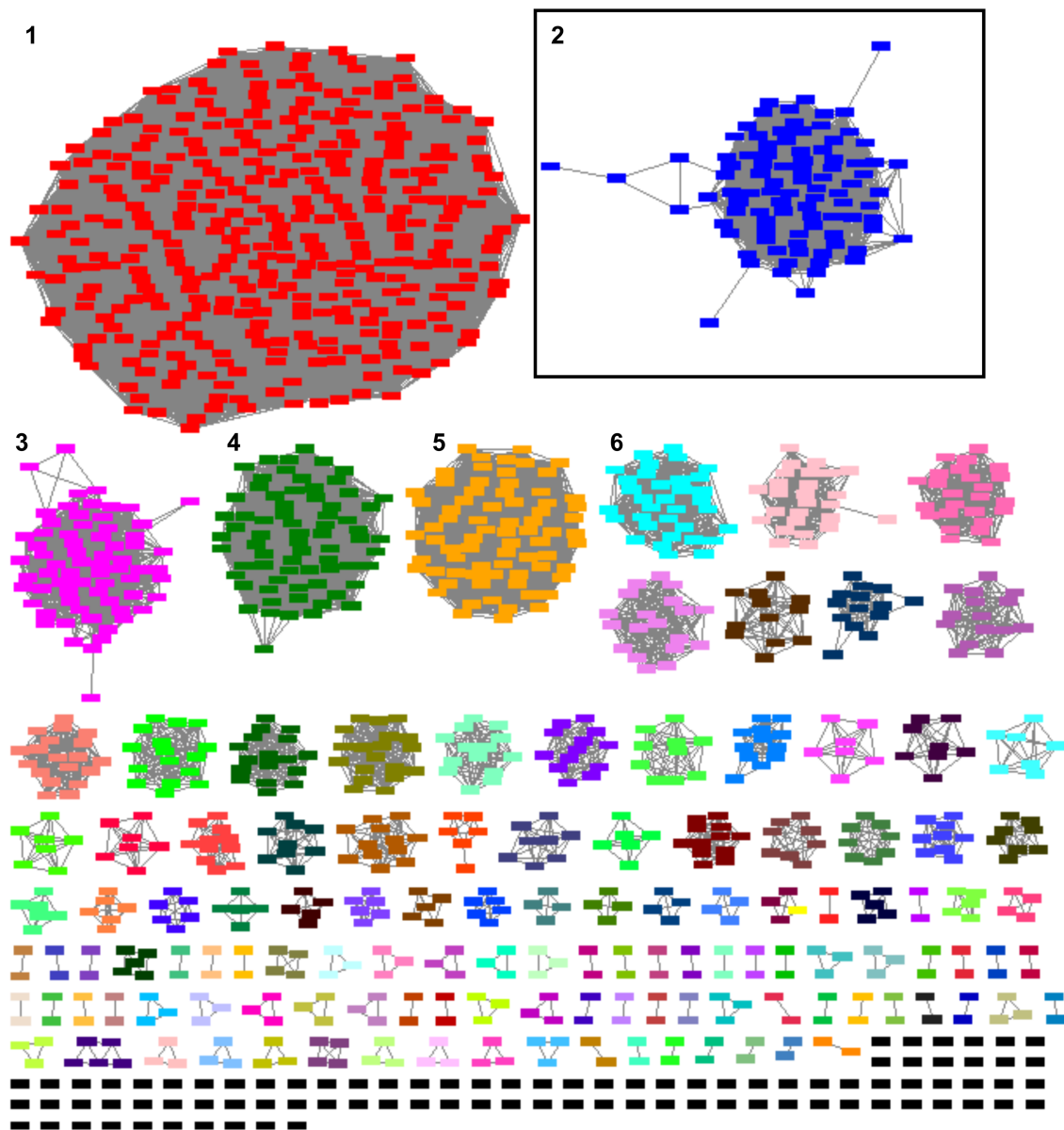
58 The temperature optima of both enzymes differ dramatically from the preferred growth  
59 temperatures of *F. agariphila* with 23 °C (Nedashkovskaya et al. 2006) and *Z. galactanivorans*  
60 with 35 °C (Barbeyron et al. 2001). Both bacteria engage in algae-associated life and tend to  
61 inhabit shallow water, which implies that such high temperatures are unexpected under natural  
62 conditions. Therefore, the temperature optimum is probably a result of the thermal stability of  
63 both enzymes caused by the stabilizing effects of the Zn<sup>2+</sup> site and the numerous hydrogen  
64 and salt bridges. Simultaneously, these structural properties ensure stability at temperatures  
65 encountered in the habitat of these marine bacteria.

66 A slight increase and a subsequent reduction in the activity of both enzymes was observed  
67 with increasing salt concentration. Both enzymes originate from a marine environment where  
68 a salinity of 3.5% (w/v), corresponding to approximately 600 mM NaCl, exists. At this  
69 concentration a negative effect on activity was observable. However, coastal areas where algal  
70 blooms tend to occur more frequently can also contain a reduced salinity due to freshwater  
71 influxes. In addition, a different salt concentration might be present within the cell. Considering  
72 that the ADHs possess an intracellular function, it might be reasonable to assume that the  
73 ADHs are not exposed to higher salt concentrations, which would also explain the beneficial  
74 effect at a lower NaCl concentration.

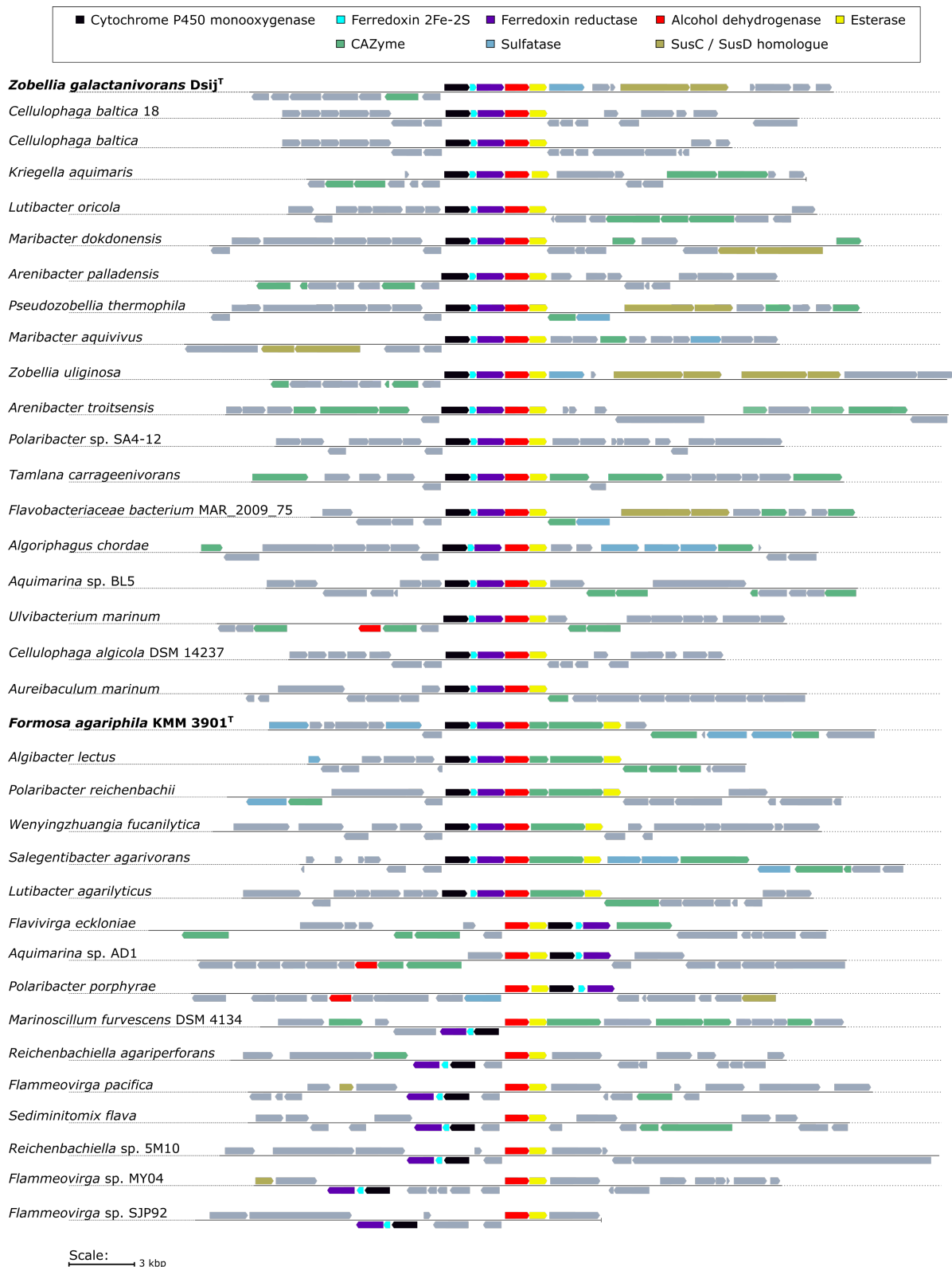
75 Incubation with EDTA and the resulting partial loss of enzyme activity demonstrated that the  
76 zinc ion located in the active site is required for the ADH activity. However, since no complete  
77 inhibition of ADH by EDTA could be obtained, some resistance to chelation can be assumed.  
78 Inhibition of both ADHs was observed in the presence of additional zinc, similar findings were  
79 described for the allyl/benzyl alcohol dehydrogenase from *Yokenella* sp. (Ying et al. 2014) and

80 the aryl alcohol dehydrogenase from *Acinetobacter baylyi* (Uthoff and Steinbüchel 2012).  
 81 Unexpectedly, a 10-14-fold increase in relative activity was observed in the presence of  $Mn^{2+}$ ,  
 82  $Ni^{2+}$  and  $Co^{2+}$ . Finding an explanation for these phenomena is challenging, perhaps one of  
 83 these ions is the natural metal cofactor of these ADHs.

84 **Figures**

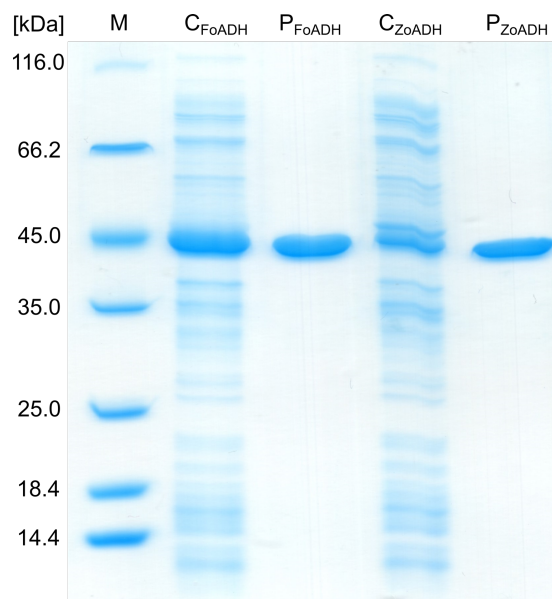


85  
 86 **Fig. S1** Sequence similarity network from FoADH and ZoADH. Both ADHs cluster with zinc-  
 87 dependent ADHs and some glutathione-dependent formaldehyde dehydrogenases. Sequence  
 88 similarity network which were obtained as a result from the FoADH and ZoADH blast against  
 89 MarDB and MarRef sequences (alignment score 150, 63.14%ident). Overall, six main clusters  
 90 (1-6) were obtained, a main cluster is defined here as a cluster that contains at least 34  
 91 sequences, with FoADH und ZoADH included in main cluster 2 (framed).



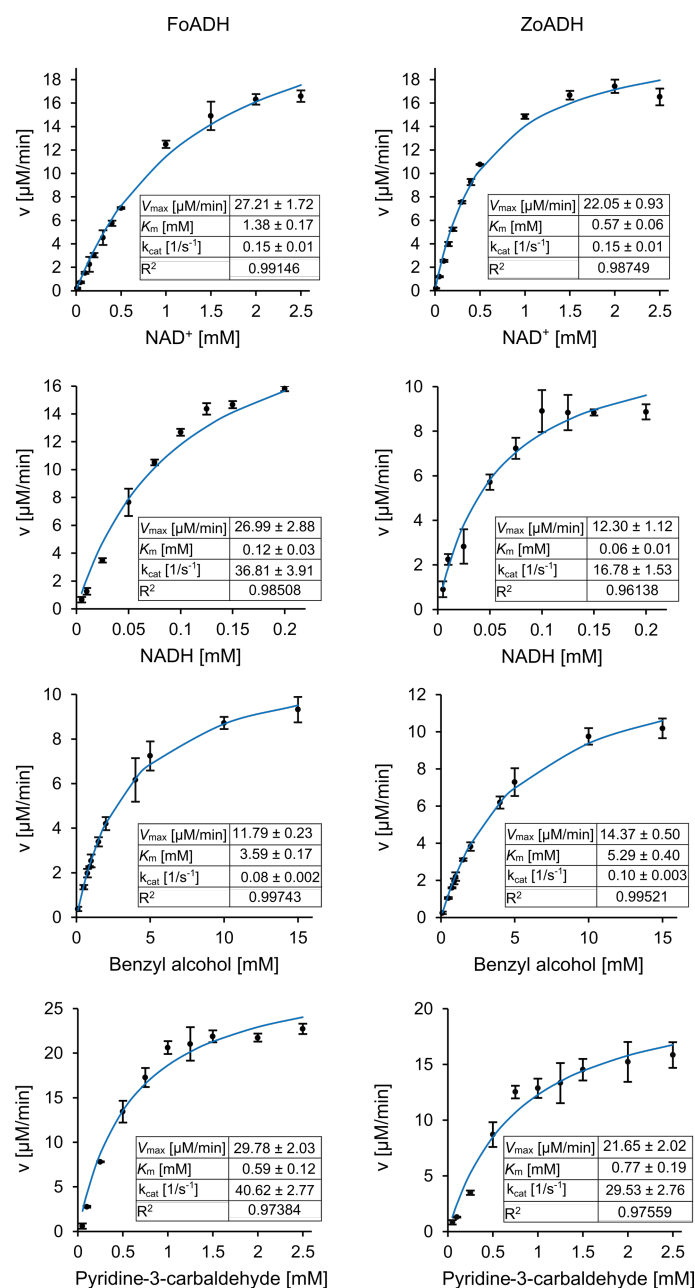
92

93 **Fig. S2** Genome neighborhood diagram of main cluster 2. The main cluster 2 of the sequence  
 94 similarity network (Fig. S1) reveals that the gene encoding for the ADH is consistently in close  
 95 proximity to the genes encoding for the enzymes of oxidative demethylation. Simultaneously,  
 96 the analysis reveals that these ADHs are represented in several marine carbohydrate utilizers.  
 97 In order to achieve a better overview, other genes not involved in carbohydrate degradation or  
 98 uptake/binding have been grayed out.



100

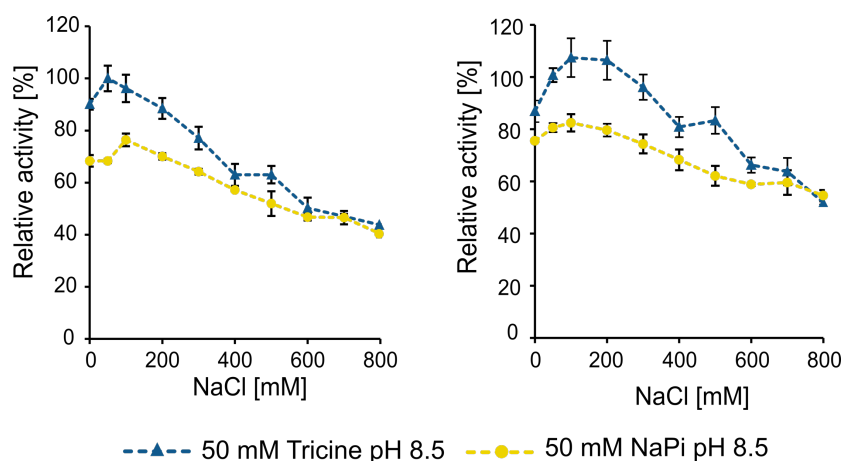
101 **Fig. S3** SDS-PAGE of purified proteins. The purified proteins (P) and the crude cell extract (C)  
102 were separated on a 12.5% gel and stained with Coomassie blue. 4.0  $\mu\text{g}$  of the proteins were  
103 loaded onto the gel. As reference (M) the Pierce™ Unstained protein molecular weight marker  
104 (Thermo Scientific, Waltham, MA, USA) was used. Both enzymes possess a theoretical  
105 molecular weight of approximately 40.9 kDa. The experiment was repeated independently with  
106 similar results.



107

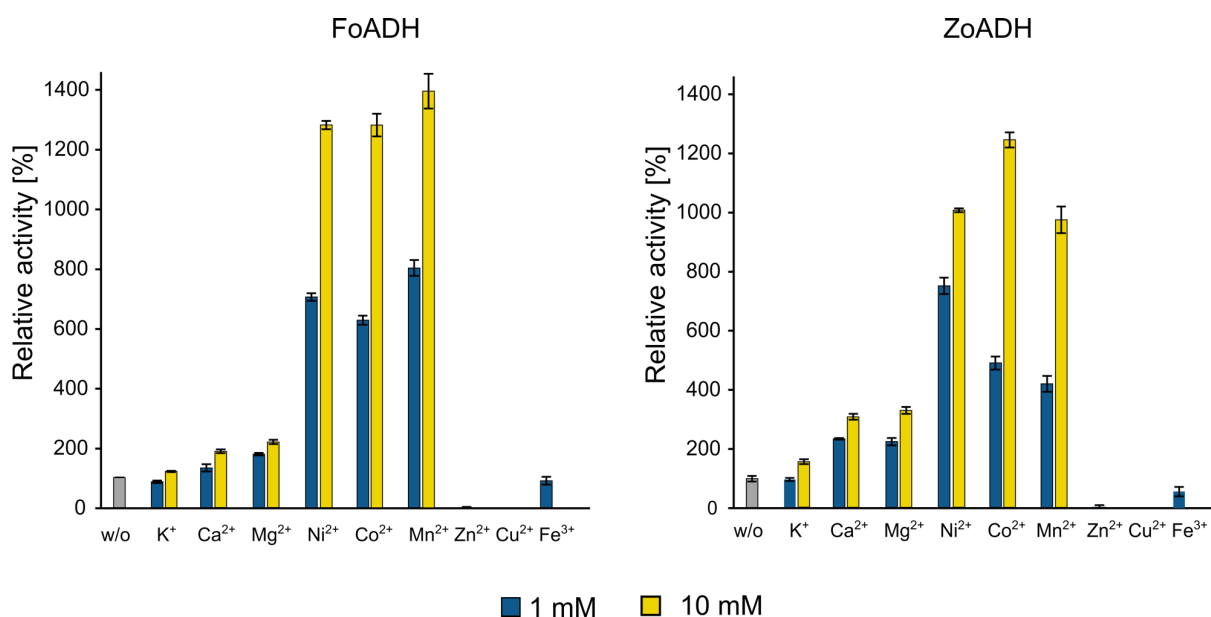
108 **Fig. S4** Kinetic data for FoADH and ZoADH. The final protein content employed for the  
 109 oxidation reactions was  $0.1 \text{ mg mL}^{-1}$ , which corresponds to a protein concentration of  $2.44 \text{ }\mu\text{M}$ .  
 110 For the determination of the kinetic parameters for NAD<sup>+</sup>, 15 mM benzyl alcohol was used as  
 111 the final substrate concentration, while a final cofactor concentration of 5 mM NAD<sup>+</sup> was used  
 112 for the determination of the kinetic parameters for benzyl alcohol. Oxidation reactions were  
 113 performed in 50 mM NaPi buffer pH 8.5 and at a reaction temperature of 70 °C. In the reduction  
 114 reaction, the final protein content used was  $5 \text{ }\mu\text{g mL}^{-1}$ , which is equivalent to a protein  
 115 concentration of  $0.012 \text{ }\mu\text{M}$ . For the determination of the kinetic parameters for NADH, 2.5 mM  
 116 pyridine-3-carbaldehyde was used as the final substrate concentration, while a final cofactor  
 117 concentration of 0.5 mM NADH was used for the determination of the kinetic parameters for  
 118 pyridine-3-carbaldehyde. Reduction reactions were carried out in 50 mM succinate buffer  
 119 pH 6.5 and at 70 °C. All measurements were carried out as triplicates, the mean values (black  
 120 dots) and their standard deviations are given.  $V_{max}$  and  $K_m$  were determined via a fitted curve  
 121 (blue line), which was calculated using standard Michaelis-Menten kinetics.

122



123

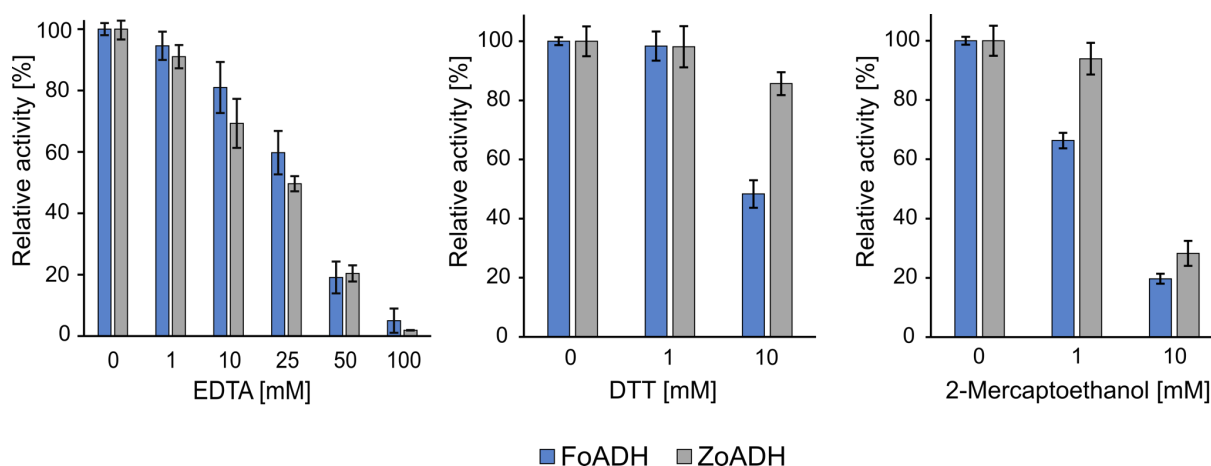
124 **Fig. S5** Effect of NaCl on enzyme activity. Determination of NaCl influence on enzyme activity  
 125 was performed by carrying out the oxidation reaction in the presence of different NaCl  
 126 concentrations varying from 0 to 800 mM. The maximum relative activity (100%) corresponds  
 127 to the measurement at a NaCl concentration of 50mM for FoADH and 100 mM for ZoADH in  
 128 the 50 mM Tricine buffer. Assay conditions were as follows: the reaction volume was 200  $\mu$ L,  
 129 10 mM benzyl alcohol was used as substrate, the final enzyme concentration was 0.1 mg mL<sup>-1</sup>.  
 130 The reaction was carried out at 25 °C in a 50 mM NaPi buffer pH 8.5 or in a 50 mM Tricine  
 131 buffer pH 8.5 and started by the addition of 0.5 mM NAD<sup>+</sup>. All measurements were performed  
 132 as triplicates, the mean is given and the error bars indicate the standard deviation.



133

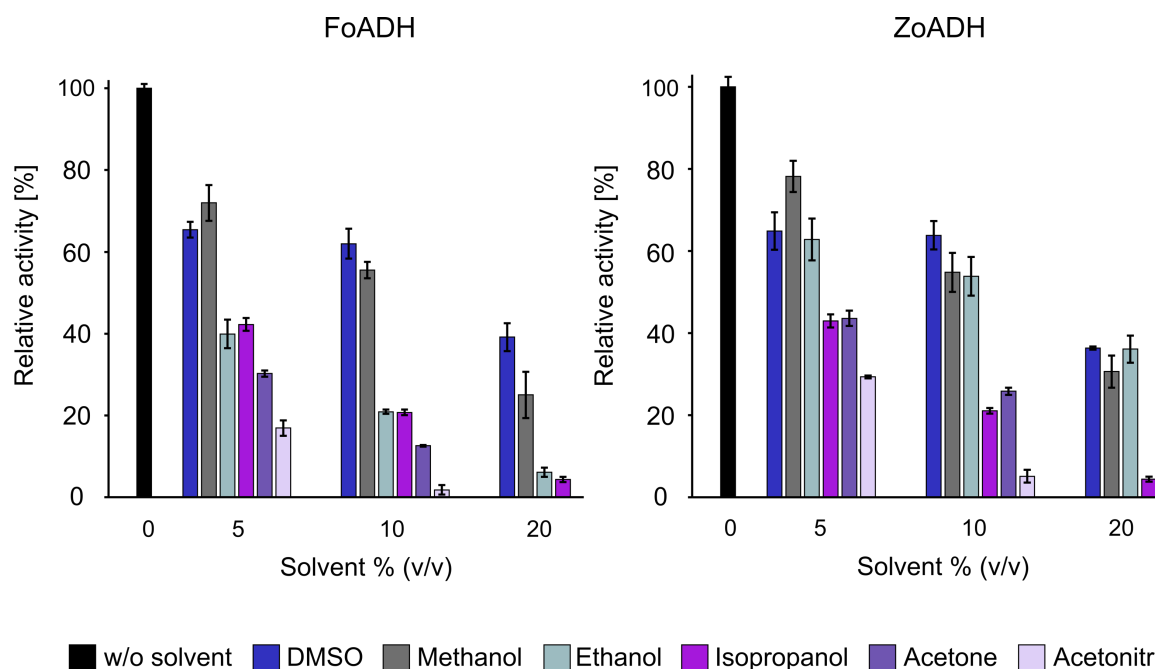
134 **Fig. S6** Influence of different metal ions on enzyme activity. The ADH with was incubated with  
 135 the metal chloride for 1 h at RT prior to measurement. The maximum relative activity (100%)  
 136 corresponds to the measurement for the control, which was incubated without a metal ion. The  
 137 measurement was performed under following conditions: a final substrate concentration of  
 138 10 mM benzyl alcohol and 0.5 mM NAD<sup>+</sup> was used. The reaction was started by the addition  
 139 of ADH at a final enzyme concentration of 0.1 mg mL<sup>-1</sup>. The measurement was performed in a  
 140 50 mM HEPES buffer pH 8.5 at 25 °C. All measurements were performed as triplicates, the  
 141 mean and the standard deviation is given.

142



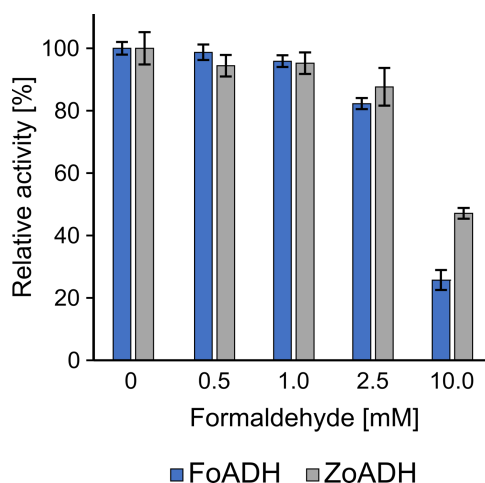
143

144 **Fig. S7** Influence of EDTA, DTT and 2-Mercaptoethanol on enzyme activity. The ADH was  
 145 incubated with the compound for 1 h at RT prior to measurement. The maximum relative  
 146 activity (100%) corresponds to the measurement for the control, which was incubated without  
 147 additional compound. The measurement was performed under following conditions: a final  
 148 substrate concentration of 10 mM benzyl alcohol and 0.5 mM NAD<sup>+</sup> was used. The reaction  
 149 was started by the addition of ADH at a final enzyme concentration of 0.1 mg mL<sup>-1</sup>. The  
 150 measurement was performed in a 50 mM HEPES buffer pH 8.5 at 25 °C. All measurements  
 151 were performed as triplicates, the mean and the standard deviation is given.



152

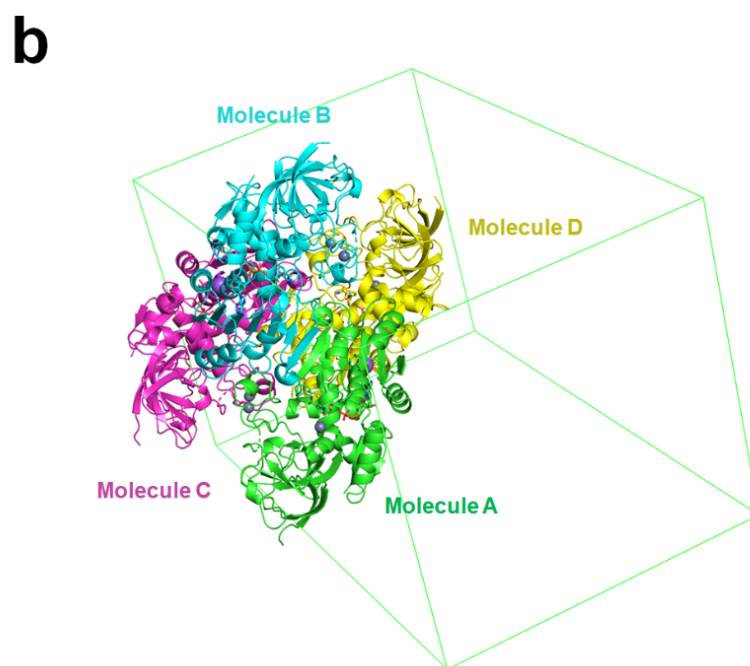
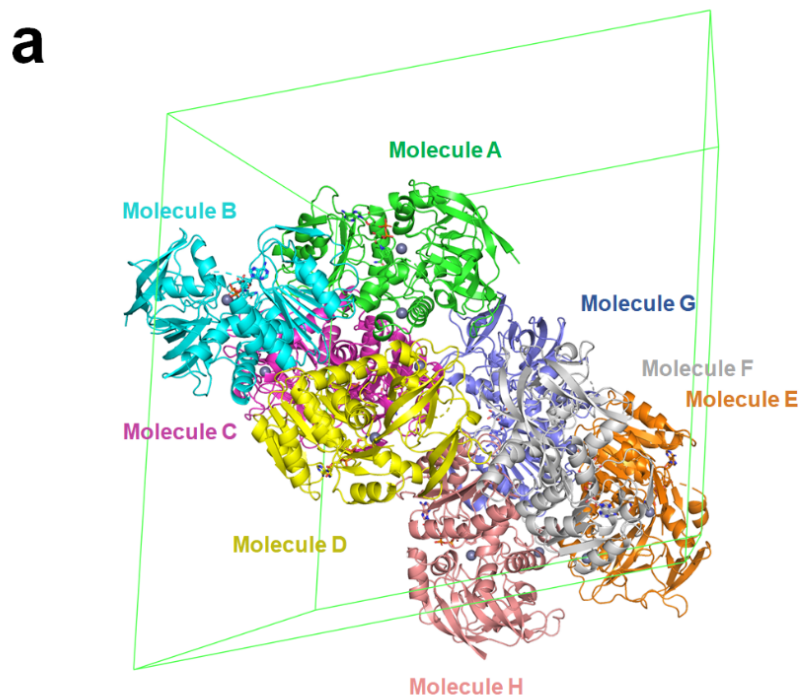
153 **Fig. S8** Influence of water-miscible solvents on enzyme activity. The oxidation reaction was  
 154 conducted in the presence of 5, 10, and 20% (v/v) solvent and compared with a control  
 155 containing no additional solvent, which corresponds to the maximum relative activity (100%).  
 156 The reaction was performed in 50 mM NaPi buffer at 25 °C. The final enzyme concentration  
 157 was 0.1 mg mL<sup>-1</sup>, 10 mM benzyl alcohol was employed as substrate and the reaction was  
 158 started by adding 0.5 mM NAD<sup>+</sup>. All measurements were performed as triplicates, the mean  
 159 and the standard deviation is given.



161

162 **Fig. S9** Influence of formaldehyde on enzyme activity. The enzymes were incubated at a  
163 concentration of  $1 \text{ mg mL}^{-1}$  with different concentrations of formaldehyde varying from 0 to  
164 50 mM for 1 hour at RT prior activity measurement to evaluate the effect of formaldehyde on  
165 enzyme activity. The measurement of the sample without formaldehyde corresponds to the  
166 maximum relative activity (100%). No activity was observed for both enzymes in the presence  
167 of 50 mM formaldehyde. The reaction was performed in 50 mM HEPES buffer pH 8.5 at  $25^\circ\text{C}$ .  
168 The final enzyme concentration was  $0.1 \text{ mg mL}^{-1}$ , 10 mM benzyl alcohol was employed as  
169 substrate and the reaction was started by adding  $0.5 \text{ mM NAD}^+$ . All measurements were  
170 performed as triplicates, the mean and the standard deviation is given.



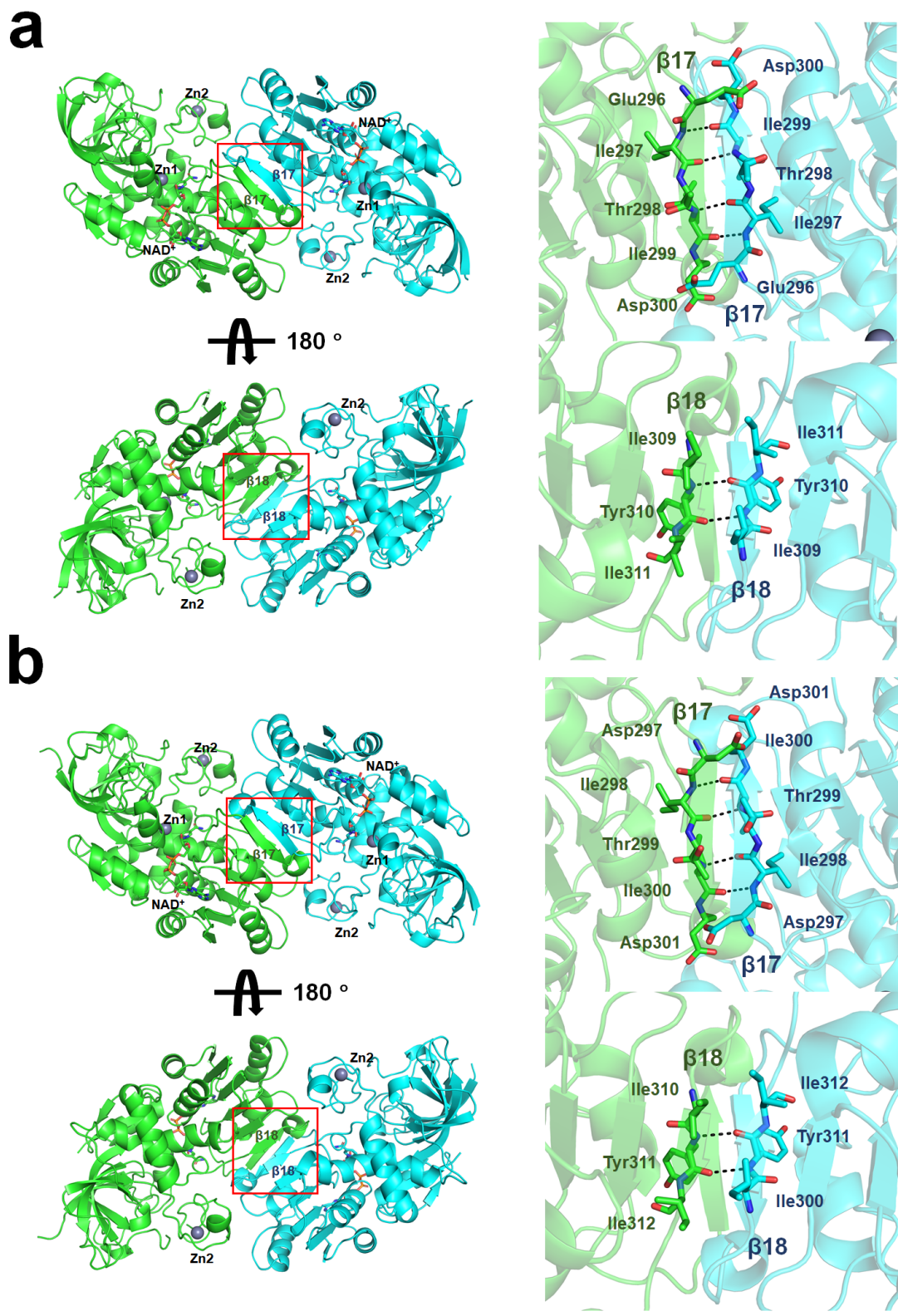


171

172 **Fig. S10** Asymmetric units of both ADHs. a) Eight FoADH molecules and b) four ZoADH

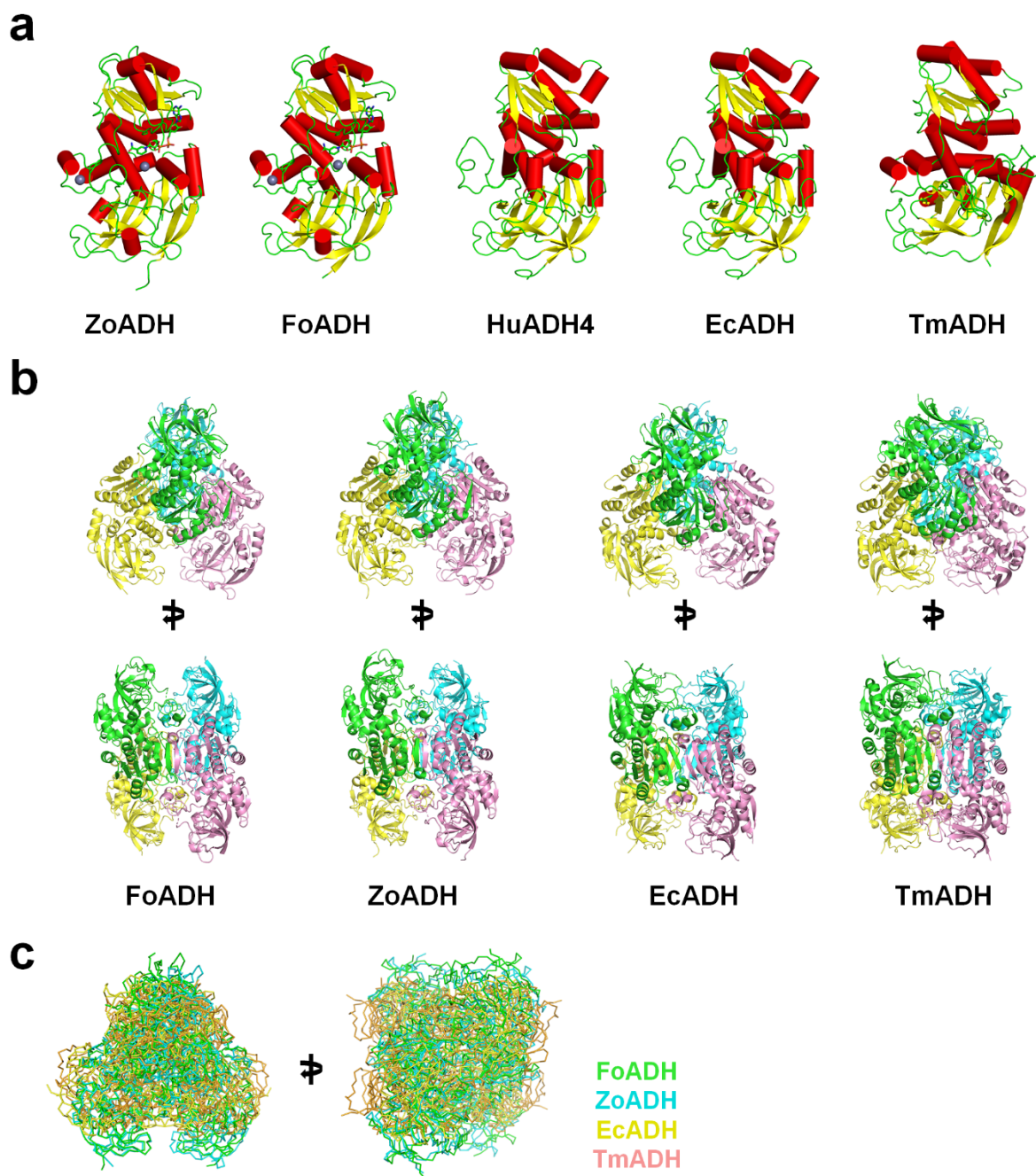
173 molecules in asymmetric unit.





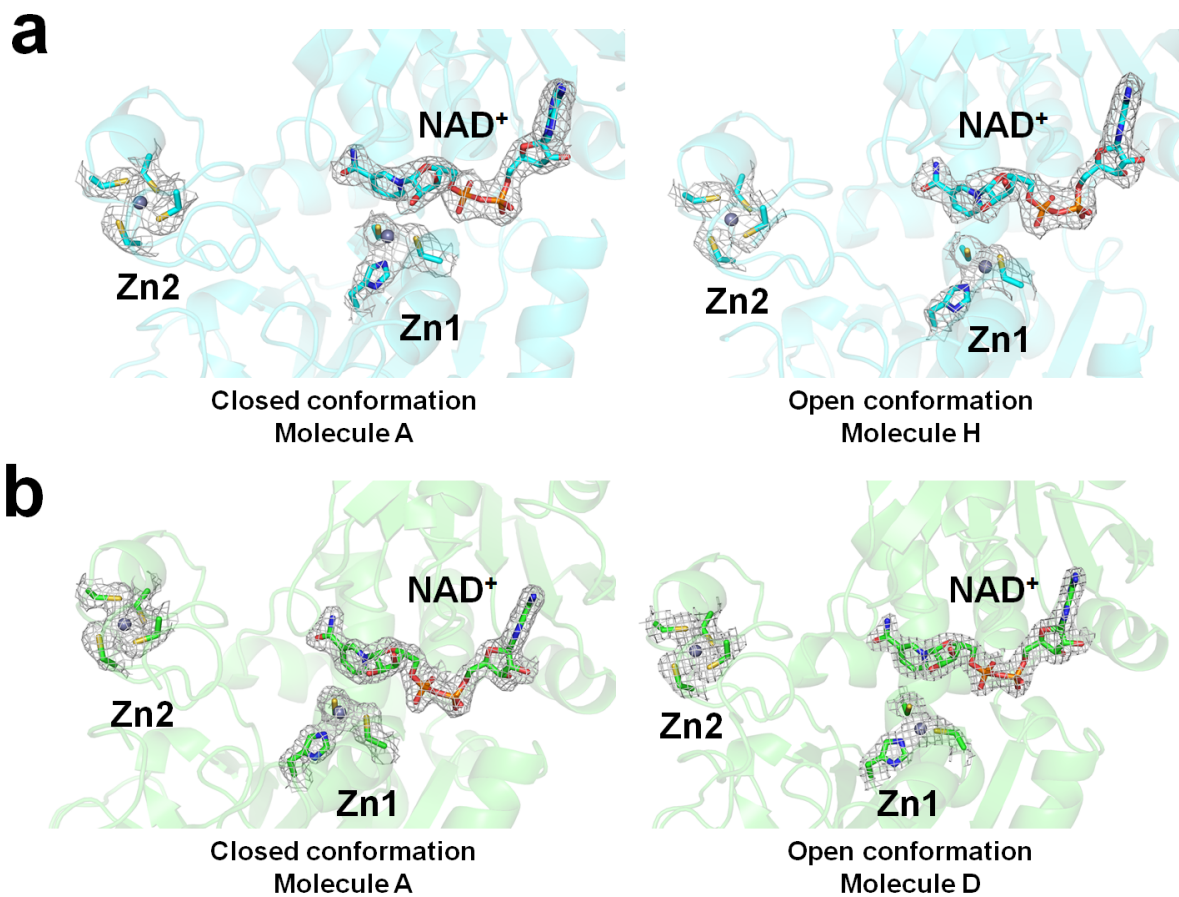
179

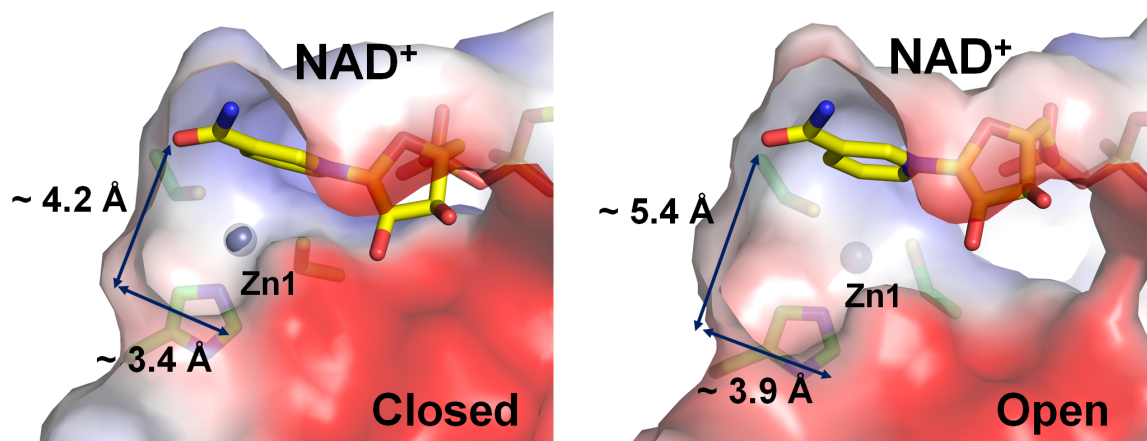
180 **Fig. S12** Dimeric interface of a) FoADH and b) ZoADH.



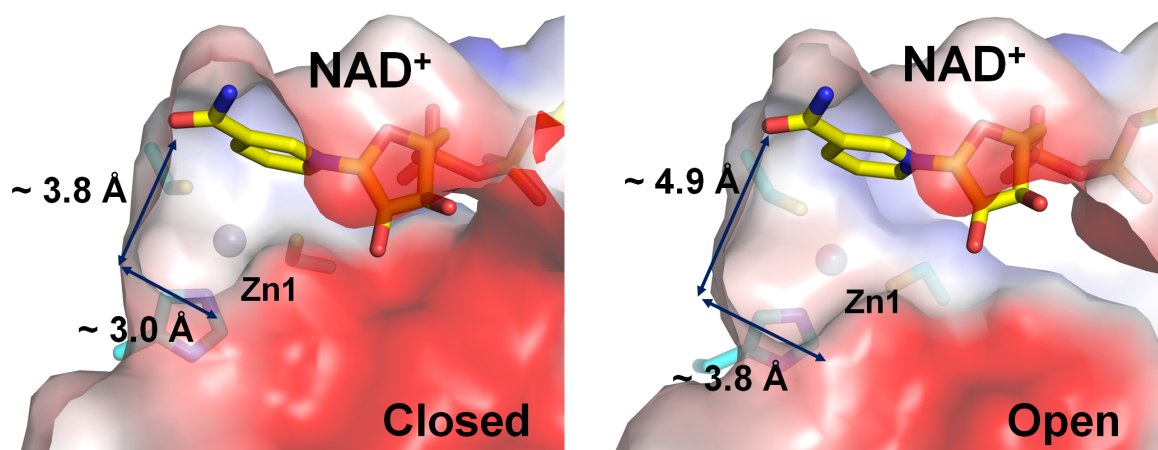
181

182 **Fig. S13** Structural comparison of ZoADH and FoADH with structural homologs. **a)**  
 183 Comparison of monomeric ZoADH and FoADH with structural homolog all-trans-retinol  
 184 dehydrogenase ADH4 from *Homo sapiens* (HuADH4, PDB code 3COS), uncharacterized zinc-  
 185 type alcohol dehydrogenase-like protein YdjJ from *Escherichia coli* (EcADH, 5vm2) and scyllo-  
 186 inosose 3-dehydrogenase from *Thermotoga maritima* (TmADH, 3IP1). **b)** Comparison and **c)**  
 187 superimposition of tetrameric assembly of FoADH, ZoADH, EcADH and TmADH.





### FoADH



### ZoADH

191

192 **Fig. S15** Substrate binding pocket of FoADH and ZoADH.

193

194 **Tables**

195 **Table S1** Primers used for knockout experiments.

<b>Primers</b>	<b>Sequence and Description</b>
OFT0040	5' TTTTTT <u>GTCGACT</u> GCGTAAAGAACCTGAGATTACCG 3'; forward primer used in construction of pFT13; Sall site underlined
OFT0041	5' TAGGCCGCTTCTTTTTTAGGATCG 3'; reverse primer used in construction of pFT12; BamHI site downstream in amplified fragment
OFT0042	5' TTTTTTCTAGAGCTACTGCACTCTTTGATTGAATAG 3'; reverse primer used in construction of pFT13; XbaI site underlined
OFT0043	5' TTTTTTCTAGAGTTGGCCGGTAAAAATGCAAAAGG 3'; forward primer used in construction of pFT12; XbaI site underlined
OFT0044	5' ACACCCTTTTGTCCGTTGATGCG 3'; forward primer to confirm deletion of <i>zgal_4674</i>
OFT0045	5' AAATCTTCCAAGTCGGCCATTGG 3'; reverse primer to confirm deletion of <i>zgal_4674</i>

196

197

198 **Table S2** Data collection and refinement statistics.

<b>Data collection</b>	<b>FoADH</b>	<b>ZoADH</b>
Beamline	11C beamline, PLS-II	11C beamline, PLS-II
Wavelength (Å)	0.9794	0.9794
Space group	P2 <sub>1</sub>	P2 <sub>1</sub> 2 <sub>1</sub> 2 <sub>1</sub>
Unit cell		
a, b, c (Å)	98.49, 157.20, 98.57	90.57, 92.67, 154.19
α, β, γ (°)	90.00, 103.50, 90.00	90.00, 90.00, 90.00
Resolution	50.0-2.50 (2.54-2.50)	50.0-2.10 (2.14-2.10)
Total reflections	98086 (4819)	76289 (3735)
Redundancy	5.7 (4.6)	12.6 (11.3)
Completeness (%)	97.5 (95.9)	99.9 (100.0)
Mean I/sigma(I)	12.79 (1.93)	15.00 (1.94)
CC1/2	0.976 (0.751)	0.989 (0.734)
CC*	0.994 (0.926)	0.997 (0.920)
<b>Refinement</b>		
Resolution	48.19-2.50	49.58-2.10
R <sub>work</sub>	0.225	0.1612
R <sub>free</sub>	0.278	0.2047
R.M.S. Deviation		
Bonds (Å)	0.010	0.009
Angles (°)	1.424	1.200
Average B-factor (Å <sup>2</sup> )		
Protein	51.20	33.45
Ligand	49.89	29.13
Water	45.75	36.81
Ramachandran (%)		
Favored	94.53	96.10
Allowed	4.77	3.69
Outliers	0.70	0.21

199 Statistics for the highest-resolution shell are shown in parentheses.

200



201 **Table S3** The ADHs lacked activity for various sugar substrates. For the measurement an  
202 incubation temperature of 40 °C was used. Sugars were used at a final substrate concentration  
203 of 30 mM. The reactions were performed in the 50 mM NaPi pH 8.5 for the oxidation and  
204 50 mM succinate pH 6.5 for the reduction reaction. The final enzyme concentration was  
205 0.1 mg mL<sup>-1</sup>. The reaction was initialized by the addition of 0.5 mM NAD<sup>+</sup> or NADH.

<b>Sugar substrates</b>	
6-O-methyl-D-galactose	D-Sucrose
D-Galactose	D-Trehalose
D-Glucose	3,6-Anhydro-D-galactose
D-Fructose	L-Rhamnose
D-Xylose	L-Arabinose
D-Mannose	

206

207

208 **Table S4** Superimposition of monomer structures of FoADH and ZoADH

	Chain	ZoADH			
		A	B	C	D
FoADH	A	0.562	0.391	0.350	0.621
	B	0.420	0.396	0.357	0.672
	C	0.402	0.383	0.396	0.543
	D	0.625	0.691	0.772	0.498
	E	0.419	0.399	0.347	0.650
	F	0.497	0.454	0.487	0.472
	G	0.435	0.405	0.381	0.647
	H	0.546	0.597	0.651	0.459

209 \* Numbers indicate r.m.s. deviation values.

210 \* Chain marked in blue have an open conformation between cofactor and catalytic domain.

211

212

213 **Table S5** Superimposition of monomeric structures of FoADH.

Chain	A	B	C	D	E	F	G	H
A		0.256	0.310	0.579	0.226	0.460	0.263	0.562
B	0.256		0.353	0.626	0.259	0.568	0.248	0.610
C	0.310	0.353		0.494	0.320	0.413	0.353	0.457
D	0.579	0.626	0.494		0.587	0.336	0.608	0.276
E	0.226	0.259	0.320	0.587		0.500	0.264	0.574
F	0.460	0.568	0.413	0.336	0.500		0.550	0.350
G	0.263	0.248	0.353	0.608	0.264	0.550		0.576
H	0.562	0.610	0.457	0.276	0.574	0.350	0.576	

214 \* Numbers indicate r.m.s. deviation values.

215 \* Chain marked in blue have an open conformation between cofactor and catalytic domain.

216

217

218 **Table S6** Superimposition of monomeric structures of ZoADH.

Chain	A	B	C	D
A		0.198	0.226	0.314
B	0.198		0.207	0.418
C	0.226	0.207		0.471
D	0.314	0.418	0.471	

219 \* Numbers indicate r.m.s. deviation values.

220 \* Chain marked in blue have an open conformation between cofactor and catalytic domain.

221

222

223

224

225 **Table S7** Hydrogen bonds and salt bridges on the interface of FoADH.

<b>Molecule A-B</b>					
<b>Hydrogen bonds</b>			<b>Salt bridges</b>		
Molecule A	Dist. [Å]	Molecule B	Molecule A	Dist. [Å]	Molecule B
Asn283 [O]	3.37	Gln93 [NE2]	Asp307 [OD1]	3.78	His100 [NE2]
Asp307 [OD2]	2.51	His100 [NE2]	Asp307 [OD2]	2.51	His100 [NE2]
Glu103 [OE2]	3.48	Arg259 [NE]	Glu103 [OE1]	3.50	Arg259 [NE]
Glu103 [OE1]	3.01	Arg259 [NH2]	Glu103 [OE2]	3.48	Arg259 [NE]
Glu305 [OE2]	3.32	Ile293 [N]	Glu103 [OE1]	3.01	Arg259 [NH2]
Ile299 [O]	2.90	Ile297 [N]	His100 [NE2]	3.56	Asp307 [OD1]
Ile297 [O]	2.86	Ile299 [N]	His100 [NE2]	2.37	Asp307 [OD2]
Glu295 [O]	2.95	Met301 [N]	Arg259 [ NE ]	3.90	Glu103 [OE1]
Ile293 [O]	3.55	Arg302 [N]			
Asn312 [O]	2.94	Asp307 [N]			
Tyr310 [O]	2.80	Tyr310 [N]			
Glu305 [OE2]	3.78	Asn312 [ ND2]			
Asp307 [OD1]	2.87	Leu314 [N]			
Gln93 [NE2]	2.87	Asn283 [O]			
His100 [NE2]	2.37	Asp307 [OD2]			
Ile293 [N]	3.54	Glu305 [OE2]			
Ile297 [N]	3.06	Ile299 [O]			
Ile299 [N]	2.88	Ile297 [O]			
Met301 [N]	3.34	Glu295 [O]			
Arg302 [N]	3.45	Ile293 [O]			
Trp306 [N]	3.30	Asn312 [O]			
Asp307 [N]	3.02	Asn312 [O]			
Tyr310 [N]	2.83	Tyr310 [O]			
Leu314 [N]	3.27	Asp307 [OD1]			

<b>Molecule C-D</b>					
<b>Hydrogen bonds</b>			<b>Salt bridges</b>		
Molecule C	Dist. [Å]	Molecule D	Molecule C	Dist. [Å]	Molecule D
Asn283 [O]	3.03	Gln93 [NE2]	Asp307 [OD1]	3.18	His100 [NE2]
Glu103 [OE1]	3.18	Arg259 [NH2]	Asp307 [OD2]	2.89	His100 [NE2]
Glu305 [OE2]	3.26	Ile293 [N]	Glu103 [OE1]	3.18	Arg259 [NH2]
Ile299 [O]	3.02	Ile297 [N]	Glu103 [OE2]	3.79	Arg259 [NH2]
Ile297 [O]	2.84	Ile299 [N]	His100 [NE2]	3.65	Asp307 [OD1]
Glu295 [O]	3.04	Met301 [N]	His100 [NE2]	2.74	Asp307 [OD2]
Ile293 [O]	3.37	Arg302 [N]	Arg259 [NE]	3.65	Glu103 [OE2]
Asn312 [OD1]	3.41	Trp306 [N]	Arg259 [NE]	3.17	Glu103 [OE1]

Asn312 [O]	3.03	Trp306 [N]	Arg259[ NH2]	3.72	Glu103 [OE1]
Asn312 [O]	3.23	Asp307 [N]			
Tyr310 [O]	2.94	Tyr310 [N]			
Asp307 [OD2]	3.44	Leu314 [N]			
Gln93 [NE2]	2.71	Asn283 [O]			
Arg259 [NE]	3.17	Glu103 [OE1]			
Ile297 [N]	3.19	Ile299 [O]			
Ile299 [N]	2.82	Ile297 [O]			
Met301 [N]	3.15	Glu295 [O]			
Arg302 [N]	3.74	Ile293 [O]			
Trp306 [N]	3.22	Asn312 [O]			
Asp307 [N]	3.03	Asn312 [O]			
Tyr310 [N]	2.88	Tyr310 [O]			
Leu314 [N]	3.86	Asp307 [OD2]			

#### Molecule A-C

Hydrogen bonds		
Molecule A	Dist. [Å]	Molecule C
Gln185 [NE2]	3.81	VAL 179 [O]
Gln185 [NE2]	3.37	Asn180 [OD1]

#### Molecule B-D

Hydrogen bonds		
Molecule B	Dist. [Å]	Molecule D
Ala211[ O ]	2.93	LYS 333 [NZ]

#### Molecule E-G

Hydrogen bonds			Salt bridges		
Molecule E	Dist. [Å]	Molecule G	Molecule E	Dist. [Å]	Molecule G
Asn283 [O]	2.93	Gln93 [NE2]	Asp307 [OD1]	3.16	His100 [NE2]
Glu103 [OE1]	2.37	Arg259 [NH2]	Asp307 [OD2]	3.28	His100 [NE2]
Glu305 [OE2]	3.65	Ile293 [N]	Glu103 [OE1]	2.37	Arg259 [NH2]
Ile299 [O]	3.12	Ile297 [N]	Glu103 [OE2]	3.57	Arg259 [NH2]
Ile297 [O]	3.02	Ile299 [N]	His100 [NE2]	2.52	Asp307 [OD2]
Glu295 [O]	3.01	Met301 [N]	Arg259 [NE]	3.44	Glu103 [OE1]
Ile293 [O]	3.53	Arg302 [N]	Arg259 [NE]	3.11	Glu103 [OE2]
Asn312 [OD1]	3.54	Trp306 [N]	LYS 317 [NZ]	3.46	Asp307 [OD1]
Asn312 [O]	3.13	Trp306 [N]	LYS 317 [NZ]	3.31	Asp307 [OD2]
Asn312 [O]	2.95	Asp307 [N]			
Tyr310 [O]	3.08	Tyr310 [N]			
Asp307 [OD2]	3.44	Leu314 [N]			
Gln93 [NE2]	2.95	Asn283 [O]			

His100 [NE2]	2.52	Asp307 [OD2]
Arg259 [NE]	3.11	Glu103 [OE2]
Arg282 [NH2]	3.79	Gln93 [OE1]
Ile293 [N]	3.66	Glu305 [OE2]
Ile297 [N]	3.36	Ile299 [O]
Ile299 [N]	3.00	Ile297 [O]
Met301 [N]	2.71	Glu295 [O]
Arg302 [N]	3.72	Ile293 [O]
Trp306 [N]	3.03	Asn312 [O]
Asp307 [N]	2.92	Asn312 [O]
Tyr310 [N]	2.83	Tyr310 [O]
Leu314 [N]	2.87	Asp307 [OD1]

### Molecule F-H

Hydrogen bonds			Salt bridges		
Molecule F	Dist. [Å]	Molecule H	Molecule F	Dist. [Å]	Molecule H
Asn283 [O]	3.00	Gln93 [NE2]	Asp307 [OD1]	3.87	His100 [NE2]
Asp307 [OD2]	2.37	His100 [NE2]	Asp307 [OD2]	2.37	His100 [NE2]
Glu103 [OE2]	3.15	Arg259 [NE]	Glu103 [OE1]	3.91	Arg259 [NE]
Glu103 [OE1]	2.64	Arg259 [NH1]	Glu103 [OE2]	3.15	Arg259 [NE]
Glu305 [OE2]	3.45	Ile293 [N]	Glu103 [OE1]	2.64	Arg259 [NH1]
Ile299 [O]	2.88	Ile297 [N]	Glu103 [OE2]	3.35	Arg259 [NH1]
Ile297 [O]	3.50	THR 298 [OG1]	His100 [NE2]	2.56	Asp307 [OD2]
Ile297 [O]	2.77	Ile299 [N]	Arg259 [NE]	3.05	Glu103 [OE2]
Glu295 [O]	3.17	Met301 [N]	Arg259 [NH2]	3.07	Glu103 [OE1]
Ile293 [O]	3.43	Arg302 [N]	Arg259 [NH2]	3.47	Glu103 [OE2]
Glu294 [O]	3.53	Arg302 [NH1]			
Asn312 [O]	3.22	Trp306 [N]			
Asn312 [O]	3.09	Asp307 [N]			
Tyr310 [O]	2.77	Tyr310 [N]			
Asp307 [OD1]	2.85	Leu314 [N]			
Gln93 [NE2]	3.10	Asn283 [O]			
His100 [NE2]	2.56	Asp307 [OD2]			
Arg259 [NE]	3.05	Glu103 [OE2]			
Arg259 [NH2]	3.07	Glu103 [OE1]			
Arg282 [NH2]	3.70	Gln93 [OE1]			
Ile293 [N]	3.90	Glu305 [OE2]			
Ile297 [N]	3.03	Ile299 [O]			
Ile299 [N]	2.80	Ile297 [O]			
Met301 [N]	3.20	Glu295 [O]			

Arg302 [N]	3.51	Ile293 [O]
Trp306 [N]	3.22	Asn312 [O]
Asp307 [N]	2.90	Asn312 [O]
Tyr310 [N]	2.84	Tyr310 [O]
Leu314 [N]	2.97	Asp307 [OD1]
<b>Molecule G-H</b>		
<b>Hydrogen bonds</b>		
Molecule G	Dist. [Å]	Molecule H
Ala211 [O]	3.21	LYS 333 [NZ]
Gly187[ N ]	3.87	Tyr175 [OH]
<b>Molecule E-F</b>		
<b>Hydrogen bonds</b>		
Molecule E	Dist. [Å]	Molecule F
Tyr175 [OH]	3.86	Gly187 [N]
Ala211 [O]	3.12	LYS 333 [NZ]
Gly187[ N ]	3.81	Tyr175 [OH]

226

227

228

229

230 **Table S8** Hydrogen bonds and salt bridges on the interface of ZoADH.

<b>Molecule A-B</b>					
<b>Hydrogen bonds</b>			<b>Salt bridges</b>		
Molecule A	Dist. [Å]	Molecule B	Molecule A	Dist. [Å]	Molecule B
Asn284 [O]	3.13	Gln93 [NE2]	Asp308 [OD2]	2.48	His100 [NE2]
Asp308 [OD2]	2.48	His100 [NE2]	Asp308 [OD1]	3.50	His100 [NE2]
Glu103 [OE1]	2.80	Arg260 [NE]	Glu103 [OE1]	2.80	Arg260 [NE]
Glu103 [OE2]	3.03	Arg260 [NH2]	Glu103 [OE2]	3.77	Arg260 [NE]
Glu306 [OE2]	3.64	Ile294 [N]	Glu103 [OE1]	3.56	Arg260 [NH2]
Ile300 [O]	3.04	Ile298 [N]	Glu103 [OE2]	3.03	Arg260 [NH2]
THR 299[ OG1]	3.67	THR 299[ OG1]	Glu 96 [OE2]	3.99	Arg283 [NH2]
Ile298 [O]	2.85	Ile300 [N]	His100 [NE2]	2.35	Asp308 [OD2]
Glu296 [O]	2.97	Met302 [N]	His100 [NE2]	3.76	Asp308 [OD1]
Ile294 [O]	3.40	Arg303 [N]	Arg260 [NE]	2.86	Glu103 [OE1]
Asn313 [O]	2.98	Asp308 [N]	Arg260 [NE]	3.67	Glu103 [OE2]
Tyr311 [O]	2.89	Tyr311 [N]	Arg260 [NH2]	3.63	Glu103 [OE1]
Asp308 [OD1]	2.90	Leu315 [N]	Arg260 [NH2]	2.90	Glu103 [OE2]
Gln93 [NE2]	2.97	Asn284 [O]	LYS 318 [NZ]	3.80	Asp308 [OD2]
His100 [NE2]	2.35	Asp308 [OD2]	LYS 318 [NZ]	3.76	Asp308 [OD1]
Arg260 [NE]	2.86	Glu103 [OE1]			
Arg260 [NH2]	2.90	Glu103 [OE2]			
Ile294 [N]	3.35	Glu306 [OE2]			
Ile298 [N]	3.00	Ile300 [O]			
Ile300 [N]	2.87	Ile298 [O]			
Met302 [N]	2.87	Glu296 [O]			
Arg303 [N]	3.37	Ile294 [O]			
Asp308 [N]	2.97	Asn313 [O]			
Tyr311 [N]	2.93	Tyr311 [O]			
Leu315 [N]	2.90	Asp308 [OD1]			

<b>Molecule C-D</b>					
<b>Hydrogen bonds</b>			<b>Salt bridges</b>		
Molecule C	Dist. [Å]	Molecule D	Molecule C	Dist. [Å]	Molecule D
Asn284 [O]	3.06	Gln93 [NE2]	Asp308 [OD1]	3.56	His100 [NE2]
Asp308 [OD2]	2.45	His100 [NE2]	Asp308 [OD2]	2.45	His100 [NE2]
Glu103 [OE1]	2.60	Arg260 [NE]	Glu103 [OE1]	2.60	Arg260 [NE]
Glu103 [OE2]	2.77	Arg260 [NH2]	Glu103 [OE2]	3.66	Arg260 [NE]
Glu306 [OE2]	3.49	Ile294 [N]	Glu103 [OE1]	3.34	Arg260 [NH2]
Ile300 [O]	3.07	Ile298 [N]	Glu103 [OE2]	2.77	Arg260 [NH2]
THR 299[ OG1]	3.63	THR 299[ OG1]	His100 [NE2]	3.75	Asp308 [OD1]

Ile298 [O]	2.84	Ile300 [N]	His100 [NE2]	2.19	Asp308 [OD2]
Glu296 [O]	3.02	Met302 [N]	Arg260[ NH1]	3.42	Glu103 [OE2]
Ile294 [O]	3.45	Arg303 [N]	Arg260[ NH1]	3.37	Glu103 [OE1]
Asn313 [O]	2.93	Asp308 [N]	Arg260 [NH2]	2.65	Glu103 [OE2]
Tyr311 [O]	2.88	Tyr311 [N]	Arg260 [NH2]	3.88	Glu103 [OE1]
Asp308 [OD1]	2.98	Leu315 [N]			
Gln93 [NE2]	2.98	Asn284 [O]			
His100 [NE2]	2.19	Asp308 [OD2]			
Arg260[ NH1]	3.37	Glu103 [OE1]			
Arg260 [NH2]	2.65	Glu103 [OE2]			
Ile294 [N]	3.47	Glu306 [OE2]			
Ile298 [N]	3.00	Ile300 [O]			
Ile300 [N]	2.92	Ile298 [O]			
Met302 [N]	3.07	Glu296 [O]			
Arg303 [N]	3.45	Ile294 [O]			
Asp308 [N]	2.95	Asn313 [O]			
Tyr311 [N]	2.86	Tyr311 [O]			
Leu315 [N]	2.87	Asp308 [OD1]			

#### Molecule A-D

Hydrogen bonds			Salt bridges		
Molecule A	Dist. [Å]	Molecule D	Molecule A	Dist. [Å]	Molecule D
Gly213 [O]	2.78	Gln330 [NE2]	Glu208 [OE1]	3.85	LYS 334 [NZ]
Ala212 [O]	2.82	LYS 334 [NZ]	Glu208 [OE2]	3.03	LYS 334 [NZ]
Glu208 [OE2]	3.03	LYS 334 [NZ]	LYS 334 [NZ]	2.95	Glu208 [OE1]
Gln330 [NE2]	2.95	Gly213 [O]			
LYS 334 [NZ]	2.95	Ala212 [O]			
LYS 334 [NZ]	2.95	Glu208 [OE1]			

#### Molecule B-C

Hydrogen bonds			Salt bridges		
Molecule B	Dist. [Å]	Molecule C	Molecule B	Dist. [Å]	Molecule C
Gln330 [NE2]	3.16	Gly213 [O]	LYS 334 [NZ]	2.82	Glu208 [OE1]
Gly213 [O]	3.15	Gln330 [NE2]	LYS 334 [NZ]	3.58	Glu208 [OE2]
Glu208 [OE1]	2.82	LYS 334 [NZ]			

231

232



233 **References**

- 234 Akal AL, Karan R, Hohl A, Alam I, Vogler M, Grötzinger SW, Eppinger J, Rueping M (2019) A  
235 polyextremophilic alcohol dehydrogenase from the Atlantis II Deep Red Sea brine pool.  
236 FEBS Open Bio 9:194–205. <https://doi.org/10.1002/2211-5463.12557>
- 237 Barbeyron T, L'Haridon S, Corre E, Kloareg B, Potin P (2001) *Zobellia galactanovorans* gen.  
238 nov., sp. nov., a marine species of Flavobacteriaceae isolated from a red alga, and  
239 classification of [*Cytophaga*] *uliginosa* (ZoBell and Upham 1944) Reichenbach 1989 as  
240 *Zobellia uliginosa* gen. nov., comb. nov. Int J Syst Evol Microbiol 51:985–997.  
241 <https://doi.org/10.1099/00207713-51-3-985>
- 242 Bubb WA, Berthon HA, Kuchel PW (1995) Tris Buffer Reactivity with Low-Molecular-Weight  
243 Aldehyds: NME Characterization of the reactions of glyceraldehyde 3-phosphate. Bioorg  
244 Chem 23:119–130. <https://doi.org/10.1006/bioo.1995.1010>
- 245 Nedashkovskaya OI, Kim SB, Vancanneyt M, Snauwaert C, Lysenko AM, Rohde M, Frolova  
246 GM, Zhukova N V., Mikhailov V V., Bae KS, Oh HW, Swings J (2006) *Formosa agariphila*  
247 sp. nov., a budding bacterium of the family Flavobacteriaceae isolated from marine  
248 environments, and emended description of the genus *Formosa*. Int J Syst Evol Microbiol  
249 56:161–167. <https://doi.org/10.1099/ijs.0.63875-0>
- 250 Smith KW, Johnson SL (1975) Borate inhibition of yeast alcohol dehydrogenase. Biochemistry  
251 34:560–565. <https://doi.org/10.1021/bi00648a016>
- 252 Trivić S, Leskovac V, Zeremski J, Stančić B, Anderson BM (1998) Influence of  
253 Tris(hydroxymethyl)aminomethane on kinetic mechanism of yeast alcohol  
254 dehydrogenase. J Enzyme Inhib 13:57–68. <https://doi.org/10.3109/14756369809035827>
- 255 Uthoff S, Steinbüchel A (2012) Purification and Characterization of an NAD<sup>+</sup>-Dependent XylB-  
256 like aryl alcohol dehydrogenase identified in *Acinetobacter baylyi* ADP1. Appl Environ  
257 Microbiol 78:8743–8752. <https://doi.org/10.1128/AEM.02224-12>
- 258 Ying X, Wang Y, Xiong B, Wu T, Xie L, Yu M, Wang Z (2014) Characterization of an  
259 allylic/benzyl alcohol dehydrogenase from *Yokenella* sp. strain WZY002, an organism  
260 potentially useful for the synthesis of  $\alpha,\beta$ -unsaturated alcohols from allylic aldehydes and  
261 ketones. Appl Environ Microbiol 80:2399–2409. <https://doi.org/10.1128/AEM.03980-13>
- 262 Zhang L, Jiang D, Li Y, Wu L, Liu Q, Dong K, Oger P (2021) Characterization of a novel type  
263 III alcohol dehydrogenase from *Thermococcus barophilus* Ch5. Int J Biol Macromol  
264 171:491–501. <https://doi.org/10.1016/j.ijbiomac.2020.12.197>

265



# Article III



RESEARCH

Open Access



# Metabolic engineering enables *Bacillus licheniformis* to grow on the marine polysaccharide ulvan

Theresa Dutschei<sup>1</sup>, Marie-Katherin Zühlke<sup>2,3</sup>, Norma Welsch<sup>2,3</sup>, Tom Eisenack<sup>2</sup>, Maximilian Hilkmann<sup>2,3</sup>, Joris Krull<sup>3,4,5</sup>, Carlo Stühle<sup>1</sup>, Stefan Brott<sup>1</sup>, Alexandra Dürwald<sup>2</sup>, Lukas Reisky<sup>1</sup>, Jan-Hendrik Hehemann<sup>3,4,5</sup>, Dörte Becher<sup>6</sup>, Thomas Schweder<sup>2,3\*</sup> and Uwe T. Bornscheuer<sup>1,3\*</sup>

## Abstract

**Background:** Marine algae are responsible for half of the global primary production, converting carbon dioxide into organic compounds like carbohydrates. Particularly in eutrophic waters, they can grow into massive algal blooms. This polysaccharide rich biomass represents a cheap and abundant renewable carbon source. In nature, the diverse group of polysaccharides is decomposed by highly specialized microbial catabolic systems. We elucidated the complete degradation pathway of the green algae-specific polysaccharide ulvan in previous studies using a toolbox of enzymes discovered in the marine flavobacterium *Formosa agariphila* and recombinantly expressed in *Escherichia coli*.

**Results:** In this study we show that ulvan from algal biomass can be used as feedstock for a biotechnological production strain using recombinantly expressed carbohydrate-active enzymes. We demonstrate that *Bacillus licheniformis* is able to grow on ulvan-derived xylose-containing oligosaccharides. Comparative growth experiments with different ulvan hydrolysates and physiological proteogenomic analyses indicated that analogues of the *F. agariphila* ulvan lyase and an unsaturated  $\beta$ -glucuronidase are missing in *B. licheniformis*. We reveal that the heterologous expression of these two marine enzymes in *B. licheniformis* enables an efficient conversion of the algal polysaccharide ulvan as carbon and energy source.

**Conclusion:** Our data demonstrate the physiological capability of the industrially relevant bacterium *B. licheniformis* to grow on ulvan. We present a metabolic engineering strategy to enable ulvan-based biorefinery processes using this bacterial cell factory. With this study, we provide a stepping stone for the development of future bioprocesses with *Bacillus* using the abundant marine renewable carbon source ulvan.

**Keywords:** Ulvan, Marine polysaccharide, Green algae, Biorefinery process, *Bacillus licheniformis*

## Background

Eutrophication and global warming impact frequency and extent of algal blooming events and thus accumulation of algal biomasses in coastal areas [1–3]. Despite algae or algal products being already used in food, cosmetics, biotechnology and pharmaceutical industry [4–6], washed up algae are still largely unexploited. As a consequence, interest has been raised to develop processes that convert this cheap biomass to valuable products [7] and first

\*Correspondence: schweder@uni-greifswald.de;  
uwe.bornscheuer@uni-greifswald.de

<sup>1</sup> Department of Biotechnology & Enzyme Catalysis, Institute of Biochemistry, University of Greifswald, 17487 Greifswald, Germany

<sup>2</sup> Department of Pharmaceutical Biotechnology, Institute of Pharmacy, University of Greifswald, 17487 Greifswald, Germany

Full list of author information is available at the end of the article



© The Author(s) 2022. **Open Access** This article is licensed under a Creative Commons Attribution 4.0 International License, which permits use, sharing, adaptation, distribution and reproduction in any medium or format, as long as you give appropriate credit to the original author(s) and the source, provide a link to the Creative Commons licence, and indicate if changes were made. The images or other third party material in this article are included in the article's Creative Commons licence, unless indicated otherwise in a credit line to the material. If material is not included in the article's Creative Commons licence and your intended use is not permitted by statutory regulation or exceeds the permitted use, you will need to obtain permission directly from the copyright holder. To view a copy of this licence, visit <http://creativecommons.org/licenses/by/4.0/>. The Creative Commons Public Domain Dedication waiver (<http://creativecommons.org/publicdomain/zero/1.0/>) applies to the data made available in this article, unless otherwise stated in a credit line to the data.

attempts are already underway [8]. Amongst a variety of compounds that could be harnessed, polysaccharides are attractive targets. They account for up to 50% of macroalgal biomass and mostly represent cell wall or storage components [9–11]. These polysaccharides are highly diverse in their structure and composition [12]. Targeting this versatile substrate pool thus requires a multitude of enzymes which are usually encoded in highly clustered genomic regions of polysaccharide degrading bacteria. These so-called polysaccharide utilization loci (PUL) encode proteins to mediate binding, degradation and uptake of saccharides [13]. Recently, we were able to elucidate a complex enzymatic cascade to completely deconstruct polymeric ulvan to monomeric sugar compounds using enzymes from the marine flavobacterium *Formosa agariphila* KM3901<sup>T</sup> recombinantly expressed in *Escherichia coli* [14, 15]. Ulvan is the main cell wall polysaccharide in the green seaweed *Ulva* spp. [16]. The sugar backbone is composed of L-rhamnose, D-xylose and D-glucuronic acid/L-iduronic acid and is highly branched and sulfated. Moreover, the monosaccharide composition varies between species and sampling sites [17]. In *F. agariphila*, ulvan lyases catalyze the initial degradation step, releasing several oligosaccharide species with a 5-dehydro-4-deoxy-D-glucuronate at the non-reducing end [14, 18]. This unsaturated moiety is then removed by glycoside hydrolases (GH), which allows further GH-mediated hydrolysis of oligosaccharides prior to or after their desulfation [14]. On the one hand, such enzyme cascades can be used for the production of rare (sulfated) sugar oligosaccharides that could be interesting due to their immunomodulating activities [19]. On the other hand, these hydrolysates may represent a starting material for biotechnological processes as alternative feedstock for common sugars like glucose for microbial fermentation [5]. Microbial engineering and systems biology can further help to develop such new biomass based bioprocesses [20, 21]. Consequently, in-depth characterization of the selected microbial production species is a prerequisite for strain optimization. The well-established biotechnological work horse *Bacillus licheniformis* is an attractive target to be investigated for the utilization of alternative algal derived biomasses: It produces a variety of enzymes to degrade plant materials, it is a generally recognized as safe (GRAS) strain, has a fast growth rate and is already of high industrial importance [22]. This bacterial cell factory naturally produces the extracellular protease subtilisin [23], which has been developed into industrial production due to its widespread use in detergents [24]. In addition, first processes that use *B. licheniformis* to convert plant biomass into valuable products have already been established. This includes metabolic engineering approaches which enabled the production of

acetoin, 2,3-butanediol or lactic acid from kitchen waste or corncob molasses [22, 25–27]. Furthermore, the production of extracellular proteins from algal feedstock [28] was already studied to broaden up the possible use of this bacterium in fermentation processes.

In order to develop an ulvan based bioprocess, we investigated a variety of bacterial strains for their ability to utilize ulvan and identified the industrially relevant bacterium *B. licheniformis* DSM13, which is able to grow on pre-digested ulvan. We investigated strain specific metabolic properties of this bacterium, which are required for ulvan utilization. Our study provides first insights into the development of a potential ulvan based bioprocess with *Bacillus* species.

## Results and discussion

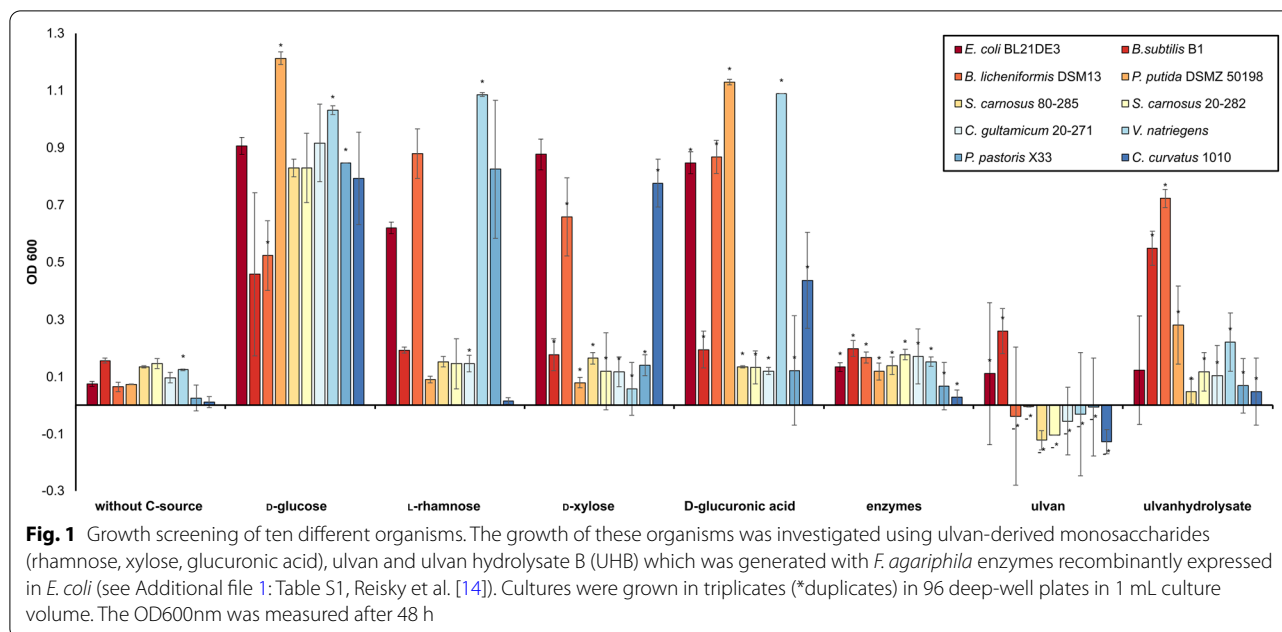
### *Bacillus licheniformis* DSM13 efficiently consumes ulvan-derived monomers

In a first attempt, we screened 10 different strains for their ability to grow on ulvan and ulvan-derived monosaccharides, as single monomers or as monosaccharide mixture (Fig. 1, Additional file 1: Fig. S1). While none of the strains grew on raw ulvan, *B. licheniformis* DSM13, *Cryptococcus curvatus* 1010 and *Pseudomonas putida* DSMZ 50198 consumed the monomer cocktail derived from ulvan digestion using the complete enzymatic cascade of *F. agariphila* that was recombinantly expressed in *E. coli* BL21(DE3) as described previously (Additional file 1: Table S1, Fig. S2) [14, 15].

This mixture, ulvan hydrolysate B (UHB), provided L-rhamnose, D-xylose, D-glucuronic acid and 5-dehydro-4-deoxy-D-glucuronate. *B. licheniformis* DSM13 grew also well on each individual monosaccharide present in the mixture, as described before [29, 30], even better than on D-glucose. Although *P. putida* DSMZ 50198 and *Bacillus subtilis* B1 consumed UHB, they were not able to grow on L-rhamnose (Fig. 1), which is known for *P. putida* [31], but disagrees with observations reported for *C. curvatus* 1010 [32]. *P. putida* DSMZ 50198 also lacks the ability to grow on D-xylose. Growth experiments identified *B. licheniformis* DSM13 as a suitable candidate for further investigations to establish an ulvan sugar-based bioprocess.

### *Bacillus licheniformis* DSM13 grows and accumulates proteases on fully digested ulvan

To investigate the suitability of the abundant macroalgal polysaccharide ulvan as feedstock for production processes, we quantified exemplarily protease activity via the AAPF-assay [33] during cultivation, like the alkaline serine protease (AprX, Q65IP4), subtilisin protease Apr (Q65LP7) and extracellular serine protease Vpr (Q65DN2). Following growth over time, *B. licheniformis*



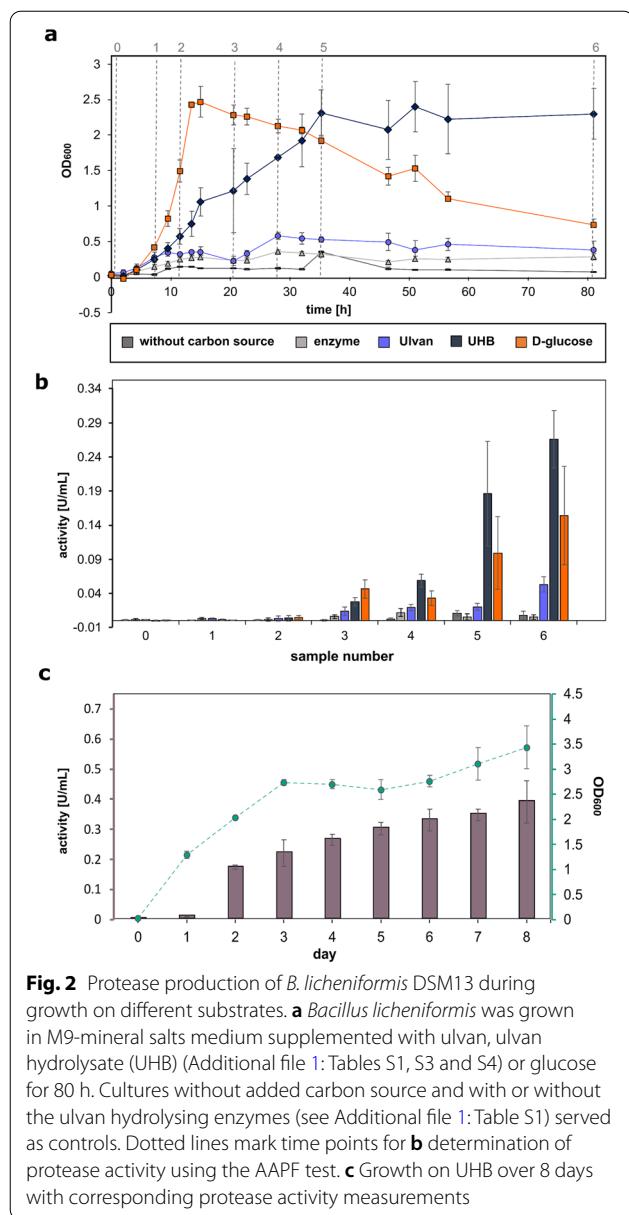
DSM13 grew more slowly on UHB compared to D-glucose, but reached a comparable maximum optical density that was stable until the end of the experiment (Fig. 2a). At the same time, protease activity increased over time (Fig. 2b) and was stable even in prolonged cultivations (Fig. 2c). These growth experiments revealed a constant stationary phase over more than 5 days for *B. licheniformis* using UHB as the sole carbon source. The resulting increased biomass until the end of the cultivation improved protease production significantly compared to the glucose-based cultivations.

#### Capabilities of *B. licheniformis* DSM13 to grow on ulvan-derived oligosaccharides

The initial growth experiments demonstrated the physiological capability of *B. licheniformis* DSM13 to utilize ulvan-specific monosaccharides (Fig. 2, Additional file 1: Fig. S3). Consumption of these monosaccharides as well as the fact that this bacterium is well known to degrade plant material [34, 35], gave reasons to suspect also the acceptance of ulvan-derived oligosaccharides. Therefore, 12 different ulvan hydrolysates were examined as potential substrates (Additional file 1: Fig. S4). These enzymatically digested ulvan-extracts cover different levels of ulvan depolymerisation as described in our previous studies and thus differ in their mono- and oligosaccharide composition [14, 15]. Again, each hydrolysate, including the aforementioned UHB, was produced using selected *F. agariphila* ulvan-degrading enzymes recombinantly expressed in *E. coli* BL21(DE3) (Additional file 1: Table S1, Fig. S2; Fig. 3a) [14]. The cell densities

achieved after 24 h of cultivation identified the required level of hydrolyzation to allow growth of *B. licheniformis* DSM13. At the same time, they indicated which enzymatic activities might be missing in *Bacillus* and would thus enable growth on higher degrees of polymerization or ulvan itself (Fig. 3b). The ulvan lyase-generated hydrolysates improved digestibility only to a small extent (P30\_PL28 > P10\_PL40), similar to P31\_GH39 and P17\_GH2 pre-digestion (Additional file 1: Fig. S4).

However, optical densities were considerably increased if the ulvan lyase activity of P30\_PL28 was either supported by the unsaturated glucuronyl hydrolase P1\_GH88 or the glycoside hydrolase P33\_GH105 (UHA). This may be due to the release of smaller oligosaccharides and unsaturated uronic acids as carbon source in UHA. The P30\_PL28 ulvan lyase cleaves the ulvan polymer between  $\alpha$ -L-rhamnose-3-sulfate-(1,4)- $\beta$ -D-glucuronic acid, which produces an unsaturated uronic acid at the non-reducing end of the released oligosaccharide, which is specific for lyases. This unsaturated uronic acid (4-deoxy- $\alpha$ -L-threo-hex-4-enopyranuronic acid) is then hydrolyzed by P33\_GH105. Indeed, previous growth experiments confirmed *B. licheniformis* DSM13 to consume 4-deoxy- $\alpha$ -L-threo-hex-4-enopyranuronic acid (Additional file 1: Fig. S3). This way, not only easily digestible monosaccharides are released from oligosaccharides using P33\_GH105, its activity also enables P30\_PL28 to cleave the oligomer even further since lyase products inhibit subsequent lyase activities [14, 18]. In addition, unsaturated uronic acids in oligosaccharides might hinder their subsequent disassembling by *B. licheniformis* DSM13.



Interestingly, additional hydrolysis steps, which also included sulfatases, did not further improve growth. This led to the assumption that the two initial major enzyme activities of the ulvan degradation pathway [14], ensured by the ulvan lyase (PL28) and unsaturated glucuronyle hydrolases (GH105, GH88), provided an oligosaccharide mixture suitable for *B. licheniformis* DSM13 to degrade ulvan. This also indicated the availability of putative CAZymes in *B. licheniformis* DSM13 to utilize L-rhamnose, D-xylose and D-glucuronic acid from ulvan oligomers and to channel them into its carbon and energy metabolism.

### Proteogenomic analysis of *B. licheniformis* DSM13

To further interpret our results and to explore the physiological potential of *B. licheniformis* to utilize ulvan derived sugars, we performed computational and proteome analyses. We analyzed the intracellular soluble as well as the extracellular proteomes of ulvan-, UHA- and UHB-cultivated cells (Fig. 3, Additional file 1: Fig. S5) compared to rhamnose and glucose cultures. In general, it is well known that *B. licheniformis* DSM13 secretes a variety of extracellular CAZymes to degrade polysaccharides [34, 35]. Correspondingly, computational analysis with the web server for automated CAZyme annotation, dbCAN2 [36, 37], identified 86 PLs, GHs and CEs to be encoded in its genome, 58 of which were captured by intracellular and extracellular proteomes (Additional file 2: Table S6; Additional file 1: Fig. S5).

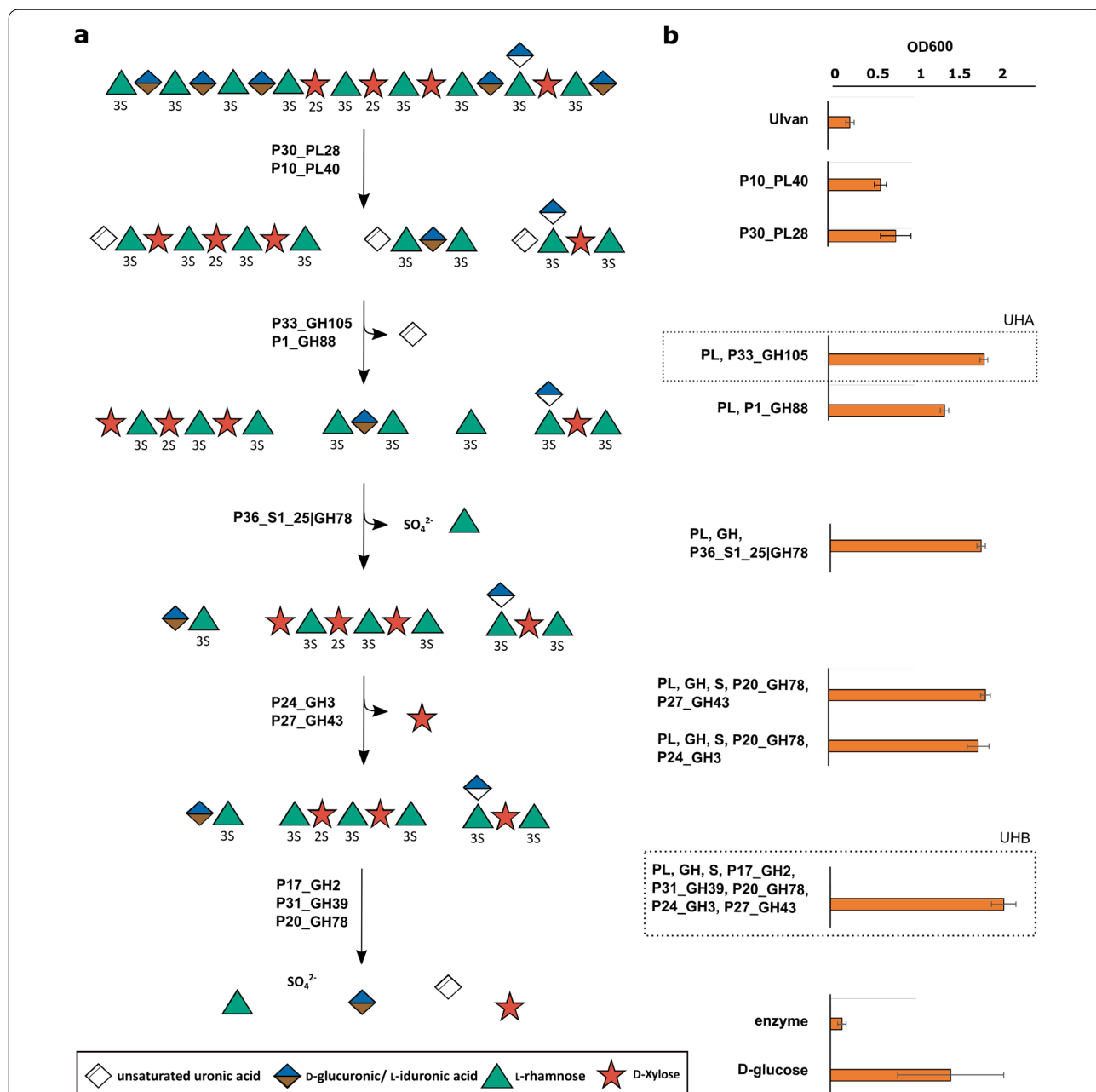
### Enzymes to cleave ulvan are lacking

Proteome and dbCAN2 analyses did not reveal suitable ulvanolytic enzyme activities of *B. licheniformis* DSM13 wild type strain, which are required for the initial digestion of ulvan, and thus confirmed our growth experiments shown in Fig. 2. The strain lacks PLs from families 24, 25, 28 and 40 [12] to cleave ulvan into oligosaccharides. Moreover, proteome analyses do not indicate PLs or GHs that depolymerize pectin and pectin components to also cleave ulvan, since corresponding proteins were either low abundant (PL11\_1 Q65KY4) or quantified across all samples (PL1\_5 Q65DC2, PL3\_1 Q65EF5 and GH28 Q65F26, Additional file 1: Fig. S5; Additional file 2: Table S6). *B. licheniformis* DSM13 encodes two GH105s (Q65FY9, Q65KY9) as candidates to catalyze the next necessary enzymatic step in ulvan disassembling, but both of them were not detected in our proteome analyses during growth on ulvan oligosaccharides. Instead, they might be involved in rhamnogalacturonan I degradation, like in *B. subtilis* [39].

### GHs that may disassemble oligosaccharides

Nevertheless, the adaptation of *B. licheniformis* DSM13 to pectin or hemicellulose usage may still allow for consumption of certain ulvan oligosaccharides as demonstrated by our growth experiments. Proteome analyses captured potentially involved GH43s, the GH43\_4 (Q65D31) being highly abundant in ulvan and ulvan hydrolysate samples (1–3% of the total extracellular proteome) (Fig. 4, Additional file 2: Table S6, S7). GH43\_4 (Q65D31, YxiA/Abn2) as well as GH43\_5 (Q65GB9, AbnA) are both extracellular enzymes that degrade arabinans [40, 41]. By contrast, in *F. agariphila* a GH43\_10 cleaved xylose moieties from ulvan-derived oligosaccharides [14]. The corresponding *B. licheniformis*



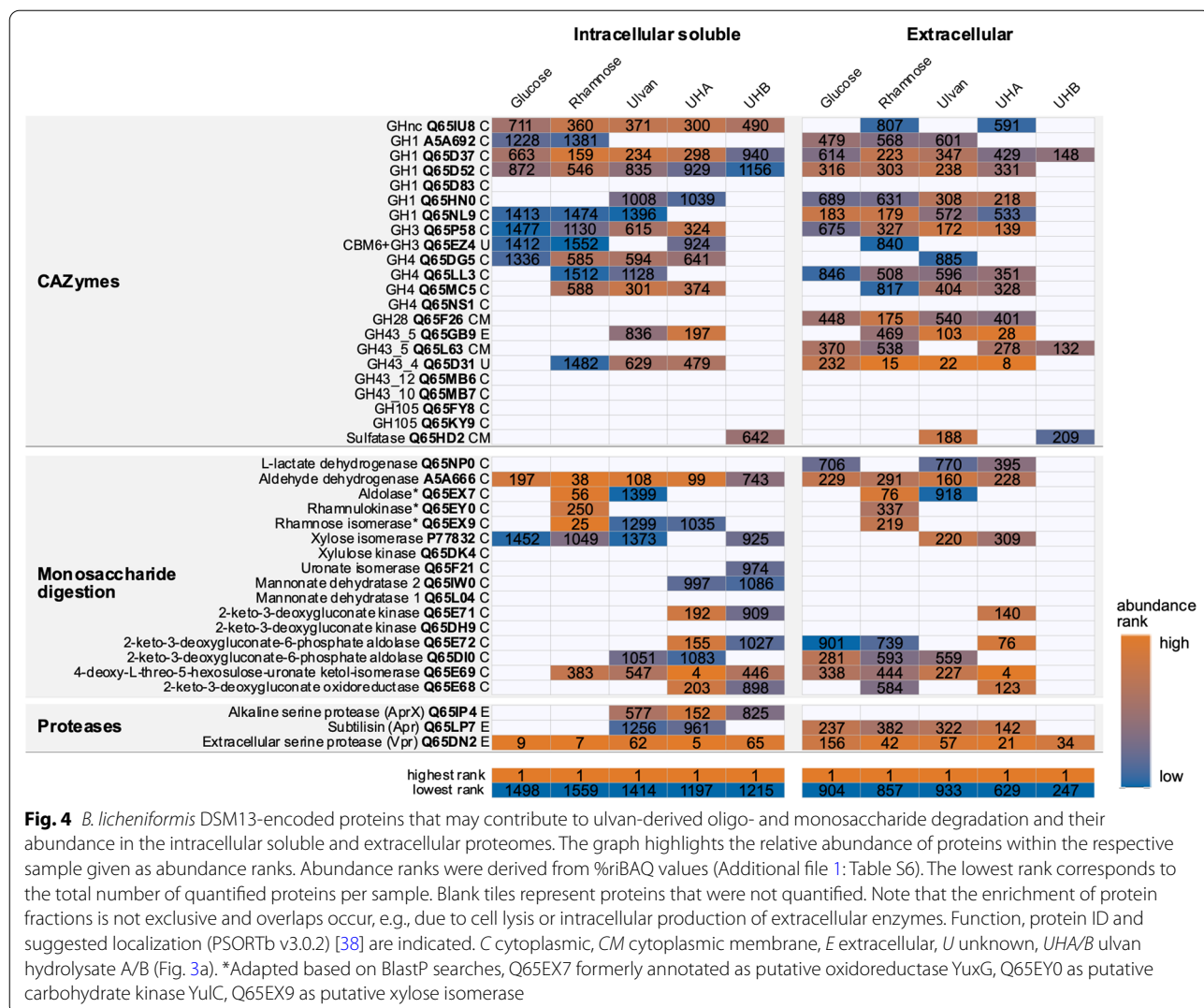


**Fig. 3** In-depth analysis of the capability of *B. licheniformis* DSM13 to degrade ulvan-derived oligosaccharides. Ulvan was digested with selected enzymes or enzyme cocktails, described before [14, 15], to produce a total of 12 different ulvan hydrolysates (Additional file 1: Fig. S4). **a** These vary in their mono- and oligosaccharide content based on **b** the enzymes used and thus provide specific carbon sources for *B. licheniformis* DSM13. The DSM13 strain was cultivated in M9-mineral medium supplemented with ulvan or enzyme-generated ulvan hydrolysates and OD600 was measured after 24 h. Growth on hydrolysates UHA and UHB, which were used for further investigations, is highlighted. (PL: mix of P10\_PL40; GH: mix of P33\_GH105, P1\_GH88; S: P36\_S1\_25|GH78)

DSM13 enzyme (Q65MB7) was not quantified by proteome analyses. However, several other GHs of family 1, 3 and 4 that might have xylosidase activity, as well as an unclassified (nc) GH, were quantified in the proteome of *B. licheniformis* DSM13 grown on ulvan extracts.

**The involvement of sulfatases remains speculative**

Ulvan degradation does not only require PLs and GHs to cleave the sugar chain, but also sulfatases to act on sulfated rhamnose or xylose units. To encounter the complexity of ulvan composition and its degree of sulfation,



**Fig. 4** *B. licheniformis* DSM13-encoded proteins that may contribute to ulvan-derived oligo- and monosaccharide degradation and their abundance in the intracellular soluble and extracellular proteomes. The graph highlights the relative abundance of proteins within the respective sample given as abundance ranks. Abundance ranks were derived from %iBAQ values (Additional file 1: Table S6). The lowest rank corresponds to the total number of quantified proteins per sample. Blank tiles represent proteins that were not quantified. Note that the enrichment of protein fractions is not exclusive and overlaps occur, e.g., due to cell lysis or intracellular production of extracellular enzymes. Function, protein ID and suggested localization (PSORTb v3.0.2) [38] are indicated. C cytoplasmic, CM cytoplasmic membrane, E extracellular, U unknown, UHA/B ulvan hydrolysate A/B (Fig. 3a). \*Adapted based on BlastP searches, Q65EX7 formerly annotated as putative oxidoreductase YuxG, Q65EY0 as putative carbohydrate kinase YulC, Q65EX9 as putative xylose isomerase

marine ulvan targeting strains encode a set of sulfatases [14, 42–44], e.g., eight sulfatases from five S1 subfamilies are encoded in the *F. agariphila* ulvan PUL. In *B. licheniformis*, only three proteins are annotated as putative sulfatases. However, for two of them, YfnI (Q65D92) and YflE (Q62XX8), it has been discovered that they are involved in cell wall lipoteichoic acid synthesis in *B. subtilis* (Additional file 1: Fig. S6) [45]. Indeed, the remaining sulfatase (Q65HD2) was abundant in ulvan and UHB secretomes (Fig. 4). We therefore cloned and overexpressed the respective gene in *E. coli*, but so far, no specific sulfatase activity of this enzyme could be detected (data not shown). At the same time, since UHB hydrolysate provides desulfated monosaccharides, its role in desulfation needs to be investigated in more detail in future studies. Nevertheless, the results underline that sulfatases are largely underexplored in *B. licheniformis* and might not even be recognized as such, e.g.

alkaline phosphatases preferentially cleave phosphate monoesters, but are also active on the sulfate counterparts [46]. In another scenario, *B. licheniformis* DSM13 could just consume desulfated ulvan fragments.

**Consumption of ulvan-derived monosaccharides**

In case of UHA the hydrolysate does not only contain oligosaccharides, but also free unsaturated uronic acids as substrates, which was demonstrated to be consumed by our growth experiments (Additional file 1: Fig. S3). Confirming this, a 4-deoxy-L-threo-5-hexosulose-uronate ketol-isomerase (Q65E69) was among the most abundant proteins in UHA samples (Fig. 4) representing 1.6% and 4.5% of the total UHA intracellular and extracellular proteome, respectively (Additional file 2: Table S6, Additional file 3: Table S7). Pathways for the other monosaccharides could also be mapped in UHA and UHB samples (Fig. 4), although they were not fully covered.

Taking multiple samples over time and comparing them to respective monosaccharide cultures could close these gaps. Monosaccharides are probably consumed successively, as glucose and xylose are not degraded simultaneously in *Bacillus* species [47, 48].

### Protease expression during growth on ulvan and oligosaccharides

In addition, the detected significantly increased protease activities of *B. licheniformis* cultivations with ulvan hydrolysates (see Fig. 2) indicated an elevated protease expression under these conditions. This was supported by our proteome analyses, where the alkaline serine protease (AprX, Q65IP4) was only quantified in ulvan and ulvan hydrolysate samples. However, the subtilisin protease Apr (Q65LP7) or the extracellular serine protease Vpr (Q65DN2) were present throughout all conditions, with high levels of Vpr (Fig. 4). Whereas putative algal-derived proteins from extraction were probably negligible (ulvan, UHA and UHB samples) as inducers of these enzymatic activities, the added *F. agariphila* enzyme extracts to generate ulvan hydrolysates injected additional protein sources into our samples. However, it is worth emphasizing that this potential nutrient source did not cause a significant biomass increase in our control growth experiments (Fig. 2a, enzyme control). The observed increased protease activities thus underline the suitability of ulvan and hydrolysates thereof as potential substrates for industrial bulk protease production processes.

### Functional expression of two initial ulvan-degrading CAZymes in *Bacillus*

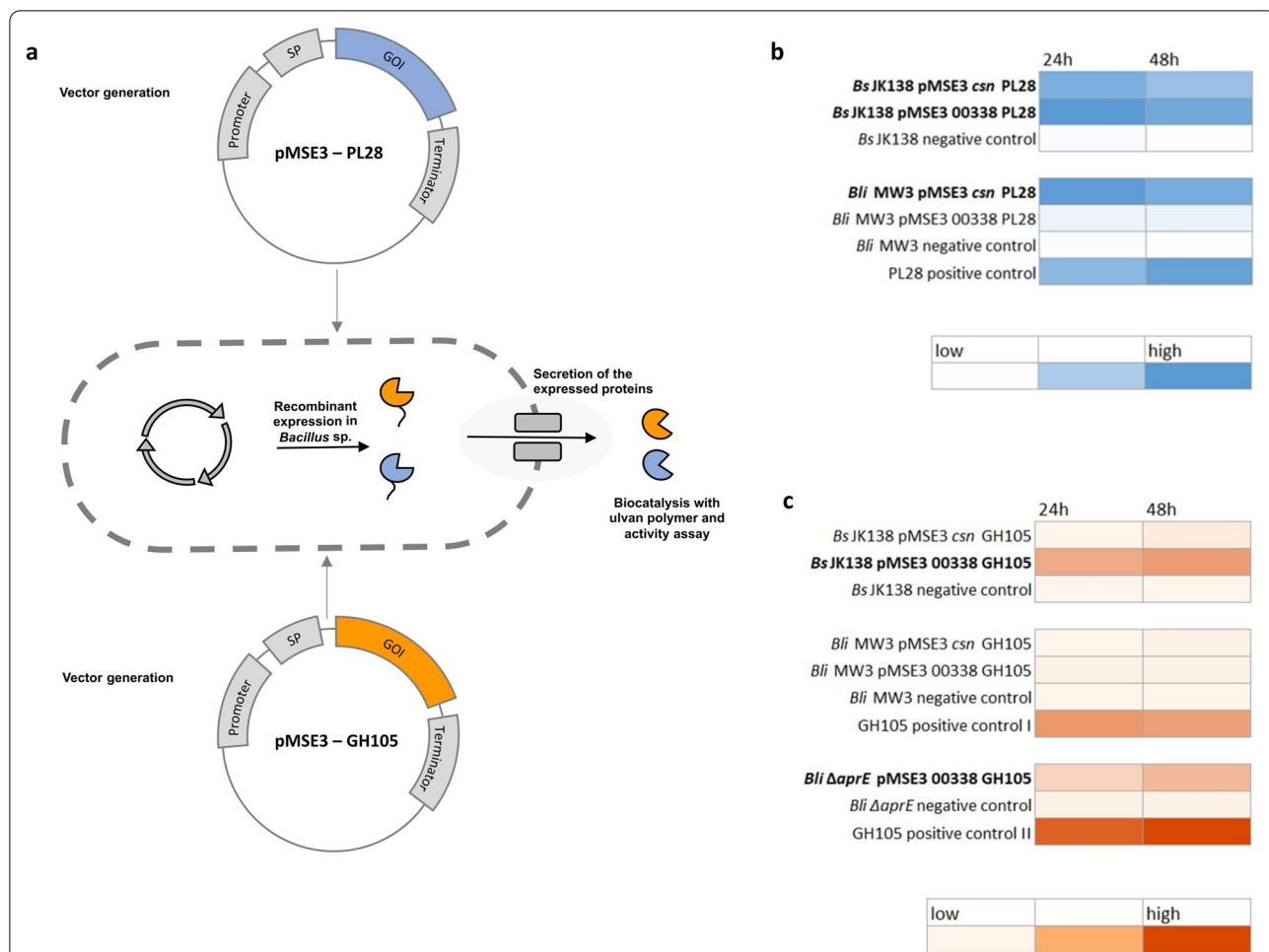
Our previous experiments have shown that *B. licheniformis* DSM13 lacks two initial enzyme activities, ulvan lyase (PL28) and unsaturated glucuronyl hydrolase (GH105, GH88), to use the ulvan polymer as sole carbon source. Therefore, we integrated the *F. agariphila* P30\_PL28 and P33\_GH105 into a *Bacillus* host-vector system, expressing them as secreted proteins to disassemble ulvan and thus enabling a self-sufficient *Bacillus* strain (Fig. 5a). Since *B. subtilis* and *B. licheniformis* share a similar CAZyme repertoire [35, 49] and showed similar growth in comparative experiments (Additional file 1: Fig. S7), *B. subtilis* JK138 and *B. licheniformis* MW3 were selected as first expression hosts. *B. licheniformis* MW3, a derivative of *B. licheniformis* DSM13, lacks the RM-system (restriction and modification system) which facilitates the genetic accessibility of this strain [50]. Starting with the signal peptide *csn* from *B. subtilis* and 00338 from *B. licheniformis* for both hosts, proteins were expressed in an active form extra- and intracellularly after growth in EnpressoB under simulated fed-batch

conditions (Additional file 1: Fig. S9). PL28 synthesis and activity was confirmed for both expression hosts by ulvan lyase assays (Fig. 5b) and C-PAGE analysis (Additional file 1: Figs. S9, S10).

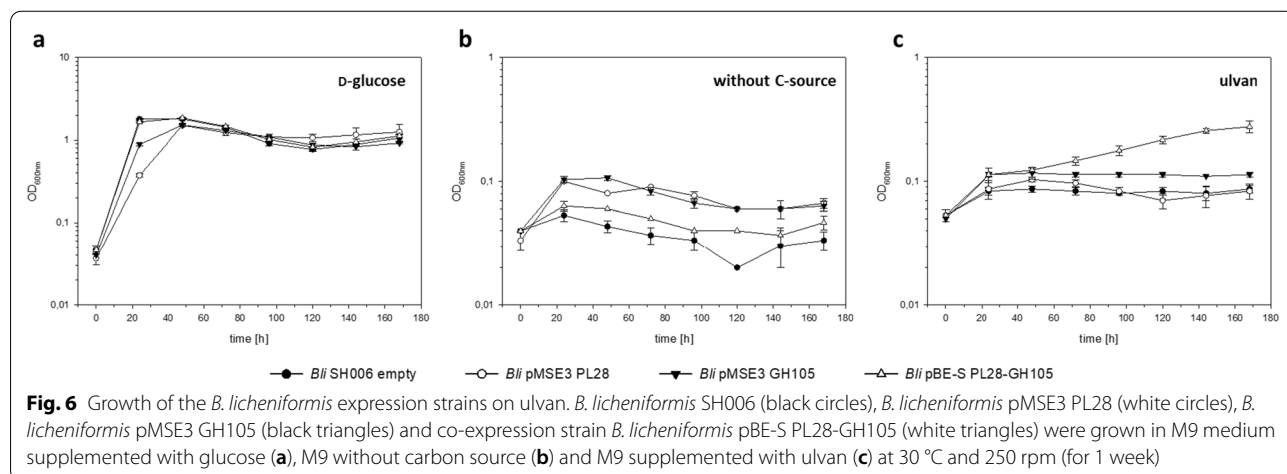
Production of the GH105 enzyme was detected in *B. subtilis* in combination with the 00338-secretion signal but not in *B. licheniformis* MW3, which was most probably caused by protease activity in this strain. Thus, we additionally used another *B. licheniformis* expression strain (*B. licheniformis* SH006), which is similar to *B. subtilis* JK138 being deficient in the main extracellular protease Apr. Indeed, functional expression of GH105 was detected in the *B. licheniformis* protease-mutant strain using the same expression cassette as for *B. subtilis* (Fig. 5b). Corresponding carbohydrate polyacrylamide gel electrophoresis (C-PAGE) analysis for GH105 activity is shown in Additional file 1: Fig. S10. Although enzyme activity was higher within the extracellular fraction, intracellular enzyme activities for PL28 and GH105 were measured in the activity assays (data not shown) and were also detected by C-PAGE (Additional file 1: Fig. S10), indicating an incomplete protein secretion. To further improve protein secretion of PL28 and GH105, all Sec dependent signal peptides of *B. subtilis* were screened to enhance protein secretion. For this purpose, the *B. subtilis* Secretory Protein Expression System (Takara Clontech) was used, which allows the fusion of 173 Sec-dependent signal peptides of *B. subtilis* to the genes of interest. Based on *B. subtilis* JK138, it could be demonstrated, that higher enzyme activities for PL28 were measured when protein secretion was mediated by the secretion signal of *wprA*, whereas none of the investigated signal peptides mediated an increase in GH105 activity (data not shown). Taken together, we were able to establish the functional expression of the two initial ulvan degrading enzymes PL28 and GH105 in *B. subtilis* and *B. licheniformis*, which may enable both organisms for applications in bioprocess development based on the alternative biomass ulvan.

### Co-expression of the PL28 and GH105 in *B. licheniformis* SH006

As soon as the functional expression of either the PL28 or the GH105 encoding gene was established, a self-sufficient strain was designed by combining both enzyme genes. In order to compare PL28 or GH105 single expression vs. co-expression of both marine enzymes in *B. licheniformis* SH006, growth experiments for protein expression (Additional file 1: Fig. S11) and ulvan utilization (Fig. 6) were carried out simultaneously for the *B. licheniformis* “empty” strain, serving as the negative control, for *B. licheniformis* pMSE3 P<sub>aprE</sub> *csn*-UL, *B. licheniformis* pMSE3 P<sub>aprE</sub> 00,338-GH and



**Fig. 5** Integration of two genes of ulvan-degrading CAZymes in *Bacillus* strains. High copy expression vectors for synthesis of PL28 and GH105 enzymes were constructed, integrated and functionally expressed in *Bacilli* (a). Extracellular PL28 (b) and GH105 (c) activities detected by lyase-assay and thiobarbituric acid-assay, respectively (Additional file 1: Figs. S8–S10)



*B. licheniformis* pBE-S PL28-GH105. Determination of enzymatic activities revealed functional expression of the PL28 enzyme in the PL28 single expression strain *B. licheniformis* pMSE3 PL28 and the co-expression strain *B. licheniformis* pBE-S PL28-GH105 (Additional file 1: Fig. S12a) whereas GH105 activity was detected in the *B. licheniformis* pMSE3 GH105 and *B. licheniformis* pBE-S PL28-GH105 strains for both investigated time points (Additional file 1: Fig. S12b). As illustrated in Additional file 1: Fig. S12a, the measured PL28 activities in *B. licheniformis* pBE-S PL28-GH105 were very low after 24 h and even in a negative range after 48 h of expression. However, this represents a strong hint for co-expression of both enzymes: the unsaturated uronic acid formed by the PL28 led to an increased absorption ( $A_{235\text{nm}}$ ), which was then reversed by the GH105 that cleaved this moiety. Corresponding C-PAGE analysis for PL28 and GH105 showed activities in all analyzed strains as shown in Additional file 1: Fig. S13. Taken together, the data of our protein expression experiments under simulated fed-batch conditions in EnpressoB medium clearly demonstrated that both marine enzymes were actively co-expressed.

In a final experiment, we thus wished to demonstrate, that *B. licheniformis*, equipped with the pBE-S PL28-GH105 co-expression vector, is able to grow on ulvan as the sole carbon source. Therefore, the same four expression strains were grown for 7 days in: (i) M9 mineral medium without carbon source, serving as the negative control; (ii) M9 mineral medium with 0.4% D-glucose, serving as the positive control; and (iii) with 1% ulvan as the sole carbon source (Fig. 6). While the single PL28 and GH105 strains lack the ability to grow on the ulvan, the co-expression strain shows an increased growth over this period of time. A C-PAGE of the culture's supernatant showed ulvan hydrolysis (Additional file 1: Fig. S14) in the PL28 and co-expression cultivation. This demonstrated PL28 and GH105 expression and activity in the M9-mineral medium supplemented with ulvan. Additionally, this experiment confirmed that the *B. licheniformis* strain needs PL28 and GH105 to grow on ulvan biomass.

## Conclusion

This study reveals the promising metabolic potential of the bacterial cell factory *B. licheniformis* to utilize the abundant and renewable marine algal polysaccharide ulvan. We demonstrated that the native *B. licheniformis* DSM13 strain can grow on ulvan-derived oligo- and monosaccharides obtained by enzymatic pre-hydrolysis. Our proteogenomic analyses indicated that *B. licheniformis* DSM13 lacks the initial ulvan degradation enzymes, but that the pre-digestion of this marine

polysaccharide with two particular enzymes suffices to generate a suitable carbon source for this bacterium. We demonstrate that a metabolically engineered *B. licheniformis* strain, equipped with two marine heterologously expressed marine enzymes for the initial breakdown of the algal polysaccharide ulvan, is able to grow on ulvan as the sole carbon and energy source. Thus, this study pinpoints a suitable metabolic engineering strategy for future strain development aiming for a cell factory for the conversion of the abundant marine polysaccharide ulvan as alternative feedstock in large-scale bioprocesses.

## Methods

### Genes and enzyme expression

We used the already available pET28a(+) based expression constructs, coding for the *Formosa agariphila* KMM3901<sup>T</sup> (collection number DSM15362 at DSMZ, Braunschweig, Germany) specific ulvan enzyme cascade [14]. Enzyme overproduction in *E. coli* was performed as described previously [14]. After cell lysis the soluble fraction was filtered (0.45  $\mu\text{m}$ ) and the resulting crude extract was aliquoted and shock frozen. The enzyme expression was confirmed via SDS-PAGE (Additional file 1: Fig. S2).

### Extraction of ulvan

Dried *Ulva* biomass from the Atlantic coast in Spain was purchased as organic sea lettuce (Kulau, Berlin, Germany). Ulvan was extracted as described before, but distilled water was used as extraction solvent [14].

### Enzyme assays

The thiobarbituric acid assay [51] adapted for reduced volumes detected 5-dehydro-4-deoxy-D-glucuronate in the culture supernatant. The protease/peptidase activity in the culture supernatant was determined via the AAPF-assay, through the release of *p*-nitroanilin (410 nm,  $E^M=9800$ ) from the substrate *N*-succinyl-Ala-Ala-Pro-Phe-*para*-nitroanilide (succinyl-AAPF-*p*-Nitroanilide). The enzyme activity was calculated from the amount of *p*-nitroanilin released per time [33].

### Strains

Ten microorganisms were selected for growth screening on ulvan extracts or hydrolysate: *Escherichia coli* Top10, *E. coli* BL21(DE3), *Bacillus subtilis* B1, *Saccharomyces cerevisiae* GRF18, *Vibrio natriegens* ATCC 14048, *Pseudomonas putida* DSMZ 50198, *Pichia pastoris* X33, *Bacillus licheniformis* DSM13, *Cupriavidus necator* H16 and *Cutaneotrichosporan curvatus* DSM 101032 (Additional file 1: Table S2). All strains were maintained as glycerol stocks, stored at  $-80^\circ\text{C}$ . The Bacilli strains *Bacillus subtilis* JK138, *Bacillus licheniformis* MW3 and *Bacillus licheniformis* SH006 were used for all

expression experiments in this study. *E. coli* DH10B (Invitrogen, Darmstadt, Germany) [F-endA1 recA1 galE15 galK16 nupG rpsL  $\Delta$ lacX74  $\Phi$ 80lacZ $\Delta$ M15 araD139  $\Delta$ (ara,leu)7697 mcrA  $\Delta$ (mrr-hsdRMS-mcrBC)  $\lambda$ -] was used as the host strain for all subcloning procedures. *Bacillus licheniformis* DSM13 mutant SH006 was constructed with a homologous recombination method using a pE194-derived shuttle vector pE194SV analogous to the pMAD system [52]. pE194SV consist of the temperature-sensitive ori and erythromycin resistance marker gene from pE194ts [53] cloned into the *Sma*I site of pUC18, in which the native *Bsa*I site was removed. Moreover, pE194SV carries a type-II-assembly mRFP cassette from pBSd141R [54]; GenBank accession number: KY995200) integrated into the *Bam*HI site of pUC18. The pE194SV based gene deletion procedure was conducted according to Nahrstedt et al. 2005, using 45 °C instead of 42 °C as non-permissive temperature [55].

For the deletion of the restriction endonuclease (*hsdR1*) within the restriction modification operon 1 and the adjacent *mcrA* gene, 5'- and 3'-homologous flanking regions were PCR amplified from DSM13 genomic DNA. The 5'-flanking region was amplified using primers P1-hsdR1 and P2-hsdR1 and the 3'-flanking region was amplified with primers P3-hsdR1 and P4-hsdR1. Primers P1-hsdR1 and P4-hsdR1 introduced *Bsa*I cut sites and unique overhangs for subsequent cloning. Both fragments were ligated by SOE-PCR [56] and cloned via *Bsa*I into pE194SV, resulting in plasmid pDhsdR1.

For the deletion of the restriction endonuclease (*hsdR2*) within the restriction modification operon 2, 5'- and 3'-homologous flanking regions were PCR amplified from DSM13 genomic DNA. The 5'-flanking region was amplified using primers P1-hsdR2 and P2-hsdR2 and the 3' flanking region was amplified with primers P3-hsdR2 and P4-hsdR2. Primers P1-hsdR2 and P4-hsdR2 introduced *Bsm*BI cut sites and unique overhangs for subsequent cloning. Both fragments were then ligated by SOE-PCR, digested with *Bsm*BI and cloned into the *Bsa*I digested pE194SV, resulting in plasmid pDhsdR2.

For the deletion of the poly- $\gamma$ -glutamic acid (*pga*) synthesis operon (*pgsBCAE*) and the *apr* gene encoding an extracellular alkaline serine protease individual cassettes comprising the 5'- and 3'-homologous flanking regions, flanked by *Bsa*I cut sites and unique overhangs were ordered as synthetic fragments. Each cassette was cloned separately via *Bsa*I into pE194SV, resulting in plasmids pDpga ( $\Delta$ *pga*) and pDapr ( $\Delta$ *apr*).

#### Preparation of a sugar rich hydrolysate

2 mg/mL ulvan in phosphate buffer (25 mM, 50 mM NaCl, pH 7.5) was incubated with 0.5% (v/v) of the respective *F. agariphila* crude enzyme (Additional file 1:

Table S1) overnight. The ulvan hydrolysates were centrifuged for 5 min at 4500 $\times$ g and were then filtered (0.2  $\mu$ m).

#### Monosaccharide composition analysis of the cultivation media

The ulvan, UHA and UHB raw media (Additional file 1: Fig. S1) were chemically hydrolysed (1 M HCl for 24 h at 100 °C). Afterwards, the samples were filtered (0.2  $\mu$ m Spin-X filter) prior to HPAEC-PAD analyses using a Dionex CarboPac PA10 column (Thermo Fisher Scientific, Waltham, Massachusetts, USA) and monosaccharide mixtures as standards for column calibration [57].

#### Cultivation of different strains with various carbon sources

The M9-mineral medium with 0.2% (w/v) yeast extract was supplemented with various sugar sources (Additional file 1: Tables S3, S4). Selected monosaccharides were D-glucose, L-rhamnose, D-xylose and D-glucuronic acid, each at a final concentration of 0.4%(w/v). A final concentration of 1%(w/v) was used in case of ulvan and ulvan hydrolysates. M9 and M9 supplemented with enzyme mixtures from the preparation of the sugar rich hydrolysates were used as controls. Precultures were prepared in respective rich media for the corresponding microorganisms (LB media, YPD for yeasts) and overnight (for yeasts 1.5 days). This preculture was used to inoculate a second preculture in M9-mineral media with 0.2%(g/L) glucose as carbon source (1:100). The main culture was inoculated (1:100) with the M9-mineral media preculture and cultured up to 4 days at 30 °C and 180 rpm. The optical density was measured at 600 nm.

#### Proteome analyses

For proteome analyses, late logarithmic phase cells from triplicates of ulvan, UHA, UHB, L-rhamnose and D-glucose cultures were separated from supernatants by centrifugation (20 min, 4000 $\times$ g, 4 °C). Intracellular soluble proteins were extracted by suspending cell pellets in lysis buffer (4% SDS, 1% NaDCA, 50 mM TEAB) adapted to Hinzke et al. [58]. Samples were incubated for 5 min at 600 rpm and 95 °C, then cooled on ice shortly and sonicated for 5 min. Cell debris was removed from the protein extract (intracellular soluble proteome) by centrifugation (10 min, 14,000 $\times$ g, room temperature). Protein concentration was determined using the Pierce™ BCA Protein Assay Kit (Thermo Fisher Scientific, Waltham, Massachusetts, US). Secreted and detached proteins (extracellular proteome) were extracted from cultivation supernatants using StrataClean beads (Agilent, Santa Clara, California, US) [59]. In brief, 20  $\mu$ L of bead solution, extracting approximately 20 – 30  $\mu$ g of protein, was removed. Beads were primed in 180  $\mu$ L 37% hydrochloric acid

(100 °C, 6 h) and then washed in TE buffer (50 mM Tris, 10 mM EDTA, pH 8.0) twice (5 min, 3500×g, room temperature). 0.2 µm-filtered supernatants were incubated with prepared beads overnight in a 360° rotating shaker at 8 rpm and 4 °C. The protein-loaded beads were pelleted by centrifugation (45 min, 10,000×g, 4 °C) and washed in TE buffer. In a last step, they were resuspended in 1 mL of ultrapure water and dried by vacuum centrifugation. 25 µg of protein from intracellular soluble protein extracts as well as protein-loaded beads were separated by 1D SDS PAGE (12% SDS gels) at 120 V. Proteins were in-gel digested using trypsin [59]. Peptides were separated by reversed phase chromatography and analyzed in an LTQ-Orbitrap Classic mass spectrometer equipped with a nanoelectrospray ion source [60]. MS/MS spectra were searched against a target decoy database using MaxQuant v. 1.6.10.43 [61]. The database covered all protein sequences predicted from the *B. licheniformis* DSM13 genome, selected *F. agariphila* KM3901<sup>T</sup> ulvan PUL-encoded enzymes (Additional file 1: Table S1) and common laboratory contaminants as well as corresponding reversed sequences (decoys). The MaxQuant computed iBAQ values (intensity-based absolute quantification [62]) were used to manually calculate %riBAQ values, giving the relative protein abundance in % per sample. Quantified *F. agariphila* KM3901<sup>T</sup> proteins were excluded from %riBAQ calculations. Proteins quantified in at least two out of the three replicates were considered for further calculations and for statistical tests. Since the total number of quantified proteins varied considerably between substrates (e.g., 933 proteins in ulvan extracellular samples compared to 247 proteins in the UHB samples), %riBAQ mean values were ranked according to their abundance (e.g., rank 1 for most abundant protein in the sample) to increase comparability between conditions. In addition, the total number of quantified proteins per sample was considered for the color code in graphs. Welch's two-sided t-test (permutation-based FDR 0.05) identified statistical significance to protein abundance differences between samples within the intracellular soluble proteome samples and within the extracellular samples using Perseus v. 1.6.0.7 [63]. Only samples with a similar number of quantified proteins were compared. CAZymes were identified using dbCAN2 [37]. The enrichment of protein fractions is not exclusive and overlaps may occur, e.g., due to cell lysis or intracellular production of extracellular enzymes. Therefore, protein localization was also predicted using PSORTb v3.0.2 [38]. Proteomic data were deposited to the ProteomeXchange Consortium via the PRIDE partner repository [64] with the dataset

identifier PXD033411. CAZymes were identified using dbCAN2 [37].

#### Development of a *Bacillus* host-vector system

The nucleotide sequence of both genes from *F. agariphila* KMM3901<sup>T</sup> P30\_PL28 and P33\_GH105 were ordered by GenScript Biotech (Leiden, Netherlands). Both synthetic genes were codon-optimized for expression in *B. licheniformis* using the GenSmart™ Codon Optimization tool (GenScript). The algorithm utilizes a matrix for the most frequently occurring codons in *B. licheniformis*. The constructs were assembled from synthetic oligonucleotides and provided in the backbone of the pUC19 vector. Amplification of the PL28 nucleotide sequence with *csn* and 00338 signal peptides (SP) was carried out in two discrete polymerase chain reactions, first with oligonucleotides MaZu8 and MaZu9 and second with MaZu7 and MaZu9 for the *csn*-SP whereas fusion of the 00338-SP was carried out with MaZu13/MaZu9 and MaZu12/MaZu9. The nucleotide sequence of GH105 with *csn*-SP was amplified with oligonucleotides MaZu10 and MaZu11 in a first PCR and, using the purified PCR product as the template, with MaZu7 and MaZu11 in a second PCR. Fusion of the 00338-SP to the GH105 sequence occurred with oligonucleotides MaZu14/MaZu11 and MaZu12/MaZu11. The PCR products were digested with *NdeI* and *KpnI* and subsequently gel-purified. After ligation into the *NdeI* and *KpnI* sites of pMSE3 *P<sub>appr</sub>* *E. coli* DH10B was transformed with the recombinant plasmids, yielding pMSE3 *P<sub>appr</sub>* *csn*-UL, pMSE3 *P<sub>appr</sub>* 00338-UL, pMSE3 *P<sub>appr</sub>* *csn*-GH and pMSE3 *P<sub>appr</sub>* 00338-GH. Sequence identity of all expression vectors was verified by sequencing (Eurofins Genomics, Ebersberg, Germany). All four expression vectors were then transferred into both *Bacillus* expression hosts, *B. subtilis* JK138 and *B. licheniformis* MW3 [50] by electroporation.

Protein expression experiments were performed under simulated fed-batch conditions in EnpressoB-Medium as recommended by the manufacturer (Biosilta) at 30 °C and 250 rpm. Samples for protein analysis (SDS-PAGE, Activity screening and carbohydrate electrophoresis [15]) were taken after 24 h and 48 h of cultivation.

#### Development of a co-expression host *B. licheniformis* SH006

Construction of the appropriate expression vector was achieved by Gibson assembly. To this purpose, PCRs of the PL28 and GH105 expression cassettes were carried out with oligonucleotides MaZu37/MaZu29 (PL28) and MaZu28/MaZu35 (GH105) using pMSE3 *P<sub>apprE</sub>* *csn*-UL and pMSE3 *P<sub>apprE</sub>* 00338-GH as the templates. The vector backbone of the medium copy-vector pBE-S was amplified with oligonucleotides MaZu38/MaZu36. The PCR

products were gel-purified and, in case of the pBE-S vector backbone, digested with *DpnI* in order to remove remaining circular plasmid DNA. All purified DNA fragments were then assembled in a vector:insert ratio of 1:2 and 3  $\mu\text{L}$  of the reaction were used for transformation of *E. coli* DH10B yielding pBE-S P<sub>aprE</sub> *csn*-UL - P<sub>aprE</sub> 00338-GH (pBE-S PL28-GH105). Sequence identity of the PL28-GH105 co-expression vector was verified and the plasmid was subsequently integrated into *B. licheniformis* SH006 by electroporation. Protein expression experiments of the newly constructed *B. licheniformis* SH006 PL28-GH105 co-expression strain were performed as before for the single constructs. Additionally, in order to demonstrate the ability of the newly constructed *B. licheniformis* SH006 PL28-GH105 strain to grow on ulvan, cultivations in M9-mineral media supplemented with either D-glucose or ulvan as the sole carbon source and also without any carbon source were carried out as described before.

#### Activity measurement of ulvan lyase (PL28) and glycoside hydrolase (GH105)

The ulvan lyase activity was detected as described before [15] using the intra- or extracellular extract of *Bacillus* sp. cultivations instead of purified protein. For the detection of the glycoside hydrolase (GH105) activity the reversed ulvan lyase assay was used, while ulvan was PL28-pre-hydrolysed and heat inactivated after 16 h. The breakdown products resulting from the ulvan lyase assays were additionally analyzed via C-PAGE, the MBTH- assay and the thiobarbituric acid assay as described before [15].

#### Construction of the plasmid libraries for PL28 and GH105 activity screening

In order to obtain both plasmid libraries with 173 different types of signal peptides DNA sequences in the required size of at least 2000 *E. coli* clones, the “*B. subtilis* Secretory Protein Expression System” (Takara/Clontech) in combination with the “In Fusion HD Cloning Plus Kit” (Takara/Clontech) was used according to the manufacturer’s instructions. To this end, the nucleotide sequences for PL28 and GH105 were amplified from pMSE3-PL28 and pMSE3-GH105 using oligonucleotides MaZu19/MaZu20 (for PL28) and MaZu21/MaZu22 (for GH105). After restriction with *NdeI* and *XbaI*, the purified PCR products and the pBE-S vector were ligated and *E. coli* DH10B was transformed with the recombinant plasmids pBE-S-PL28 and pBE-S-GH105. After validation of sequence identity for PL28 and GH105, all different signal peptide sequences included in the provided SP library were integrated into the vector backbones of pBE-S-PL28 and pBE-S-GH105 following the manufacturer’s instructions. In brief, the *EagI* and *MluI* digested vector was ligated with the 173 SP-containing DNA mixture using

the “In Fusion Cloning” technology. Chemically competent *E. coli* Stellar cells (included in the kit) were transformed with 2  $\mu\text{L}$  of the “In Fusion” reaction and selected on LB agar plates with ampicillin. All colony forming units (cfu) were rinsed from the plate to isolate the SP-plasmid library, which was subsequently integrated into the *Bacillus* expression hosts by electroporation.

#### Abbreviations

CAZyme: Carbohydrate active enzyme; GH: Glycoside hydrolase; UL: Ulvan lyase; U: Ulvan; UH: Ulvan hydrolysate; UHA: Ulvan hydrolysate resulting from the digestion of ulvan with the enzymes P30\_PL28 and P33\_GH105; UHB: Ulvan hydrolysate resulting from the digestion of ulvan with the whole ulvan specific enzyme cascade according to Reisky et al. [14].

#### Supplementary Information

The online version contains supplementary material available at <https://doi.org/10.1186/s12934-022-01931-0>.

**Additional file 1: Table S1.** Proteins and accession numbers. **Table S2.** Bacterial strains. **Table S3.** M9-mineral media D-glucose composition. **Table S4.** M9-mineral media additives. **Table S5.** Primer list. **Figure S1.** Sugar composition of the cultivation media. **Figure S2.** SDS-PAGE of *F. agariphila* KMM3901<sup>T</sup> enzymes expressed recombinantly in *E. coli*. **Figure S3.** Consumption of 5-dehydro-4-deoxy-D-glucuronate from *B. licheniformis* DSM13 during cultivation. **Figure S4.** Growth of *B. licheniformis* DSM13 on different ulvan hydrolysates. **Figure S5.** *B. licheniformis* DSM13 CAZyme repertoire and their expression. **Figure S6.** Alignment *B. licheniformis* DSM13 sulfatases with lipoteichoic acid synthases. **Figure S7.** Comparison of different *Bacillus* sp. to digest ulvan hydrolysate and ulvan derived monosaccharides. **Figure S8.** Growth curves of PL28 and GH105 *Bacillus* sp. expression strains. **Figure S9.** Activity assays from *Bacillus* sp. PL28 and GH105 expression strains. **Figure S10.** C-PAGE results from *Bacillus* sp. PL28 and GH105 expression strains. **Figure S11.** Growth of the different *B. licheniformis* expression strains. **Figure S12.** Activity assay results from *B. licheniformis* SH006, PL28 and GH105 single- and co-expression strain. **Figure S13.** C-PAGE results from *B. licheniformis* SH006 PL28, GH105 and co-expression strains. **Figure S14.** C-PAGE from the cultivation supernatant of *B. licheniformis* strains in M9-mineral media.

**Additional file 2: Table S6.** Summary of the proteomic results.

**Additional file 3: Table S7.** Results of statistical analyses.

#### Acknowledgements

We thank Alek Bolte for the help in the monosaccharide composition analysis and Sebastian Grund for the mass spectroscopy measurements. In addition, we thank our Bachelor student Maik Behrens for her supporting work.

#### Author contributions

UTB, LR and TS designed the study, supervised its execution and co-wrote the manuscript. TD wrote the main manuscript with the support of MKZ and NW. TD performed the initial screening of organism and growth and activity assays, with TE and CS. The proteome analysis was performed by TE and MKZ. DB coordinated MS measurements. The computational analysis was performed by MKZ, AD and SB. JK performed the sugar monosaccharide composition analysis in the lab of JHH. SB expressed and purified the putative sulfatases and performed the activity assays. NW developed the *Bacillus* host-vector system and the strain *Bacillus* design with MH. All authors read and approved the final manuscript.

#### Funding

Open Access funding enabled and organized by Projekt DEAL. This study was supported by the German Federal Ministry of Education and Research (BMBF) in the frame of the Plant<sup>3</sup> MarZucker project (03WIR2205A/C) and the German Research Foundation (DFG) for the Research Unit FOR 2406 “Proteogenomics



of Marine Polysaccharide Utilization" (POMPU) by Grants to U.T.B. (BO 1862/17-2), J.-H.H. (HE 7217/2-2), and T.S. (SCHW 595/10-2).

#### Availability of data and materials

Proteomic data were deposited to the ProteomeXchange Consortium via the PRIDE partner repository [64] with the dataset identifier PXD033411.

#### Declarations

##### Consent for publication

All authors have read and approved the final version of the manuscript.

##### Competing interests

The authors declare no competing interests.

##### Author details

<sup>1</sup>Department of Biotechnology & Enzyme Catalysis, Institute of Biochemistry, University of Greifswald, 17487 Greifswald, Germany. <sup>2</sup>Department of Pharmaceutical Biotechnology, Institute of Pharmacy, University of Greifswald, 17487 Greifswald, Germany. <sup>3</sup>Institute of Marine Biotechnology e.V., 17489 Greifswald, Germany. <sup>4</sup>Max Planck-Institute for Marine Microbiology, 28359 Bremen, Germany. <sup>5</sup>Center for Marine Environmental Sciences (MARUM), University of Bremen, 28359 Bremen, Germany. <sup>6</sup>Department of Microbial Proteomics, Institute for Microbiology, University of Greifswald, 17487 Greifswald, Germany.

Received: 28 June 2022 Accepted: 26 September 2022

Published online: 10 October 2022

#### References

- Wang M, Hu C, Barnes BB, Mitchum G, Lapointe B, Montoya JP. The great Atlantic Sargassum belt. *Science*. 2019;365:83–7.
- Smětacek V, Zingone A. Green and golden seaweed tides on the rise. *Nature*. 2013;504:84–8.
- Field CB. Primary production of the biosphere: integrating terrestrial and oceanic components. *Science*. 1998;281:237–40.
- Hehemann J-H, Boraston AB, Czjzek M. A sweet new wave: structures and mechanisms of enzymes that digest polysaccharides from marine algae. *Curr Opin Struct Biol*. 2014;28:77–86.
- Filote C, Santos SCR, Popa VI, Botelho CMS, Volf I. Biorefinery of marine macroalgae into high-tech bioproducts: a review. *Environ Chem Lett*. 2020;19:969–1000.
- Laurens LML, Lane M, Nelson RS. Sustainable seaweed biotechnology solutions for carbon capture, composition, and deconstruction. *Trends Biotechnol*. 2020;38:1232–44.
- Cesário MT, da Fonseca MMR, Marques MM, de Almeida MCMD. Marine algal carbohydrates as carbon sources for the production of biochemicals and biomaterials. *Biotechnol Adv*. 2018;36:798–817.
- Kim HT, Lee S, Kim KH, Choi I-G. The complete enzymatic saccharification of agarose and its application to simultaneous saccharification and fermentation of agarose for ethanol production. *Bioresour Technol*. 2012;107:301–6.
- Murata M, Nakazoe J. Production and use of marine algae in Japan. *Jpn Agric Res Q JARQ*. 2001;35:281–90.
- Lahaye M, Gomez-Pinchetti J-L, del Rio MJ, Garcia-Reina G. Natural decoloration, composition and increase in dietary fibre content of an edible marine algae, *Ulva rigida* (Chlorophyta), grown under different nitrogen conditions. *J Sci Food Agric*. 1995;68:99–104.
- Kloareg B, Quatrano RS. Structure of the cell walls of marine algae and ecophysiological functions of the matrix polysaccharides. *Oceanogr Mar Biol Annu Rev*. 1988;26:259–315.
- Bäumgen M, Dutschei T, Bornscheuer UT. Marine polysaccharides: occurrence, enzymatic degradation and utilization. *ChemBioChem*. 2021;22:2247–56.
- Cantarel BL, Coutinho PM, Rancurel C, Bernard T, Lombard V, Henrissat B. The carbohydrate-active enzymes database (CAZy): an expert resource for glycogenomics. *Nucleic Acids Res*. 2009;37:D233–8.
- Reisky L, Préchoux A, Zühlke M-K, Bäumgen M, Robb CS, Gerlach N, et al. A marine bacterial enzymatic cascade degrades the algal polysaccharide ulvan. *Nat Chem Biol*. 2019;15:803–12.
- Bäumgen M, Dutschei T, Bartosik D, Suster C, Reisky L, Gerlach N, et al. A new carbohydrate-active oligosaccharide dehydratase is involved in the degradation of ulvan. *J Biol Chem*. 2021. <https://doi.org/10.1016/j.jbc.2021.101210>.
- Cardoso SM, Carvalho LG, Silva PJ, Rodrigues MS, Pereira ORP, Pereira L. Bioproducts from seaweeds: a review with special focus on the Iberian Peninsula. *Curr Org Chem*. 2014. <https://doi.org/10.2174/138527281807140515154116>
- Lahaye M, Robic A. Structure and functional properties of ulvan, a polysaccharide from green seaweeds. *Biomacromol*. 2007;8:1765–74.
- Reisky L, Stanetty C, Mihovilovic MD, Schweder T, Hehemann J-H, Bornscheuer UT. Biochemical characterization of an ulvan lyase from the marine flavobacterium *Formosa agariphila* KMM 3901T. *Appl Microbiol Biotechnol*. 2018;102:6987–96.
- Jose ML, Rosario C, Jon AA, Jesus L. Immunomodulating activities of acidic sulphated polysaccharides obtained from the seaweed *Ulva rigida*. *Int Immunopharmacol*. 2007;7:879–88.
- Wargacki AJ, Leonard E, Win MN, Regitsky DD, Santos CNS, Kim PB, et al. An engineered microbial platform for direct biofuel production from brown macroalgae. *Science*. 2012;335:308–13.
- Stephanopoulos G. Challenges in engineering microbes for biofuels production. *Science*. 2007;315:801–4.
- Lü C, Ge Y, Cao M, Guo X, Liu P, Gao C, et al. Metabolic engineering of *Bacillus licheniformis* for production of acetoin. *Front Bioeng Biotechnol*. 2020;8:125.
- Wells JA, Estell DA. Subtilisin—an enzyme designed to be engineered. *Trends Biochem Sci*. 1988;13:291–7.
- Huebner U, Bock U, Schuegerl K. Production of alkaline serine protease subtilisin Carlsberg by *Bacillus licheniformis* on complex medium in a stirred tank reactor. *Appl Microbiol Biotechnol*. 1993;40:182–8.
- Song CW, Chelladurai R, Park JM, Song H. Engineering a newly isolated *Bacillus licheniformis* strain for the production of (2R,3R)-butanediol. *J Ind Microbiol Biotechnol*. 2020;47:97–108.
- Nilegaonkar SS, Bhosale SB, Dandage CN, Kapadi AH. Potential of *Bacillus licheniformis* for the production of 2,3-butanediol. *J Ferment Bioeng*. 1996;82:408–10.
- Sakai K, Yamanami T. Thermotolerant *Bacillus licheniformis* TY7 produces optically active l-lactic acid from kitchen refuse under open condition. *J Biosci Bioeng*. 2006;102:132–4.
- Pervez S, Shahid F, Aman A, Qader SAU. Algal biomass: a sustainable, economical and renewable approach for microbial production of pectinolytic enzymes using submerged and solid state fermentation techniques. *Biocatal Biotransformation*. 2017;35:442–9.
- Caspi R, Billington R, Fulcher CA, Keseler IM, Kothari A, Krummenacker M, et al. The MetaCyc database of metabolic pathways and enzymes. *Nucleic Acids Res*. 2018;46:D633–9.
- Wang L, Zhao B, Liu B, Yu B, Ma C, Su F, et al. Efficient production of l-lactic acid from corn cob molasses, a waste by-product in xylitol production, by a newly isolated xylose utilizing *Bacillus* sp. strain. *Bioresour Technol*. 2010;101:7908–15.
- Ramos JL, Duque E, Huertas MJ, Haïdour A. Isolation and expansion of the catabolic potential of a *Pseudomonas putida* strain able to grow in the presence of high concentrations of aromatic hydrocarbons. *J Bacteriol*. 1995;177:3911–6.
- Fonseca Á, Boekhout T, Fell JW. Chapter 138—Cryptococcus Vuillemin (1901). In: Kurtzman CP, Fell JW, Boekhout T, editors. *Yeasts*. 5th ed. London: Elsevier; 2011. p. 1661–737.
- Kannan Y, Koga Y, Inoue Y, Haruki M, Takagi M, Imanaka T, et al. Active subtilisin-like protease from a hyperthermophilic archaeon in a form with a putative prosequence. *Appl Environ Microbiol*. 2001;67:2445–52.
- Voigt B, Schroeter R, Schweder T, Jürgen B, Albrecht D, van Dijk JM, et al. A proteomic view of cell physiology of the industrial workhorse *Bacillus licheniformis*. *J Biotechnol*. 2014;191:139–49.
- Veith B, Herzberg C, Steckel S, Feesche J, Maurer KH, Ehrenreich P, et al. The complete genome sequence of *Bacillus licheniformis* DSM13, an organism with great industrial potential. *J Mol Microbiol Biotechnol*. 2004;7:204–11.

36. Zhang H, Yohe T, Huang L, Entwistle S, Wu P, Yang Z, et al. dbCAN2: a meta server for automated carbohydrate-active enzyme annotation. *Nucleic Acids Res.* 2018;46:W95–101.
37. Yin Y, Mao X, Yang J, Chen X, Mao F, Xu Y. dbCAN: a web resource for automated carbohydrate-active enzyme annotation. *Nucleic Acids Res.* 2012;40:W445–51.
38. Yu NY, Wagner JR, Laird MR, Melli G, Rey S, Lo R, et al. PSORTb 3.0: improved protein subcellular localization prediction with refined localization subcategories and predictive capabilities for all prokaryotes. *Bioinformatics.* 2010;26:1608–15.
39. Silva IR, Jers C, Meyer AS, Mikkelsen JD. Rhamnogalacturonan I modifying enzymes: an update. *New Biotechnol.* 2016;33:41–54.
40. Voigt B, Antelmann H, Albrecht D, Ehrenreich A, Maurer K-H, Evers S, et al. Cell physiology and protein secretion of *Bacillus licheniformis* compared to *Bacillus subtilis*. *Microb Physiol.* 2009;16:53–68.
41. Inácio JM, de Sá-Nogueira I. Characterization of *abn2* (*xyiA*), encoding a *Bacillus subtilis* GH43 arabinanase, *Abn2*, and its role in arabino-polysaccharide degradation. *J Bacteriol.* 2008;190:4272–80.
42. Koch H, Freese HM, Hahnke RL, Simon M, Wietz M. Adaptations of *Alteromonas* sp. 76-1 to polysaccharide degradation: a CAZyme plasmid for ulvan degradation and two alginateolytic systems. *Front Microbiol.* 2019;10:504.
43. Foran E, Buravenkov V, Kopel M, Mizrahi N, Shoshani S, Helbert W, et al. Functional characterization of a novel “ulvan utilization loci” found in *Alteromonas* sp. LOR genome. *Algal Res.* 2017;25:39–46.
44. Salinas A, French CE. The enzymatic ulvan depolymerisation system from the alga-associated marine flavobacterium *Formosa agariphila*. *Algal Res.* 2017;27:335–44.
45. Matsuoaka S, Hashimoto M, Kamiya Y, Miyazawa T, Ishikawa K, Hara H, et al. The *Bacillus subtilis* essential gene *dgkB* is dispensable in mutants with defective lipoteichoic acid synthesis. *Genes Genet Syst.* 2011;86:365–76.
46. Andrews LD, Zalatan JG, Herschlag D. Probing the origins of catalytic discrimination between phosphate and sulfate monoester hydrolysis: comparative analysis of alkaline phosphatase and protein tyrosine phosphatases. *Biochemistry.* 2014;53:6811–9.
47. Gärtner D, Geissendörfer M, Hillen W. Expression of the *Bacillus subtilis* *xyl* operon is repressed at the level of transcription and is induced by xylose. *J Bacteriol.* 1988;170:3102–9.
48. Sun J-D, Tang C, Zhou J, Wei P, Wang Y-J, An W, et al. Production of poly- $\gamma$ -glutamic acid ( $\gamma$ -PGA) from xylose-glucose mixtures by *Bacillus amyloliquefaciens* C1. *3 Biotech.* 2021;11:100.
49. Sharma A, Satyanarayana T. Comparative genomics of *Bacillus* species and its relevance in industrial microbiology. *Genom Insights.* 2013;6:25–36.
50. Waschkau B, Waldeck J, Wieland S, Eichstädt R, Meinhardt F. Generation of readily transformable *Bacillus licheniformis* mutants. *Appl Microbiol Biotechnol.* 2008;78:181–8.
51. Itoh T, Ochiai A, Mikami B, Hashimoto W, Murata K. A novel glycoside hydrolase family 105: the structure of family 105 unsaturated rhamnogalacturonyl hydrolase complexed with a disaccharide in comparison with family 88 enzyme complexed with the disaccharide. *J Mol Biol.* 2006;360:573–85.
52. Arnaud M, Chastanet A, Débarbouillé M. New vector for efficient allelic replacement in naturally nontransformable, low-GC-content, gram-positive bacteria. *Appl Environ Microbiol.* 2004;70:6887–91.
53. Villafane R, Bechhofer DH, Narayanan CS, Dubnau D. Replication control genes of plasmid pE194. *J Bacteriol.* 1987;169:4822–9.
54. Radeck J, Meyer D, Lautenschläger N, Mascher T. *Bacillus SEVA* siblings: a Golden Gate-based toolbox to create personalized integrative vectors for *Bacillus subtilis*. *Sci Rep.* 2017;7:14134.
55. Nahrstedt H, Waldeck J, Gröne M, Eichstädt R, Feesche J, Meinhardt F. Strain development in *Bacillus licheniformis*: construction of biologically contained mutants deficient in sporulation and DNA repair. *J Biotechnol.* 2005;119:245–54.
56. Heckman KL, Pease LR. Gene splicing and mutagenesis by PCR-driven overlap extension. *Nat Protoc.* 2007;2:924–32.
57. Engel A, Händel N. A novel protocol for determining the concentration and composition of sugars in particulate and in high molecular weight dissolved organic matter (HMW-DOM) in seawater. *Mar Chem.* 2011;127:180–91.
58. Hinzke T, Markert S. Efficient protein extraction for proteomics and metaproteomics (also suitable for low biomass samples). *Protoc Io.* 2017;10:6.
59. Bonn F, Bartel J, Büttner K, Hecker M, Otto A, Becher D. Picking vanished proteins from the void: how to collect and ship/share extremely dilute proteins in a reproducible and highly efficient manner. *Anal Chem.* 2014;86:7421–7.
60. Otto A, Bernhardt J, Meyer H, Schaffer M, Herbst F-A, Siebourg J, et al. Systems-wide temporal proteomic profiling in glucose-starved *Bacillus subtilis*. *Nat Commun.* 2010;1:137.
61. Cox J, Mann M. MaxQuant enables high peptide identification rates, individualized p.p.b-range mass accuracies and proteome-wide protein quantification. *Nat Biotechnol.* 2008;26:1367–72.
62. Schwanhäusser B, Busse D, Li N, Dittmar G, Schuchhardt J, Wolf J, et al. Global quantification of mammalian gene expression control. *Nature.* 2011;473:337–42.
63. Tyanova S, Temu T, Sinitcyn P, Carlson A, Hein MY, Geiger T, et al. The Perseus computational platform for comprehensive analysis of (prote)omics data. *Nat Methods.* 2016;13:731–40.
64. Vizcaino JA, Csordas A, del Toro N, Dienes JA, Griss J, Lavidas I, et al. 2016 update of the PRIDE database and its related tools. *Nucleic Acids Res.* 2016;44:D447–56.

## Publisher's Note

Springer Nature remains neutral with regard to jurisdictional claims in published maps and institutional affiliations.

Ready to submit your research? Choose BMC and benefit from:

- fast, convenient online submission
- thorough peer review by experienced researchers in your field
- rapid publication on acceptance
- support for research data, including large and complex data types
- gold Open Access which fosters wider collaboration and increased citations
- maximum visibility for your research: over 100M website views per year

At BMC, research is always in progress.

Learn more [biomedcentral.com/submissions](https://biomedcentral.com/submissions)



## Additional file 1\_ supplementary table and figures

### Metabolic engineering enables *Bacillus licheniformis* to grow on the marine polysaccharide ulvan

Theresa Dutschei<sup>1</sup>, Marie-Katherin Zühlke<sup>2,3</sup>, Norma Welsch<sup>2,3</sup>, Tom Eisenack<sup>2</sup>, Maximilian Hilkmann<sup>2,3</sup>, Joris Krull<sup>3,4,5</sup>, Carlo Stühle<sup>1</sup>, Stefan Brott<sup>1</sup>, Alexandra Dürwald<sup>2</sup>, Lukas Reisky<sup>1</sup>, Jan-Hendrik Hehemann<sup>3,4,5</sup>, Dörte Becher<sup>6</sup>, Thomas Schweder<sup>2,3‡</sup> and Uwe T. Bornscheuer<sup>1,3‡</sup>

<sup>1</sup>Department of Biotechnology & Enzyme Catalysis, Institute of Biochemistry, University of Greifswald, 17487 Greifswald, Germany

<sup>2</sup>Department of Pharmaceutical Biotechnology, Institute of Pharmacy, University of Greifswald, 17487 Greifswald, Germany

<sup>3</sup>Institute of Marine Biotechnology e.V., 17489 Greifswald, Germany

<sup>4</sup>Max Planck-Institute for Marine Microbiology, 28359 Bremen, Germany

<sup>5</sup>University of Bremen, Center for Marine Environmental Sciences (MARUM), 28359 Bremen, Germany

<sup>6</sup>Department of Microbial Proteomics, Institute for Microbiology, University Greifswald, 17487 Greifswald, Germany

‡ Corresponding authors:

Thomas Schweder, [schweder@uni-greifswald.de](mailto:schweder@uni-greifswald.de)

Uwe T. Bornscheuer, [uwe.bornscheuer@uni-greifswald.de](mailto:uwe.bornscheuer@uni-greifswald.de)

## Additional tables

- Table S1: Proteins and accession numbers
- Table S2: Bacterial strains and plasmids
- Table S3: M9-mineral media D-glucose composition
- Table S4: M9-mineral media additives
- Table S5: Primer list
- The Supplementary Tables S6 and S7 are available as separate Excel files.

## Additional figures

- Figure S1: Sugar composition of the cultivation media
- Figure S2: SDS-PAGE of *F. agariphila* KMM3901<sup>T</sup> enzymes expressed recombinantly in *E. coli*
- Figure S3: Consumption of 5-dehydro-4-deoxy-D-glucuronate from *B. licheniformis* DSM13 during cultivation
- Figure S4: Growth of *B. licheniformis* DSM13 on different ulvan hydrolysates
- Figure S5: *B. licheniformis* DSM13 CAZyme repertoire and their expression
- Figure S6: Alignment *B. licheniformis* DSM13 sulfatases with lipoteichoic acid synthases
- Figure S7: Comparison of different *Bacillus* sp. to digest ulvan hydrolysate and ulvan derived monosaccharides
- Figure S8: Growth of the *Bacillus* sp. PL28 and GH105 expression strains
- Figure S9: Activity assays of *Bacillus* sp. PL28 and GH105 expression strains
- Figure S10: C-PAGE results from *Bacillus* sp. PL28 and GH105 expression strains.
- Figure S11: Growth of the different *B. licheniformis* expression strains.
- Figure S12: Activity assay results from *B. licheniformis* SH006, PL28 and GH105 single- and co-expression strain.
- Figure S13: C-PAGE results from *B. licheniformis* SH006 PL28, GH105 and co-expression strains.
- Figure S14: C-PAGE from the cultivation supernatant of *B. licheniformis* strains in M9-mineral media.

**Table S1:** List of *F. agariphila* proteins used to produce ulvan hydrolysates. (UHA) P30\_PL28 and P33\_GH105 and (UHB) all listed enzymes. All proteins were recombinantly expressed in *E. coli* as described previously [1].

Name	Locus tag	Uniprot ID	Functional annotation	size [kDa]
P1_GH88	*21900	T2KLZ3	Unsaturated glucuronylhydrolase (GH88)	44.1
P10_PLnc	*21990	T2KNA3	Ulvan lyase (PLnc)	92.6
P17_GH2	*22060	T2KN75	$\beta$ -Galactosidase (GH2)	112.9
P18_S1_7	*22070	T2KPK5	Arylsulfatase (S1_7)	53.1
P20_GH78	*22090	T2KNB2	$\alpha$ -L-rhamnosidase (GH78)	100.4
P24_GH3	*22130	T2KMH0	$\beta$ -Glucosidase (GH3)	79.3
P27_GH43	*22160	T2KN85	$\beta$ -Xylosidase (GH43)	67.3
P30_PL28	*22190	T2KNC2	Ulvan lyase (PL28)	44.1
P31_GH39	*22200	T2KM23	Glycoside hydrolase (GH39)	54.6
P33_GH105	*22220	T2KPL9	Glycoside hydrolase (GH105)	40.7
P36_S1_25	*22250	T2KM26	$\alpha$ -L-rhamnosidase/-sulfatase (GH78/S1_25)	134.3
	*=BN863			

**Table S2:** Bacterial strains and plasmids

Strain	Description or genotype	Reference or source
<i>Escherichia coli</i> TOP10	<i>F</i> - <i>mcrA</i> Δ( <i>mrr</i> - <i>hsdRMS</i> - <i>mrcB</i> ) φ80 <i>lacZ</i> Δ <i>M15</i> Δ <i>lacX74 nupG</i> <i>recA1 araD139</i> Δ( <i>ara-leu</i> )7697 <i>galK16 rpsL</i> (StR) <i>endA1 fhuA2</i> λ-	Originally purchased from Invitrogen by Thermo Fisher Scientific (Waltham, MS, USA)
<i>Escherichia coli</i> BL21(DE3)	B F <sup>-</sup> <i>ompT gal dcm lon</i> <i>hsdSB</i> (rB—mB-) λ(DE3 [ <i>lacI</i> <i>lacUV</i> -T7 gene 1 <i>ind1 sam7 nin5</i> ])	Originally purchased from New England Biolabs (Ipswich, MS, USA)
<i>Bacillus subtilis</i> B1	Wildtype	Department of Biotechnology & Enzyme Catalysis (University of Greifswald)
<i>Bacillus licheniformis</i> DSM13	Wildtype	Department of Pharmaceutical Biotechnology (University of Greifswald) originating from Veith et al [2]
<i>Staphylococcus carnosus</i> 80-285	Wildtype	Kindly provided by the Enzymicals AG (Greifswald, Germany)
<i>Staphylococcus carnosus</i> 20-282	Wildtype	Kindly provided by the Enzymicals AG (Greifswald, Germany)
<i>Saccharomyces cerevisiae</i> GRF18	Wildtype	Department of Biotechnology & Enzyme Catalysis (University of Greifswald)
<i>Vibrio natriegens</i> ATCC 14048	Wildtype	Originating from the ATCC (Manassas, V, USA)
<i>Pseudomonas putida</i> DSMZ 50198	Wildtype	Originating from the DSMZ (Braunschweig, German)
<i>Pichia pastoris</i> X33	Wildtype	Originally from Invitrogen by Thermo Fisher Scientific (Waltham, MS, USA)
<i>Cutaneotrichosporan curvatus</i> DSM 101032	Wildtype	Department of Computational Synthetic Biology (TU Darmstadt) as described by Hofmeyer <i>et al.</i> [3]
<i>Cupriavidus necator</i> H16	Wildtype	Department of Microbial proteomics (University of Greifswald) as described by Pohlmann <i>et al.</i> [4]
<i>Bacillus licheniformis</i> MW3	Δ <i>hsdR1</i> , Δ <i>hsdR2</i>	Waschkau <i>et al.</i> 2008 [5]
<i>Bacillus subtilis</i> JK138	<i>sfp+</i> , Δ <i>sacA::SpecR</i> , Δ <i>lytC::lox72</i> , Δ <i>bpr-spo::lox72</i> , Δ <i>nprB::lox72</i> , Δ <i>mpr::lox72</i> , Δ <i>aprE::lox72</i> , Δ <i>nprE::lox72</i> , Δ <i>vpr::lox72</i> , Δ <i>epi::lox72</i> , Δ <i>wprA::lox72</i> , Δ <i>srfA::(comS,lox72)</i> , Δ <i>pksX::lox72</i> , Δ <i>pps::lox72</i> , Δ <i>amyE::lox72</i>	Krüger <i>et al.</i> 2022
<i>Bacillus licheniformis</i> SH006	Δ <i>hsdR1</i> , Δ <i>hsdR2</i> , Δ <i>pga</i> , Δ <i>apr</i>	this study
pE194SV	pE194 derivative; <i>E. coli</i> / <i>Bacillus</i> -shuttle vector; <i>EmR</i> ; ori pE194; <i>AmpR</i> , ori pUC18	This work
pDhsdR1	pE194SV with Δ <i>hsdR1</i> homology flanking region	This work
pDhsdR2	pE194SV with Δ <i>hsdR2</i> homology flanking region	This work
pDpga	pE194SV with Δ <i>pga</i> homology flanking region	This work
pDapr	pE194SV with Δ <i>apr</i> homology flanking region	This work

**Table S3:** D-glucose-supplemented M9-mineral medium

<b>M9 - mineral media stock solution</b>	<b>Final concentration per 1 L</b>
M9 salt solution	1x
20 % glucose	0.4 %
1 M MgSO <sub>4</sub>	1 mM
1 M CaCl <sub>2</sub>	0.3 mM
Biotin (1 mg/ml)	4.09 nM
Thiamine (1mg/ml)	3.77 nM
Trace element solution (100x)	1 x

**Table S4:** M9-mineral medium additives

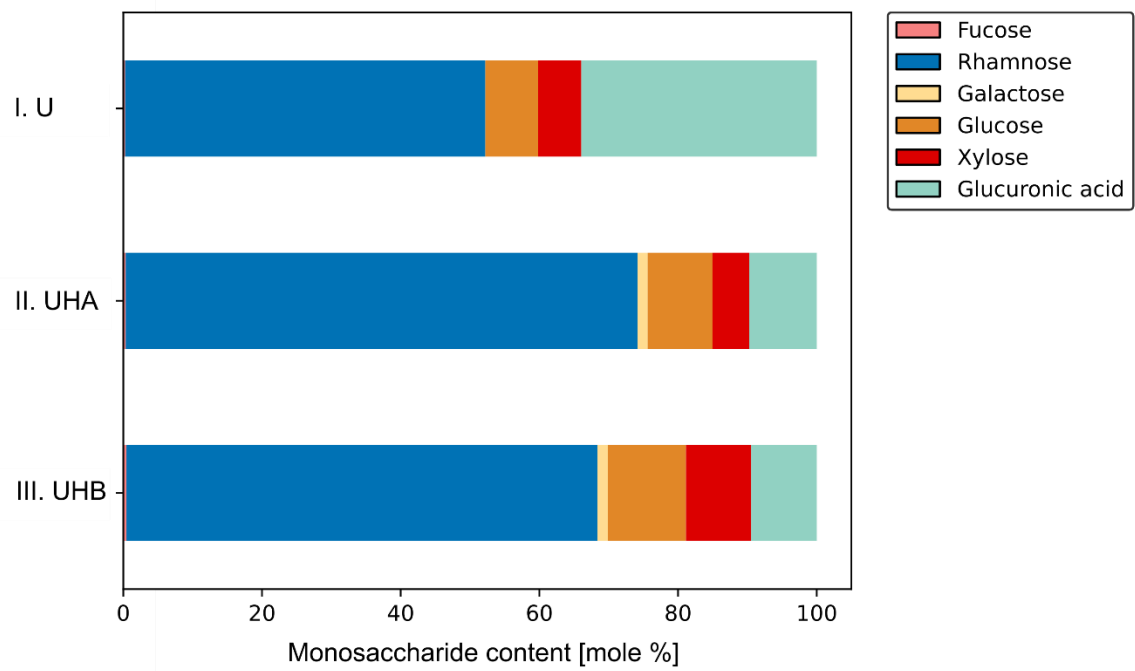
<b>Additive</b>	<b>Component</b>	<b>Concentration in stock solution</b>
M9 salts (10x)	Na <sub>2</sub> HPO <sub>4</sub> *2 H <sub>2</sub> O	422.6 mM
	KH <sub>2</sub> PO <sub>4</sub>	141.4 mM
	NaCl	93.6 mM
	NH <sub>4</sub> Cl	93.5 mM
	ddH <sub>2</sub> O	1 L
Ulvan solution	Ulvan	2 %
	Sodium phosphate buffer	25 mM
	Sodium chloride	50 mM
	pH 7.5	
Ulvan hydrolysate	Ulvan	2 %
	Sodium phosphate buffer	25 mM
	Sodium chloride	50 mM
	pH 7.5	
	Enzyme mix	5 µL/mL per enzyme
Enzyme mix	Sodium phosphate buffer	25 mM
	Sodium chloride	50 mM
	pH 7.5	
	Enzyme mix	5 µL/mL per crude extract enzyme from table S1
Trace element solution 100 x	FeCl <sub>3</sub>	13.1 mM
	ZnCl <sub>2</sub>	0.62 mM
	0.1 M CaCl <sub>2</sub> • 2H <sub>2</sub> O	76 µM
	0.2 M CoCl <sub>2</sub> • 6 H <sub>2</sub> O	42 µM
	0.1 M HBO <sub>3</sub>	162 µM
	1 M MnCl <sub>2</sub> • 4 H <sub>2</sub> O	8.1 µM
	KI	0.5 mM
	Na <sub>2</sub> MoO <sub>4</sub>	1 mM
EDTA	13.4 mM	
Yeast extract		2 % (w/v)
Sodium chloride		15 % (w/v)



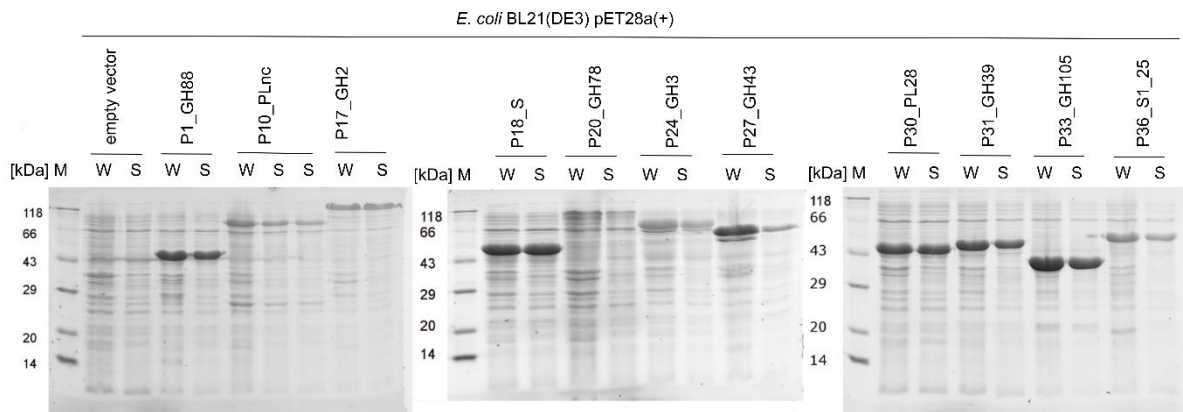
**Table S5:** List and sequences of primers used in this study.

Primer	Sequence 5' → 3'
MaZu7	ACGTCATATGAAAATCAGTATGCAAAAAGCAGATTTTTGGAAAAAAGCAGCGATCTCATTACT TGTTTTACCCATGTTTTTACCCTGATGATGAGCG
MaZu8	CACCATGTTTTTACCCTGATGATGAGCGAAACGGTTTTTGCGCCAAACGGCACCGGATGAA GACACAAGCGCCATTACGAG
MaZu9	ACGTGGTACCTTACAGGCTTTCGACTGCGATGGCTTTCCAGACGC
MaZu10	CACCATGTTTTTACCCTGATGATGAGCGAAACGGTTTTTGCGCCAAACGGCCTTAACCATA GCGAAATCGAAGC
MaZu11	ACGTGGTACCTTATTCTTCCAGTTTTCAAGACTTCGCTTCCTGCCATCAG
MaZu12	ACGTCATATGTTGATCAACAAAAGCAAAAAGTTTTTCGTTTTTCTTTCATTTTTGTTATGATG CTGAGCCTCTCATTGTGAATGGG
MaZu13	GATGCTGAGCCTCTCATTGTGAATGGGGAAGTTGCAAAAGCCCAAACGGCACCGGATGAA GACACAAGCGCC
MaZu14	GATGCTGAGCCTCTCATTGTGAATGGGGAAGTTGCAAAAGCCCAAACGGCCTTAACCAT AGCGAAATCGAAGCG
MaZu19	ACGTACCATATGCAAACGGCACCGGATGAAGACACAAGCGCC
MaZu20	ACGTACTCTAGACAGGCTTTCGACTGCGATGGCTTTCCAGAC
MaZu21	ACGTACCATATGCAAAAAGGCCTTAACCATAGCGAAATCGAAGCG
MaZu22	ACGTACTCTAGATTCTTCCAGTTTCAAGACTTCGCTTCCTGCCATCAG
MaZu28	TGATAAGCGTTGGTTGGCAATCTTATCGGGCTATGCATTTATAAAATG
MaZu29	GCATAGCCCGATAAGATTGCCAAACCAACGCTTATCAATAGAAAAAGAGCATTTTTTGAAAC AAAATTC
MaZu35	TGCGTTAGCAATTTAACTGTGATAAACTACCGCATTAATAGAAAAAGAGCATTTTTTGAAACA AAAATTC
MaZu36	TAATGCGGTAGTTTATCACAGTTAAATTGCTAACGCAGTCAGGCACCGT
MaZu37	GTTTTTAAAGGCTTTTAAAGCCGTCTGTACGTTTCTTAACATCTGATGTCTTTGCTTGCGAATG TTCATCT
MaZu38	TTAGGAACGTACAGACGGCTTAAAAGCCTTAAAAACGTTTTTAAAGGGTTTGTAGACAAGG TAAAGGATAAAACAG
P1-hsdR1	CTGCAGGGTCTCAACCCGAACAGCGTAAGGCTGATG
P2-hsdR1	CCGTAATTTGAATCTATTAGACAAACATCTTTTGTAGGAATG
P3-hsdR1	GATGTTTGTCTAATAGATTCAAATTACGGGCCTTG
P4-hsdR1	TCTAGAGGTCTCATGAGATCGGTTTTATGAAAGCGTC
P1-hsdR2	CTGCAGCGTCTCAACCCGATAAAAGGATTACTGTGCG
P2-hsdR2	TCCATGTTGTCACAACCTATTGTTGAGAATAAAGGAAAAGGAG
P3-hsdR2	CCTTTATTCTCAACAATAGGTTGTGACAACATGGAAAG
P4-hsdR2	TCTAGACGTCTCATGAGGTGCTTTCATCAATCGTAAATC

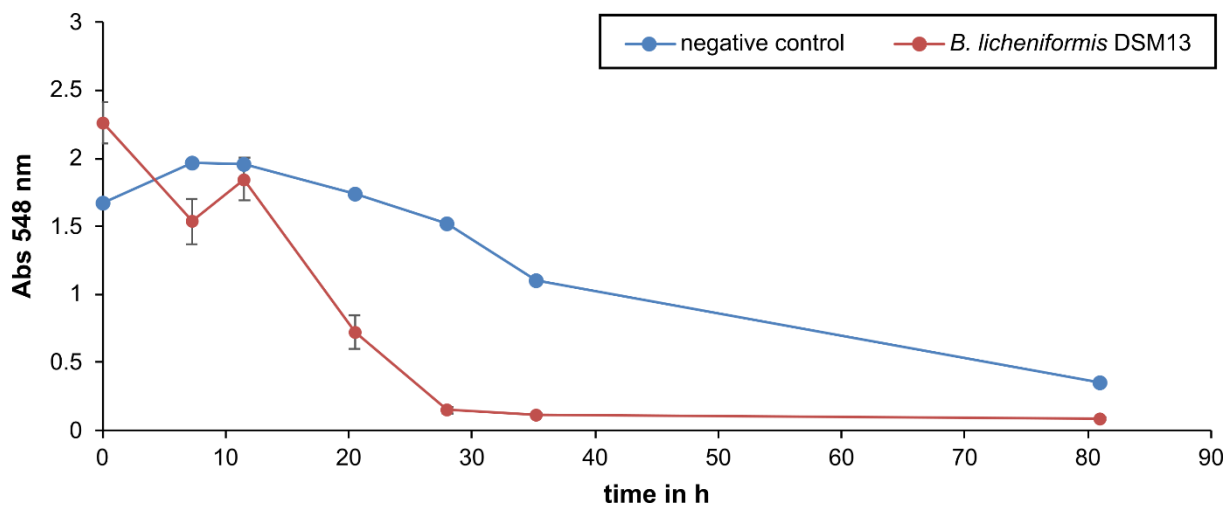
**Table S6:** Summary of the proteomic results (available as separate Excel file)**Table S7:** Results of statistical analyses (Welch's T-test, FDR 0.05) (available as separate Excel file)



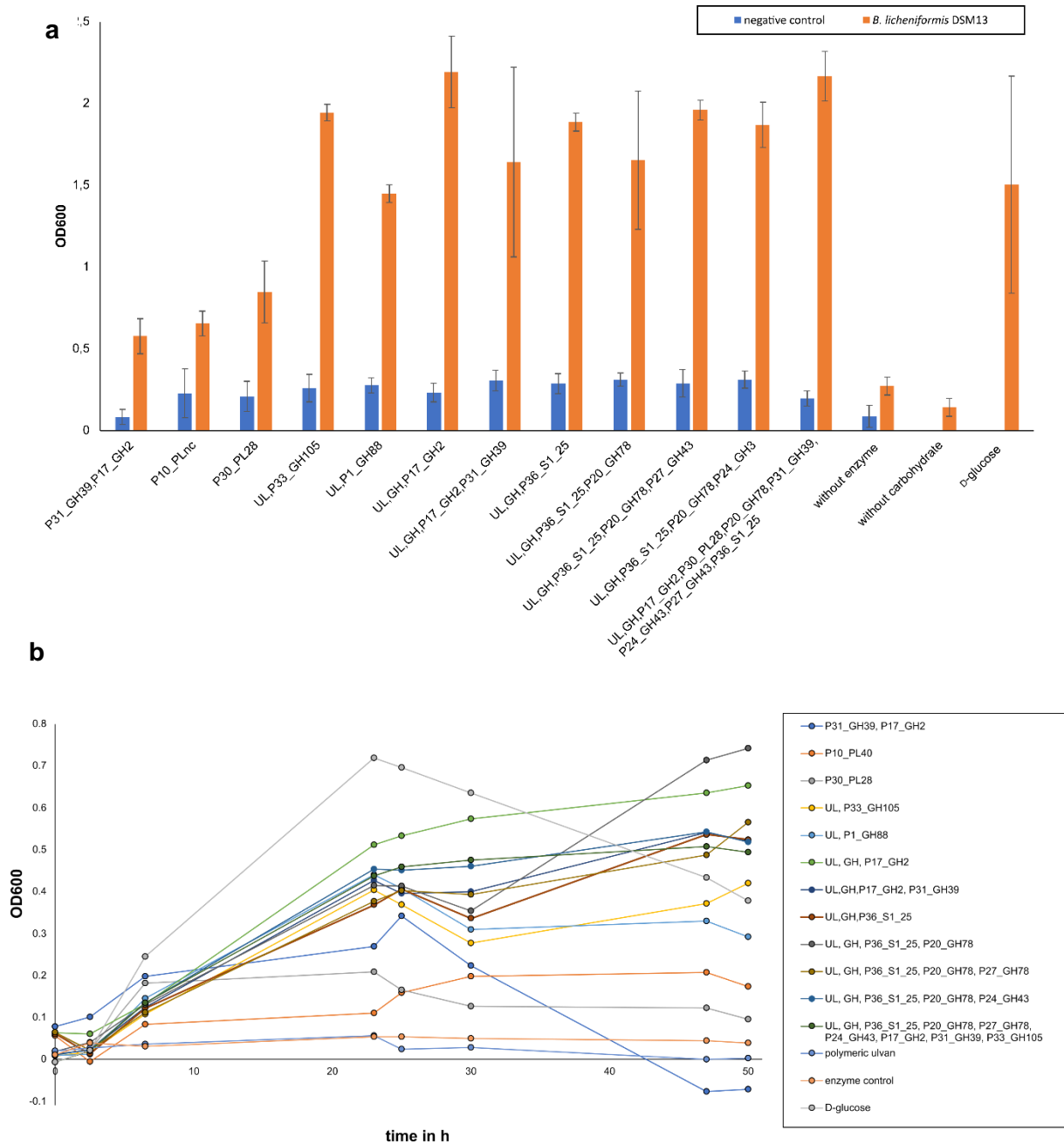
**Fig. S1** Sugar composition of the cultivation media. The complex carbon sources were analysed for their detailed monosaccharide composition via acid hydrolysis and HPAEC-PAD. Ulvan (U), the partially P30\_PL28 and P33\_GH105-hydrolyzed ulvan (UHA) and the completely digested ulvan (UHB) using the whole cascade of ulvan degrading enzymes [1].



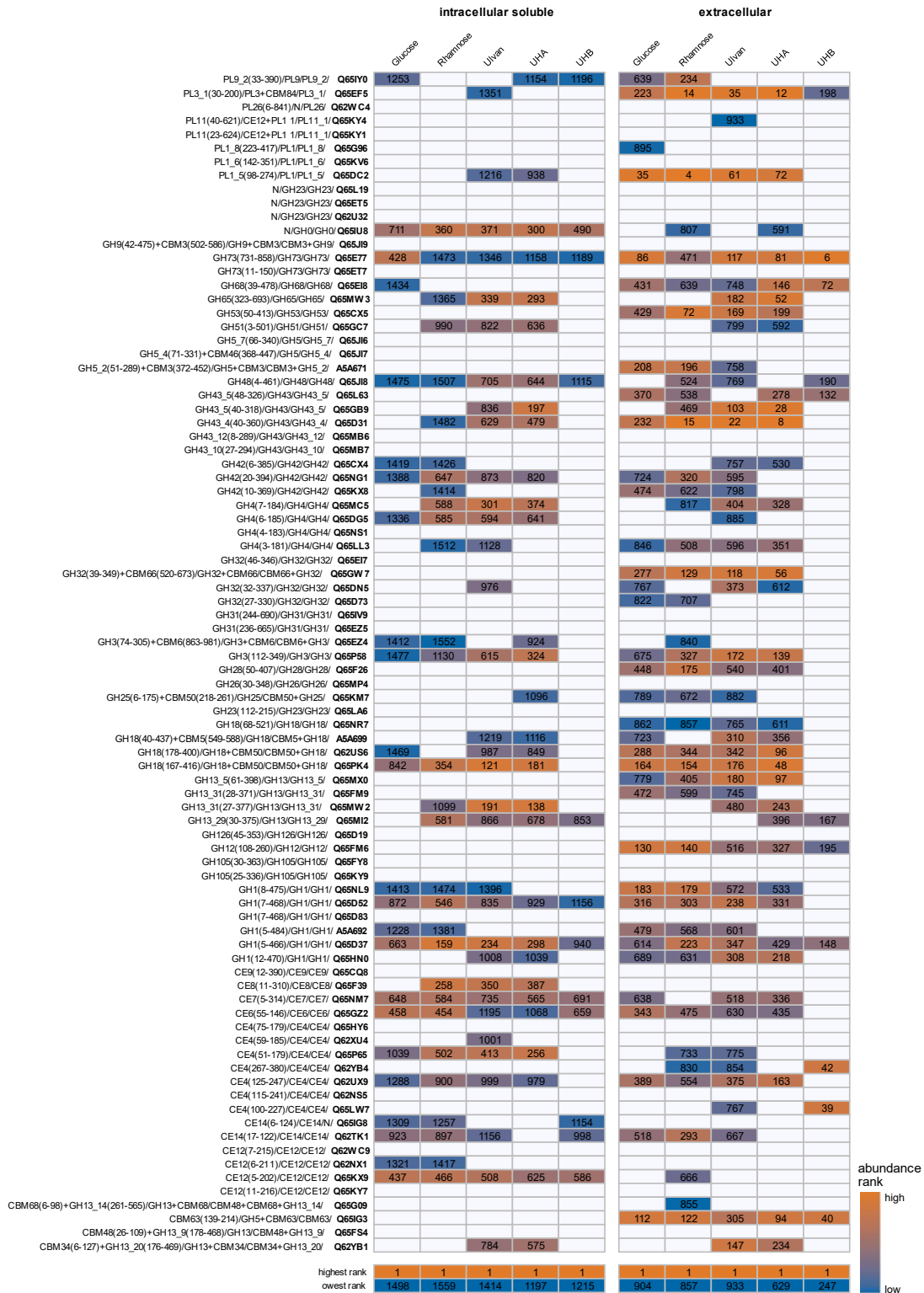
**Fig. S2** SDS-PAGE of *F. agariphila* KMM3901<sup>T</sup> enzymes expressed recombinantly in *E. coli* BL21(DE3) as described by Reisky *et al.* [1]. The cells were normed (7/OD) and the whole cell (W) extract and soluble protein (S) fraction were analyzed by SDS-PAGE containing 1% (V/V) trichloroethanol (TCE). The protein bands were visualised under UV and the pictures were colour-inverted and decolorized. The protein marker Roti<sup>®</sup>-Mark from Carl Roth (Karlsruhe, Germany) was used.



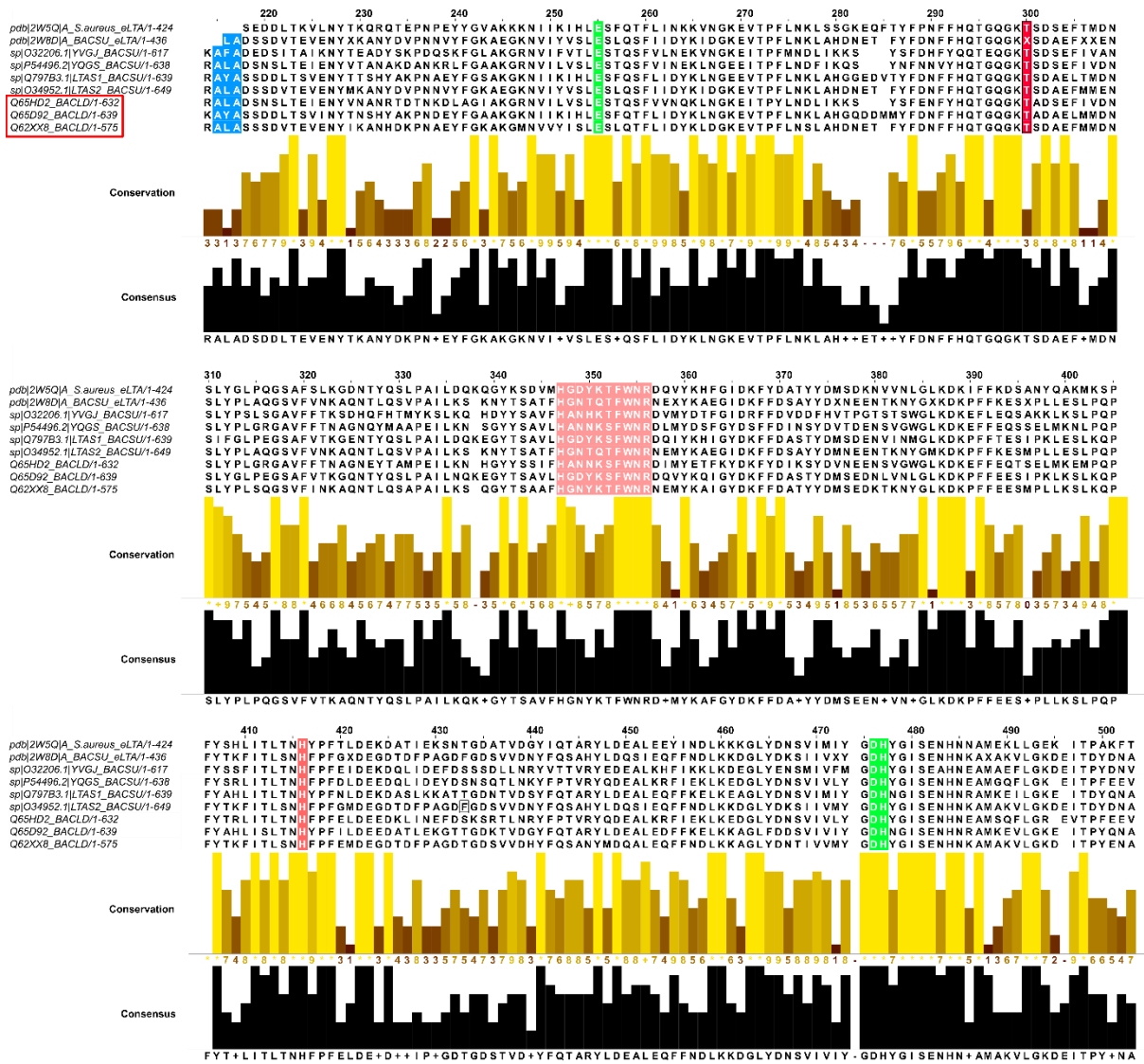
**Fig. S3** Consumption of 5-dehydro-4-deoxy-D-glucuronate by *B. licheniformis* DSM13 during cultivation. Thiobarbituric acid assay determined 5-dehydro-4-deoxy-D-glucuronate in cultivation supernatants (M9-ulvan hydrolysate UHB, see Fig. 3a). Cell-free medium served as negative control.



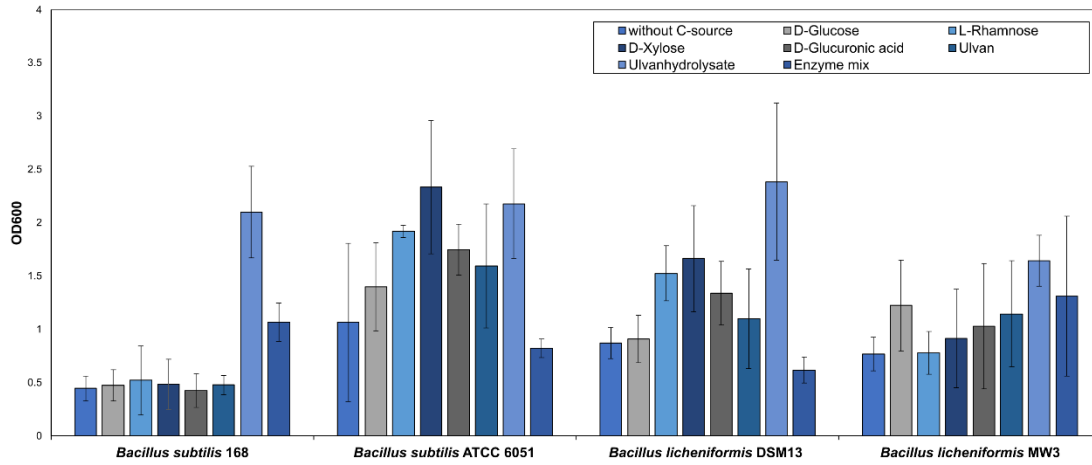
**Fig. S4** Growth of *B. licheniformis* DSM13 on ulvan (without enzyme) and ulvan hydrolysates representing different levels of degradation. For hydrolysis, different *F. agariphila* enzymes, enzyme combinations or all enzymes (recombinantly expressed in *E. coli*) were used (Table S1). *B. licheniformis* DSM13 was cultivated in 1 mL in 96 deep-well plates and OD600 was measured after 48 h (a). This graph represents the full dataset of the Figure 2 in the main text. For investigation of the growth behaviour the culture was cultivated in 200  $\mu$ L scale in a low-well plate and measured for 48 h (b).



**Fig. S5** List of PLs, GHs and CEs identified by dbCAN2 [6] and their abundance in the intracellular soluble and extracellular proteomes. The graph indicates the relative abundance of proteins within the respective sample given as abundance ranks. Abundance ranks were derived from %riBAQ values (Table S6). The lowest rank corresponds to the total number of quantified proteins per sample. Blank tiles represent proteins that were not quantified. UHA/B: Ulvan hydrolysate A/B (see Fig. 3a). Protein IDs are highlighted in bold together with the full output of dbCAN2 analyses (HMMER/Hotpep/DIAMOND/Protein ID).

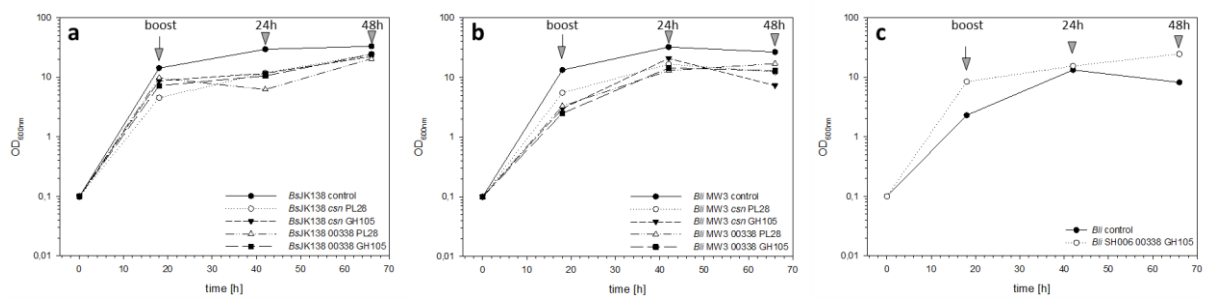


**Fig. S6** Alignment of sulfatases from *B. licheniformis* DSM13 with lipoteichoic acid synthases of other Gram-positive bacteria. The lipoteichoic acid synthases (LTA) were the highest hit in the BlastP search. LTAs consist of a transmembrane and an extracellular domain. Amino acid residues in the region of the extracellular LTA (eLTA) domain (210 to 585 As) are displayed. LTAs are synthesized as membrane proteins and are cut at a cleavage sequence AXA (blue). T300 (marked in red) is the catalytic residue in the eLTA of *S. aureus*, while H416 is involved in the reaction mechanism (protonation of the leaving group). Residues marked in green are important for the binding of Mn<sup>2+</sup>. Residues 347-356 (HxD/NxxFW/YNR) are important for substrate binding [7].

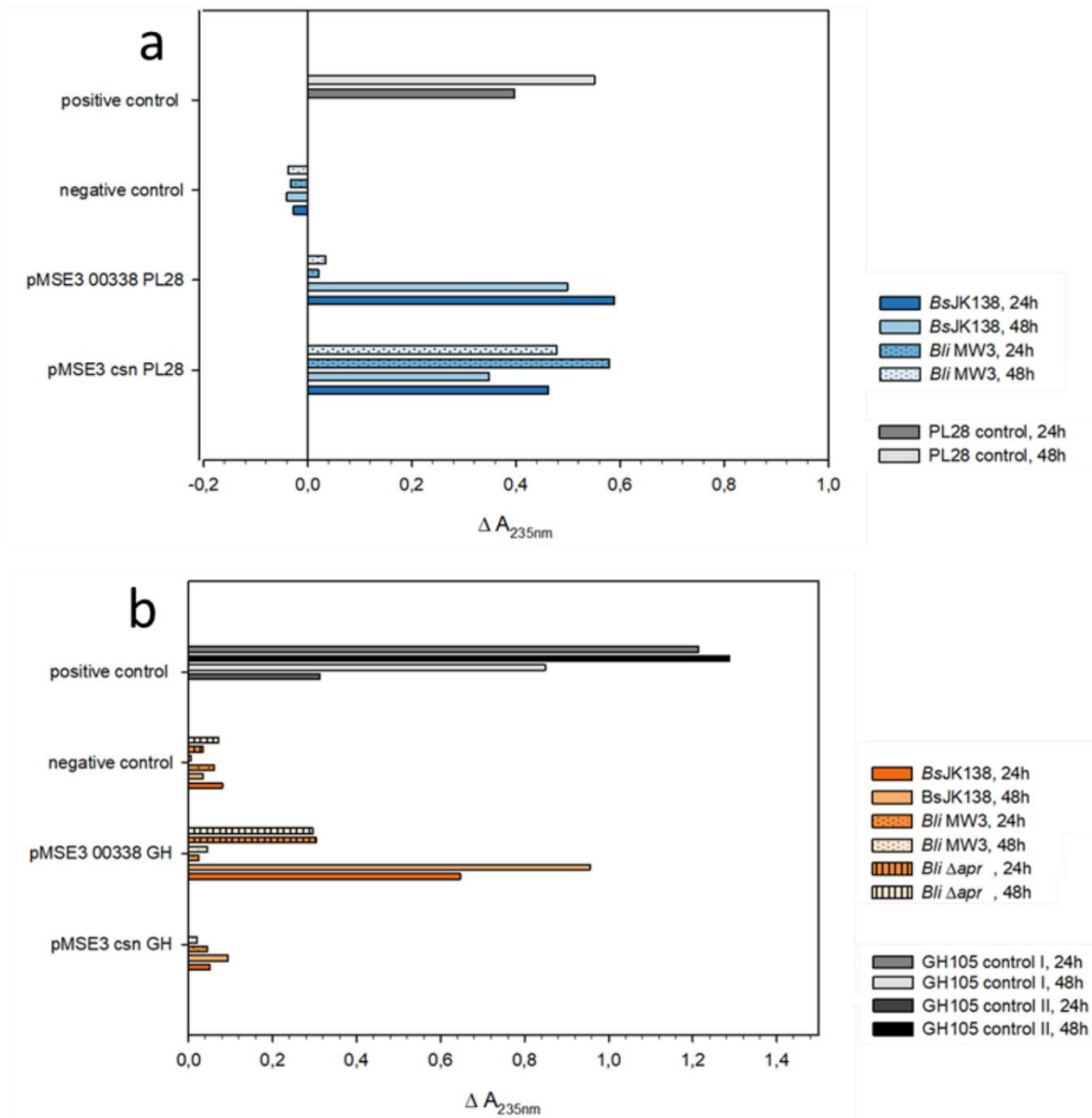


**Fig. S7** Comparison of different *Bacillus* sp. for the conversion of ulvan hydrolysate and ulvan derived monosaccharides. The strains were cultivated in 1 mL Belitzky-Minimal media [8] with variation of the carbon source in a 96-deep well-plate. General growth in OD600nm was measured after 24 h, showing a general acceptance of the ulvan hydrolysate for all four *Bacillus* sp. in the chosen Belitzky-Minimal medium conditions.

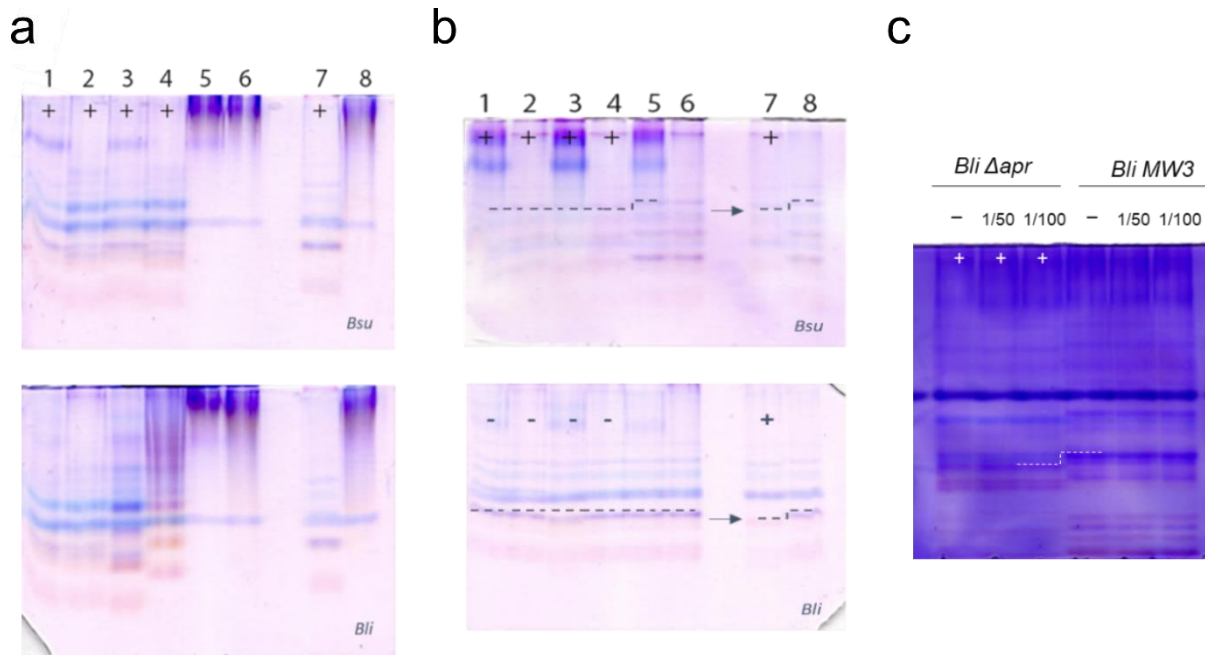




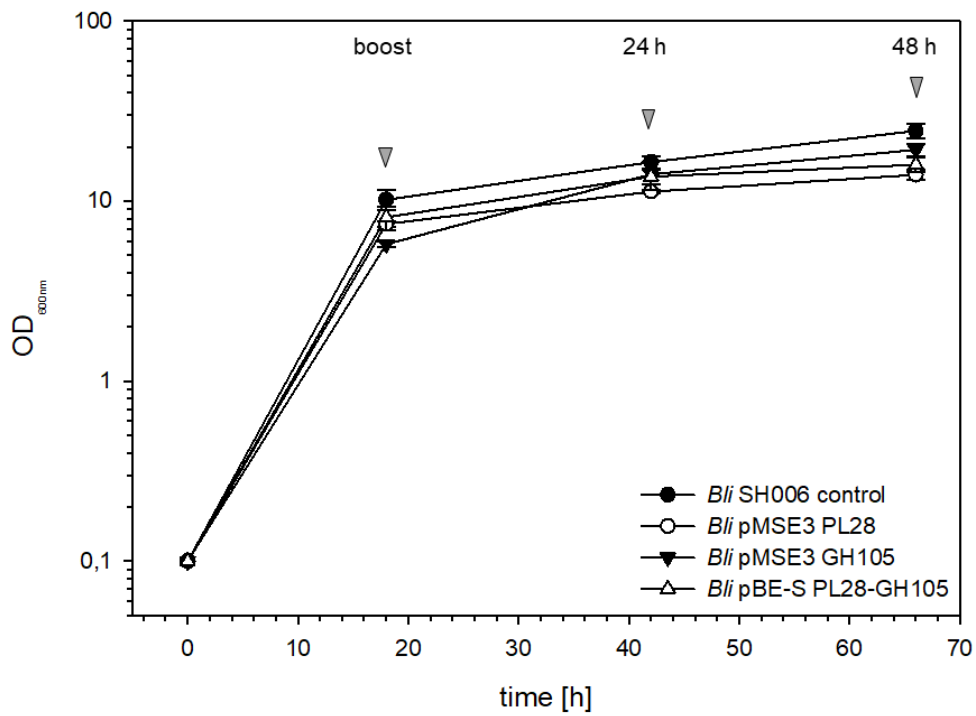
**Fig. S8** Growth of the PL28 and GH105 *Bacillus* expression strains. *B. subtilis* JK138. **(a)**, *B. licheniformis* MW3 **(b)** and *B. licheniformis* SH006 ( $\Delta$ csr) **(c)** were grown under simulated fed-batch conditions in Espresso-B medium at 30°C and 250 rpm. Sampling points for activity measurements, 24 h and 48 h after the boost are indicated.



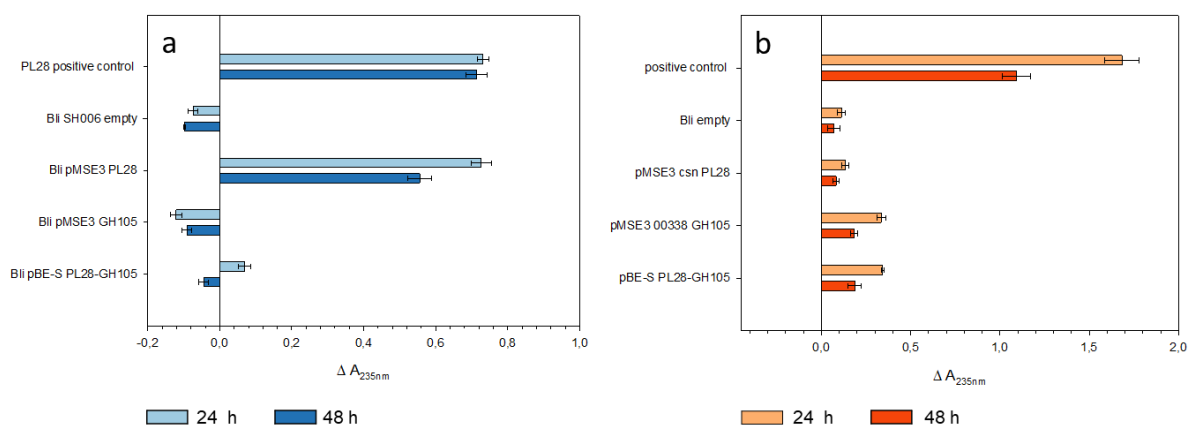
**Fig. S9** Activity assay results from *Bacillus* sp. PL28 and GH105 expression strains. (a) Results of the ulvan lyase (UL) assay measurement of the lyase product formation at 235 nm over 60 min. The deviation of the absorption of the end-start reveals the lyase product formation (lyase activity), while the deviation of the absorption start-end shows the reversed reaction of the GH105 activity (b) cleaving of the lyase moiety using prehydrolyzed ulvan from the recombinantly expressed ulvan lyase PL28.



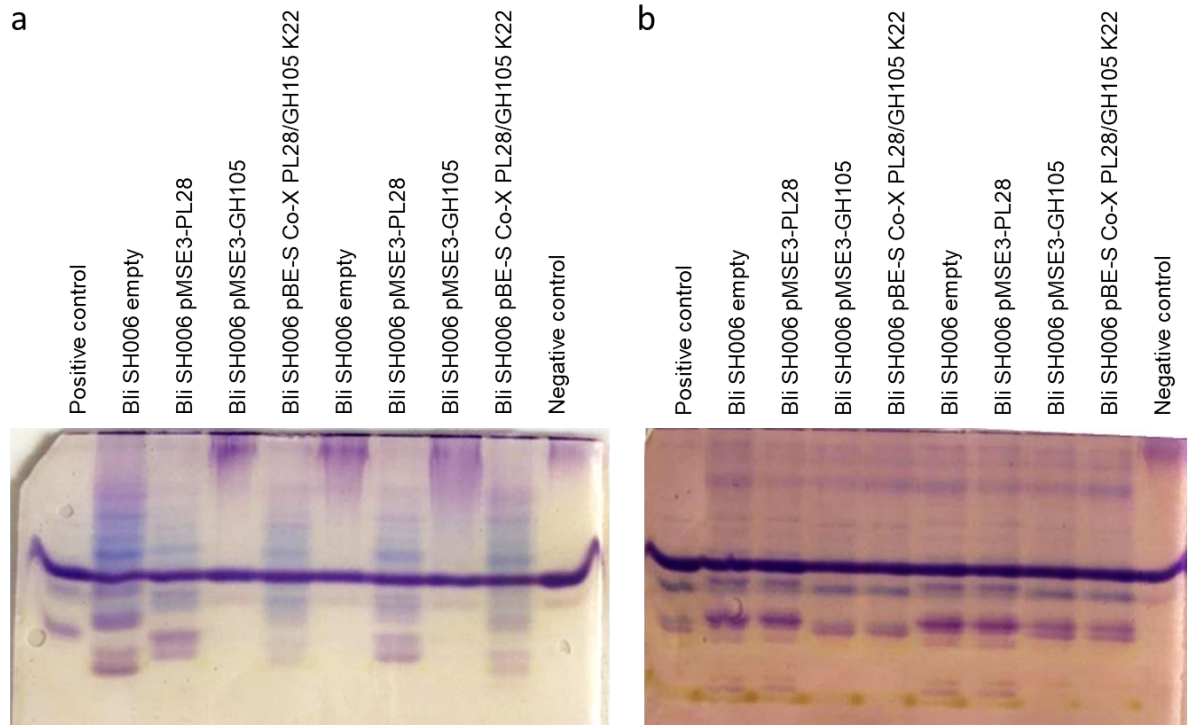
**Fig. S10** C-PAGE results from *Bacillus* sp. PL28 and GH105 expression strains. **(a)** The C-PAGE (carbohydrate polyacrylamide gel electrophoresis) corresponds to the ulvan lyase assay shown in Fig. S10 to the results of the ulvan lyase (UL) expression and **(b)** reaction of the GH105 activity cleaving of the lyase moiety using prehydrolyzed ulvan from the recombinantly expressed ulvan lyase PL28. Intracellular (in) and extracellular (ex) fractions of *B. subtilis* JK138 (*Bsu*) and *B. licheniformis* DSM13 (*Bli*) were analyzed. Lane 1: TB1 csn-UL ex, Lane 2: TB1 csn-UL in, Lane 3: TB1 00338-UL ex, Lane 4: TB1 00338-UL in, Lane 5: Ko (empty vector) ex, Lane 6: Ko (empty vector), Lane 7: positive control, Lane 8: negative control. **(c)** C-PAGE after 24 h of GH105 expression in *B. licheniformis* SH006 (*Bli*  $\Delta apr$ ) and *B. licheniformis* MW3 (*Bli* MW3) with the addition of the protease inhibitor in 1/100, 1/50 and no protease (-) addition.



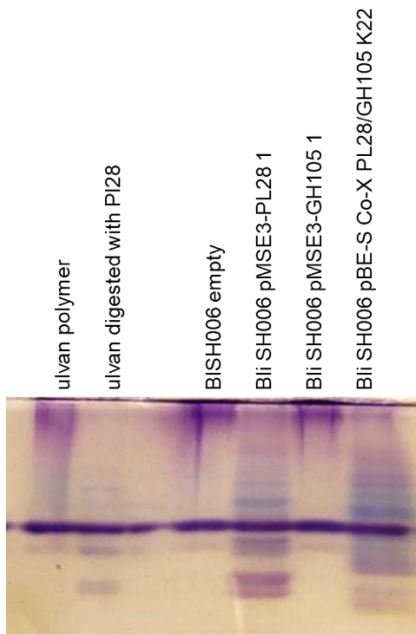
**Fig. S11** Growth of the different *B. licheniformis* expression strains. *B. licheniformis* SH006, *B. licheniformis* pMSE3 PL28, *B. licheniformis* pMSE3 GH105 and *B. licheniformis* pBE-S PL28-GH105 were grown under simulated fed-batch conditions in Espresso-B medium at 30°C and 250 rpm. Sampling points for activity measurements, 24 h and 48 h after the boost are indicated.



**Fig. S12** Activity assay results from *B. licheniformis* SH006, PL28 and GH105 single- and co-expression strain. **(a)** Results of the ulvan lyase (PL28) assay measurement of the lyase product formation at 235 nm over 60 min. The deviation of the absorption of the end-start shows the lyase product formation (lyase activity). **(b)** The deviation of the absorption start-end shows the reversed reaction of the GH105 activity by cleaving of the lyase moiety using prehydrolyzed ulvan from the recombinantly expressed ulvan lyase PL28. Corresponding C-PAGE gels are shown in Fig. S13.



**Fig. S13** C-PAGE results from *B. licheniformis* SH006 PL28, GH105 and co-expression strains. The results correspond to the ulvan lyase assay shown in Fig. S12. (a) Shows the C-PAGE result of the PL28 ulvan lyase activity (extracellular fraction) of the strain constructs *B. licheniformis* SH006 (Bli SH006) empty, pMSE3\_PL28, pMSE3- GH105 or pBE-S Co-X PL28/GH105 K22 (b) shows the reaction of the GH105 cleaving of the lyase moiety using prehydrolyzed ulvan.



**Fig. S14** C-PAGE from the cultivation supernatant of *B. licheniformis* strains in M9-mineral media. *B. licheniformis* (Bli) SH006 PL28, GH105 and coexpression strains were cultivated in M9-mineral media (see Fig. 6) for seven days. A supernatant sample was loaded, as negative control the ulvan polymer and as a positive control the predigested ulvan with PL28 was loaded on the gel.

## References

1. Reisky L, Précoux A, Zühlke MK, Baumgen M, Robb CS, Gerlach N, et al. A complex enzyme cascade degrades the polysaccharide ulvan from green algae. *Nat Chem Biol.* 2019;803–12.
2. Veith B, Herzberg C, Steckel S, Feesche J, Maurer KH, Ehrenreich P, et al. The complete genome sequence of *Bacillus licheniformis* DSM13, an organism with great industrial potential. *J Mol Microbiol Biotechnol.* 2004;7:204–11.
3. Hofmeyer T, Hackenschmidt S, Nadler F, Thürmer A, Daniel R, Kabisch J. Draft genome sequence of *Cutaneotrichosporon curvatus* DSM 101032 (Formerly *Cryptococcus curvatus*), an oleaginous yeast producing polyunsaturated fatty acids. *Genome Announc.* 2016;4:e00362-16.
4. Pohlmann A, Fricke WF, Reinecke F, Kusian B, Liesegang H, Cramm R, et al. Genome sequence of the bioplastic-producing “Knallgas” bacterium *Ralstonia eutropha* H16. *Nat Biotechnol.* 2006;24:1257–62.
5. Waschkau B, Waldeck J, Wieland S, Eichstädt R, Meinhardt F. Generation of readily transformable *Bacillus licheniformis* mutants. *Appl Microbiol Biotechnol.* 2008;78:181–8.
6. Yin Y, Mao X, Yang J, Chen X, Mao F, Xu Y. dbCAN: a web resource for automated carbohydrate-active enzyme annotation. *Nucleic Acids Res.* 2012;40:W445–51.
7. Lu D, Wörmann ME, Zhang X, Schneewind O, Gründling A, Freemont PS. Structure-based mechanism of lipoteichoic acid synthesis by *Staphylococcus aureus* LtaS. *Proc Natl Acad Sci. Proceedings of the National Academy of Sciences;* 2009;106:1584–9.
8. Stülke J, Hillen W. Regulation of Carbon Catabolism in *Bacillus* Species. *Annu Rev Microbiol.* 2000;54:849–80.





## List of Publications

1. S. Brott, K. H. Nam, F. Thomas, T. Dutschei, L. Reisky, M. Behrens, H. C. Grimm, G. Michel, T. Schweder, and U. T. Bornscheuer. „Unique Alcohol Dehydrogenases Involved in Algal Sugar Utilization by Marine Bacteria.” *Appl. Microbiol. Biotechnol.* **2023**, *107*, 2363–84.
2. N. A. Tarazona, R. Wei, S. Brott, L. Pfaff, U. T. Bornscheuer, A. Lendlein, and R. Machatschek. “Rapid Depolymerization of Poly(Ethylene Terephthalate) Thin Films by a Dual-Enzyme System and Its Impact on Material Properties.” *Chem Catal.* **2022**, *2*, 3573–89.
3. T. Dutschei, M. K. Zühlke, N. Welsch, T. Eisenack, M. Hilkmann, J. Krull, C. Stühle, S. Brott, A. Dürwald, L. Reisky, J. H. Hehemann, D. Becher, T. Schweder, and U. T. Bornscheuer. “Metabolic Engineering Enables *Bacillus Licheniformis* to Grow on the Marine Polysaccharide Ulvan.” *Microb. Cell Factories* **2022**, *21*, 207
4. M. Kollipara, P. Matzel, M. Sowa, S. Brott, U. T. Bornscheuer, and M. Höhne. „Characterization of Proteins from the 3N5M Family Reveals an Operationally Stable Amine Transaminase.” *Appl. Microbiol. Biotechnol.* **2022**, *106*, 5563–74.
5. S. Brott, F. Thomas, M. Behrens, K. Methling, D. Bartosik, T. Dutschei, M. Lalk, G. Michel, T. Schweder, and U. T. Bornscheuer. „Connecting Algal Polysaccharide Degradation to Formaldehyde Detoxification.” *ChemBioChem* **2022**, *23*, e202200269
6. S. Brott, L. Pfaff, J. Schuricht, J. N. Schwarz, D. Böttcher, C. P. S. Badenhorst, R. Wei, and U. T. Bornscheuer. „Engineering and Evaluation of Thermostable IsPETase Variants for PET Degradation.” *Eng. Life Sci.* **2022**, *22*, 192–203.



## Acknowledgments

Mein erstes und größtes Danke geht an Prof. Dr. Uwe Bornscheuer, da er mir die Möglichkeit gab, in seiner Arbeitsgruppe an so einem spannenden und gleichzeitig vielseitigen Thema zu arbeiten. Ich konnte dadurch so viel Wissen und Methoden sammeln und mich dadurch auch als Wissenschaftler weiterentwickeln. Gleichzeitig bedanke ich mich auch dafür, dass ich auch auf dem Thema meiner Masterarbeit, dem Plastik-Abbau, weiterarbeiten durfte und auch dort erfolgreich Studien publizieren konnte.

Ich möchte mich auch bei meinen Kooperationspartnern Prof. Dr. Thomas Schweder, Prof. Dr. François Thomas, Prof. Dr. Gurvan Michel und Prof. Dr. Ki Hyun Nam für die Möglichkeit der Zusammenarbeit und deren Beitrag zu den Studien bedanken.

Ein großer Dank geht an alle Mitglieder des POMPU-Teams. Vor allem Theresa Dutschei erhält ein großes Dankeschön, da sie stets eine Antwort auf meine Fragen besaß und mir zahlreiches Hintergrundwissen zu Beginn meines PhD vermachte. Jana Husarcikova danke ich für die zahlreichen kleinen Gespräche und die Beantwortung von Fragen zur Bedienung der Äkta. Michelle Teune danke ich ebenfalls für die tolle Gemeinschaftsarbeit am *Novel Enzymes* Poster und das Beantworten von Fragen. Daniel Bartosik danke ich für die Zusammenarbeit und für die gemeinsamen Grillabende, die durch Schluckauf-Garantie unvergesslich geworden sind.

Ich möchte mich auch bei allen Mitgliedern des Arbeitskreises für Biotechnologie und Enzymkatalyse für die tolle Arbeitsatmosphäre bedanken. Ein großer Dank geht an Dominique, Mark und Thomas, welche stets für Ordnung und Sicherheit im Labor sorgen.

Marian, Ina und Thomas danke ich für die wundervollen Momente im Labor und am heiligen Tisch der Motivation, welche mir immer neue Kraft für die stressigen Momente im Laboralltag gegeben haben. Viel Erfolg für eure Zukunft wünscht euch eurer Paparazzi, der Bezwingen des *Hollow Knights*, der Entenangler-Profi und Experte für *fancy* Präsentationen.

Meinen indirekten Laborplatznachbar Yannik danke ich für den Spaß im Labor und die unzähligen Möglichkeiten über das neuste *One Piece* Kapitel zu quatschen. Ich bin sicher, irgendwann hätte auch unsere Revolution gegen die Labor-Deputies funktioniert.

Mein tiefster Dank geht auch an meine Bachelorstudentin und studentischen Hilfskraft Maïke Behrens, welche wertvolle Beiträge zu den Studien geleistet hat und viel Spaß in den alltäglichen Laboralltag brachte. Des Weiteren möchte ich mich auch bei Nadja, Jule und Nils bedanken, welche das Biotechnologie-Praktikum zu einem echten Highlight machten.

Zum Abschluss möchte ich mich noch bei meiner Familie für die Unterstützung während meines gesamten Studiums und des Schreibens dieser Arbeit bedanken.